

**MOLECULAR ARCHITECTURES FOR IMPROVED BIOMATERIALS DERIVED
FROM VEGETABLE OILS – APPLICATION TO ENERGY STORAGE AND
LUBRICANTS**

A dissertation submitted to the Committee on Graduate Studies in Partial Fulfillment of the Requirements
for the Degree of Doctor of Philosophy in the Faculty of Arts and Science

TRENT UNIVERSITY

Peterborough, Ontario, Canada

© Copyright by Navindra Soodoo (2022)

Environmental and Life Sciences Ph.D. Graduate Program

September 2022

ABSTRACT

MOLECULAR ARCHITECTURES FOR IMPROVED BIOMATERIALS DERIVED FROM VEGETABLE OILS – APPLICATION TO ENERGY STORAGE AND LUBRICANTS

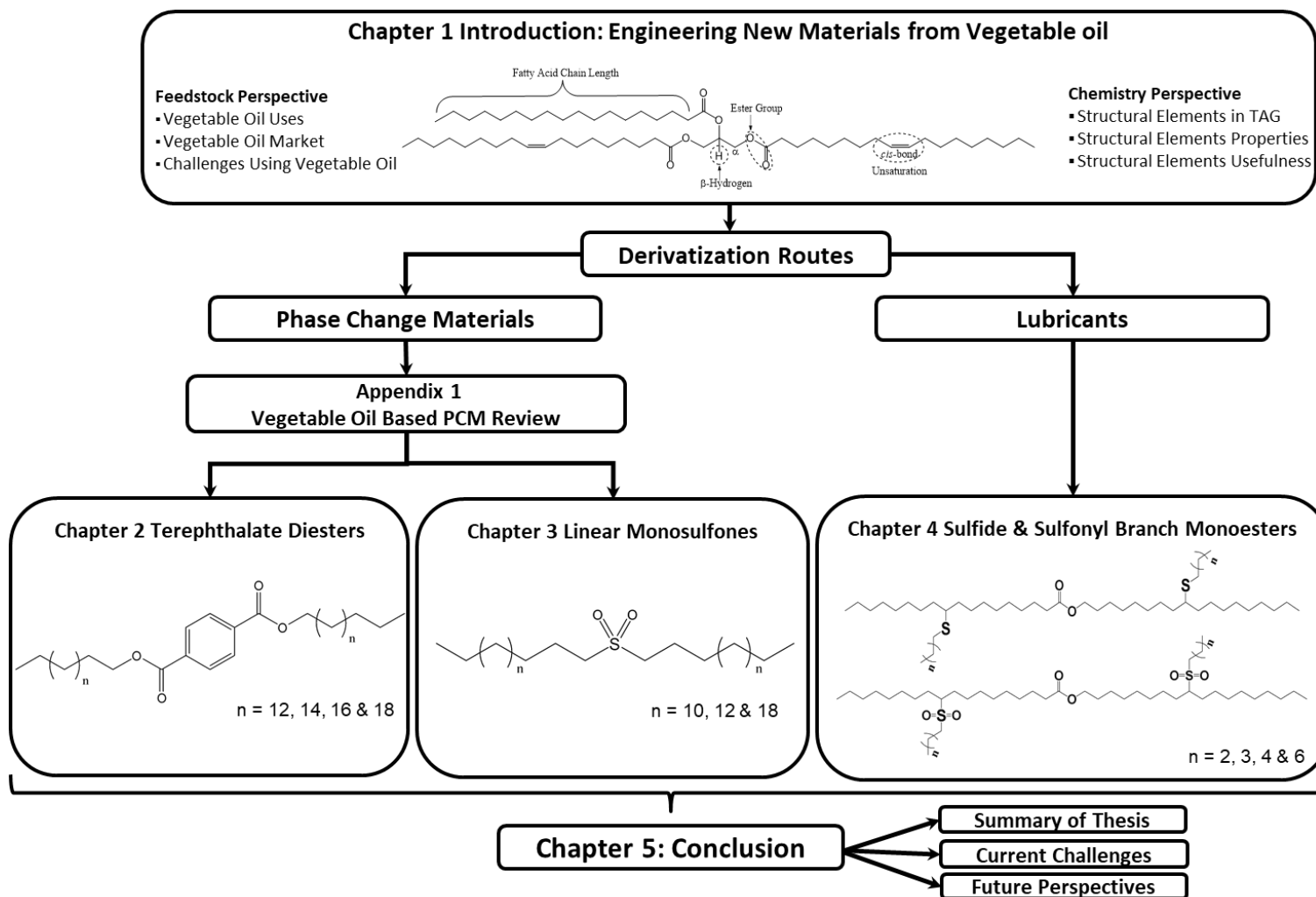
Navindra Soodoo

The replacement of petroleum with renewable feedstock for energy and materials has become a priority because of concerns over the environment and finite nature of petroleum. The structures of the available natural biomass feedstocks fall short in delivering key functionality required in materials such as lubricants and phase change energy storage materials (PCMs). The approach taken in this thesis was to combine select functional groups with vegetable oil derivatives to create novel PCMs and lubricants which deliver desired functionality. One series of diester PCMs were prepared with terephthalic acid and fatty alcohols to address known shortcomings of esters. The second class of PCMs are sulfones prepared from oxidation of fatty sulfides to improve thermal energy storage. Overall, the new PCMs presented narrow phase change temperature ranges, high transition temperature (between 67 to 110°C), high transition enthalpy (210 to 266J/g), minimal supercooling and congruent phase transitions unaffected by cooling rates. They also demonstrated higher thermal degradation stability with onset of degradation from 290 to 310°C. The series of lubricants studied consists of sulfide and sulfonyl functional groups attached to the unsaturation sites of oleyl oleate as pendant groups to improve the thermal and flow properties. The new lubricants present subzero crystallization temperatures, very low crystallization enthalpy and dynamic viscosity as high as 180mPas.

Furthermore, they also presented high onset of degradation (up to 322°C) and oxidation (up to 298°C). The PCMs and lubricants of the present thesis demonstrate that select functional groups can be used with common structural elements of vegetable oil such as fatty acids, ester groups and unsaturation sites to make a variety of molecular structures capable of delivering desired properties.

Keywords: Renewable, Plant Oil; Vegetable Oil (VO) Green Chemistry; Phase Change Material (PCM); Lubricant; Terephthalate Diester; Esterification, Benzene, Sulfone; Thioetherification; Oleyl Oleate; Branching; Intermolecular Interactions; Structure-Property Relationships; Melting Temperature; Enthalpy; Entropy, Thermal Stability; Cold flow; Viscosity; Crystal Structure; Polymorphism.

Graphical Summary of Thesis



Declaration on Publications

This dissertation includes three published studies and one submitted to a peer-reviewed journal. The table below lists the thesis chapters and citation of the published/submitted work:

Study #	Thesis Chapter	Citation
1.	Chapter 2	Navindra Soodoo , K.D. Poopalam, L. Bouzidi, and S.S. Narine, <i>Exploiting Aromaticity in Fatty Terephthalate Diesters to Enhance Melting Point and Prevent Polymorphism</i> . <i>Solar Energy Materials and Solar Cells</i> , 2022 https://doi.org/10.1016/j.solmat.2022.111650
2.	Chapter 3	Navindra Soodoo , L. Raghunanan, L. Bouzidi, and S.S. Narine, <i>Phase behavior of monosulfones: Use of high polarity sulfonyl groups to improve the thermal properties of lipid-based materials for PCM applications</i> . <i>Solar Energy Materials and Solar Cells</i> , 2019. https://doi.org/10.1016/j.solmat.2019.110115
4.	Chapter 4	Navindra Soodoo , L. Bouzidi, and S.S. Narine, <i>Exploiting the Chemical Properties of Sulfur to Improve Thermal, Viscosity and Antioxidative Properties of Branched Lipid-Based Lubricants</i> . Accepted to <i>Industrial & Engineering Chemistry Research</i> , 2022
5.	Appendix 1	Navindra Soodoo , K.D. Poopalam, L. Bouzidi, and S.S. Narine, <i>Fundamental Structure-Function Relationships in Vegetable Oil Based Phase Change Materials: A Critical Review</i> . https://doi.org/10.1016/j.est.2022.104355

I hereby declare that this thesis incorporates published as well as submitted studies that are the result of collaborations:

In the published/submitted studies, I, Navindra Soodoo, developed ideas and experimental designs, performed data collection, analyses and interpretation.

All the published/submitted studies are co-authored by (i) Laziz Bouzidi who provided: conceptualization, formal analysis, writing, reviewing and editing, methodology, software, validation, terminology, validation and visualization on the manuscripts and (ii) Suresh Narine my supervisor, who provided conceptualization, formal analysis, writing, reviewing and editing, supervision, visualization, funding acquisition, project administration, validation and methodology of the manuscripts. Study 2 (*Chapter 3*) was co-authored by Latchmi Raghunanan who also provided advice for the data analyses and feedback on the manuscript. Study 1 and 3 (*Chapters 2 and 4*) were co-authored by Kosheela Devi Poo Palam who assisted with experimental work, data curation, writing, reviewing and editing.

Acknowledgments

Firstly, I want to express my sincere thanks to my academic supervisor Dr. Suresh S. Narine for giving me this excellent opportunity to challenge myself and believe in myself. I thank him for his magnificent guidance and immense support that helped me tremendously to complete this work. Without the priceless learning and countless experiences obtained from him, I would not be able to finish this work. I thank him for being very supportive in a circumstances when I had issues with my health and family.

Thanks to my supervisory committee, Dr. Andrew Vreugdenhil, Dr. Chris Metcalfe and Dr. Stephen Hill, for their kind advice and motivations for the progress of my research. My special thanks to Dr. Laziz Bouzidi for his kind advice and suggestions for my research. His doors are always open for discussion on research and writing. He was always there, providing me with the right direction to focus on my work.

A million thanks to Linda Cardwell, Mary-Lynn Scriver and Rekha Singh for their kind support in handling the administration of my studies and, their immense support showered during my difficult times when emotional support was much needed. I would like to thank all my family and friends with a special mention to Rukhmini Ramlall, Ganda Soodoo, Kosheela Devi Poopalam, Latchmi Raghunanan, Tingkai Zhang, Marceano Narine, Aminikee Thompson, Frank Woon-A-Tai and IKD family.

I would like to thank the Grain Farmers of Ontario, Northwater Capital, Greater Peterborough Area Economic Development Corporation, Ontario Ministry of Agriculture, Food and Rural Affairs, Industry Canada, Natural Sciences and Engineering Research Council of Canada and Trent University for their financial support.

Table of Contents

ABSTRACT	II
GRAPHICAL SUMMARY OF THESIS	III
DECLARATION ON PUBLICATIONS	IV
ACKNOWLEDGMENTS	VI
TABLE OF CONTENTS	VII
LIST OF TABLES	XI
LIST OF FIGURES	XIII
LIST OF SCHEMES	XIX
LIST OF ABBREVIATION AND SYMBOLS	XXI
LIST OF APPENDICES	XXII
APPENDIX 1	XXII
1 CHAPTER 1 INTRODUCTION	1
1.1 INTRODUCTION METHODOLOGY	1
1.2 VEGETABLE OIL STRUCTURE.....	2
1.2.1 <i>Fatty Acids</i>	2
1.2.2 <i>Unsaturation Sites</i>	3
1.2.3 <i>Ester Functional Group</i>	3
1.3 DERIVATIZATION OF TAGS AND TRANSFORMATION ROUTES.....	5
1.3.1 <i>Derivatization Sites</i>	5
1.3.2 <i>Transformation Routes</i>	5
1.3.3 <i>Challenges for Producing PCMs and Lubricants from VOs</i>	6
1.3.4 <i>Advantages and Limitations of TAGs</i>	7
1.4 PCMS AND LUBRICANTS	8
1.4.1 <i>PCMs and Thermal Energy Storage</i>	8
1.4.2 <i>Lubricants and Lubrication</i>	8
1.4.3 <i>Desirable Properties for PCMs and Lubricants</i>	9
1.5 PCM AND LUBRICANT IN GLOBAL MARKETPLACE.....	11
1.5.1 <i>The Global PCM Market</i>	11
1.5.2 <i>The Global Lubricant Market</i>	13
1.6 CURRENT VO-BASED PCMS AND LUBRICANTS	14
1.6.1 <i>PCMs Derived from TAG</i>	14
1.6.2 <i>Lubricants Derived from TAG</i>	15
1.7 THERMODYNAMICS OF PHASE TRANSITIONS.....	15
1.8 USING VO STRUCTURES AND SULFUR BASED GROUPS TO PREPARE NEW PCMS AND LUBRICANTS	16
1.8.1 <i>VO structures</i>	16
1.8.2 <i>Sulfur Based Functional Groups</i>	17
1.8.3 <i>Overview of Sulfur Chemistry</i>	17
1.9 THESIS SCOPE AND THEME OBJECTIVES	20

1.9.1	<i>Project 1: Terephthalate diester PCMs</i>	21
1.9.2	<i>Project 2: Linear saturated monosulfone PCMs</i>	25
1.9.3	<i>Project 3: Sulfide and sulfonyl branched monoesters lubricants</i>	28
1.10	REFERENCES	32

2 CHAPTER 2 EXPLOITING AROMATICITY IN FATTY TEREPHTHALATE DIESTERS TO ENHANCE MELTING POINT AND PREVENT POLYMORPHISM

41

2.1	INTRODUCTION	41
2.2	MATERIALS AND METHODS	47
2.2.1	<i>Materials</i>	47
2.2.2	<i>Synthesis of the terephthalate diesters</i>	47
2.2.3	<i>Characterization methods</i>	49
2.3	RESULTS & DISCUSSION	52
2.3.1	<i>Chemical characterization</i>	52
2.3.2	<i>Thermal stability</i>	53
2.3.3	<i>Thermal transition properties</i>	55
2.4	CRYSTAL STRUCTURE ELUCIDATION	62
2.4.1	<i>Crystal structure of the terephthalate diesters</i>	62
2.4.2	<i>Molecular packing efficiency</i>	65
2.4.3	<i>Crystal phase collimation</i>	67
2.5	COMPARISON OF ESTER GROUP ROTATIONAL DEGREE OF FREEDOM	70
2.6	CONCLUSIONS	72
2.7	REFERENCES	74

3 CHAPTER 3 PHASE BEHAVIOR OF MONOSULFONES: USE OF HIGH POLARITY SULFONYL GROUPS TO IMPROVE THE THERMAL PROPERTIES OF LIPID-BASED MATERIALS FOR PCM APPLICATIONS.....

80

3.1	INTRODUCTION	80
3.2	MATERIALS & METHODS	84
3.2.1	<i>Materials</i>	84
3.2.2	<i>Synthesis of the sulfones</i>	84
3.2.3	<i>Characterization methods</i>	85
3.3	RESULTS	87
3.3.1	<i>Chemical characterization and confirmation of the synthesized compounds</i>	87
3.3.2	<i>Thermal stability</i>	89
3.3.3	<i>Phase change properties of the sulfones</i>	90
3.3.4	<i>Crystal structure elucidation</i>	93
3.4	DISCUSSION	102
3.4.1	<i>Thermal stability</i>	102
3.4.2	<i>Phase change temperature</i>	104
3.4.3	<i>Phase change enthalpy</i>	106
3.5	CONCLUSION	109
3.6	REFERENCES	110

4 CHAPTER 4 EFFECT OF PENDANT SULFIDE AND SULFONYL GROUPS ON THE THERMAL, FLOW AND ANTIOXIDATIVE PROPERTIES OF LIPID BASED ALIPHATIC MONOESTERS.....

116

4.1	INTRODUCTION	116
4.2	MATERIALS & METHODS	119
4.2.1	<i>Materials</i>	119
4.2.2	<i>Preparation of Oleyl Oleate Monoesters</i>	120
4.2.3	<i>Preparation of Sulfide-Branched Oleyl Oleate Monoesters (A2-S-n)</i>	120
4.2.4	<i>Preparation of Sulfonyl-Branched Oleyl Oleate Monoesters (A2-SO₂-n)</i> ..	121
4.3	CHARACTERIZATION METHODS	121
4.3.1	<i>Proton Nuclear Magnetic Resonance (¹H-NMR)</i>	121
4.3.2	<i>Electrospray Ionization - Mass Spectrometry (ESI-MS)</i>	122
4.3.3	<i>Viscosity and Flow Behavior</i>	122
4.3.4	<i>Differential Scanning Calorimetry (DSC)</i>	123
4.3.5	<i>Thermogravimetric Analysis (TGA)</i>	124
4.3.6	<i>Polarized Light Microscopy (PLM)</i>	125
4.4	RESULTS AND DISCUSSION.....	125
4.4.1	<i>Synthesis and Structural Characterization</i>	125
4.4.2	<i>Thermal Stability</i>	127
4.4.3	<i>Thermal Transition Behavior</i>	128
4.4.4	<i>PLM Observations</i>	132
4.4.5	<i>Flow Behavior and Viscosity</i>	136
4.4.6	<i>Oxidative Stability</i>	141
4.4.7	<i>Comparison Of Oleyl Oleate, Sulfide and Sulfonyl Branched Oleyl Oleate Monoesters with Mineral Oils and Biobased Lubricants.</i>	145
4.5	CONCLUSION.....	148
4.6	REFERENCES	149
5	CONCLUSIONS	158
5.1	CONCLUSION FOR THE PCMS STUDY: MONOSULFONES AND TEREPHTHALATE DIESTERS	158
5.1.1	<i>Objectives and Hypotheses Achieved</i>	159
5.2	CONCLUSION FOR SULFIDE AND SULFONYL BRANCHED OLEYL OLEATE MONOESTERS LUBRICANTS	162
5.2.1	<i>Objectives and Hypotheses Achieved</i>	162
5.3	CHALLENGES AND FUTURE PERSPECTIVES	164
5.3.1	<i>Challenges and Perspectives with the VO Feedstock</i>	164
5.3.2	<i>Challenges and Perspectives for VO-based PCMs and Lubricants</i>	166
5.4	REFERENCES	168
6	APPENDIX.....	170
6.1	FUNDAMENTAL STRUCTURE-FUNCTION RELATIONSHIPS IN VEGETABLE OIL BASED PHASE CHANGE MATERIALS: A CRITICAL REVIEW.....	170
6.1.1	<i>Abstract</i>	170
6.1.2	<i>Chemical nomenclature and list of abbreviations</i>	172
6.1.3	<i>Introduction</i>	173
6.1.4	<i>Methodology</i>	177
6.1.5	<i>Derivatization of TAGs to produce PCMs</i>	178
6.1.6	<i>Gibb's free energy of the phase change</i>	179
6.1.7	<i>Thermal phase change behaviour</i>	182
6.1.8	<i>Effect of Symmetry – Case of the Monoesters PCMs</i>	189

6.1.9	<i>Diesters and Diamides PCMs</i>	193
6.1.10	<i>Sugar Esters PCMs – Effect of Branching and Isomerism on TES</i>	196
6.1.11	<i>Entropy of fusion (ΔS_m) of linear saturated functional PCMs</i>	199
6.1.12	<i>Thermal Stability</i>	204
6.1.13	<i>Thermal Conductivity</i>	208
6.1.14	<i>Applications of VO-based PCMs</i>	211
6.1.15	<i>Challenges and Future Trends</i>	213
6.1.16	<i>Conclusion</i>	216
6.1.17	<i>Acknowledgment</i>	219
6.1.18	<i>References</i>	1

List of Tables

Table 1-1. Parameters used to characterize PCMs and lubricants.	10
Table 1-2. Effect of VO structures on key PCM and lubricant properties. Adv.: advantageous and Dis.: disadvantageous.....	17
Table 1-3. Geometry, hybridization and bond angle of sulfide, sulfoxide and sulfonyl groups.....	18
Table 2-1. DSC crystallization and melting results of the terephthalates diesters. Average standard deviation is $\pm 0.5^{\circ}\text{C}$ for the temperatures and $\pm 5\text{J/g}$ for the enthalpies.	56
Table 2-2. Supercooling ($T_{on}^m - T_{on}^c$), span of crystallization ($\Delta T^c = T_{on}^c - T_{off}^c$) and span of melting ($\Delta T^m = T_{on}^m - T_{off}^m$) of the terephthalate diesters and other vegetable oil based PCMs.....	57
Table 2-3. Theoretical Staking Length (TSL)* and Experimental Stacking Length (ESL)* of terephthalate diesters.....	63
Table 2-4. Crystal phase composition and phase change data of 18-TA-18 and 18-6-18 diacid diester and 18-6-18 diol diester with comparable molecular structure. Average standard deviation is $\pm 0.5^{\circ}\text{C}$ for the temperature values and $\pm 5\text{J/g}$ for the enthalpies....	68
Table 2-5. $^1\text{H-NMR}$ chemical shifts and FT-IR wavenumbers of 18-TA-18, 18-6-18 diacid and diol diesters.....	70
Table 3-1. Chemical name, $^1\text{H NMR}$ shifts, and ESI-MS results of the sulfones.....	88
Table 3-2. Crystallization and melting results of the sulfones under the 20.0, 5.0 and 0.1 C/min cooling protocols. Standard deviation is $> 0.3^{\circ}\text{C}$ for the temperatures and $> 8\text{ J/g}$ for the enthalpies.....	90

Table 3-3. Phase composition of the sulfones and melting temperatures at the various cooling protocols.....	99
Table 4-1. DSC crystallization and melting results for oleyl oleate, sulfide and sulfonyl branched oleyl oleate monoesters. Average standard deviation is ± 0.5 °C for the temperatures and ± 5 J/g for the enthalpies. The molar enthalpy (kJ/mol) is also reported in bracket.....	129
Table 4-2. Parameter A and b of the sigmoidal function for A-S-3 and A2-SO2-3.	135
Table 4-3. Oxidation induction time (OIT) of various sulfide-based and commercial antioxidants used in lubrication formulation from largest to smallest.....	144
Table 4-4. Comparison of flow properties of select commercial lubricants and biolubricants of similar carbon chain length.....	146
Table 0-1. Fit parameters for the exponential rise to a maximum function for the series of linear PCMs. (<i>Equation 3</i>).....	184
Table 0-2. Estimated dipole moments (Debye, D) for main functional groups and comparison of T_m for PCMs with three representative fixed carbon chain (C_{20} , C_{28} and C_{38}).....	186
Table 0-3. Parameters of the fit to an exponential rise to a maximum function (<i>Equation 3</i>) of T_m of asymmetric monoesters versus total carbons curves (Figure 0-3a-b).	191

List of Figures

Figure 1-1. Structure of the ester group. red: carbon, blue: hydrogen, yellow: oxygen. ...	3
Figure 1-2. Classification of (a) PCMs and (b) Lubricants. The classes highlighted in yellow is the area of focus in this thesis.	9
Figure 1-3. Global PCM market share by (a) end-user application and (b) chemical composition.....	12
Figure 1-4. Global lubricant market share by (a) end-user industry and (b) by base oil type.....	13
Figure 1-5. (a) PCMs and (b) lubricants molecular architectures derived using TAG....	14
Figure 1-6. Dipole moments in Debye (D) of different functional groups with R representing the aliphatic saturated hydrocarbon chain and sulfonyl-sulfonyl interaction of sulfonyl groups.	26
Figure 2-1. (a) TGA and DTG curves of 18-TA-18 and (b) versus molecular mass of the terephthalate diesters (▲), diol diesters (●) and diacid diesters (■). Dashed lines are fits to exponential rise to a maximum function ($f = y_0 + a(1 - \exp(-x/x_0))$); $R^2 \geq 0.9613$) and serve as guides for the eye. Errors bars are standard deviations from at least three replicates.	53
Figure 2-2. (a) Cooling and (b) heating traces (both at 3°C/min) of the terephthalate diesters.	56
Figure 2-3. Melting (a) Temperature (T_m) and (b) Enthalpy (ΔH_m) versus fatty chain length (n) of the n-TA-n terephthalate diesters (▲), n-2-n (●), n-4-n (■), n-6-n (◆) saturated aliphatic diol diesters, and 18-6-18 diacid diester (◆). (c) ΔT_m : difference in T_m	

between n-TA-n and n-6-n diol diesters. Errors bars are standard deviation of three replicates.	59
Figure 2-4. (a) SAXD and (b) WAXD spectra of the terephthalate diesters (n-TA-n). (c) Cross-sectional packing of the 18-TA-18.	63
Figure 2-5. (a) SAXD and (b) WAXD patterns of 18-TA-18, 18-6-18 diacid diester and 18-6-18 diol diester	66
Figure 2-6. Cross-sectional packing of the (a) 18-6-18 diol diester in triclinic subcell and (b) 18-6-18 diacid diester in orthorhombic subcell.....	67
Figure 2-7. (a) cooling and (b) heating curves (both at 3 °C/min) of 18-TA-18, 18-6-18 diacid diester and 18-6-18 diol diester.....	68
Figure 3-1. (a) FTIR spectra of 12-S-12 and 12-SO ₂ -12, (i) C-S stretch, (ii) O=S=O sym. stretch, (iii) O=S=O asym stretch, (iv) C-H bending and (v) sp ³ C-H stretching; (b) 1H NMR spectrum of 12-SO ₂ -12.....	88
Figure 3-2. (a) TGA and DTG weight loss curves of 12-SO ₂ -12, (b) 5 % and weight temperatures of the sulfones. Dashed lines in (b) are guides for the eye.	89
Figure 3-3. (a) crystallization and (b) melting thermograms of the sulfones cooled at 0.1 (red), 5 (black) and 20 °C/min (blue). (c) Zoom into the low temperature regions of the crystallization thermograms of the sulfones cooled at 5 °C/min.	91
Figure 3-4. Variation of the characteristics of the main crystallization and melting peaks; (a) Temperature (T_{cl} , T_{ml}), (b) enthalpy (ΔH_{cl} , ΔH_{ml}). Dashed lines are guides for the eye.	93
Figure 3-5. SAXD spectra of the sulfones crystals with labelled miller indices (00l). (a) 10-SO ₂ -10, (b) 12-SO ₂ -12, and (c) 18-SO ₂ -18. Cooling rates are labelled as 20, 5, 0.1	

and, 0.1 °C/min after 4 months. (d) shows the effect of cooling rates on the sulfones ESL.

..... 95

Figure 3-6. XRD long-range c-axis stacking of (a) 10-SO₂-10, (b) 12-SO₂-12, and 18-SO₂-18. The sulfonyl group (sulfur (yellow) and oxygens (blue)) is shown at the center of the molecule..... 97

Figure 3-7. WAXD patterns of (a) 10-SO₂-10, (b) 12-SO₂-12, and (c) 18-SO₂-18. The d-spacing values are shown on top of the peaks (vertical lines are guides for the eye). .. 98

Figure 3-8. Cross-sectional packing of the 18-SO₂-18 -polymorph in the triclinic subcell. The shaded region represents the 010 planes containing the sulfonyl groups..... 100

Figure 3-9. (a) Onset of weight loss (T_{ON}) as determined at 5 % weight loss and (b) maximum derivative weight loss temperature (T_D) of the sulfones compared with other PCMs mined from the literature. 102

Figure 3-10. T_{m1} of the present sulfones and selected organic compounds mined from the literature. Symbols: sulfones (▲); monoesters (●); monoamides (■); alkanes (◆); carboxylic acids (⊖); ethers (★); alcohols (⊕); diamides (×); and diesters (×) .. 104

Figure 3-11. Enthalpy of melting (ΔH_{m1}) of the sulfones with organic PCMs: sulfones (▲); monoesters (●); alkanes (■); ethers (◆); alcohols (⊖); diamides (★); diesters (⊕); and monoamides (×). 107

Figure 4-1. (a) TGA and DTG curves of A2-S-3 (red dashed lines), A2-SO₂-3 (black dashed lines) and oleyl oleate (blue dashed lines) (b) 10 % w/w mass loss versus molecular mass of A2-S-*n* (▲), A2-SO₂-*n* (●), oleyl oleate (■) and T_D versus molecular mass of A2-S-*n* (▲), A2-SO₂-*n* (●) and oleyl oleate (■). 127

Figure 4-2. (a) Cooling and (b) Heating thermograms (both at 5 °C/min) of oleyl oleate, A2-S-3 and A2-SO2-3. P_1 , P_2 : main peaks of crystallization or melting, P_R : recrystallization peak, T_g : glass transition temperature. 129

Figure 4-3. (a) Correlation of data from DSC cooling thermograms of A2-S-3 and A2-SO2-3 with PLM observations at selected temperatures, (b) zoom into a crystallite hexagonal face and representation of associated α -polymorph, and (c) progression in crystallite size as determined by area versus temperature (dashed lines are fits to a sigmoidal function, *Equation 3*). 134

Figure 4-4. Shear stress - shear rate curves obtained at 40 °C for A2-S-3 and A2-SO2-3. Solid lines are fits to the Herschel-Bulkley model (*Equation 1*). 137

Figure 4-5. Viscosity versus temperature curves of (a) sulfide (filled) and sulfonyl (unfilled) branched oleyl oleate monoesters. (b) viscosity difference between the sulfonyl and sulfide branched oleyl oleate monoesters (Δv) versus temperature for $n=2 - 6$ 138

Figure 4-6. (a) Viscosity at 40°C of the sulfide and sulfonyl branched oleyl oleate monoesters versus branch chain length (n). *Dashed line are guides for the eyes.* (b) Difference in viscosity between sulfonyl branch and sulfide functional group (Δv) taken at 25 °C, 40 °C and 90 °C. Error bars are standard deviation of three replicates. 139

Figure 4-7. Parameters of the fit of sulfide and sulfonyl branched oleyl oleate monoesters to the GvVE versus branch chain length n (a) parameter A , (b) coefficient m 140

Figure 4-8. DSC heating (10°C/min) thermograms at of oleyl oleate (A), ester branched oleyl oleate (A4-C-3), sulfonyl branched oleyl oleate (A2-SO2-3) and sulfide branched oleyl oleate (A2-S-3). Onset temperatures of oxidation (T_{on}^{ox}) are indicated by arrows.

Right panel: molecular structures of above compounds with protons prone to oxidation highlighted in blue and yellow boxes.	142
Figure 5-1. T_{ON} versus molecular mass for terephthalate diesters (▲) and monosulfones (●).	159
Figure 5-2. T_m versus fatty chain length (n) of terephthalate diesters and monosulfones.	160
Figure 0-1. (a) T_m and (b) ΔH_m of linear saturated PCMs with one functional group versus total carbons atoms (n), <i>Dashed lines are guides for the eyes</i>	183
Figure 0-2. Relationship between dipole moment and T_m for PCMs with three fixed carbon chain (C ₂₀ , C ₂₈ and C ₃₈) and polar functional group capable of forming dipole-dipole intermolecular interaction between each other (* in Table 0-1). <i>Dashed lines are guide for the eyes only</i>	187
Figure 0-3. (a) T_m versus fatty acid chain length of monoesters with (a) C ₁ -C ₄ alcohol, (b) C ₅ -C ₁₈ alcohol, (c) T_m of monoesters with fixed fatty acid chain (C ₁₂₋₁₈) versus alcohol chain length and (d) ΔH_m of monoesters versus fatty acid chain length. <i>Dashed lines are guide for the eyes</i>	190
Figure 0-4. (a) T_m and (b) ΔH_m of the symmetrical diesters and diamides versus spacer chain length (R'') (symbols Δ & \blacktriangle : R & R' = 11; \circ & \bullet : R & R' = 13; \square & \blacksquare : R & R' = 15; \diamond & \blacklozenge : R & R' = 17; unfilled: diesters and filled: diamides). Error bars represent the standard deviations of three runs. <i>Dashed lines are guides for the eye</i>	193
Figure 0-5. (a) T_m and (b) ΔH_m of the sugar esters versus total carbons (n). Symbols: (▲) glycerol, (●) erythritol, (■) xylitol, (◆) galactitol and (●) mannitol. <i>Dashed lines are guides for the eye</i>	197

Figure 0-6. Molar entropy of melting (ΔS_m) versus total carbons: (a) linear saturated monofunctional PCMs, (b) monoesters; diesters; and diamides (spacer chain (m)). *Dashed lines are fits of the data to straight lines.* 200

Figure 0-7. Rate of change in ΔS_m of the individual categories of PCM. *Dashed line is a guide for the eye.*..... 201

Figure 0-8. Correlation between Molar entropy of melting versus molar enthalpy of melting of the PCMs. *Dashed lines are fits of the data to straight lines.*..... 203

Figure 0-9. Onset of degradation (T_{ON}) of (a) monofunctional and difunctional PCMs and (b) branched multifunctional sugar ester PCMs. *Dashed lines are guides for the eye.* 205

Figure 0-10. Thermal conductivity of PCMs mined from the literature measured at room temperature versus (a) total number of carbons (n); and (b) total number of hydrogen bonds per molecule. *Dashed lines are guides for the eyes.* 210

List of Schemes

Scheme 1-1. Triacylglycerol (TAG) molecular structure. Reactive sites are indicated surrounded by dashed curves.	2
Scheme 1-2. Hydrolysis of ester group under (i) acid, and (ii) basic conditions.	4
Scheme 1-3. Thermal degradation mechanism of ester group via the cis-elimination of β -hydrogen.	4
Scheme 1-4. Structure of the n-TA-n terephthalate diesters investigated (n = 12, 14, 16, & 18).	21
Scheme 1-5. Chemical structures of (a) monoesters (R-COO-R') where R and R' = fatty acid and fatty alcohol chain moieties, respectively, (b-c) Diol and Diacid diesters (n-m-n) where n= fatty chain length, and m= inter-ester chain. Curved and double arrows indicate rotation at the alkoxy bonds and separation distance between the ester groups, respectively.	22
Scheme 1-6. Structure of the n-SO ₂ -n monosulfones investigated (n = 10, 12, & 18)....	25
Scheme 1-7. Structures of the four sulfide (A ₂ -S-n) and four sulfonyl-branch oleyl oleate monoesters (A ₂ -SO ₂ -n) investigated in this work (n= 2, 3, 4 and 6).	29
Scheme 2-1. Chemical structures of (a) monoesters (R-COO-R') where R and R' = fatty acid and fatty alcohol chain moieties, respectively, (b-c) Diol and Diacid diesters (n-m-n) where n= fatty chain length, and m= inter-ester chain. Curved and double arrows show rotation at the alkoxy bonds and separation distance between the ester groups, respectively.	43
Scheme 2-2. Structure of the n-TA-n terephthalate diesters.	46

Scheme 2-3. ¹ H-NMR chemical shifts and FT-IR wavenumber associated with the ester group for 18-TA-18, 18-6-18 diacid and 18-6-18 diol diesters.	71
Scheme 3-1. Structure of the lipid-based sulfones (n-SO ₂ -n) synthesized in this work. (a) 10-SO ₂ -10, (b) 12-SO ₂ -12 and (c) 18-SO ₂ -18.	83
Scheme 4-1. (a) Oleyl oleate (A)-curved arrow denotes the rotation of ester group, (b) sulfide (A ₂ -S-n) and (c) sulfonyl (A ₂ -SO ₂ -n) doubly branched monoesters. S and SO ₂ : sulfide and sulfonyl functional groups, respectively and n:length of the branched carbon chain.	118
Scheme 4-2. Synthetic route to prepare sulfide and sulfonyl branched oleyl oleate monoesters from oleyl oleate.	126
Scheme 0-1. Saturated organic phase change materials derived from triacylglycerols (TAGs). (R, R' and R'' denotes the number of carbon atoms in the aliphatic chains) ...	176
Scheme 0-2. Schematic representation of the two-dimensional projection for the packing of (a) even numbered and (b) odd numbered alkanes.	185
Scheme 0-3. Wedge-and-dash projection molecular structures of the sugar esters. The solid and dash wedges represent the hydrocarbon chains that are coming out and going into the plane, respectively. R = 11, 13, 15 and 17 for molecules in the sugar alcohol series.	196

List of Abbreviation and Symbols

List of abbreviations	
TES	Thermal Energy Storage
LHTES	Latent Heat Thermal Energy Storage
POs	Plant Oils
VOs	Vegetable Oils
TAGs	Triacylglycerols
PCMs	Phase Change Materials
NMR	Nuclear Magnetic Resonance
DSC	Differential Scanning calorimetry
XRD	Xray Diffraction
MW	Molecular Weight
HVAC	Heating, Ventilation, And Air Conditioning
T_m	Melting Temperature
T_c	Crystallization Temperature
ΔH_m	Melting Enthalpy
ΔS_m	Melting Entropy
K	Thermal Conductivity
T_{ON}	Onset Temperature
n_s	Melting Point Singularity
R^2	Coefficient of Correlation
n_0	Characteristic Carbon Number
SI	Supporting Information
ΔG	Gibbs Free Energy
$\alpha_{\Delta S}$	Rate Of Change Of ΔS_m
β	Beta Polymorph
β'	Beta Prime Polymorph
D	Debye
M	Spacer Chain Length
R	Length of Carbon Chain
C–O	Alkoxy Moiety
–COO–	Ester Group
–CONH–	Amide Group
–COOH	Carboxylic Group
–OH	Hydroxyl Group
–SO ₂ –	Sulfonyl Group
–CH ₂ –	Methylene Unit

List of Apendices

Appendix 1

6.1 Fundamental Structure-Function Relationships in Vegetable Oil Based Phase Change Materials: A Critical Review: Manuscript published in *Journal of Energy Storage* (<https://doi.org/10.1016/j.est.2022.104355>)

1 Chapter 1 Introduction

1.1 Introduction Methodology

Chapter 1 introduces vegetable oils (VOs) as a potential feedstock alternative to petroleum. The structures of VOs are detailed in *Section 1.2*. The chemical routes available to derivatize and transform VOs into functional materials are presented in *Section 1.3*. A brief overview of PCMs and lubricants is presented in *Section 1.4*. The commercial importance of PCMs and lubricants is described in *Section 1.5*. The structures of the major classes of PCMs and lubricants that were synthesized from VO derivatives are presented in *Section 1.6*. The thermodynamics concepts used to explain the thermal behavior and properties of the new VO-based compounds from a molecular structure perspective are presented in *Section 1.7*. The VO-based structures and sulfur based functional groups which are used to prepare the new compounds are discussed in *Section 1.8*.

A critical review of the literature on VO-based PCMs establishing predictive structure-function relationships was completed. This review is published in *Journal of Energy Storage* (<https://doi.org/10.1016/j.est.2022.104355>) and presented in **Appendix 1**.

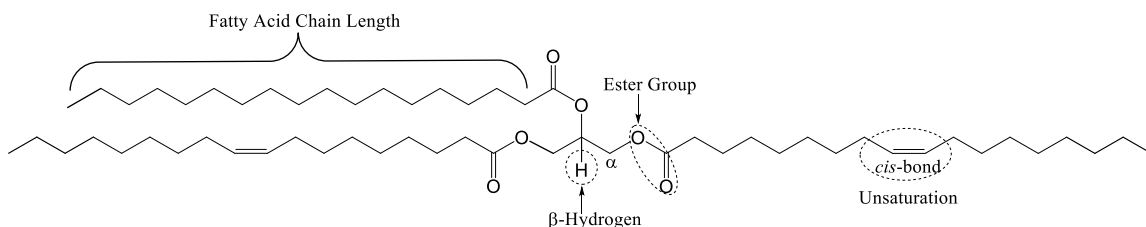
Chapter 2 present the study of terephthalate diesters. The insertion of the benzene group between linear saturated fatty chains was intended to reduce molecular flexibility and mitigate polymorphism. **Chapter 3** present the study of monosulfones. The high polarity sulfonyl group was inserted between linear saturated fatty chains to increase the intermolecular forces.

Chapter 4 present the study of sulfide- and sulfonyl branched oleyl oleate monoesters. The branching of oleyl oleate with sulfide and sulfonyl pendant groups was proposed to achieve low pour points, predictable viscosity profiles and an increase in oxidative stability

1.2 Vegetable Oil Structure

Most VO's such as coconut, corn, cottonseed, canola, olive, peanut, safflower, sesame, soybean, and sunflower oil are naturally composed of 88-96% triacylglycerols (TAGs) with some minor amounts of diacylglycerols (DAGs, usually < 5%) [1, 2]. Other minor components are tocopherols and tocotrienols and phytosterols ($\leq 1\%$) [3]. TAG is a triester derived from glycerol and three fatty acids. The structure of TAG is shown in

Scheme 1-1.



Scheme 1-1. Triacylglycerol (TAG) molecular structure. Reactive sites are indicated surrounded by dashed curves.

1.2.1 Fatty Acids

Fatty acids in VO's naturally range from 8 to 24 carbon atoms and comprise 0 to 7 carbon double bonds, depending on the plant type and growth conditions [4]. The most common

naturally occurring linear saturated fatty acids are capric (C10), lauric (C12), myristic (C14), palmitic (C16) and stearic acids (C18); whereas the common linear unsaturated fatty acids are oleic (C18:1), linoleic(C18:2), linolenic acid (C18:3) and arachidonic acids (C20:4) [5].

1.2.2 Unsaturation Sites

The C=C double bonds can exist in a *cis*- or *trans*-configuration. The *cis*-configuration is kinked whereas the *trans*-configuration is straight [6]. The unsaturation sites are oxidatively unstable because the protons allylic to each C=C bond can be readily abstracted to generate radicals which propagate auto-oxidation [7].

1.2.3 Ester Functional Group

Each fatty acid is attached to the TAG glycerol backbone by the ester group (**Scheme 1-1**). The ester group is composed of a carbonyl (C=O) group and an alkoxy (C–O–C) group attached to the carbonyl carbon (**Figure 1-1**). The ester group is trigonal planar with a bond angle of 120° because of the carbonyl carbon sp² hybridized orbitals.

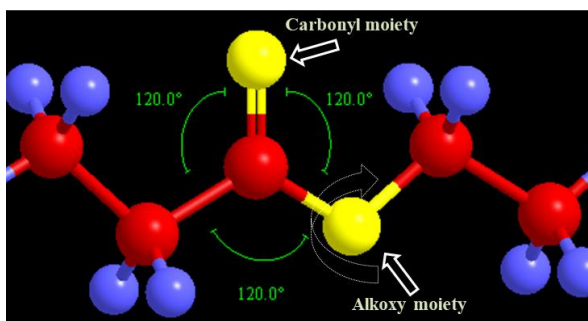


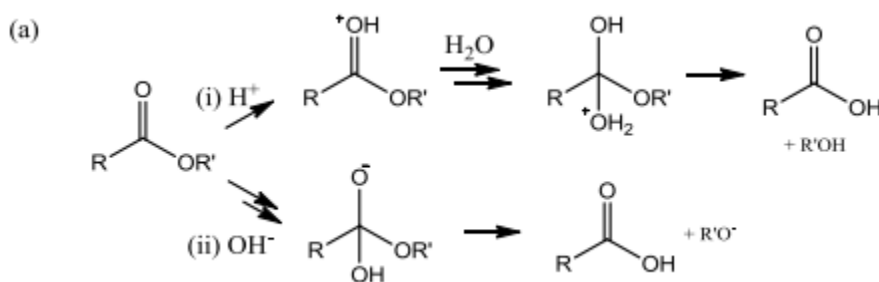
Figure 1-1. Structure of the ester group. red: carbon, blue: hydrogen, yellow: oxygen.

1.2.3.1 Rotatability and Polarity

The alkoxy moiety on the ester group has a low rotational energy barrier which makes the bond easily rotatable thus providing great flexibility to the TAG [8, 9]. Additionally, ester groups have low polarity and cannot form strong intermolecular interactions [10].

1.2.3.2 Hydrolytic Susceptibility

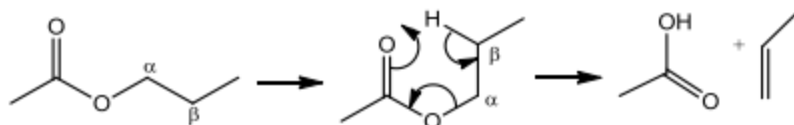
TAG ester groups are hydrolytically unstable and can be broken under acidic or basic conditions to give free acids (**Scheme 1-2**). The acids products make ester hydrolysis autocatalytic adding to the limitations on TAG durability in applications [11].



Scheme 1-2. Hydrolysis of ester group under (i) acid, and (ii) basic conditions.

1.2.3.3 β -hydrogen Elimination and γ -hydrogen Transfer

TAGs can be thermally degraded at elevated temperatures via β -hydrogen elimination (shown in **Scheme 1-3**) and also by γ -hydrogen transfer [12, 13].



Scheme 1-3. Thermal degradation mechanism of ester group via the cis-elimination of β -hydrogen.

The β -hydrogen is acidic and cleave as a hydrogen ion. The acidity of β -hydrogen (pKa \sim 10) is significantly lower compared to hydrogens on the ester group (pKa \sim 20) of linear esters and those attached to the fatty chains (pKa \sim 50) [14]. The β -hydrogen is particularly undesirable because it degrades the TAG molecule when abstracted.

1.3 Derivatization of TAGs and Transformation Routes

1.3.1 Derivatization Sites

The derivatization sites on a TAG (**Scheme 1-1**) are ester functional groups and C=C double bonds. Ester functional groups are susceptible to nucleophilic substitution reaction with a variety of nucleophiles at the electrophilic carbon because its alkoxy group is a good leaving group. The C=C double bond can undergo addition reactions and oxidative cleavage reactions.

1.3.2 Transformation Routes

TAGs can be hydrolyzed to obtain linear saturated and unsaturated fatty acids [11, 15]. The carboxylic group can be chemically modified to obtain different functional groups. For instance, fatty alcohols are produced by reducing the carboxylic group using a reducing agent [16]. A variety of linear saturated and unsaturated fatty esters can be prepared through esterification reaction of fatty acids and fatty alcohols of varying chain lengths and combinations [17]. Fatty amines can be prepared from fatty acids via nitrile process [15]. A variety of linear saturated and unsaturated fatty amides can be prepared through amidation reaction of fatty acids and fatty amines of varying chain lengths and combinations. Fatty carbonates are synthesized from carbonate interchange reaction using

fatty alcohol and dialkyl carbonate with n-dibutyltin catalyst [18]. The standard route for the preparation of fatty ethers is through Williamson ether synthesis via the reaction of fatty alcohol with fatty halide under a base catalyst [19]. Thioetherification of a fatty halide with a fatty thiol produces a fatty sulfide which is then further oxidized with hydrogen peroxide to fatty sulfones [20, 21].

Pendant groups can be introduced at the C=C double bond sites via synthetic routes such as epoxidation/ring-opening [22-25], etherification [26] and thioetherification [27]. Moreover, the C=C double bond can be hydrogenated to alkanes, converted to ketones, aldehydes and carboxylic functional groups via ozonolysis and converted to vicinal diols via dihydroxylation. Halide and hydroxyl groups can be introduced via halohydrin reaction and hydroxyl group can be introduced using hydroboration reaction and ether group via oxymercuration reaction [14].

1.3.3 Challenges for Producing PCMs and Lubricants from VOs

Renewable feedstocks are investigated as alternative to petroleum for fuel and materials. The transition involves important actors in the value chain including milling, derivatization and transformation facilities, manufacturing industry, regulators and end users [28]. These come with several barriers and challenges ranging from ethical concerns with the use of edible crops to economic viability and consumer acceptance and concerns over the complexity, economic viability and environmental impact of the synthetic routes used [29, 30]. One also understands that the development may take several years to reach the market.

Prior to using VOs as feedstock, physical and chemical refining is necessary to remove undesirable molecules such as free fatty acids, phospholipids, waxes, aldehydes and

ketones to obtain pure TAGs. Multiple synthetic routes are needed for converting TAGs into crude PCMs and lubricants [31, 32]. These synthetic routes should preferably be environmentally friendly. The resulting crude PCMs and lubricants may need to be purified to ensure optimal performance. The refining, multiple synthesis steps, characterization and analysis can increase the cost of production of the VO-based PCMs and lubricants. It is therefore imperative to develop economical methods and tests [33].

Consumer acceptance of VO-based PCMs and lubricants is a major concern related to performance and cost. VO-based PCMs are approximately two times more expensive than petroleum-based PCMs and lubricants are up to three times more expensive than mineral oil-based lubricants [34].

1.3.4 Advantages and Limitations of TAGs

TAGs in their unmodified state have advantageous as well as disadvantageous attributes for use in PCMs or lubricants formulations. The C=C double bonds and β -hydrogens of TAGs are undesirable in both PCMs and lubricants because of poor thermo-oxidative stability and eventual changes to the chemical and physical integrity that they impart [35]. TAGs are subject to large supercooling effects, demonstrate polymorphism and cause broad and incongruent phase transitions which are detrimental to PCM function [36]. Although having undisputable lubrication advantages over mineral oil such as low volatility, better lubricity, higher viscosity index and flash points, TAGs have inherent poor cold-flow performance, limited viscosity range and unpleasant smell [37].

1.4 PCMs and Lubricants

1.4.1 PCMs and Thermal Energy Storage

There are three common ways to store thermal energy: (i) conversion to thermochemical energy, (ii) sensible and (iii) latent heat [38]. These are achieved using dedicated materials. In thermochemical energy storage, thermal energy is stored and released by reversible chemical reactions [39]. In sensible heat storage, the energy is used to change the temperature of a storage medium (usually solid or liquid) without phase change [40]. Latent heat thermal energy storage (LHTES) involves the heat absorbed or released by a material during a phase transition and is achieved by PCMs [41].

1.4.2 Lubricants and Lubrication

Lubricants are materials whose primary function is to prevent contact between two solid surfaces, thereby minimizing friction and wear, and thus, increasing the materials lifetime and efficiency of the work performed [42]. A typical lubricant is formulated with a base-stock component (70-90%) and various additives [43]. Lubricants may contain 2 to 5% or fewer additives [44]. The role of the additive is generally to improve one or more of the key performance characteristics of the base oil, or to add market value by extending its functionalities, for example, by facilitating corrosion inhibition properties, or improving solvency and antioxidant properties [45, 46].

Figure 1-2 presents the classification of PCMs [47] and lubricants [48] as established in the literature.

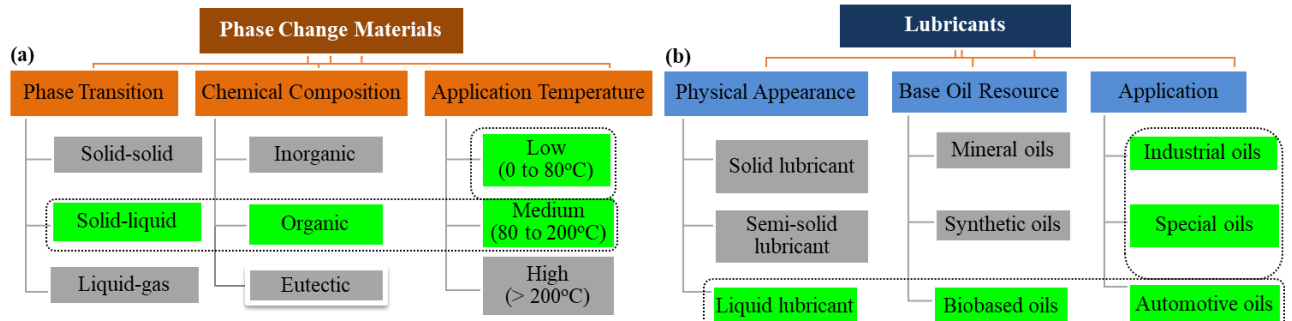


Figure 1-2. Classification of (a) PCMs and (b) Lubricants. The classes highlighted in green is the area of focus in this thesis.

As outlined in **Figure 1-2**, PCMs can be classified by (i) phase transition type which can either be solid-solid, solid-liquid or liquid-gas, (ii) chemical composition which can be inorganic, organic and eutectic and (iii) application temperatures which are categorized as low, medium and high. Likewise, lubricants can be categorized by (i) physical appearance which are solid, semi-solid and liquid (ii) base oil resources which are categorized as mineral oil, synthetic oil and biobased oil and (iii) application which are categorized as industrial, special and automotive.

1.4.3 Desirable Properties for PCMs and Lubricants

PCMs and lubricants are characterized by the following parameters shown in **Table 1-1**.

Table 1-1. Parameters used to characterize PCMs and lubricants.

PCM		Lubricants	
Parameter	Relevance	Parameter	Relevance
Transition temperature	Should be fixed to store and release heat at a specific temperature	Pour point (PP)	Should have low pour points to maintain its flow characteristics at low temperature
Transition Full width at half maximum (FWHM)	Peak should be narrow and sharp to rapidly absorb/release heat	Cloud point (CP)	Should have low cloud point to prevent clogging of filters at low temperatures
Transition congruency	Should have same thermogram after numerous thermal cycling	Transition Full width at half maximum (FWHM)	Peak should be broad to demonstrate slow crystallization process.
Enthalpy	Should have high enthalpy to store more heat per given mass	Enthalpy	Peak should have low enthalpy to store less heat and correlate with low crystallization
Crystal structure	Should pack in the highest stability phase	Viscosity	Should have correct viscosity to form stable oil film at specified temperature and speed of operation.
Polymorphism	Should display minimal to no polymorphism to store all heat in one crystal form	Flow type	Should have the desirable flow behavior for specific application
Thermal stability	Should have high thermal stability to operate at elevated temperatures with minimal or no degradation	Thermal stability	Should have high thermal stability to operate at elevated temperatures with minimal or no degradation
Thermal conductivity	Should have high thermal conductivity to increase the rate heat flow into the material	Oxidative stability	Should have high oxidative stability to perform in the presence of oxygen and air under high temperature environment.
Volume change	Should have small volume change to avoid damaging/	Viscosity index (VI)	Should have high VI to reduce change in viscosity with

PCM		Lubricants	
Parameter	Relevance	Parameter	Relevance
	exploding containers		temperature
Supercooling	Should have fast self-nucleation to display minimal to no supercooling	Corrosion	Should have anti-corrosive properties to protect its metallic containment systems from corroding
Phase segregation	Should have minimal to no phase segregation after numerous thermal cycling	Tribofilm	Should have good adhesion to metal surface to form a thin tribofilm.
Flashpoint	Should have high flash points to reduce the concentration of vapor that would spontaneously ignite with air	Flashpoint	Should have high flash points to reduce the concentration of vapor that would spontaneously ignite with air
Fire Point	Should have high fire points to reduce the concentration of vapor that would burn continuously with air	Fire Point	Should have high fire points to reduce the concentration of vapor that would burn continuously with air
Biodegradability	Should have high biodegradability to be broken down by the action of microorganisms in presence of oxygen, nitrogen and minerals	Biodegradability	Should have high biodegradability to be broken down by the action of microorganisms in presence of oxygen, nitrogen and minerals

1.5 PCM and Lubricant in Global Marketplace

1.5.1 The Global PCM Market

The global PCM market size in 2020 was worth US\$1.2 billion and is projected to reach US\$3.1 billion by 2026 at a compound annual growth rate of 17% [49]. **Figure 1-3a** and **b** show the global PCM market share by end-user application and chemical composition type, respectively. As shown in **Figure 1-3a**, 65% of the PCM volume is consumed in building/construction and HVAC applications [50]. The majority of these PCM are organic (65% mainly paraffin and polyethylene glycols) and inorganic PCMs (30%) [51].

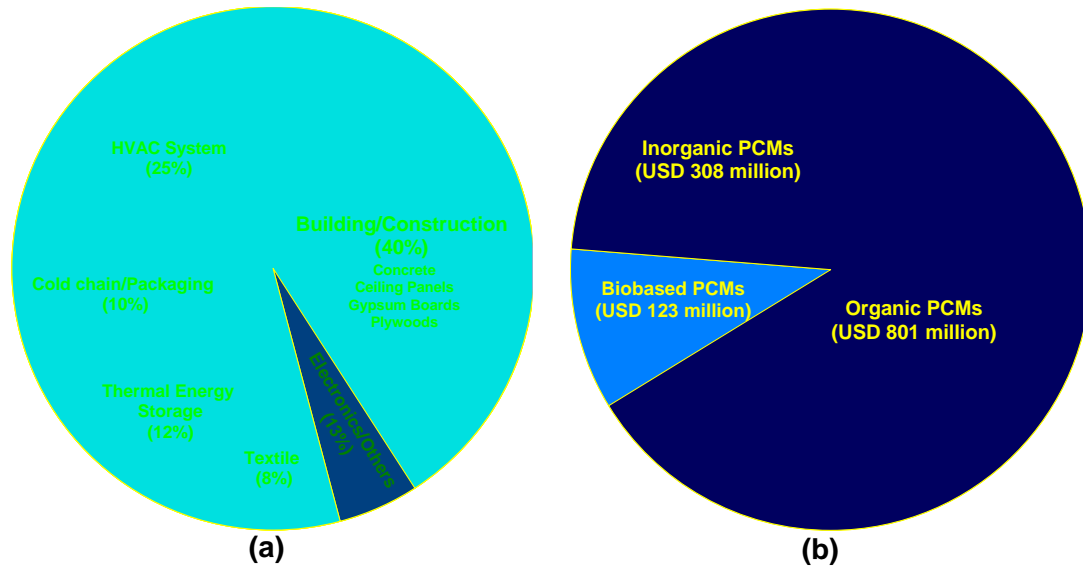


Figure 1-3. Global PCM market share by (a) end-user application and (b) chemical composition

Currently, the global PCM market is dominated by inorganic salt hydrates and organic paraffin waxes but there is a strong demand for renewable PCMs and for environment-friendly TES technologies. The paraffin waxes are leading the organic PCM market with approximately 53% of the total organic PCM market share and is forecasted to gain 18.3% by 2027 [52]. Bio-based PCMs, particularly those derived from TAGs are gaining commercial attention encouraged by continued performance and economic improvements. The major suppliers of paraffin PCMs are Rubitherm Technologies and Honeywell Electronic Materials; major suppliers of inorganic PCMs and products are Climator Technologies and Cold Chain Technologies and major suppliers of biobased PCMs (mainly fatty acids) are Entropy Solutions and Croda International [53].

1.5.2 The Global Lubricant Market

The global lubricant market size in 2020 was worth US\$157 billion with a total of 37 million metric tons [54]. The lubricant market is projected to reach US\$230 billion by 2027 at a compound annual growth rate of 3.4% [54]. **Figure 1-4a** and b show the global lubricant market volume share (%) by end-user industry and base oil type respectively. As can be seen in **Figure 1-4a**, 57% of the lubricant volume is consumed by the automotive and transportation industry [55].

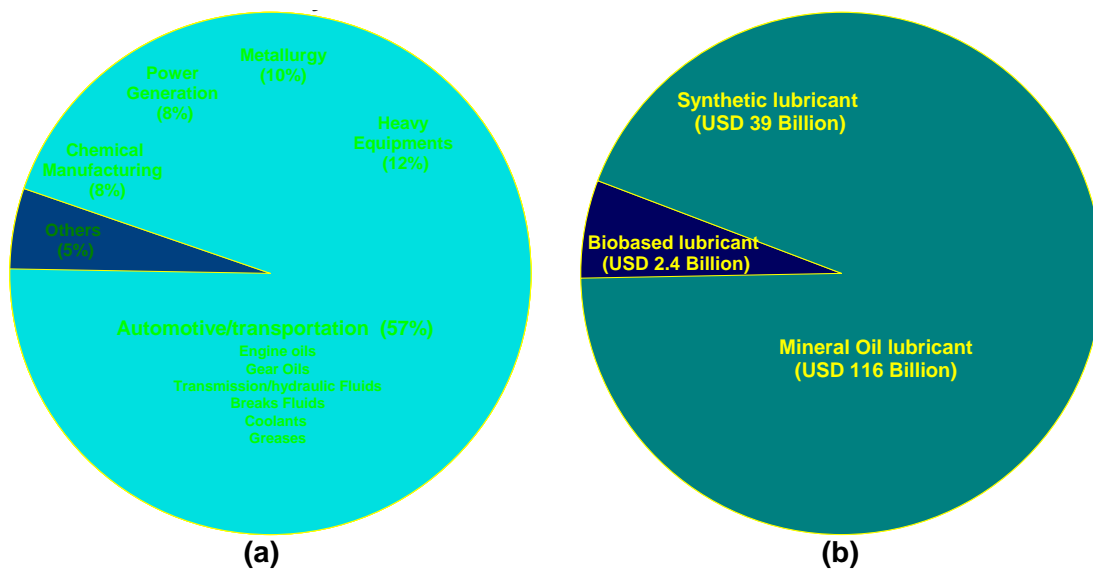


Figure 1-4. Global lubricant market share by (a) end-user industry and (b) by base oil type

The majority of lubricants supplied to the automotive and transportation industry are mineral oils and synthetic oils. The demand for bio-based lubricants is currently motivated by growing environmental awareness, adoption of stringent government regulations and increasing consumer acceptance [45]. The suppliers are well-established

players in the lubricant marketplace with Royal Dutch Shell, Exxon Mobile, Chevron Corporation, Total and British Petroleum being top five [55].

1.6 Current VO-based PCMs and Lubricants

Figure 1-5 shows the structures of the major classes of PCMs and lubricants that were synthesized from TAG derivatives.

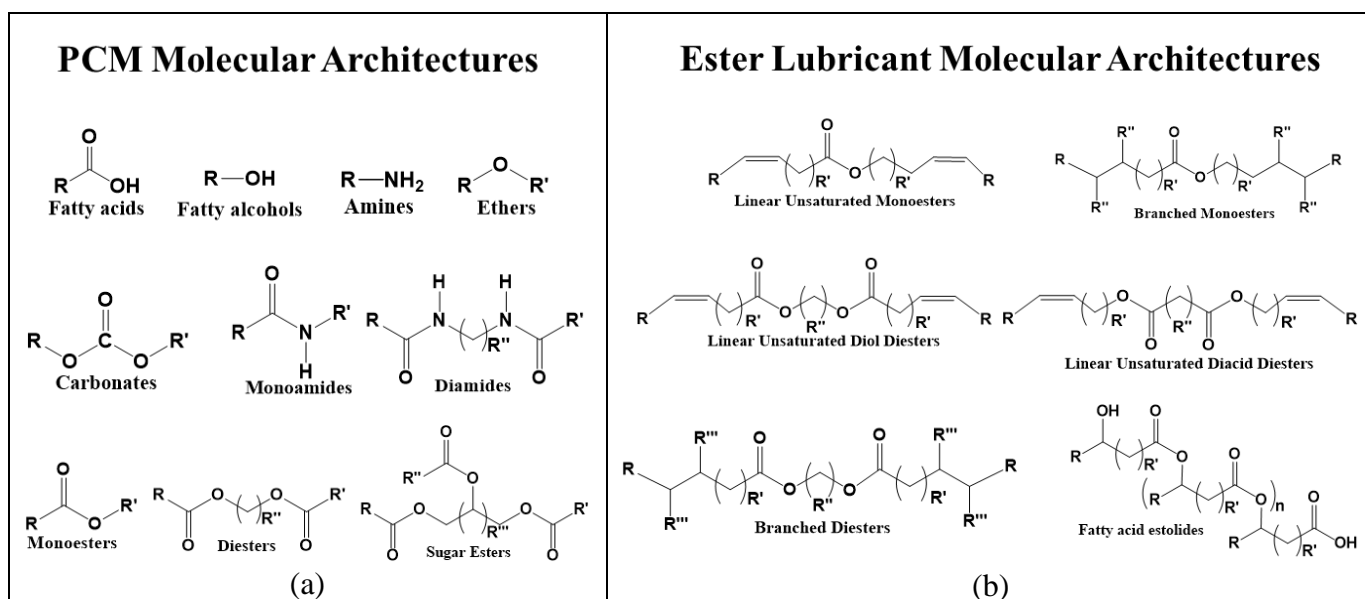


Figure 1-5. (a) PCMs and (b) lubricants molecular architectures derived using TAG.

1.6.1 PCMs Derived from TAG

The general structures of the PCMs derived from TAGs are shown in **Figure 1-5a**. They include fatty acids and their eutectic mixtures [56-62], fatty alcohols [63-67], fatty carbonates [63], fatty ethers [68], fatty amines [68], monoesters, diesters, polyol-esters [69-73], monoamides and diamides [74-76]. These PCMs generally present high

enthalpy, narrow phase change temperature ranges and minimum requirements for supercooling. They are also thermally stable and withstand thermal cycling without loss of performance.

1.6.2 Lubricants Derived from TAG

Figure 1-5b shows the classes of ester-based lubricants derived from TAG. The classes of lubricants include functionalized TAGs [77-79], linear saturated monoesters [80], unsaturated monoesters [81-84], branched monoesters [85], linear unsaturated and branched diacid and diol diesters [86-93] and polyesters [86, 94, 95]. Broadly, derivatized VO esters of **Figure 1-5b** are classified into two categories: (1) linear esters mimetics of synthetic oils and (2) branched esters mimetics of polyalphaolefins [96]. Polyesters such as estolides have been extensively studied as lubricant base fluids. The VO-based lubricants have common structural elements that are associated with improved lubricating properties such as linear fatty chain segments, polar functional groups, low unsaturation and branched chains [97].

1.7 Thermodynamics of Phase Transitions

At the melting point (T_m) of a PCM or lubricant the solid and liquid phase exist in thermal equilibrium. When T_m is reached, the Gibb's free energies of the solid and liquid phases become equal and the change in Gibb's free energy upon melting ΔG_m can be written as [98]:

$$\Delta G_m = 0 = \Delta H_m - T_m \Delta S_m \quad \text{Equation 4}$$

Where ΔH_m is the enthalpy of melting and ΔS_m is the entropy of melting.

Equation 4 gives:

$$T_m = \frac{\Delta H_m}{\Delta S_m} \quad \text{Equation 5}$$

Equation 5 provides a pathway to link the solid-liquid phase transition temperature to ΔH_m and ΔS_m of structures thereby possibly distinguishing individual contributions to ΔH_m through their intermolecular forces and to ΔS_m through the molecular “disorder” introduced by flexibility and spatial configuration [99]. *Equation 5* was used in this thesis as guidance to appreciate the contribution of specific structural elements to the thermal transition parameters of PCMs and lubricants given the particular molecular structure.

1.8 Using VO Structures and Sulfur based Groups to Prepare New PCMs and Lubricants

1.8.1 VO structures

Table 1-2 provides a summary of the overall effect and contribution of VO structures to key PCM and lubricants properties. The contribution is classified as advantageous or disadvantageous depending on capability to deliver function.

Table 1-2. Effect of VO structures on key PCM and lubricant properties. Adv.: advantageous and Dis.: disadvantageous.

Structural element	Influence when present in a PCM or lubricant structure			
	PCM		Lubricant	
Saturated fatty chain	<ul style="list-style-type: none"> • Increase crystal packing • Increase dispersion forces • Increase T_m and ΔH_m • Increase thermal stability • Low supercooling 	Adv	<ul style="list-style-type: none"> • Increase viscosity • Increase flash point • Increase thermal stability • create thicker tribofilm 	Adv
	<ul style="list-style-type: none"> • Increases ΔS_m • Varying polymorphism • Low thermal conductivity • Low application temperature 	Dis	<ul style="list-style-type: none"> • Increase pour point • Increase cloud point • Limited viscosity range • Poor corrosion protection 	Dis
Unsaturation		Adv	<ul style="list-style-type: none"> • Decrease pour point • Decrease cloud point • Tribofilm adhesion 	Adv
	<ul style="list-style-type: none"> • Decrease T_m and ΔH_m • Reduce crystal packing • Low oxidative stability 	Dis	<ul style="list-style-type: none"> • Low oxidative stability • Increase reactivity • Decrease viscosity 	Dis
Ester groups	<ul style="list-style-type: none"> • Increase thermal stability • Increase biodegradability 	Adv	<ul style="list-style-type: none"> • Tribofilm adhesion • Improve flow behavior • Increase biodegradability 	Adv
	<ul style="list-style-type: none"> • Increase flexibility • Decrease T_m and ΔH_m 	Dis	<ul style="list-style-type: none"> • Decrease viscosity • Mild polarity 	Dis
β -hydrogen		Adv	<ul style="list-style-type: none"> • No desirable properties 	Adv
	<ul style="list-style-type: none"> • Decrease thermal stability • Decrease oxidative stability 	Dis	<ul style="list-style-type: none"> • Decrease thermal stability • Decrease oxidative stability 	Dis

1.8.2 Sulfur Based Functional Groups

1.8.3 Overview of Sulfur Chemistry

Sulfur is a p-block element in row III and group VI (atomic number 16) below oxygen and between phosphorus and chlorine on the periodic table. Approximately 50% of available sulfur is derived from elemental deposits, 30% from smelter gases and 20% is recovered from pyrites [100].

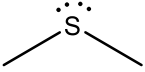
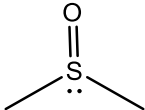
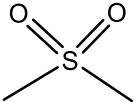
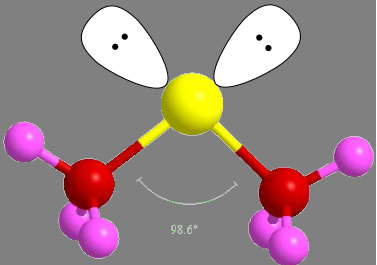
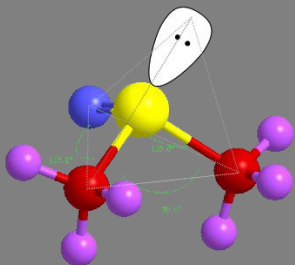
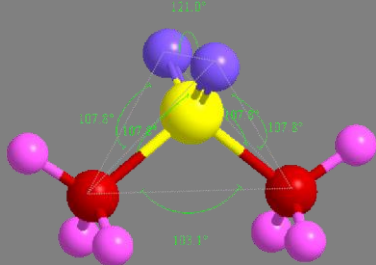
Sulfur can form thermally stable C–S covalent bonds with carbon atoms with a bond strength of 362kJ/mol which is slightly weaker than C–C bond which is 376kJ/mol. This small difference suggests that the C–S bond is slightly more sensitive to thermal degradation when exposed to temperature similar to the C–C bond [14].

Sulfur (electronegativity number EN =2.58) is similar to carbon (EN =2.56) which means the electrons in the C–S covalent bond are evenly shared and therefore have no permanent bond dipole to form dipole-dipole attraction [101]. Sulfur is less electronegative than oxygen (EN =3.44) and nitrogen (EN =3.04). However, since the atomic radius of a sulfur atom (1.05Å) is larger than carbon (0.77Å) and oxygen (0.66Å), sulfur electronic cloud is more easily distorted to form instantaneous dipoles.

The molecular geometry, hybridization and bond angle of sulfide, sulfoxide and sulfonyl groups are shown in **Table 1-3**. When the sulfur atom is present in the fatty chain as a sulfide functional group (C–S–C), the sulfur atom is sp³ hybridized with bent molecular geometry with bond angle that varies between 92 and 109° due to the lone pair-lone pair repulsion [14]. When it is present as sulfoxide group (C–SO–C), the sulfur atom is sp³d hybridized with trigonal pyramidal molecular geometry [102]. When the sulfur atom is present in the fatty chain as sulfonyl group (C–SO₂–C), the sulfur atom is sp³d² hybridized with tetrahedral molecular geometry [103].

Table 1-3. Geometry, hybridization and bond angle of sulfide, sulfoxide and sulfonyl groups.

Chemical	Sulfide	Sulfoxide	Sulfone
----------	---------	-----------	---------

Property			
Geometry	Bent	Trigonal pyramidal	Tetrahedral
Hybridization	sp^3	sp^3d	sp^3d^2
Average Bond angles	C-S-C = 92 to 109°	C-S-C = 98° [104] O-S-C = 105°	C-S-C = 103° [105, 106] O-S-O = 120° O-S-C = 107°
3D of functional group in a hydrocarbon chain			

1.8.3.1 Sulfonyl Groups in PCMs and Lubricants

Sulfonyl groups are known to be the most stable and inert group amongst organosulfur functional groups since the sulfur valence shell is fully occupied and is therefore in the highest possible oxidation state. Three main characteristics of the sulfonyl group may improve PCMs as well as lubricants: (i) molecular symmetry, (ii) tetrahedral molecular geometry and (iii) high polarity [106]. The benefits of using the sulfonyl group include improved T_m and ΔH_m for PCMs and high viscosity and improved cold-flow performance for lubricants.

1.8.3.2 Sulfide Group in Lubricants

Sulfide-branch groups have the ability to convert hydroperoxides to non-radical derivatives and can be useful to increase the oxidative stability of lubricant molecules [107]. Sulfide-branch groups can mitigate chain propagation by eliminating free radicals generated in the initiation stage of oxidation [35]. This reaction is relatively rapid, removes peroxides as they are formed, and thus breaks the hydrocarbon oxidation chain

[108]. The sulfide pendant group will also help lower the crystallization temperature and enthalpy of transition.

1.9 Thesis Scope and Theme Objectives

Current research on VO-based materials targets the production of performing materials using benign and economical means. The present work adopts a methodology in which the compounds are built considering the roles that the constituent structures would play in performance. PCMs and lubricants are selected because of their industrial importance and contrasting property requirements.

The building blocks of the compounds prepared for this thesis include VO structural elements and select functional groups which would deliver improved performance. The focus was on key properties relevant to PCMs and lubricants i.e., thermal stability, thermal transition behavior, crystal structure, flow behavior and oxidation stability. The role of the structural elements such as functional groups, fatty acid chain, double bonds, and pendant groups is considered for the analysis of these properties.

The objectives of the thesis are to:

1. Derive from VO structure and select sulfur based functional groups performing PCMs and lubricants of industrial relevance.
2. Understand the relationships between the chemical functionality and the resultant physical functionality of these PCMs and lubricants.
3. Establish predictive structure-function relationships that can be used to direct the design of lipid-based performing materials.

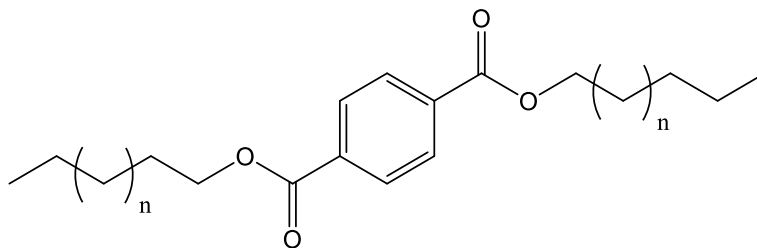
The thesis encompasses three (03) projects: two related to PCM and one to lubricants. The projects are presented each in four sub-sections: (1) the structures of the project's compounds, (2) the weaknesses observed in the current VO based materials, (3) the suggested solutions to solve these problems and (4) outline of the project specific objectives and hypotheses.

1.9.1 Project 1: Terephthalate diester PCMs

1.9.1.1 Structure of the compounds

The compounds involved in this project consist of reacting terephthalic acid (TA) with linear saturated fatty alcohols of length n to prepare terephthalate diesters.

Terephthalate diesters with (n -TA- n , $n = 12, 14, 16, \& 18$; **Scheme 1-4**) were prepared and investigated.

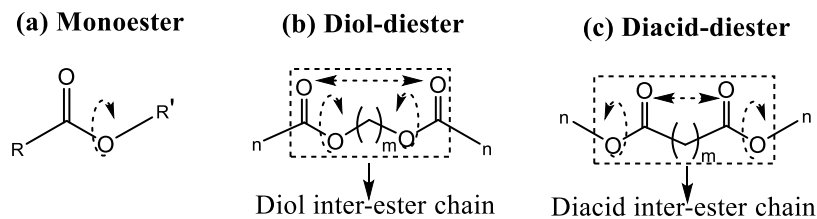


Scheme 1-4. Structure of the n -TA- n terephthalate diesters investigated ($n = 12, 14, 16, \& 18$).

1.9.1.2 Weaknesses: Flexibility, polymorphism and low T_m in linear saturated esters

Linear saturated monoesters (R -COO- R' in Scheme 1-5a) have high molecular flexibility which promotes polymorphism and is a major limitation when utilizing the solid-liquid phase transition in TES applications [109-111]. The ester groups alkoxy moiety (C-O-C)

rotates freely and provides flexibility to the alcohol chain which increases entropy (shown in **Scheme 1-5**) [8, 112].



Scheme 1-5. Chemical structures of (a) monoesters ($R-COO-R'$) where R and R' = fatty acid and fatty alcohol chain moieties, respectively, (b-c) Diol and Diacid diesters ($n-m-n$) where n = fatty chain length, and m = inter-ester chain. Curved and double arrows indicate rotation at the alkoxy bonds and separation distance between the ester groups, respectively.

The introduction of a second ester group to prepare linear saturated diol (**Scheme 1-5b**) and diacid (**Scheme 1-5c**) diesters does not significantly improve the phase change properties. The presence of a second ester group in the aliphatic chain introduces two inherent undesirable properties (i) intramolecular steric repulsion [113] and (ii) directionality which dictates how the two C–O–C moieties rotate and affect the aliphatic chain flexibility [114-116]. The intramolecular steric repulsion can be minimized by increasing the inter-ester chain length m (**Scheme 1-5b-c**). In both diol and diacid diesters; as the two ester groups are further separated, the intramolecular steric repulsion decreases which increases T_m and ΔH_m [113, 116, 117]. T_m and ΔH_m are shown to be maximum when the two ester groups are separated by an inter-ester chain length of 6 carbons regardless of the fatty chain length [113].

The directionality of the alkoxy group was shown to play a role in the phase change properties [116]. In diol diesters, the C–O–C moiety directs rotation “inwards” (curved arrows **Scheme 1-5b**) into the short inter-ester chain segment and leads to better packing efficiency in the crystalline phase, whereas in diacid diesters the C–O–C moiety directs rotation “outwards” (curved arrows **Scheme 1-5c**) into the long aliphatic chain, thereby increasing the probability of coexistence of a larger number of conformational arrangements. The coexistence of several conformational arrangements in diol and diacid diesters leads to poor packing efficiency and tendency for the material to crystallize in less stable phases [116, 118].

1.9.1.3 Solution: Approach to reduce diester’s flexibility and polymorphism and increase T_m

In order to reduce the flexibility and mitigate polymorphism in linear saturated diesters, one can introduce an inter-ester group which (i) is appropriately sized to reduce the intramolecular steric repulsion between two ester groups (ii) prevent flexibility at the center of the molecule and (iii) contribute to the total intermolecular attractions.

The insertion of a planar benzene ring between two ester groups (**Scheme 1-4**) instead of a hydrocarbon chain can mitigate ester groups intramolecular steric repulsion and restrain the ester group flexibility. The benzene ring size (5Å) is a sufficient separation distance to reduce intramolecular steric repulsion similar to what was accomplished by a 5.5Å - long hydrocarbon interchain in diacid and diol diesters [116]. The benzene ring can anchor the center of the molecule, reduce conformational arrangements and avoid polymorphism [116, 118].

1.9.1.4 Specific Objectives and Hypotheses of Project 1

1. Will the size of the planar benzene ring provide a sufficient distance between two ester groups to limit ester groups intramolecular steric repulsion?

It is hypothesized that a 5Å-long benzene ring will mitigate steric repulsion of the ester group electronic clouds and reduce the number of conformational arrangements similar to the 5.5Å hydrocarbon chain in diol and diacid diesters.

2. Will the flat nature of the planar benzene ring in symmetrical terephthalate diesters improve crystal packing?

It is hypothesized that the planar benzene ring will result in a closer stacking arrangement in the crystal phase when compared to linear saturated monoesters and linear saturated diol and diacid diesters. It is expected that the planar benzene ring will lower ΔS_m compared to the diol and diacid inter-ester chains which have higher degree of freedom to exist in higher conformational arrangements.

3. Will the π - π intermolecular attraction from the benzene group increase T_m and ΔH_m

It is hypothesized that the π - π intermolecular interaction between rigid benzene rings will contribute to the total intermolecular forces.

4. Will thermal transition temperature and thermal stability properties of the terephthalate diesters vary predictably with chain length?

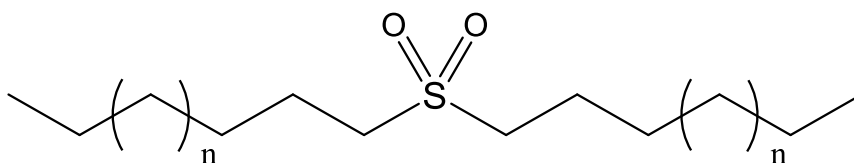
A decrease of steric repulsions, a closer stacking arrangement and an increase in intermolecular attraction would lead to the increase of ΔH_m and T_m and thermal stability. It is hypothesized that ΔH_m and T_m and thermal stability will vary predictably with fatty chain length due to the incremental contribution of CH_2 units to the dispersion

forces. The solid-liquid phase transition temperature and onset of mass loss temperature are expected to increase following trends similar to linear hydrocarbons.

1.9.2 Project 2: Linear saturated monosulfone PCMs

1.9.2.1 Structure of the compounds

The compounds involved in this project consist of reacting linear saturated monosulfides with hydrogen peroxide to prepare linear saturated monosulfones. Linear saturated monosulfones ($n\text{-SO}_2\text{-}n$, with $n = 10, 12, \& 18$, **Scheme 1-6**) were prepared and investigated.



Scheme 1-6. Structure of the $n\text{-SO}_2\text{-}n$ monosulfones investigated ($n = 10, 12, \& 18$).

1.9.2.2 Weakness: Limited thermal energy storage properties in current VO-based PCMs

The existing VO-based PCMs have low T_m due to weak intermolecular interactions which prevent their application in important areas, such as rapidly expanding solar energy and industrial waste heat sectors [119, 120]. Higher temperature VO-based PCMs can be achieved in principle by using long saturated fatty chains. However, the available chain length for VO-based PCM synthesis is limited to the most abundant naturally occurring fatty acid, i.e., C_{18} and its derivatives.

The introduction of polar functional groups into the fatty chain can substantially add to the net attractions through the dipole-dipole forces [121, 122]. The polar functional

groups such as the ester ($-\text{COO}-$), carboxylic ($-\text{COOH}$), amine ($-\text{NH}_2$) hydroxyl ($-\text{OH}$), amide ($-\text{CONH}-$), groups can form hydrogen bonds between adjacent molecules have already been used to prepare monoesters, fatty acids, fatty amines, fatty alcohols and monoamides PCMs with T_m limited to 80°C [36].

1.9.2.3 Solution: Using high polarity sulfonyl groups to expand energy storage properties

The sulfonyl group ($-\text{SO}_2-$) is selected because its permanent dipoles are expected to provide large intermolecular sulfonyl-sulfonyl attraction which would significantly increase intermolecular attraction and increase T_m . As shown in **Figure 1-6**, the polarity of ($-\text{SO}_2-$) is higher than that of other functional groups available for incorporation into PCM structures [10, 123].

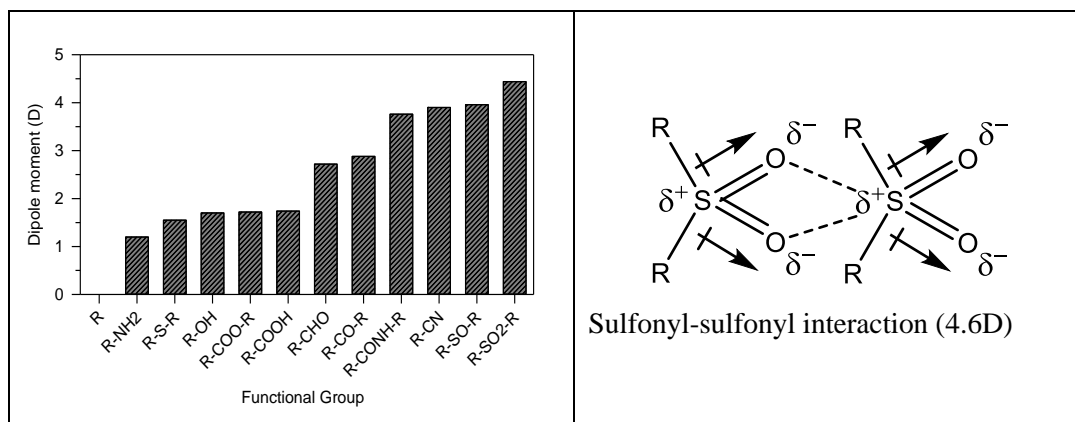


Figure 1-6. Dipole moments in Debye (D) of different functional groups with R representing the aliphatic saturated hydrocarbon chain and sulfonyl-sulfonyl interaction of sulfonyl groups.

The tetrahedral geometry of the sulfonyl group is expected to keep the molecule linear and facilitate uniform and close-packing arrangement. There are therefore opportunities to increase T_m above the 80°C achieved with other functional groups, increase or match ΔH_m and improve onset temperature of degradation.

1.9.2.4 Specific Objectives and Hypotheses of Project 2

1. Will the incorporation of the high polarity sulfonyl group in the linear saturated aliphatic fatty chain increase T_m and ΔH_m ?

It is hypothesized that the incorporation of a sulfonyl functional group to saturated aliphatic fatty chains will provide strong sulfonyl-sulfonyl attraction that will add to the dispersion forces of the hydrocarbon chains to noticeably increase T_m and ΔH_m .

2. Will the symmetrical design of the molecules mitigate the effect of size on crystal packing?

It is hypothesized that the symmetry of the molecule about the sulfonyl group will mitigate the detrimental effect of the sulfonyl group large size while maximizing its contribution to the intermolecular attractions. The linear fatty chains in a symmetrical configuration are expected to add to the crystal stability.

3. Will the monosulfones experience polymorphism?

The monosulfones will possibly display polymorphic behavior and experience solid-solid transition or melt-mediated recrystallization because of the long fatty acid chains flexibility and bulky nature of the sulfonyl functional group.

4. Will the linear saturated monosulfones have higher T_m and ΔH_m than PCMs with other monofunctional groups?

Because of the large dipole moment of the sulfonyl group, the monosulfones are expected to have larger T_m and ΔH_m than PCMs with single amide, carboxylic, hydroxyl, amine, ester functional groups which have lower dipole moments. It is expected that T_m of the monosulfones will be suitable for application requiring T_m above 80 such as in solar water heating systems, solar cookers and heat recovery systems.

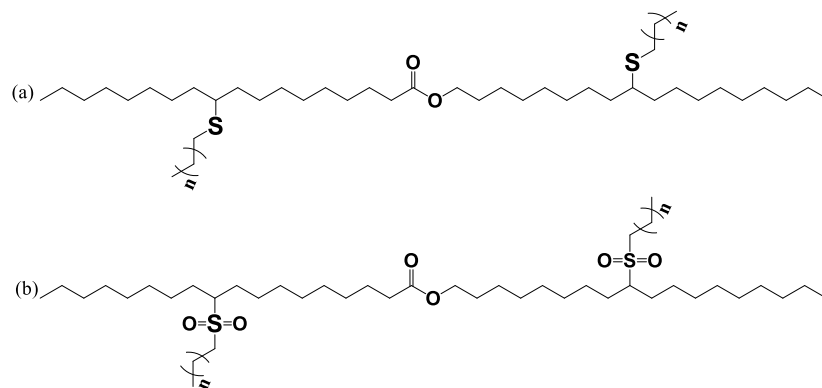
5. Will thermal transition and thermal stability properties of the monosulfones change predictably with fatty chain length?

It is expected that the thermal transition and thermal stability will vary predictably with fatty chain length due to incremental increase of the dispersion forces similar to what is observed for hydrocarbons.

1.9.3 Project 3: Sulfide and sulfonyl branched monoesters lubricants

1.9.3.1 Structure of the compounds

The compounds involved in this project consist of sulfide branched oleyl oleate monoesters (A2-S-n, **Scheme 1-7a**) and sulfonyl branched oleyl oleate monoesters (A2-SO₂-n, **Scheme 1-7b**). Sulfide and sulfonyl branched oleyl oleate monoesters with pendant chain length n = 2, 3, 4 & 6 were prepared and investigated.



Scheme 1-7. Structures of the four sulfide (A2-S-n) and four sulfonylethyl-branch oleyl oleate monoesters (A2-SO₂-n) investigated in this work (n= 2, 3, 4 and 6).

1.9.3.2 Weakness: Poor oxidative stability, high onset of crystallization, low thermal stability and low viscosity range

The naturally abundant oleic acid [124-126] and its widely available and inexpensive derivative oleyl oleate are undesirable for direct use lubricant because of poor oxidative stability, high onset of crystallization, low thermal stability and low viscosity range [127]. The branching of oleyl oleate with ester pendant groups increased oxidative stability and thermal stability, reduced the onset of crystallization and increased the viscosity range [128-131]. For example, linear unsaturated monoesters [81-84], unsaturated diacid diesters [92, 132-134] and unsaturated diol diesters [88, 114] presented onsets of crystallization (T_{on}^c) between -30°C and 20°C and viscosity between 10mPa.S and 40mPa.S; whereas, branched ester lubricants with ester pendant groups present T_{on}^c as low as -55°C and viscosity ranging from 100mPa.S to 500mPa.s [81, 82, 87, 88, 93, 114, 135-138]. However, the branched ester lubricants with ester pendant groups have low oxidative stability at elevated temperatures and low viscosities because

the ester groups cannot form dipole-dipole attractions. From a synthetic perspective, unsaturated ester lubricants are mainly branched with ester pendant groups using epoxidation/ring opening synthetic route which yields crude mixtures of branched products that require tedious purification processes.

1.9.3.3 Solution: Using Sulfide and Sulfonyl Pendant Group

Oleyl oleate was branched with sulfide and sulfonyl pendant groups to improve the oxidative stability, viscosity, flow behavior and cold-flow properties. Similarly to ester pendant groups, the bulkier sulfide and sulfonyl pendant groups will be able to suppress onset of crystallization and provide wider viscosity ranges due to higher polarity and large size. The bulkier sulfonyl group could be able to delay early stage of crystallization.

The sulfide pendant groups can impart higher oxidative stability to the ester molecule due to their ability to eliminate hydroperoxide radicals at elevated temperatures. The sulfide pendant groups should have higher oxidative stability compared to sulfonyl and ester groups.

Unlike the epoxidation/ring-opening route, which produces a mixture of branched ester lubricants in the crude [27, 139-150], thiolene synthesis yield a single sulfide branched product in the crude [151].

1.9.3.4 Specific Objectives and Hypotheses of Project 3

1. Will branching with sulfide and sulfonyl pendant groups improve the thermal stability of monoesters and would the effect be predictable?

The thermal stability of sulfide and sulfonyl branched monoesters is expected to vary predictably with total chain length and functional groups polarity. The sulfonyl group is expected to impart higher thermal stability than the sulfide group.

2. Will branching with sulfide and sulfonyl pendant groups improve the oxidative stability of monoesters and would the effect be predictable?

The sulfide branched monoesters are expected to have higher oxidative stability than the oleyl oleate monoester, sulfonyl branched oleyl oleate monoester and ester branched oleyl oleate monoesters.

3. Will branching with sulfide and sulfonyl pendant groups improve the thermal transition properties of the monoesters and would the effect be predictable?

The onset temperatures of crystallization and melting are expected to (a) vary predictably with total chain length, (b) be influenced differently by the sulfide and sulfonyl group, and (c) be depressed with the introduction of internally branched groups.

4. Will the sulfide and sulfonyl pendant groups dictate the flow behavior of the monoesters?

It is expected that the sulfide and sulfonyl branched monoesters will have Newtonian flow behavior at temperatures above their onset of melting.

5. Will branching with sulfide and sulfonyl pendant groups provide desired viscosity profiles in monoesters and would the changes be predictable?

The viscosity of the sulfide and sulfonyl branched monoesters is expected to be set by the type of functional group and vary predictably with chain length.

1.10 References

1. No, S.-Y., *Inedible vegetable oils and their derivatives for alternative diesel fuels in CI engines: A review*. Renewable and Sustainable Energy Reviews, 2011. **15**(1): p. 131-149.
2. Demirbas, A., *Progress and recent trends in biodiesel fuels*. Energy Conversion and Management, 2009. **50**(1): p. 14-34.
3. Hammond, E., *Vegetable oils/ Types and properties*. 2003.
4. Zhang, C., et al., *Recent advances in vegetable oil-based polymers and their composites*. Progress in Polymer Science, 2017. **71**: p. 91-143.
5. Gunstone, F.D., J.L. Harwood, and A.J. Dijkstra, *The Lipid Handbook with CD-ROM, Third Edition*. 2007: CRC Press.
6. Dominguez, L.J. and M. Barbagallo, *Chapter 3 - Not All Fats Are Unhealthy*, in *The Prevention of Cardiovascular Disease Through the Mediterranean Diet*, A. Sánchez-Villegas and A. Sánchez-Tainta, Editors. 2018, Academic Press. p. 35-58.
7. Frankel, E.N., *Chapter 1 - Free radical oxidation*, in *Lipid Oxidation (Second Edition)*, E.N. Frankel, Editor. 2012, Woodhead Publishing. p. 15-24.
8. Bunn, C.W., *The melting points of chain polymers*. Journal of Polymer Science Part B: Polymer Physics, 1996. **34**(5): p. 799-819.
9. Wiberg, K.B. and K.E. Laidig, *Barriers to rotation adjacent to double bonds. 3. The carbon-oxygen barrier in formic acid, methyl formate, acetic acid, and methyl acetate. The origin of ester and amide resonance*. Journal of the American Chemical Society, 1987. **109**(20): p. 5935-5943.
10. Ouellette, R.J. and J.D. Rawn, *1 - Structure and Bonding in Organic Compounds*, in *Organic Chemistry* R.J. Ouellette and J.D. Rawn, Editors. 2018, Academic Press. p. 1-30.
11. Knothe, G. and J.T.P. Derksen, *Recent Developments in the Synthesis of Fatty Acid Derivatives*. 1999: Taylor & Francis.
12. Gosselink, R.W., et al., *Reaction Pathways for the Deoxygenation of Vegetable Oils and Related Model Compounds*. ChemSusChem, 2013. **6**(9): p. 1576-1594.
13. Vonghia, E., et al., *Pathways for the deoxygenation of triglycerides to aliphatic hydrocarbons over activated alumina*. Energy & Fuels, 1995. **9**(6): p. 1090-1096.
14. Clayden, J., N. Greeves, and S. Warren, *Organic Chemistry*. 2012: OUP Oxford.

15. Foley, P., et al., *Derivation and synthesis of renewable surfactants*. Chemical Society Reviews, 2012. **41**(4): p. 1499-1518.
16. Kushairi, A., et al., *Oil palm economic performance in Malaysia and R&D progress in 2017*. Journal of Oil Palm Research, 2018. **30**(2): p. 163-195.
17. Gunstone, F., *The chemistry of oils and fats: sources, composition, properties and uses*. 2009: John Wiley & Sons.
18. Kenar, J.A., G. Knothe, and A.L. Copes, *Synthesis and characterization of dialkyl carbonates prepared from mid-, long-chain, and guerbet alcohols*. Journal of the American Oil Chemists' Society, 2004. **81**(3): p. 285-291.
19. Williamson, A., *XLV. Theory of ætherification*. The London, Edinburgh, and Dublin Philosophical Magazine and Journal of Science, 1850. **37**(251): p. 350-356.
20. Soodoo, N., et al., *Phase behavior of monosulfones: Use of high polarity sulfonyl groups to improve the thermal properties of lipid-based materials for PCM applications*. Solar Energy Materials and Solar Cells, 2019. **201**: p. 110115.
21. Kazemi, M., H. Kohzadi, and O. Abdi, *Alkylation of thiols in green mediums*. J. Mater. Environ. Sci, 2015. **6**: p. 1451-1456.
22. Adhvaryu, A., S.Z. Erhan, and J.M. Perez, *Tribological studies of thermally and chemically modified vegetable oils for use as environmentally friendly lubricants*. Wear, 2004. **257**(3-4): p. 359-367.
23. Castro, W., et al., *A study of the oxidation and wear properties of vegetable oils: Soybean oil without additives*. Journal of the American Oil Chemists Society, 2006. **83**(1): p. 47-52.
24. Fox, N.J. and G.W. Stachowiak, *Vegetable oil-based lubricants - A review of oxidation*. Tribology International, 2007. **40**(7): p. 1035-1046.
25. Lathi, P.S. and B. Mattiasson, *Green approach for the preparation of biodegradable lubricant base stock from epoxidized vegetable oil*. Applied Catalysis B-Environmental, 2007. **69**(3-4): p. 207-212.
26. Kulkarni, R.D., et al., *Epoxidation of mustard oil and ring opening with 2-ethylhexanol for biolubricants with enhanced thermo-oxidative and cold flow characteristics*. Industrial Crops and Products, 2013. **49**: p. 586-592.
27. Kade, M.J., D.J. Burke, and C.J. Hawker, *The power of thiol-ene chemistry*. Journal of Polymer Science Part A: Polymer Chemistry, 2010. **48**(4): p. 743-750.
28. ExpertMarketResearch, *Global Vegetable Oil Market*. 2022.
29. Galloway, R., *Market demand and outlook*, in *High Oleic Oils*. 2022, Elsevier. p. 261-274.
30. Almasi, S., et al., *A review on bio-lubricant production from non-edible oil-bearing biomass resources in Iran: Recent progress and perspectives*. Journal of Cleaner Production, 2021. **290**: p. 125830.
31. Naji, S.Z., C.T. Tye, and A.A. Abd, *State of the art of vegetable oil transformation into biofuels using catalytic cracking technology: Recent trends and future perspectives*. Process Biochemistry, 2021. **109**: p. 148-168.
32. Belousov, A.S., et al., *Recent advances in sustainable production and catalytic transformations of fatty acid methyl esters*. Sustainable Energy & Fuels, 2021.

33. Hásl, T., et al., *Cost/Performance Analysis of Commercial-Grade Organic Phase-Change Materials for Low-Temperature Heat Storage*. *Energies*, 2020. **13**(1): p. 5.
34. Nowak, P., K. Kucharska, and M. Kamiński, *Ecological and Health Effects of Lubricant Oils Emitted into the Environment*. *International journal of environmental research and public health*, 2019. **16**(16): p. 3002.
35. Soleimani, M., et al., *Antioxidants Classification and Applications in Lubricants*. 2018.
36. Soodoo, N., et al., *Fundamental structure-function relationships in vegetable oil based phase change materials: A critical review*. *Journal of Energy Storage*, 2022. **51**: p. 104355.
37. Salih, N. and J. Salimon, *A Review on New Trends, Challenges and Prospects of Ecofriendly Friendly Green Food-Grade Biolubricants*. 2021.
38. Sharma, S.D. and K. Sagara, *Latent Heat Storage Materials and Systems: A Review*. *International Journal of Green Energy*, 2005. **2**(1): p. 1-56.
39. Prieto, C., et al., *Review of technology: Thermochemical energy storage for concentrated solar power plants*. *Renewable and Sustainable Energy Reviews*, 2016. **60**: p. 909-929.
40. Lugolole, R., et al., *Thermal performance comparison of three sensible heat thermal energy storage systems during charging cycles*. *Sustainable Energy Technologies and Assessments*, 2018. **30**: p. 37-51.
41. Mehling, H. and L.F. Cabeza, *Phase Change Materials and Their Basic Properties*. *Thermal Energy Storage for Sustainable Energy Consumption*, 2007: p. 257-277.
42. Puhan, D., *Lubricant and Lubricant Additives*, in *Tribology in Materials and Manufacturing-Wear, Friction and Lubrication*. 2020, IntechOpen.
43. Daschner, E., *Lubrication Fundamentals: Revised and Expanded*. 2017.
44. Perez, J.M., *Oxidative properties of lubricants using thermal analysis*. *Thermochimica Acta*, 2000. **357-358**: p. 47-56.
45. Chan, C.-H., et al., *Tribological behavior of biolubricant base stocks and additives*. *Renewable and Sustainable Energy Reviews*, 2018. **93**: p. 145-157.
46. Willermet, P.A., et al., *Mechanism of formation of antiwear films from zinc dialkyldithiophosphates*. *Tribology International*, 1995. **28**(3): p. 177-187.
47. Nazir, H., et al., *Recent developments in phase change materials for energy storage applications: A review*. *International Journal of Heat and Mass Transfer*, 2019. **129**: p. 491-523.
48. Rawat, S.S. and A.P. Harsha, *Current and Future Trends in Grease Lubrication*, in *Automotive Tribology*, J.K. Katiyar, et al., Editors. 2019, Springer Singapore: Singapore. p. 147-182.
49. ExpertMarketResearch, *Global Advanced Phase Change Materials Market Outlook*. 2022.
50. FortuneBusinessInsights, *Phase Change Materials Market*. 2022.
51. Yuan, Y., Zhang, N., Tao, W., Cao, X. and He, Y., *Fatty acids as phase change materials: a review*. *Renewable and Sustainable Energy Reviews*, 2014. **29**: p. 482-498.
52. GlobalMarketInsights, *Phase Change Materials Market*. 2022.

53. marketsandmarkets.com, *Phase Change Material (PCM) Market by Type (Organic, Inorganic, Bio-based), Application (Building & Construction, HVAC, Cold Chain & Packaging, Thermal Energy Storage, Textile, Electronics), and Region - Global Forecast to 2022*. 2017.
54. MaximizeMarketResearch, *Global Lubricant Market: Industry Analysis and Forecast (2021-2027) by Type, Fluid Type, and Region*. 2021.
55. Intelligence, M., *LUBRICANTS MARKET - GROWTH, TRENDS, AND FORECAST (2020 - 2027)*. 2020.
56. Kahwaji, S. and M.A. White, *Prediction of the properties of eutectic fatty acid phase change materials*. *Thermochim. Acta*, 2018. **660**: p. 94-100.
57. Huang, X.L., et al., *Novel phase change materials based on fatty acid eutectics and triallyl isocyanurate composites for thermal energy storage*. *J. Appl. Polym. Sci.*, 2017. **134**(27): p. 44866.
58. Yuan, Y., Zhang, N., Tao, W., Cao, X. and He, Y., *Fatty acids as phase change materials: a review*. *Renew Sust Energ Rev*, 2014. **29**: p. 482-498.
59. Suppes, G.J., M.J. Goff, and S. Lopes, *Latent heat characteristics of fatty acid derivatives pursuant phase change material applications*. *Chem Eng Sci*, 2003. **58**(9): p. 1751-1763.
60. Rozanna, D., et al., *Fatty Acids as Phase Change Materials (PCMs) for Thermal Energy Storage: A Review*. *Int. J. Green Energy*, 2005. **1**(4): p. 495-513.
61. Alkan, C. and A. Sari, *Fatty acid/poly(methyl methacrylate) (PMMA) blends as form-stable phase change materials for latent heat thermal energy storage*. *Sol Energy*, 2008. **82**(2): p. 118-124.
62. Kenisarin, M.M., *Thermophysical properties of some organic phase change materials for latent heat storage. A review*. *Sol Energy*, 2014. **107**: p. 553-575.
63. Kenar, J.A., *Latent heat characteristics of biobased oleochemical carbonates as potential phase change materials*. *Solar Energy Materials and Solar Cells*, 2010. **94**(10): p. 1697-1703.
64. Kumar, R., S. Vyas, and A. Dixit, *Fatty acids/1-dodecanol binary eutectic phase change materials for low temperature solar thermal applications: Design, development and thermal analysis*. *Solar Energy*, 2017. **155**: p. 1373-1379.
65. van Miltenburg, J.C., H.A.J. Oonk, and L. Ventola, *Heat Capacities and Derived Thermodynamic Functions of 1-Octadecanol, 1-Nonadecanol, 1-Eicosanol, and 1-Docosanol between 10 K and 370 K*. *Journal of Chemical & Engineering Data*, 2001. **46**(1): p. 90-97.
66. van Miltenburg, J.C., G.J.K. van den Berg, and M. Ramirez, *Heat Capacities and Derived Thermodynamic Functions of 1-Dodecanol and 1-Tridecanol between 10 K and 370 K and Heat Capacities of 1-Pentadecanol and 1-Heptadecanol between 300 K and 380 K and Correlations for the Heat Capacity and the Entropy of Liquid n-Alcohols*. *Journal of Chemical & Engineering Data*, 2003. **48**(1): p. 36-43.
67. Zeng, J.L., et al., *Thermal conductivity enhancement of MWNTs on the PANI/tetradecanol form-stable PCM*. *Journal of Thermal Analysis and Calorimetry*, 2008. **91**(2): p. 443-446.

68. Hasl, T. and I. Jiricek, *The Prediction of Heat Storage Properties by the Study of Structural Effect on Organic Phase Change Materials*. Energy Procedia, 2014. **46**: p. 301-309.
69. Alper Aydın, A., *High-chain fatty acid esters of 1-octadecanol as novel organic phase change materials and mathematical correlations for estimating the thermal properties of higher fatty acid esters' homologous series*. Solar Energy Materials and Solar Cells, 2013. **113**: p. 44-51.
70. Aydın, A.A. and A. Aydın, *High-chain fatty acid esters of 1-hexadecanol for low temperature thermal energy storage with phase change materials*. Solar Energy Materials and Solar Cells, 2012. **96**: p. 93-100.
71. Aydın, A.A. and H. Okutan, *High-chain fatty acid esters of myristyl alcohol with odd carbon number: Novel organic phase change materials for thermal energy storage—2*. Solar Energy Materials and Solar Cells, 2011. **95**(8): p. 2417-2423.
72. Floros, M.C. and S.S. Narine, *Latent heat storage using renewable saturated diesters as phase change materials*. Energy, 2016. **115**: p. 924-930.
73. Raghunanan, L. and S.S. Narine, *Influence of structure on chemical and thermal stability of aliphatic diesters*. The Journal of Physical Chemistry B, 2013. **117**(47): p. 14754-14762.
74. Poopalam, K.D., et al., *Lipid-derived monoamide as phase change energy storage materials*. International Journal of Energy Research, 2019. **0**(0).
75. Poopalam, K.D., et al., *Aliphatic fatty diamide as renewable phase change materials for thermal energy storage*. Journal of Energy Storage, 2021. **42**: p. 102934.
76. Floros, M.C., et al., *Lipid derived diamide phase change materials for high temperature thermal energy storage*. Solar Energy, 2016. **139**: p. 23-28.
77. Reeves, C.J., et al., *The influence of fatty acids on tribological and thermal properties of natural oils as sustainable biolubricants*. Tribology International, 2015. **90**: p. 123-134.
78. Rani, S., M.L. Joy, and K.P. Nair, *Evaluation of physiochemical and tribological properties of rice bran oil – biodegradable and potential base stock for industrial lubricants*. Industrial Crops and Products, 2015. **65**: p. 328-333.
79. Cecilia, J.A., et al., *An Overview of the Biolubricant Production Process: Challenges and Future Perspectives*. Processes, 2020. **8**(3).
80. !!! INVALID CITATION !!! [147, 148].
81. Bouzidi, L., et al., *Lubricating and waxy esters, I. Synthesis, crystallization, and melt behavior of linear monoesters*. Chemistry and Physics of Lipids, 2012. **165**(1): p. 38-50.
82. Bouzidi, L., et al., *Lubricating and waxy esters. 4. Synthesis, crystallization behavior, melt behavior, and flow behavior of linear monoesters incorporating 9-Decenol and 9-Decenoic acid*. Industrial & Engineering Chemistry Research, 2013. **52**(7): p. 2740-2749.
83. Rodrigues Jr, J.d.A., et al., *Correlating chemical structure and physical properties of vegetable oil esters*. Journal of the American Oil Chemists' Society, 2006. **83**(4): p. 353-357.
84. Allen, C.A.W., et al., *Predicting the viscosity of biodiesel fuels from their fatty acid ester composition*. Fuel, 1999. **78**(11): p. 1319-1326.

85. !!! INVALID CITATION !!! [157-160].
86. Padmaja, K.V., et al., *10-Undecenoic acid-based polyol esters as potential lubricant base stocks*. Industrial Crops and Products, 2012. **35**(1): p. 237-240.
87. Li, S., L. Bouzidi, and S.S. Narine, *Lubricating and Waxy Esters. 6. Synthesis and Physical Properties of (E)-Didec-9-enyl Octadec-9-enedioate and Branched Derivatives*. Industrial & Engineering Chemistry Research, 2014. **53**(51): p. 20044-20055.
88. Narine, S., et al., *Esters for use as a base stock and in lubricant applications*. 2014, Trent University.
89. Yasa, S.R., et al., *Synthesis of 10-undecenoic acid based C22-dimer acid esters and their evaluation as potential lubricant basestocks*. Industrial Crops and Products, 2017. **103**: p. 141-151.
90. Abdo, W., et al., *Synthesis and lubricity properties analysis of branched dicarboxylate esters based lubricant*. Malaysian Journal of Analytical Sciences, 2015. **19**: p. 106-117.
91. Abdo, W., J. Salimon, and A. Yarmo, *Lubricity Characterizations of Sebacic Acid Based Ester*. International Journal on Advanced Science, Engineering and Information Technology, 2014. **4**: p. 01-06.
92. Salimon, J., et al., *Lubricity and Tribological Properties of Dicarboxylic Acid and Oleyl Alcohol Based Esters*. Sains Malaysiana, 2015. **44**: p. 405-412.
93. Raghunanan, L. and S.S. Narine, *Engineering Green Lubricants II: Thermal Transition and Flow Properties of Vegetable Oil-Derived Diesters*. ACS Sustainable Chemistry & Engineering, 2016. **4**(3): p. 693-700.
94. Chen, Y., et al., *Fatty Acid Estolides: A Review*. Journal of the American Oil Chemists' Society, 2020. **97**(3): p. 231-241.
95. Cermak, S.C. and T.A. Isbell, *Synthesis and physical properties of estolide-based functional fluids*. Industrial Crops and Products, 2003. **18**(2): p. 183-196.
96. Schneider, M.P., *Plant-oil-based lubricants and hydraulic fluids*. Journal of the Science of Food and Agriculture, 2006. **86**(12): p. 1769-1780.
97. Zainal, N., et al., *A review on the chemistry, production, and technological potential of bio-based lubricants*. Renewable and Sustainable Energy Reviews, 2018. **82**: p. 80-102.
98. Yalkowsky, S.H. and D. Alantary, *Estimation of Melting Points of Organics*. Journal of Pharmaceutical Sciences, 2018. **107**(5): p. 1211-1227.
99. Mackay, D. and R.S. Boethling, *Handbook of Property Estimation Methods for Chemicals: Environmental Health Sciences*. 2000: CRC Press.
100. Oae, S., *Organic Chemistry of Sulfur*. 2012: Springer US.
101. Waterhouse, A.L., G.L. Sacks, and D.W. Jeffery, *Understanding Wine Chemistry*. 2016: Wiley.
102. Wen, Y.-C., H.-C. Kuo, and H.-W. Jia, *Multinuclear NMR spectroscopy for differentiation of molecular configurations and solvent properties between acetone and dimethyl sulfoxide*. Journal of Molecular Structure, 2016. **1109**: p. 154-160.
103. Clark, T., et al., *Why are dimethyl sulfoxide and dimethyl sulfone such good solvents?* J. Mol. Model., 2008. **14**(8): p. 689-697.

104. Reuter, H., *Structural parameters of dimethyl sulfoxide, DMSO, at 100 K, based on a redetermination by use of high-quality single-crystal X-ray data.* Acta crystallographica. Section E, Crystallographic communications, 2017. **73**(Pt 10): p. 1405-1408.
105. Rudolph, F.A.M., et al., *The X-ray Structures of Sulfones.* Journal of Chemical Crystallography, 2010. **40**(3): p. 253-265.
106. Clark, T., et al., *Why are dimethyl sulfoxide and dimethyl sulfone such good solvents?* Journal of Molecular Modeling, 2008. **14**(8): p. 689-697.
107. Rubinshtein, I.A. and E.P. Sobolev, *Antioxidant properties of organic sulfur compounds and criteria for evaluating these properties.* Chemistry and Technology of Fuels and Oils, 1965. **1**(1): p. 59-64.
108. Denison, G.H. and P.C. Condit, *Oxidation of Lubricating Oils.* Industrial & Engineering Chemistry, 1945. **37**(11): p. 1102-1108.
109. Wei, Z., et al., *Paraffin/methyl stearate/multi-walled carbon nanotubes composite phase change materials with wide service temperature and high latent heat.* International Journal of Energy Research, 2021. **45**(9): p. 13636-13645.
110. Sullivan, P.K., *Solid-Phase Behavior of Several Long-Chain n-Paraffins, Esters, and a Ketone.* Journal of research of the National Bureau of Standards. Section A, Physics and chemistry, 1974. **78A**(2): p. 129-141.
111. Hua, J., et al., *Preparation and thermal reliability of N-butyl stearate/methyl palmitate composite phase change material.* Journal of Thermal Analysis and Calorimetry, 2017. **128**(3): p. 1273-1278.
112. Ravotti, R., et al., *Analysis of bio-based fatty esters PCM's thermal properties and investigation of trends in relation to chemical structures.* Applied Sciences, 2019. **9**(2).
113. Floros, M.C., et al., *Lipid derived diamide phase change materials for high temperature thermal energy storage.* Solar Energy, 2016. **139**: p. 23-28.
114. Raghunanan, L. and S.S. Narine, *Engineering Green Lubricants I: Optimizing Thermal and Flow Properties of Linear Diesters Derived from Vegetable Oils.* ACS Sustainable Chemistry & Engineering, 2016. **4**(3): p. 686-692.
115. Sasanuma, Y., Y. Nonaka, and Y. Yamaguchi, *Conformational characteristics and configurational properties of poly(ethylene succinate) and poly(butylene succinate) and structure–property–function relationships of representative biodegradable polyesters.* Polymer, 2015. **56**: p. 327-339.
116. Raghunanan, L., M.C. Floros, and S.S. Narine, *Thermal stability of renewable diesters as phase change materials.* Thermochimica Acta, 2016. **644**: p. 61-68.
117. Li, W.-D. and E.-Y. Ding, *Preparation and characterization of a series of diol distearates as phase change heat storage materials.* Materials letters, 2007. **61**(21): p. 4325-4328.
118. Padley, F.B., J.L. Harwood, and F.D. Gunstone, *The lipid handbook.* 1986: Chapman & Hall.
119. Prabu, S.S. and M. Asokan, *A study of waste heat recovery from diesel engine exhaust using phase change material.* International Journal of ChemTech Research, 2015. **8**: p. 711-717.

120. Papapetrou, M., et al., *Industrial waste heat: Estimation of the technically available resource in the EU per industrial sector, temperature level and country*. Applied Thermal Engineering, 2018. **138**: p. 207-216.
121. Brown, R.J.C. and R.F.C. Brown, *Melting Point and Molecular Symmetry*. Journal of Chemical Education, 2000. **77**(6): p. 724.
122. Yalkowsky, S.H., *Carnelley's Rule and the Prediction of Melting Point*. Journal of Pharmaceutical Sciences, 2014. **103**(9): p. 2629-2634.
123. Vladimir I. Minkin, Osip A. Osipov, and Y.A. Zhdanov, *Dipole moments in organic chemistry*. 2012, Springer, Boston, MA, USA: Springer Science & Business Media.
124. KINNEY, A.J., *DEVELOPMENT OF GENETICALLY ENGINEERED SOYBEAN OILS FOR FOOD APPLICATIONS*. Journal of Food Lipids, 1996. **3**(4): p. 273-292.
125. Ghazani, S.M. and A.G. Marangoni, *Healthy Fats and Oils*, in *Reference Module in Food Science*. 2016, Elsevier.
126. Al-Bachir, M. and H. Sahloul, *Fatty acid profile of olive oil extracted from irradiated and non-irradiated olive fruits*. International Journal of Food Properties, 2017. **20**(11): p. 2550-2558.
127. Alibaba. *High Quality Oleyl Oleate; CAS:3687-45-4; Best Price from China, Factory Hot sale Fast Delivery*. 2021; Available from: <https://www.alibaba.com/product-detail/High-Quality-Oleyl-Oleate>.
128. Zainal, N.A., et al., *A review on the chemistry, production, and technological potential of bio-based lubricants*. Renewable and Sustainable Energy Reviews, 2018. **82**: p. 80-102.
129. Salimon, J., B.M. Abdullah, and N. Salih, *Optimization of the oxirane ring opening reaction in biolubricant base oil production*. Arabian Journal of Chemistry, 2016. **9**: p. S1053-S1058.
130. Mudhaffar, B. and J. Salimon, *Epoxidation of vegetable oils and fatty acids: catalysts, methods and advantages*. Journal of Applied Sciences, 2010. **10**(15): p. 1545-1553.
131. Saurabh, T., et al., *Epoxidation of vegetable oils: a review*. Int. J. Adv. Eng. Technol, 2011. **2**(4): p. 491-501.
132. Yasa, S.R., et al., *Synthesis of 10-undecenoic acid based C22-dimer acid esters and their evaluation as potential lubricant basestocks*. 2017. **103**: p. 141-151.
133. Ahmed, W.A., J. Salimon, and M.A. Yarmo, *Lubricity Characterizations of Sebacic Acid Based Ester*. International Journal on Advanced Science, Engineering and Information Technology, 2014. **4**(1): p. 1-6.
134. Ahmed, W.A., et al., *Synthesis and Lubricity Properties Analysis of Branched Dicarboxylate Esters Based Lubricant*. Malaysian Journal of Analytical Sciences, 2015. **19**(1): p. 106-117.
135. Li, S., L. Bouzidi, and S.S. Narine, *Lubricating and Waxy Esters, V: Synthesis, Crystallization, and Melt and Flow Behaviors of Branched Monoesters Incorporating 9-Decenol and 9-Decenoic Acid*. Industrial & Engineering Chemistry Research, 2014. **53**(31): p. 12339-12354.

136. Raghunanan, L. and S.S. Narine, *Branched Biobased Diesters with Exceptional Low Temperature and Flow Properties for Use in Lubricant Formulations*. ACS Sustainable Chemistry & Engineering, 2016. **4**(5): p. 2542-2549.
137. Bouzidi, L., et al., *Lubricating and Waxy Esters II: Synthesis, Crystallization, and Melt Behavior of Branched Monoesters*. Vol. 51. 2012. 14892–14902.
138. Raghunanan, L. and S.S. Narine, *Engineering Green Lubricants IV: Influence of Structure on the Thermal Behavior of Linear and Branched Aliphatic Fatty Acid-Derived Diesters*. ACS Sustainable Chemistry & Engineering, 2016. **4**(9): p. 4868-4874.
139. Northrop, B.H. and R.N. Coffey, *Thiol–ene click chemistry: Computational and kinetic analysis of the influence of alkene functionality*. Journal of the American Chemical Society, 2012. **134**(33): p. 13804-13817.
140. Bantchev, G.B., et al., *Free Radical Addition of Butanethiol to Vegetable Oil Double Bonds*. Journal of Agricultural and Food Chemistry, 2009. **57**(4): p. 1282-1290.
141. Biresaw, G., G.B. Bantchev, and S.C. Cermak, *Tribological properties of vegetable oils modified by reaction with butanethiol*. Tribology Letters, 2011. **43**(1): p. 17-32.
142. Arukali, S., P.K. V., and P.R.B. N., *Tribology and oxidation studies of fatty acid sulfide derivatives synthesized via thiol-ene “Click” additions*. European Journal of Lipid Science and Technology, 2016. **118**(3): p. 495-502.
143. F., W.J., et al., *Synthesis of Soybean Oil-Based Thiol Oligomers*. ChemSusChem, 2011. **4**(8): p. 1135-1142.
144. Ionescu, M., et al., *Functionalized vegetable oils as precursors for polymers by thiol-ene reaction*. European Polymer Journal, 2015. **67**: p. 439-448.
145. Zhao, Y.H., et al., *Thiol–ene chemistry of vegetable oils and their derivatives under UV and air: a model study by using infrared spectroscopy and mass spectrometry*. RSC Advances, 2017. **7**(6): p. 3343-3352.
146. Montero de Espinosa, L. and M.A.R. Meier, *Plant oils: The perfect renewable resource for polymer science?!* European Polymer Journal, 2011. **47**(5): p. 837-852.
147. Desroches, M., et al., *Synthesis of Biobased Polyols by Thiol–Ene Coupling from Vegetable Oils*. Macromolecules, 2011. **44**(8): p. 2489-2500.
148. Sammaiah, A., K.V. Padmaja, and R.B.N. Prasad, *Tribology and oxidation studies of fatty acid sulfide derivatives synthesized via thiol-ene “Click” additions*. European Journal of Lipid Science and Technology, 2016. **118**(3): p. 495-502.
149. Türünc, O. and M.A. Meier, *Fatty acid derived monomers and related polymers via thiol-ene (click) additions*. Macromolecular rapid communications, 2010. **31**(20): p. 1822-1826.
150. Samuelsson, J., et al., *Thiol–ene coupling reaction of fatty acid monomers*. Journal of Polymer Science Part A: Polymer Chemistry, 2004. **42**(24): p. 6346-6352.
151. Griesbaum, K., *Problems and possibilities of the free-radical addition of thiols to unsaturated compounds*. Angewandte Chemie International Edition in English, 1970. **9**(4): p. 273-287.

2 Chapter 2 Exploiting Aromaticity in Fatty Terephthalate Diesters to Enhance Melting Point and Prevent Polymorphism

2.1 Introduction

Latent heat thermal energy storage (LHTES) exploits the latent heat absorbed or released by a material during a phase transition, typically the solid - liquid transition. Materials used to store latent heat are called phase change materials (PCM). The working temperature for PCMs in LHTES applications is melting point (T_m) and energy storage capacity is determined by melting enthalpy (ΔH_m). The thermal conductivity (κ) of PCMs is also an important parameter as it measures ability of heat to quickly transfer across the material and impacts the time for the phase change to occur. It is desirable for PCMs to melt congruently with sharp phase transitions, crystallize with minimum supercooling, be thermally and chemically stable, non-toxic, non-corrosive, green and inexpensive [1].

There are generally two types of PCMs: (i) organic and (ii) inorganic. Inorganic PCMs are mainly salts and salt hydrates [2]. Salts present T_m between 192 to 1271°C and ΔH_m between 172 to 2678J/g. Salt hydrates present T_m between ~8 to 117°C and ΔH_m between ~115 to 280J/g. Moreover, both salt and salt hydrates typically have κ between ~0.4 to 2.5W/mK [3, 4]. Salt hydrates have inherent undesirable properties such as incongruent phase transition, poor thermal stability, large supercooling and high corrosiveness to metal containers [5-7]. The majority of organic PCMs currently in use

for LHTES are paraffins which are sourced from petroleum. T_m of paraffins with carbon chain length C_1 to C_{400} range from -180°C to 132°C . T_m of the most commercially available paraffins is typically between $\sim 30^\circ\text{C}$ to $\sim 80^\circ\text{C}$. Paraffins also present lower ΔH_m (~ 160 to $\sim 260\text{J/g}$) and limited κ ($\sim 0.25\text{W/m}^\circ\text{C}$) [4, 8] compared to inorganic PCMs. They present much lower T_m (typically ~ 30 to $\sim 80^\circ\text{C}$), lower ΔH_m (~ 160 to $\sim 260\text{J/g}$) and limited κ ($\sim 0.25\text{W/m}^\circ\text{C}$) [4, 8] compared to inorganic PCMs.

Current research on sustainable alternatives to petroleum based PCMs focus on renewable feedstocks and the use of facile and green or benign chemistries to build molecular architectures which would lead to improved and customizable phase change properties. The results obtained with PCMs sourced from lipids and particularly vegetable oils, for example, extend beyond and also compliments what is available from paraffins. The study of aliphatic fatty architectures which include functional groups such as esters [9-25], amides [23, 24, 26-28] and sulfones [29] has allowed access to an array of organic materials with excellent phase change properties. Furthermore, as the present study shows, PCMs derived from vegetable oils have great potential for further improvement.

The present study is a continuation of our work on fatty ester PCMs [20, 22, 23, 30], aimed at mitigating some of the main impediments to improving the phase change properties of ester compounds such as the inherent rotatability of the ester group, which limits required collimation of the crystal types in the solid phase in order to achieve narrow crystallization and melting temperature ranges. As shown in the general chemical

hydrocarbons without ester groups [33, 34]. For example, T_m of methyl octadecanoate ($R=17$ & $R'=1$) which has the ester group positioned towards the end of the aliphatic chain is 13°C higher than that of butyl octadecanoate ($R=17$ & $R'=4$) for which the ester group is positioned more into the aliphatic chain (37°C vs. 24°C) [13, 16].

The presence of a second ester group does improve, although not significantly, the phase change properties. Overall, diesters show slightly higher T_m ($40^\circ\text{C} - 77^\circ\text{C}$) and ΔH_m ($200\text{J/g} - 240\text{J/g}$) [20, 22, 23, 25, 35-38] compared to monoesters ($T_m = 20^\circ\text{C} - 60^\circ\text{C}$ and $\Delta H_m = 150\text{J/g} - 230\text{J/g}$) [9-19]. The presence of a second ester group in the aliphatic chain introduces two inherent undesirable properties (i) intramolecular steric repulsion between the electronic clouds of the ester groups [23] and (ii) directionality which dictates how the two **C–O–C** moieties rotate and affect the aliphatic chain flexibility [22, 39, 40]. The intramolecular steric repulsion can be minimized by increasing the inter-ester chain length m . It has been shown in both diol and diacid diesters that as the two ester groups are further separated, the intramolecular steric repulsion decreases which increases T_m and ΔH_m [22, 23]. T_m and ΔH_m was maximum when the two ester groups are separated apart by an inter-ester chain length of 6 carbons regardless of the fatty chain length [23].

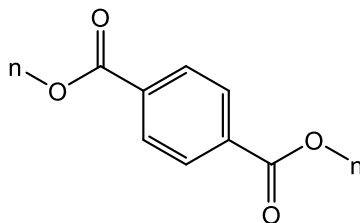
The directionality of the alkoxy group was shown to play a role in the phase change properties [22]. In diol diesters, the **C–O–C** moiety directs rotation “inwards” (curved arrows **Scheme 2-1b**) into the short inter-ester chain segment and leads to better packing efficiency in the crystalline phase, whereas in diacid diesters the **C–O–C** moiety directs

rotation “outwards” (curved arrows **Scheme 2-1c**) into the long aliphatic chain, thereby increasing the probability of coexistence of a larger number of conformational arrangements. The coexistence of several conformational arrangements leads to poorer packing efficiency and tendency of the material to crystallize in less stable polymorphs [22].

The above studies suggests that to further improve on the phase change properties of ester compounds, one needs to simultaneously mitigate ester groups intramolecular steric repulsion and restrain the inherent ester group rotation. In the present work terephthalate diesters (**Scheme 2-2**) which has a benzene ring between the two ester groups instead of a linear inter-ester chain were investigated. It is hypothesized that the presence of the benzene ring between the two ester groups would potentially limit ester groups intramolecular steric repulsion and restrain the ester group rotation by combination of benzene ring π - π intermolecular attraction and resonance stabilization effect. Terephthalate diesters have been used as polymer additives [41-43], grease thickeners [44], ink formulations [45] and plasticizer compositions [46]. However, thermal and crystallographic information on terephthalate diesters is limited, and to the best of our knowledge no research has been conducted on their potential as PCMs for LHTES applications.

To investigate hypothesized benefits of the benzene ring for improving the phase change properties of diesters, four (4) symmetrical aliphatic terephthalate diesters (*n-TA-n*, **Scheme 2-2**) having fatty chain length $n = 12, 14, 16,$ and 18 , namely dodecyl terephthalate (*12-TA-12*), tetradecyl terephthalate (*14-TA-14*), hexadecyl terephthalate

(16-TA-16) and octadecyl terephthalate (18-TA-18) were synthesized and studied in this work.



Scheme 2-2. Structure of the *n*-TA-*n* terephthalate diesters.

The molecular structure and purity of the synthesized *n*-TA-*n* diesters were confirmed using Fourier transformed Infrared Spectroscopy (FT-IR), proton Nuclear Magnetic Resonance (¹H-NMR) and Electrospray Ionization Mass Spectrometry (ESI-MS). Powder X-ray diffraction (XRD) run on samples crystallized at vastly different cooling rates (0.1, 3 and 20°C/min) was used to elucidate crystal structure and gain insights into underlying intermolecular interactions. Thermal stability and thermal transition properties were investigated using Thermogravimetric Analysis (TGA) and Differential Scanning Calorimetry (DSC), respectively.

Terephthalate diesters were compared with diacid diester [22] and diol diester analogues [23] from our previous work to distinguish the role of the aromatic benzene ring in molecular conformation and intermolecular interactions and its effect on polymorphism and phase change properties. The data were used to assess the change in rotatability and flexibility of the alkoxy moiety, and in intramolecular steric repulsion. As in previous studies only thermal stabilities measured by TGA [22] were examined for diacid diesters, in this study four symmetrical saturated aliphatic diacid diesters with fixed $n= 18$ and

varying ($m= 2, 4, 6, 10$) were also synthesized and examined in terms of thermal transition behavior and crystal structure as was done for the n -TA- n compounds, to facilitate direct comparison. The side-by-side studies of 18-TA-18 with 18-6-18 diol and diacid diesters (some information used in our previous studies [22, 23]) allowed for a comparison of the molecular packing efficiency and crystal phase collimation as well as a determination of the mitigation of the flexibility and steric hindrances introduced by the benzene ring.

2.2 Materials and Methods

2.2.1 Materials

Terephthalic acid, octadecanoic acid, ethanedioic acid, butanedioic acid, hexanedioic acid, decanedioic acid, 1-dodecanol, 1-tetradecanol, 1-hexadecanol, and 1-octadecanol, with purities $\geq 98\%$ were purchased from Sigma-Aldrich (Oakville, Ontario Canada) and used as received. The purity of the acetone and anhydrous ethanol was higher than 99%. HPLC grade (99.999%) chloroform (CHCl_3) and methanol (MeOH) were purchased from VWR (Mississauga ON, Canada) and used as received.

2.2.2 Synthesis of the terephthalate diesters

The n -TA- n ($n = 12, 14, 16, 18$) compounds were synthesized via the Fischer esterification reaction between terephthalic acid (TA) and the following linear saturated fatty alcohols: 1-dodecanol ($n= 12$), 1-tetradecanol ($n= 14$), 1-hexadecanol ($n= 16$) and 1-octadecanol ($n= 18$). The synthesis of each terephthalate diester was conducted in a three-neck flask using 2 molar equivalents of fatty alcohol with 1 molar equivalent of

terephthalic acid in a solvent-free reaction without a catalyst. The reaction was carried out at 90°C with constant stirring at 500rpm using a magnetic bar under nitrogen atmosphere. The reaction temperature was maintained for 6 hours to bring the reaction to completion. The crude reaction product was recrystallized with a hot (50-60°C) mixture of acetone and ethanol (1:1 ratio). The recrystallization step was repeated twice and the purified product dried 24 hours in a vacuum oven at 60°C before chemical characterization.

The *18-m-18* ($m = 2, 4, 6, 10$) diacid diesters were synthesized using an established esterification method [22]. In a typical reaction, 2 molar equivalents of 1-octadecanol were added to either ethanedioic acid ($m = 2$), butanedioic acid ($m = 4$), hexanedioic acid ($m = 6$) and decanedioic acid ($m = 10$) in a round bottom flask. Several drops of sulfuric acid were added to the flask as a catalyst, and the reaction mixture was connected to a vacuum line equipped with a solvent trap. The temperature of the reaction was slowly increased to 130°C and the mixture was stirred with a magnetic stir bar at this temperature for 3 hours under vacuum. The reaction mixture was then cooled to room temperature and recrystallized from an acetone/ethanol mixture. Yields were greater than 90%. The purified terephthalate diesters and diacid diesters were white crystals in the solid state and colourless, odourless liquids in the melt. Each reaction was performed once. The purity for all the diesters as determined with triplicates was $> 95 \pm 1.5\%$.

2.2.3 Characterization methods

2.2.3.1 Fourier Transform Infrared Spectroscopy (FTIR)

ATR-FTIR spectra were collected using a Thermo Scientific Nicolet 380 FTIR spectrometer (Thermo Electron Scientific Instruments LLC, USA) with 64 scans collected for each sample over a range of 400 to 4000 cm^{-1} at a spectral resolution of 1 cm^{-1} .

2.2.3.2 Proton nuclear magnetic resonance (^1H NMR)

The molecular structures of the prepared compounds were confirmed by ^1H NMR recorded on a Varian Unity-INOVA at 499.695MHz in CDCl_3 (Agilent Technologies, Santa Clara, CA, USA) with a 1s relaxation delay. The spectra were processed with ACD Labs NMR Processor, version 12.01.

2.2.3.3 Electrospray Ionization - Mass Spectrometry (ESI-MS)

Mass spectra were collected on an API 3000 triple quadrupole Thermo QExactive Orbitrap mass spectrometer (Thermo Fischer Scientific, San Jose, CA) equipped with an electron ion spray (ESI) source in the positive ion mode. The samples (1ppm wt./vol) were prepared using CHCl_3 : MeOH 70:30 (v/v) and analyzed at a resolution of 17,500.

2.2.3.4 Thermogravimetric analysis (TGA)

Thermogravimetric analysis was performed on a TGA Q500 (TA Instruments, Newcastle, DE, USA). The sample (10-15mg) was heated on a platinum pan from room temperature to 600 $^{\circ}\text{C}$ at a rate of 10 $^{\circ}\text{C}/\text{min}$ under a nitrogen flow of 60.0 mL/min . The thermal stability of the terephthalate diesters was characterized by the onset temperature of

degradation (T_{ON}) as determined at 5% of weight loss. The TGA derivative (DTG) and its peak temperature (T_D) were used to assess the weight loss mechanism. The reported TGA values are the mean and standard deviations of triplicates. Note the thermal stability data of the 18-*m*-18 aliphatic diesters were previously published by our group [22].

2.2.3.5 Differential Scanning Calorimetry (DSC)

The thermal transition properties of the compounds were measured using a Q200 DSC (TA Instruments, Newcastle, DE) equipped with a refrigerated cooling system. Samples were processed in hermetic aluminum pans. Each sample (4-6mg) was equilibrated at 150°C for 10min to erase the thermal history, then cooled at a prescribed rate (3 and 20°C/min) down to -90°C, where it was held isothermally for 10min and subsequently heated to 150°C at 10°C/min. Additionally, cooling was carried out at 0.1°C/min within a restricted temperature range. In this case, the samples were cooled to 30°C below their melting temperatures, held isothermally for 10min and subsequently heated to 150°C at 10°C/min. The data was analyzed using the “TA Universal Analysis” software. The reported values are the means and standard deviations of triplicates.

2.2.3.6 Powdered X-Ray Diffraction (XRD)

A PANalytical Empyrean X-ray diffractometer (XRD) equipped with Cu-K α radiation ($\lambda = 0.1542\text{nm}$, 45kV and 40mA) and a PIXcel^{3D} detector (PANalytical B.V., Lelyweg, The Netherlands) was used to elucidate the crystal structure of the compounds. In order to allow for comparison, each sample was crystallized following the DSC crystallization protocols (20, 3, and 0.1°C/min) in a temperature-controlled stage (Linkam LS 350, Linkam Scientific Instruments, Tadworth, Surrey, UK). The crystallized samples were

loaded into #50 glass capillary tubes (Hampton Research, California USA) and measured at room temperature. The XRD patterns were recorded between 0.2° and 70° (2θ) in 0.013° steps, with 200s intervals. The procedure was automated and controlled by the PANalytical's Data Collector (V 3.0c) software.

The XRD data provide information on the cross-sectional packing of the fatty chain. Bragg's short d-spacing allows to distinguish the crystal subcell structure and the Bragg's long d-spacing allows access to the packing of the molecules along the direction normal [47]. XRD data are typically presented in two 2θ -regions: the wide-angle scattering (WAXD) region which 2θ is generally $>15^\circ$ and the small-angle scattering (SAXD) region which 2θ is generally $<15^\circ$.

The analysis of the XRD data was performed according to the literature [48-51]. There are three well-known polymorphic forms that occur in fatty acids, esters, and amides: the alpha (α), beta prime (β') and beta (β) polymorphs [24, 26, 29, 37]. These crystal forms generally increase in crystal stability, melting point and density [51]. The α -polymorph is characterized by a very strong reflection at 4.1-4.2Å indicative of a hexagonal subcell structure. The β' -polymorph is characterized with two reflections at 3.8Å and 4.2Å indicative of an orthorhombic subcell arrangement and the β -polymorph is characterized with strong reflections at 3.6Å, 3.8Å and 4.6Å along with other small peaks of a triclinic (or monoclinic, if the angles α and γ are 90°) parallel subcell [47].

A theoretical molecular length (TML) which is taken as the length of the straight chain is compared to the lamellar thickness or "experimental stacking lengths (ESL)" to

determine if the molecules bend in order to stack along the c-axis and form the crystal. The ESL is determined from the SAXD region, which gives the periodical packing of the molecules along the axis normal (c-axis). The lamellar thickness is easily revealed from the SAXD using the horizontal and perpendicular periodicities to determine the angle of tilt and the ESL. The TML is calculated by Pythagorean theorem using standard molecular bond lengths and bond angles, i.e., assuming the molecule is straight. The analysis of the packing structure consists of comparing the ESL to the TML plus a methyl end terrace separation distance (typically 1.5Å). If the ESL equals the TML with the separation distance, then the packing of the molecules is straight. If the ESL is shorter than the molecular packing would necessarily involve bending of the molecules to fit into the experimental packing periodicity.

2.3 Results & Discussion

2.3.1 Chemical characterization

The *n-TA-n* chemical structures of the terephthalate diesters and 18-*m*-18 diacid diesters prepared in this work were confirmed with FT-IR, ¹H NMR, and ESI-MS. The results are provided and briefly discussed in the *Supporting Information (SI)*. The FT-IR, ¹H-NMR and ESI-MS spectra are presented in *SI* in *Fig SI(a)*, *SI(b)* and *Fig S2* respectively. ¹H-NMR and ESI-MS data are provided in *SI* in *Table S1*. Because the chemical characterization of the compounds prepared for the present study is not novel, it is not discussed further.

2.3.2 Thermal stability

TGA and DTG curves of 18-TA-18 are represented in **Figure 2-1a** as an example. The TGA results for the other terephthalate diesters are provided in *SI* in *Fig. S3*. **Figure 2-1b** shows T_{ON} versus molecular mass for the terephthalate diesters and includes previously acquired data for the diol diesters and diacid diesters [22]. Note that all final mass conversions reached at least 99.9%.

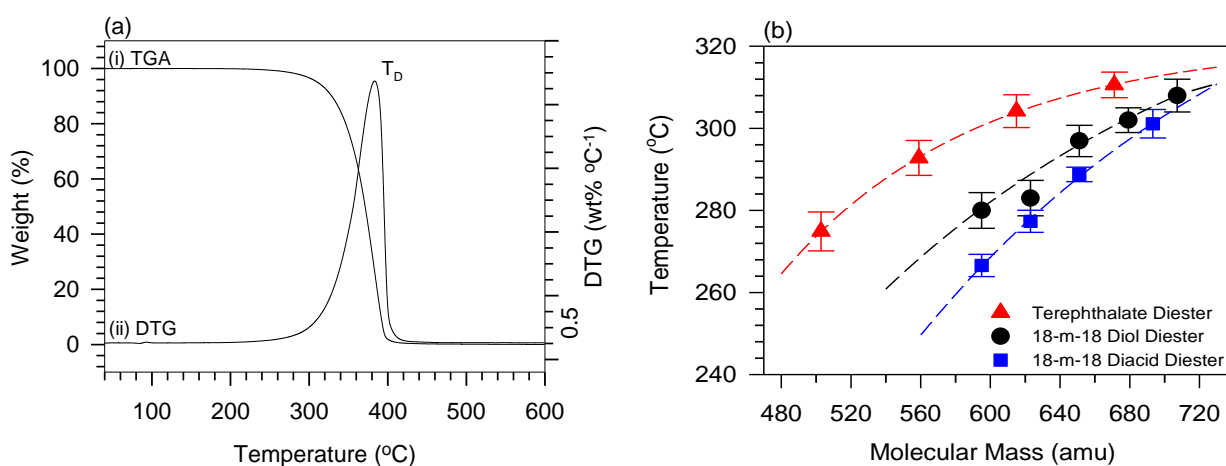


Figure 2-1. (a) TGA and DTG curves of 18-TA-18 and (b) versus molecular mass of the terephthalate diesters (\blacktriangle), diol diesters (\bullet) and diacid diesters (\blacksquare). Dashed lines are fits to exponential rise to a maximum function ($f = y_0 + a(1 - \exp(-x/x_0))$); $R^2 \geq 0.9613$) and serve as guides for the eye. Errors bars are standard deviations from at least three replicates.

DTG of all the terephthalates diesters presented a sharp drop at T_D (**Figure 2-1a**) characteristic of a single-stage mass loss mechanism dominated by evaporation [52]. As expected, T_{ON} of the terephthalate diesters (\blacktriangle in **Figure 2-1b**) increased with molecular mass following an apparent exponential rise to a maximum function ($f = y_0 + a(1 - \exp(-x/x_0))$), $R^2 \geq 0.9999$ – fit parameters are provided in SI in Table S3). This is understandable as larger molecules require higher activation energy to evaporate with the limitation of increasing vibrations that take over surface attractions [53].

Figure 2-1b shows that for any given molecular mass, T_{ON} of the terephthalate diesters (\blacktriangle) is higher than T_{ON} of diol diesters (\bullet) which is slightly higher than T_{ON} of diacid diesters (\blacksquare). The difference between T_{ON} of the terephthalate diesters and aliphatic diesters is attributable to the contributions of the benzene ring mainly through the π - π attractions which increase the activation energy for evaporation compared to the aliphatic inter-ester chains of the diol and diacid diesters. The relatively small difference in T_{ON} between the diol diesters and the diacid diesters is attributable to the difference in the direction of their alkoxy moieties which increases the rotatability of the aliphatic chain beyond the ester group adding to the molecular flexibility and therefore requiring lower activation energy for evaporation.

One can note in **Figure 2-1b** that as the molecular mass increases, the gap in T_{ON} between the terephthalate diesters, diol diester and diacid diesters decreases and converges toward the same plateau (320°C). The convergence occurs because of mass

transfer limitation effect [54]. The probability of the aliphatic chain to exist in higher number of conformational arrangements increases with increasing chain length, resulting in decreasing dispersion forces and increasing entropy which limit the thermal stability [54].

2.3.3 Thermal transition properties

The DSC cooling and heating curves (both at 3°C/min) of the terephthalate diesters are presented in **Figure 2-2a** and **b**, respectively. The corresponding thermal data are presented in **Table 2-1**. The thermal transition data of the diacid diesters also collected in the present work are provided in *SI* in *Fig S4* and *Table S3*. The thermal transition behavior of the terephthalate diesters is characterized by strong and narrow single exotherms on cooling (**Figure 2-2a**) mirrored by strong and narrow single endotherms on heating (**Figure 2-2b**) indicating the formation and subsequent melting of one crystal phase. Furthermore, T_m and ΔH_m were not significantly affected by cooling rate (**Table 2-1**).

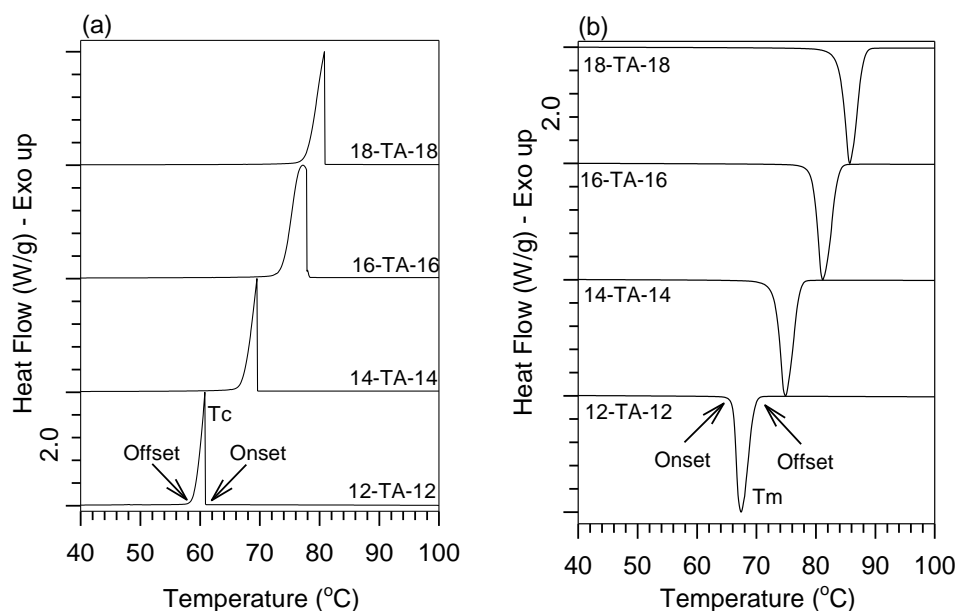


Figure 2-2. (a) Cooling and (b) heating traces (both at 3°C/min) of the terephthalate diesters.

Table 2-1. DSC crystallization and melting results of the terephthalates diesters. Average standard deviation is $\pm 0.5^\circ\text{C}$ for the temperatures and $\pm 5\text{J/g}$ for the enthalpies.

Cooling rate	20.0 °C/min		3.0 °C/min		0.1 °C/min	
	Crystallization					
	T_c (°C)	ΔH_c (J/g)	T_c (°C)	ΔH_c (J/g)	T_c (°C)	ΔH_c (J/g)
12-TA-12	59.3	197	62.4	196	61.6	187
14-TA-14	69.2	209	70.9	206	70.0	207
16-TA-16	73.1	257	76.7	245	76.4	249
18-TA-18	83.0	225	81.3	229	79.2	213

Heating rate	20.0 °C/min		3.0 °C/min		0.1 °C/min	
Melting						
	T_m (°C)	ΔH_m (J/g)	T_m (°C)	ΔH_m (J/g)	T_m (°C)	ΔH_m (J/g)
12-TA-12	67.2	208	67.5	201	67.3	188
14-TA-14	74.7	210	75.0	207	74.5	208
16-TA-16	81.3	260	81.0	253	81.5	253
18-TA-18	85.6	223	85.8	234	85.6	216

The thermal transition data relevant to PCM performance for diol diesters [23, 36, 37], diacid diesters and other linear saturated aliphatic PCMs such as monoamides [26], diamides [24] and sulfones [29] are compared with the terephthalate diesters in **Table 2.2**.

Table 2-2. Supercooling ($T_{on}^m - T_{on}^c$), span of crystallization ($\Delta T^c = T_{on}^c - T_{off}^c$) and span of melting ($\Delta T^m = T_{on}^m - T_{off}^m$) of the terephthalate diesters and other vegetable oil based PCMs.

PCMs	Cooling rate (°C/min)	Supercooling (°C)	Span of crystallization (°C)	Span of melting (°C)	Reference
Terephthalate diesters	0.1	1.4±1.5	2.0±0.8	3.7±0.4	This work
	3.0	2.3±0.8	3.4±0.6	3.9±0.5	
	20.0	5.5±1.0	7.5±0.5	3.7±0.6	
Diol diesters	5.0	4.5±1.5	3.0±2.2	4.0±2.5	[23, 36, 37]
Diacid diesters	0.1	1.3±0.5	1.1±0.4	4.7±0.6	This work
	3.0	2.4±1.8	3.7±0.7	4.4±0.5	
	20.0	5.6±2.8	9.4±2.2	4.7±0.7	
Monosulfones	0.1	1.2±0.5	0.8±0.5	9.1±0.5	[29]
	5.0	1.5±0.4	6.5±0.5	9.2±0.5	
	20.0	2.3±0.5	14.2±0.5	10.0±0.5	
Monoamides	0.1	1.41±0.2	1.1±0.2	4.1±0.4	[26]
	3.0	1.4±0.6	3.3±1.1	5.4±0.8	
	20.0	1.7±1.9	10.3±0.5	4.8±0.8	

PCMs	Cooling rate (°C/min)	Supercooling (°C)	Span of crystallization (°C)	Span of melting (°C)	Reference
Diamides	0.1	0.4±0.4	0.9±0.5	3.7±0.5	[24]
	3.0	0.5±0.4	3.9±0.4	4.2±0.5	
	20.0	2.6±1.5	11.0±2.3	5.3±2.5	

As can be seen in **Table 2-2**, supercooling ($T_{on}^m - T_{on}^c$), which measures the extent at which the PCM remain in the liquid phase below the melting point is small and comparable for all the PCMs listed including the terephthalate diesters, indicating a high rate of nucleation regardless of type and number of functional groups [55]. Also, the spans of crystallization ($\Delta T^c = T_{on}^c - T_{off}^c$) and melting ($\Delta T^m = T_{on}^m - T_{off}^m$) of the terephthalate diesters are relatively small and comparable to those of the aliphatic diesters, monoamides and diamides. ΔT^c and ΔT^m are regarded as essential criteria when selecting PCMs for LHTES applications since they are indicative of the time that the PCM takes to effectively store and release heat at the working temperature [56], without taking into consideration thermal conductivity differences.

T_m and ΔH_m versus fatty chain length (n) of the terephthalate diesters, saturated aliphatic diol diesters [23] and 18-6-18 diacid diester are presented in **Figure 2-3a** and **b**, respectively. The dashed curves in **Figure 2-3a** are fit to an exponential rise to a maximum function. The fit parameters are provided in *SI* in *Table S4*.

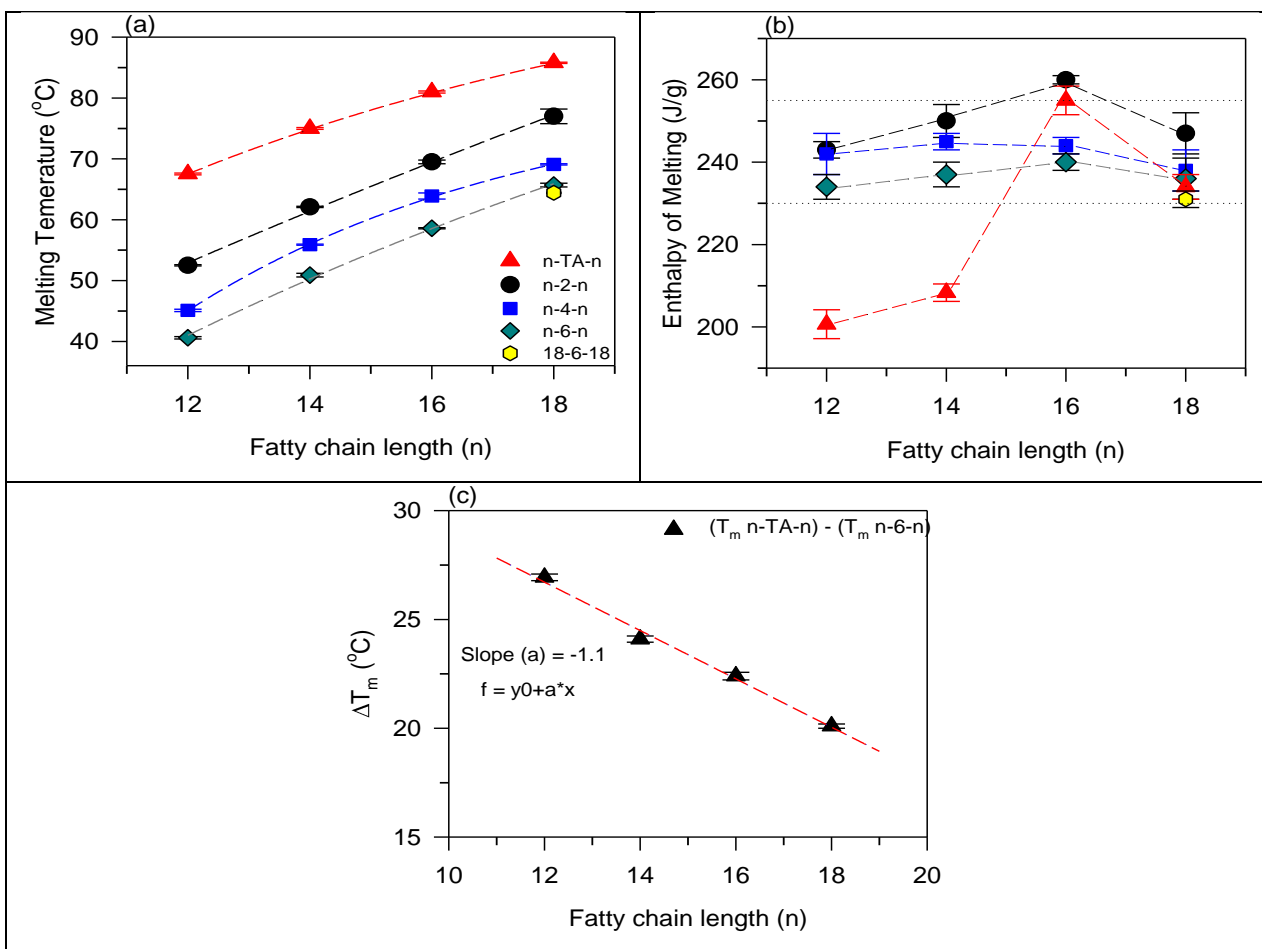


Figure 2-3. Melting (a) Temperature (T_m) and (b) Enthalpy (ΔH_m) versus fatty chain length (n) of the n-TA-n terephthalate diesters (\blacktriangle), n-2-n (\bullet), n-4-n (\blacksquare), n-6-n (\blacklozenge) saturated aliphatic diol diesters, and 18-6-18 diacid diester (\blacklozenge). (c) ΔT_m : difference in T_m between n-TA-n and n-6-n diol diesters. Errors bars are standard deviation of three replicates.

As shown in **Figure 2-3a**, T_m versus n of all the diesters follows an exponential rise to a maximum function ($f = y_0 + a(1 - \exp(x/x_0))$); $R^2 > 0.9977$). **Figure 2-3a** shows that for

any given fatty chain (n fixed), T_m of terephthalate diesters is higher than that of diol diesters and 18-6-18 diacid diester regardless of inter-ester chain length. The higher T_m of the terephthalate diesters compared to the saturated aliphatic diesters is due to the presence of the strong π - π attractions between the benzene rings. The benzene ring inherent quadrupole moment which arises from the π -system positively charges the atoms in the ring, correspondingly leaving a negatively charged electron cloud above and below the ring [57, 58]. When the benzene rings are stacked, their opposite charges interact to form π - π intermolecular forces that are relatively stronger than dispersion forces between fatty aliphatic chains [59-62]. The presence of the benzene ring π - π attraction anchors the diester molecule at the center, preventing high energy molecular conformational arrangements, which can lead to polymorphism in the crystalline phase, to take place. Further, the rigid ring influences the ester groups and the aliphatic chains to uniformly align. The π - π attractions add to the dispersion forces to increase the overall intermolecular attractions in the terephthalate diester compounds [61].

Figure 2-3c shows that the difference in melting point (ΔT_m) between n -TA- n and n -6- n diol diesters decreases linearly with increasing fatty chain length ($R^2 = 0.9910$; slope = -1.1) indicating a consistent loss of stiffness of the aliphatic chain attached to the ring. The data suggest that compared to the aliphatic diesters, the π - π attractions between the planar benzene rings caused a stiffening of the aliphatic chain which reduces the ester group degrees of freedom and number of conformers [61-63].

As can be observed in **Figure 2-3b**, ΔH_m values of the 16-TA-16 and 18-TA-18 terephthalate diesters, diol diesters and 18-6-18 diacid diester are high and in the same range as the aliphatic counterparts ($230-255 \pm 5$ J/g). ΔH_m of 12-TA-12 and 14-TA-14 is lower compared to the other but is higher than 200J/g which is considered as high for PCM applications. The lower ΔH_m for 12-TA-12 and 14-TA-14 when compared with their aliphatic 12-*m*-12 and 14-*m*-14 diol diesters (see **Figure 2-3b** for *m*= 2,4 and 6) can be explained by a simple application of the Gibbs free energy equation at the transition (*Equation 1*) using the data of **Figure 2-3** which shows that their entropy of fusion is much lower than that of their aliphatic counterparts. The low entropy is a confirmation that less aliphatic chain conformational arrangements such as the gauche, anti and eclipse conformations are available and therefore allowing less disordered states [54].

$$T_m = \frac{\Delta H_m}{\Delta S_m} \quad \text{Equation 1}$$

As detailed in section 3.4 below, the XRD reveals that the terephthalates studied here, including 12-TA-12 and 14-TA-14, crystallized in the thermodynamically stable β -polymorph with the fatty segments closest to the ring forced to align, achieving an optimal packing which contributes to high melting temperature and crystal order at the detriment of the enthalpy. As the chain length increases, ΔH_m increases to drop after $n = 16$. This is attributable to a degradation in chain periodicity because for the longer molecules the benzene ring no longer anchors the fatty segments close to the methyl end which increases “disorder” and adversely affects the enthalpy. The effect of the benzene ring on the fatty chains is further discussed in section 3.4.

2.4 Crystal structure elucidation

2.4.1 *Crystal structure of the terephthalate diesters*

The analysis of the XRD of samples cooled at 0.1, 3.0 and 20°C/min indicated that the crystal structure of the terephthalate diesters is not affected by kinetics. The SAXD and WAXD patterns of the samples crystallized at 3°C/min are presented in **Figure 2-4a-b**, respectively. The short d-spacing data are reported in **Figure 2-4a** at the peaks for convenience. The long d-spacing data (Theoretical Stacking Length (TSL) and Experimental Stacking Length (ESL)) is provided in **Table 2-3**. The intensity of the SAXD harmonics is a fingerprint of electronic density and gauge the quality of the periodicity along the axis normal. The cross-sectional packings of the of 18-TA-18 is shown in **Figure 2-4c**. The *010* plane of 18-TA-18 where the π - π attractions [64] occur is highlighted in **Figure 2-4c**.

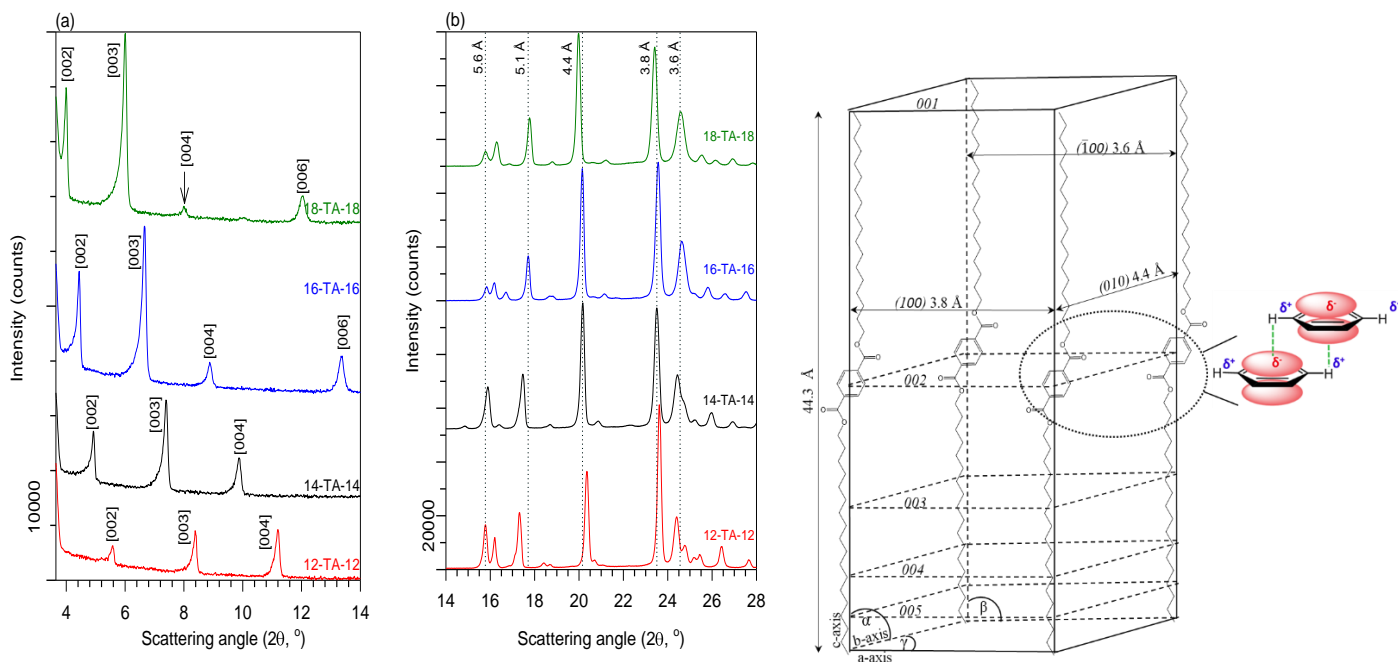


Figure 2-4. (a) SAXD and (b) WAXD spectra of the terephthalate diesters (n-TA-n). (c) Cross-sectional packing of the 18-TA-18.

Table 2-3. Theoretical Staking Length (TSL)* and Experimental Stacking Length (ESL)* of terephthalate diesters.

Compound	Stacking length (Å)	
	ESL (Å)	TSL (Å)
12-TA-12	31.6	37.6
14-TA-14	35.8	43.9
16-TA-16	39.8	50.1
18-TA-18	44.1	56.4

* TSL is calculated for straight molecule, and ESL is determined from SAXD.

The SAXD patterns of the terephthalate diesters (**Figure 2-4a**) indicate periodic stacking along the molecular axis without tilt. ESL is shorter by 4Å than TSL for all the compounds (**Table 2-3**). This indicates a single molecular packing structure in which the fatty chains are arranged in an all-*trans*-zigzag conformation with the planar benzene groups oriented in a parallel-sandwich stack (**Figure 2-4c**). The single molecular packing conformation is also observed in polyethylene terephthalates [61] and polyarylates [65]. The all-*trans*-zigzag type conformation is energetically favored since it minimizes the intramolecular steric repulsion between the two ester groups and the electronic π -cloud of the benzene ring [66, 67]. Additionally, the all-*trans*-zigzag type of conformation confirms the two esters' groups were sufficiently separated apart by the benzene group.

The phase composition of the terephthalate diesters was interpreted from the WAXD data. As shown in **Figure 2-4b**, all the terephthalate diesters exhibited strong and sharp reflections at 4.5-4.4Å and 3.8Å and a relatively medium reflection at 3.6Å which correspond to the (010), (100) and (110) planes, respectively, of the thermodynamically stable β -polymorph in the triclinic parallel subcell structure. The terephthalate diesters triclinic subcell has angles $\alpha \neq \gamma \neq \beta \neq 90^\circ$, and axes $a \neq b \neq c$. This crystal form is directly associated with the phase detected by DSC (T_c and T_m in **Figure 2-2a** and **b**, respectively).

Figure 2-4a show that while the intensity of the second and third SAXD harmonics increases with increasing n , the intensity of the higher harmonics (004 and 006 for example) decreases. This indicates that as the aliphatic chain becomes longer, the periodicity along the direction normal steadily degrades. Similar gradual weakening of

the SAXD reflections with increasing chain length has been reported for alkenes and alkanes [68]. The degradation of the chain periodicity is understandable because as the aliphatic chains become longer, the chains acquire higher conformational arrangements and thus microstates which increases the entropy [54].

2.4.2 *Molecular packing efficiency*

Figure 2-5a-b compare the SAXD and WAXD patterns, respectively, of 18-*TA*-18 terephthalate diester, 18-6-18 diacid diester and 18-6-18 diol diester. The SAXD patterns of these compounds (**Figure 2-5a**) indicate periodical stacking along the molecular axis without tilt similar to 18-*TA*-18 (**Figure 2-5c**). Their cross-sectional packings are shown in **Figure 2-6a-b**.

The SAXD of 18-*TA*-18 showed a high intensity *002*-peak but 18-6-18 diacid diester or 18-6-18 diol diester did not (**Figure 2-6a**). The *002* peak in 18-*TA*-18 indicate the benzene rings are periodically stacked at the center of the aliphatic chain and such periodicity is most likely driven by the benzene ring π - π attraction. The absence of the *002* peak in the 18-6-18 diacid diester or 18-6-18 diol diester confirms that their inter-ester chains are disordered.

The *003* SAXD peak of 18-*TA*-18 was also much stronger compared to the 18-6-18 diacid diester or 18-6-18 diol diester (*003* peaks in **Figure 2-6a**) indicating that the hydrocarbon segments closest to the benzene ring pack more rigidly than those closest to the aliphatic inter-ester chain. This suggests that the π - π attraction which anchors the

center of the aliphatic chain also contributes to aligning the neighboring fatty chain segments in more rigid configurations by restricting their number of conformations. The higher than 003 order harmonics did not show any significant differences indicating similar periodicities for the fatty chain segments close to the methyl ends. This suggests that the effect of the benzene ring on the arrangement of the fatty chains does not extend beyond the third harmonic. The probability to exist in higher conformation for the segment close to the methyl end remains similar to other fatty compounds and much larger than for the fatty chain inner segments [54].

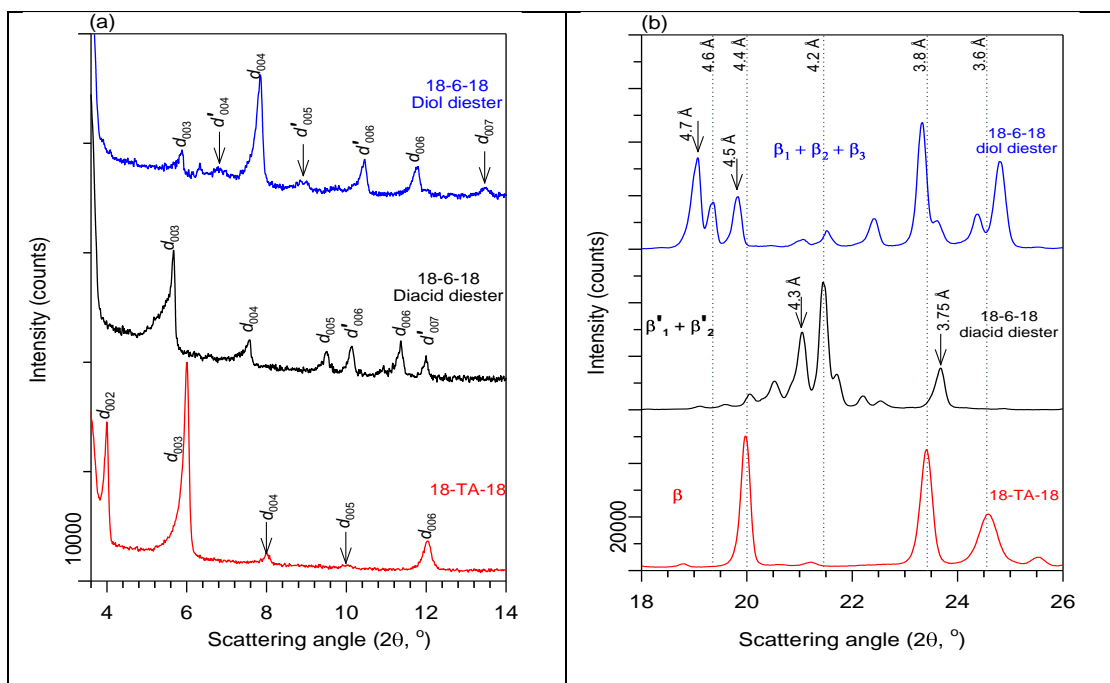


Figure 2-5. (a) SAXD and (b) WAXD patterns of 18-TA-18, 18-6-18 diacid diester and 18-6-18 diol diester

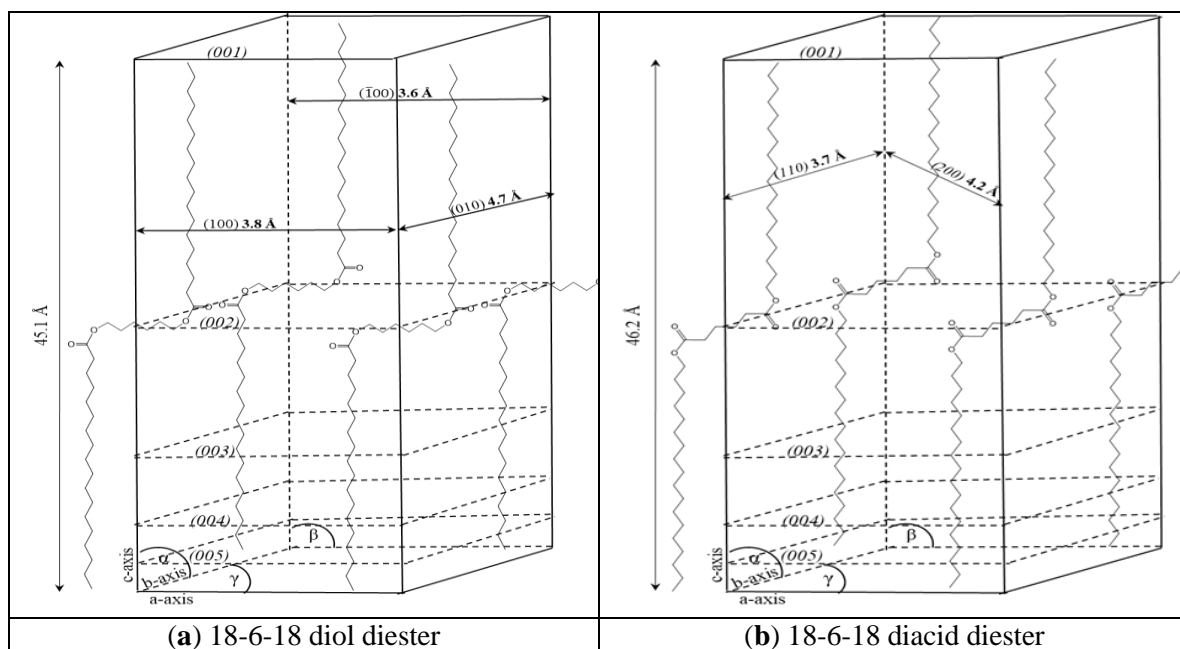


Figure 2-6. Cross-sectional packing of the (a) 18-6-18 diol diester in triclinic subcell and (b) 18-6-18 diacid diester in orthorhombic subcell.

2.4.3 Crystal phase collimation

DSC cooling and melting curves of 18-TA-18, 18-6-18 diacid diester and 18-6-18 diol diester are shown in **Figure 2-7a-b**, respectively. The polymorphism and thermal data of these compounds are shown in **Figure 2-7a-b**, respectively. The polymorphism and thermal data of these compounds are provided in **Table 2-4**. The polymorph(s) which were detected by XRD for 18-TA-18 terephthalate diester, 18-6-18 diacid diester and 18-6-18 diol diester were resolved using the 1st and 2nd derivative of the heat flow signal using the method reported by Bouzidi et al. 2005 [69]. The peak maxima and calculated area of the resolved peaks (which represent T_m and ΔH_m of the successive melting of the phases occurring in the material) were associated with the different polymorphs which were evidenced by XRD according to their successive stability (Ostwald's step rule).

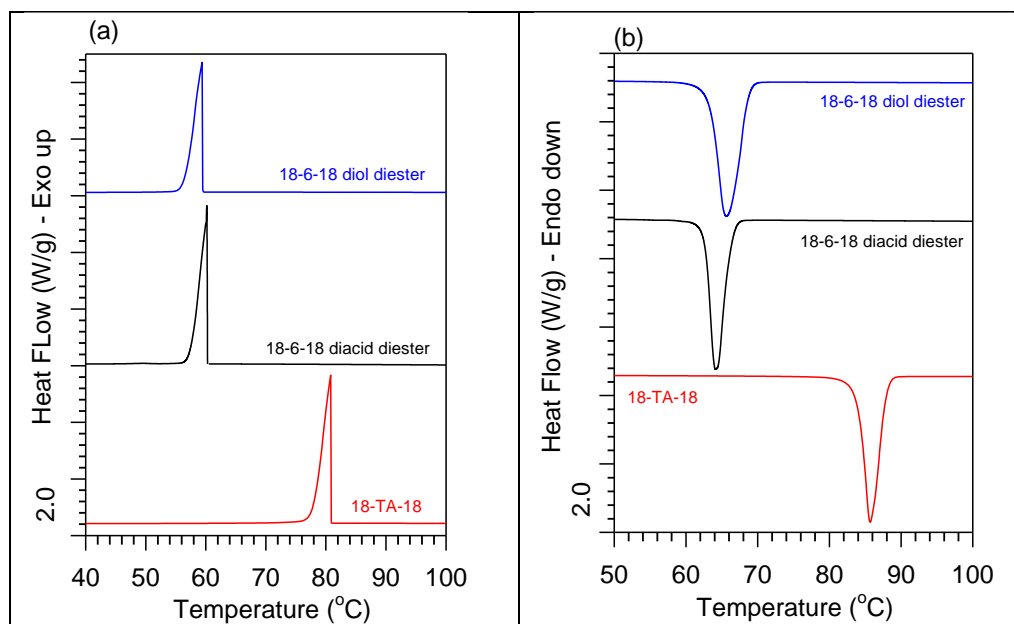


Figure 2-7. (a) cooling and (b) heating curves (both at 3 °C/min) of 18-TA-18, 18-6-18 diacid diester and 18-6-18 diol diester.

Table 2-4. Crystal phase composition and phase change data of 18-TA-18 and 18-6-18 diacid diester and 18-6-18 diol diester with comparable molecular structure. Average standard deviation is $\pm 0.5^{\circ}\text{C}$ for the temperature values and $\pm 5\text{J/g}$ for the enthalpies.

PCM	Polymorph	T_m ($^{\circ}\text{C}$)	ΔH_m (J/g)	ΔS_m ($\text{J/g}^{\circ}\text{C}$)	FWHM ($^{\circ}\text{C}$)	Span of melt ($^{\circ}\text{C}$)	Reference
18-TA-18	β	85.8	234	2.7	2	4.1	This work
18-6-18 Diol diester	β_1	67.5	38	3.6	3.4	5.4	[23]
	β_2	66.1	41				
	β_3	65.2	157				
18-6-18 Diacid diester	β'_1	64.6	104	3.6	2.7	3.6	This work
	β'_2	63.9	128				

The 18-6-18 diacid diester and 18-6-18 diol diester demonstrated polymorphic behavior; in contrast the 18-TA-18 did not (see crystal phase composition in **Table 2-4**). The single polymorph (β) formed by the 18-TA-18 is the most stable crystal phase detected in the diesters and melts 18°C higher than the most stable crystal phases formed by the diol and diacid diesters (see **Table 2-4**). The difference in polymorphism between the diacid and diol diesters is due to the directionality of the ester group which dictates which part of the molecule is rotatable. For instance, the rotatable C–O bond is outwards in diacid diesters and directs rotation to the whole fatty chain (**Scheme 2-1c**) whereas it is inwards in diol diesters and directs rotation into the inter-ester chain (**Scheme 2-1b**). Because of the more restricted rotation, diol diesters pack into more ordered arrangements, forming higher stability polymorphs (β vs. β' in the 18-6-18 compounds for example – see **Table 2-4**).

The thermal data in **Table 2-4** show that the presence of the benzene ring π - π attraction in the 18-TA-18 increased the T_m compared to the saturated aliphatic diesters. The increase in T_m was not mirrored by any significant deviation of ΔH_m which indicates that the entropy of fusion was lower for the 18-TA-18 compared to the 18-6-18 diol and diacid diester. For example, ΔS_m of 18-TA-18 is 25% lower than both that of 18-6-18 diacid and diol diester (**Table 2-4**) which suggests a large reduction in the degrees of freedom. This would only occur if strong constraints were imposed by the benzene ring on molecular mobility, including the rotatability of the ester group.

The ranking of the different crystals formed by diacid and diol diesters in terms of stability and relative amount strongly suggests that the benzene ring affects molecular

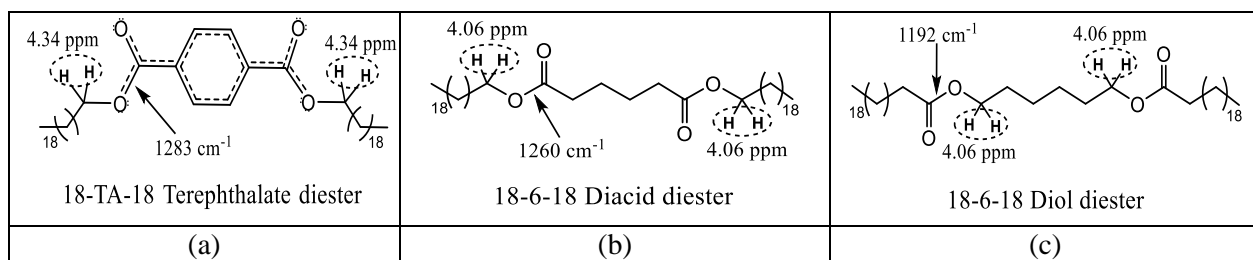
dynamics beyond the ester groups. The differences in the ΔS_m between the terephthalate and the other diesters correlate well with the differences in quality of the periodicity as inferred from the intensity of the SAXD peaks. The thermal and phase composition data is consistent with the SAXD finding in that they also indicate that the benzene ring restrains rotation of the ester group and limits flexibility at least on the fatty segments closest to the functional groups.

2.5 Comparison of Ester group rotational degree of freedom

A deeper look into the $^1\text{H-NMR}$ and FT-IR chemical analysis of the terephthalate diesters, diol diesters and diacid diesters along with theory on the aromaticity of the benzene ring provides insights to support a mechanism involving restraining rotation of the ester group. For comparison, the chemical shifts and characteristic wavenumbers from $^1\text{H-NMR}$ and FT-IR associated with the ester group in *18-TA-18*, *18-6-18* diacid and *18-6-18* diol diesters are shown in **Table 2-5** and illustrated in **Scheme 2-3**.

Table 2-5. $^1\text{H-NMR}$ chemical shifts and FT-IR wavenumbers of *18-TA-18*, *18-6-18* diacid and diol diesters.

Structure (bold)	18-TA-18		18-6-18 diacid diester		18-6-18 diol diester	
$^1\text{H-NMR}$ chemical shift (± 0.1 ppm)						
O=C-O-CH₂-	δ 4.34 ppm		δ 4.06 ppm		δ 4.06 ppm	
FT-IR Wavenumber (± 0.5 cm ⁻¹)						
O=C-O-C stretch	1283 cm ⁻¹	(0.159 ev)	1260 cm ⁻¹	(0.156 ev)	1192 cm ⁻¹	(0.148 ev)



Scheme 2-3. $^1\text{H-NMR}$ chemical shifts and FT-IR wavenumber associated with the ester group for 18-TA-18, 18-6-18 diacid and 18-6-18 diol diesters.

The $^1\text{H-NMR}$ chemical shifts in **Table 2-5** show that 18-TA-18 requires a higher frequency (4.34ppm) than the 18-6-18 diacid diester and 18-6-18 diol diester (4.06ppm for both) to bring the $-\text{O}=\text{C}-\text{O}-\text{CH}_2-$ protons into resonance. This implies the electron density around the adjacent alkoxy oxygen atom in the 18-TA-18 molecule is deshielded relative to the 18-6-18 diacid diester and 18-6-18 diol diester.

A plausible explanation for the deshielding of 18-TA-18 adjacent alkoxy protons in **Scheme 2-3a** is that the alkoxy oxygen electron lone pair is resonating into the conjugated π -system and stabilizes the $\text{C}^+=\text{O}=\text{C}$ resonance bond. Additionally, as shown in **Table 2-5**, $\text{O}=\text{C}-\text{O}-\text{C}$ (bold) alkoxy bond of 18-TA-18 has a higher wavenumber (1283 cm^{-1}) compared to 18-6-18 diacid diester (1260 cm^{-1}) and 18-6-18 diol diester (1192 cm^{-1}) indicating that it requires more energy to be stretched due to its characteristic double bond formed by the resonance effect (**Scheme 2-3a**) [70].

The double bond nature of the alkoxy resonance structure revealed by the $^1\text{H-NMR}$ and FT-IR data is supported by the literature. The two ester groups in terephthalate diesters are known to be electron-withdrawing groups because the carbonyl group can

accommodate lone pairs of electrons while the benzene ring is an electron-donating group [71, 72]. The delocalization of π -electrons in systems comprising a benzene ring and adjacent functional groups capable of accepting π -electrons like aldehydes, ketones, esters and carboxylic groups creates an extended conjugation bridge within the molecule in the vicinity of which resonance energy dramatically increases [73]. For example, the resonance energy which in benzene is 1.62eV increases to 3.09eV in benzoic acid because the π -electrons in the benzene ring flow into the carboxylic group through the extended conjugation [59]. Also, computational studies of polyethylene terephthalate show that due to resonance stabilization, the ester group attached to the benzene ring requires a higher rotational energy (5-8kcal/mol) to undergo torsional rotation at room temperature [62] compared to a typical C–C single bond which requires ~2.9kcal/mol [63]. The concerted electron delocalization immobilizes the rotation of the otherwise easily rotatable C–O–C bond on the ester group by forming a C⁺–O=C double bond which would increase the energy barrier for rotation of the ester group. This stabilization of the C–O–C flexibility causes the stiffening of the fatty chain and increase in molecule rigidity and therefore reduces the degrees of freedom and number of conformers [61-63].

2.6 Conclusions

The potential of benzene rings to improve fatty diester PCM thermal performance was demonstrated to reside in their π - π attractions and resonance effect. Also, the two ester groups were sufficiently separated by the benzene ring and prevented steric repulsion. The benzene ring improved the crystal structure and suppressed the polymorphism shown by the saturated aliphatic diesters. It favored the formation of a much higher stability

crystal form (the β form), and as shown with SAXD, resulted in improvements in the quality of the periodicity in the solid state beyond the middle of the molecule. The benzene ring stabilizing effect manifested by an increased T_m compared to the saturated aliphatic diesters without significant decrease in ΔH_m . This effect is quantified by a much smaller ΔS_m ($> 75\%$) which indicates a dramatic decrease in the number of conformational arrangements and a much lower disorder.

The thermal and crystal structure data are consistent with rotation restraint on the ester group and limit to flexibility on the fatty segments introduced by the benzene group's extended conjugated π -system. The planar benzene ring provided strong π - π intermolecular attractions and high resonance energy that restrained the ester groups, restricted the rotation of the dangling hydrocarbon chains and reduced steric repulsion. $^1\text{H-NMR}$ and FT-IR analysis revealed that the concerted electron delocalization immobilizes the rotation of the otherwise easily rotatable alkoxy C–O–C bond on the ester group by forming a C⁺=O=C bond through resonance. It is suggested to reduce the rotational degree of freedom of the ester group by increasing the energy barrier to rotation. This also causes the stiffening of the fatty chains and hence decrease of the number of conformational arrangements.

On a practical note, the renewability of the feedstock and the solvent and catalyst-free routes to prepare terephthalate diesters further make them very attractive choices for medium temperature TES applications. Additionally, the thermal and crystallographic results generated here can be used to make informed chemical modifications that improve the performance of lipid derived PCMs.

2.7 References

1. Cabeza, L.F., A. Castell, C. Barreneche, A. de Gracia, and A.I. Fernández, *Materials used as PCM in thermal energy storage in buildings: A review*. *Renew Sust Energ Rev*, 2011. **15**(3): p. 1675-1695.<http://dx.doi.org/10.1016/j.rser.2010.11.018>.
2. Soliman, F.S., *Paraffin: an Overview*. 2020: IntechOpen.
3. Hirsche, J., K.R. Gluesenkamp, A. Mallow, and S. Graham. *Review of Inorganic Salt Hydrates with Phase Change Temperature in Range of 5 to 60° C and Material Cost Comparison with Common Waxes*. in *5th International High Performance Buildings Conference at Purdue*. 2018. West Lafayette, Indiana, United States of America.
4. Pielichowska, K. and K. Pielichowski, *Phase change materials for thermal energy storage*. *Progress in Materials Science*, 2014. **65**: p. 67-123.<https://doi.org/10.1016/j.pmatsci.2014.03.005>.
5. Kenisarin, M. and K. Mahkamov, *Salt hydrates as latent heat storage materials: Thermophysical properties and costs*. *Solar Energy Materials and Solar Cells*, 2016. **145**: p. 255-286.<https://doi.org/10.1016/j.solmat.2015.10.029>.
6. Solé, A., L. Miró, C. Barreneche, I. Martorell, and L.F. Cabeza, *Corrosion Test of Salt Hydrates and Vessel Metals for Thermochemical Energy Storage*. *Energy Procedia*, 2014. **48**: p. 431-435.<https://doi.org/10.1016/j.egypro.2014.02.050>.
7. Mohamed, S.A., F.A. Al-Sulaiman, N.I. Ibrahim, M.H. Zahir, A. Al-Ahmed, R. Saidur, B.S. Yilbaş, and A.Z. Sahin, *A review on current status and challenges of inorganic phase change materials for thermal energy storage systems*. *Renewable and Sustainable Energy Reviews*, 2017. **70**: p. 1072-1089.<https://doi.org/10.1016/j.rser.2016.12.012>.
8. Sharma, A., S. Sharma, and D. Buddhi, *Accelerated thermal cycle test of acetamide, stearic acid and paraffin wax for solar thermal latent heat storage applications*. *Energy Conversion and Management*, 2002. **43**(14): p. 1923-1930.[https://doi.org/10.1016/S0196-8904\(01\)00131-5](https://doi.org/10.1016/S0196-8904(01)00131-5).
9. Aydın, A.A. and H. Okutan, *High-chain fatty acid esters of myristyl alcohol with odd carbon number: Novel organic phase change materials for thermal energy storage—2*. *Solar Energy Materials and Solar Cells*, 2011. **95**(8): p. 2417-2423.<https://doi.org/10.1016/j.solmat.2011.04.018>.
10. Aydın, A.A. and A. Aydın, *High-chain fatty acid esters of 1-hexadecanol for low temperature thermal energy storage with phase change materials*. *Solar Energy Materials and Solar Cells*, 2012. **96**: p. 93-100.<https://doi.org/10.1016/j.solmat.2011.09.013>.
11. Alper Aydın, A., *High-chain fatty acid esters of 1-octadecanol as novel organic phase change materials and mathematical correlations for estimating the thermal properties of higher fatty acid esters' homologous series*. *Solar Energy Materials and Solar Cells*, 2013. **113**: p. 44-51.<https://doi.org/10.1016/j.solmat.2013.01.024>.
12. Nikolić, R., M. Marinović-Cincović, S. Gadžurić, and I.J. Zsigrai, *New materials for solar thermal storage—solid/liquid transitions in fatty acid esters*. *Solar*

- Energy Materials and Solar Cells, 2003. **79**(3): p. 285-292.[https://doi.org/10.1016/S0927-0248\(02\)00412-9](https://doi.org/10.1016/S0927-0248(02)00412-9).
13. van Bommel, M.J., H.A.J. Oonk, and J.C. van Miltenburg, *Heat Capacity Measurements of 13 Methyl Esters of n-Carboxylic Acids from Methyl Octanoate to Methyl Eicosanoate between 5 K and 350 K*. Journal of Chemical & Engineering Data, 2004. **49**(4): p. 1036-1042.<https://doi.org/10.1021/jc0499364>.
 14. Agafonova, L.E., R.M. Varushchenko, A.I. Druzhinina, O.V. Polyakova, and Y.S. Kolesov, *Heat capacity, saturation vapor pressure, and thermodynamic functions of ethyl esters of C3–C5 and C18 carboxylic acids*. Russian Journal of Physical Chemistry A, 2011. **85**(9): p. 1516.<https://doi.org/10.1134/s0036024411090020>.
 15. Stamatiou, A., M. Obermeyer, L.J. Fischer, P. Schuetz, and J. Worlitschek, *Investigation of unbranched, saturated, carboxylic esters as phase change materials*. Renewable Energy, 2017. **108**: p. 401-409.<https://doi.org/10.1016/j.renene.2017.02.056>.
 16. Sari, A., A. Biçer, and A. Karaipekli, *Synthesis, characterization, thermal properties of a series of stearic acid esters as novel solid–liquid phase change materials*. Materials Letters, 2009. **63**(13-14): p. 1213-1216.<https://doi.org/10.1016/j.matlet.2009.02.045>.
 17. Ravotti, R., O. Fellmann, N. Lardon, L. Fischer, A. Stamatiou, and J. Worlitschek, *Synthesis and Investigation of Thermal Properties of Highly Pure Carboxylic Fatty Esters to Be Used as PCM*. Applied Sciences, 2018. **8**(7): p. 1069.<https://doi.org/10.3390/app8071069>.
 18. Robustillo, M.D., D.F. Barbosa, A.J.d.A. Meirelles, and P.d.A.P. Filho, *Solid–liquid equilibrium in ternary mixtures of ethyl oleate, ethyl laurate and ethyl palmitate*. Fluid Phase Equilibria, 2013. **339**: p. 58-66.<https://doi.org/10.1016/j.fluid.2012.11.030>.
 19. Ravotti, R., O. Fellmann, N. Lardon, J.L. Fischer, A. Stamatiou, and J. Worlitschek, *Analysis of Bio-Based Fatty Esters PCM's Thermal Properties and Investigation of Trends in Relation to Chemical Structures*. Applied Sciences, 2019. **9**(2).<https://doi.org/10.3390/app9020225>.
 20. Floros, M.C. and S.S. Narine, *Saturated linear diesters from stearic acid as renewable phase change materials*. Materials Letters, 2014. **137**: p. 252-255.<https://doi.org/10.1016/j.matlet.2014.09.041>.
 21. Floros, M.C. and S.S. Narine, *Latent heat storage using renewable saturated diesters as phase change materials*. Energy, 2016. **115**: p. 924-930.<https://doi.org/10.1016/j.energy.2016.09.085>.
 22. Raghunanan, L., M.C. Floros, and S.S. Narine, *Thermal stability of renewable diesters as phase change materials*. Thermochimica Acta, 2016. **644**: p. 61-68.<https://doi.org/10.1016/j.tca.2016.10.009>.
 23. Floros, M.C., K.L.C. Kaller, K.D. Poopalam, and S.S. Narine, *Lipid derived diamide phase change materials for high temperature thermal energy storage*. Solar Energy, 2016. **139**: p. 23-28.<https://doi.org/10.1016/j.solener.2016.09.032>.
 24. Poopalam, K.D., L. Raghunanan, L. Bouzidi, S.K. Yeong, and S.S. Narine, *The anomalous behaviour of aliphatic fatty diamides: Chain length and hydrogen*

- bonding interactions*. Solar Energy Materials and Solar Cells, 2019. **201**: p. 110056. <https://doi.org/10.1016/j.solmat.2019.110056>.
25. Aydın, A.A., *Diesters of high-chain dicarboxylic acids with 1-tetradecanol as novel organic phase change materials for thermal energy storage*. Solar Energy Materials and Solar Cells, 2012. **104**: p. 102-108. <https://doi.org/10.1016/j.solmat.2012.04.030>.
 26. Poopalam, K.D., L. Raghunanan, L. Bouzidi, S.K. Yeong, and S.S. Narine, *Lipid-derived monoamide as phase change energy storage materials*. International Journal of Energy Research, 2019. <https://doi.org/10.1002/er.4711>.
 27. Alkan, C., G. Canik, H. Dunya, and A. Sari, *Synthesis and thermal energy storage properties of ethylene dilauroyl, dimyristoyl, and dipalmitoyl amides as novel solid-liquid phase change materials*. Solar Energy Materials and Solar Cells, 2011. **95**: p. 1203–1207. <https://doi.org/10.1016/j.solmat.2011.01.018>.
 28. Canik, G. and C. Alkan, *Hexamethylene dilauroyl, dimyristoyl, and dipalmytoyl amides as phase change materials for thermal energy storage*. Solar Energy, 2010. **84**. <https://doi.org/10.1016/J.SOLENER.2010.01.016>.
 29. Soodoo, N., L. Raghunanan, L. Bouzidi, and S. Narine, *Phase behavior of monosulfones: Use of high polarity sulfonyl groups to improve the thermal properties of lipid-based materials for PCM applications*. Solar Energy Materials and Solar Cells, 2019. **201**: p. 110115. <https://doi.org/10.1016/j.solmat.2019.110115>.
 30. Tessier, M.J., M.C. Floros, L. Bouzidi, and S.S. Narine, *Exergy analysis of an adiabatic compressed air energy storage system using a cascade of phase change materials*. Energy, 2016. **106**: p. 528-534. <https://doi.org/10.1016/j.energy.2016.03.042>.
 31. Bunn, C.W., *The melting points of chain polymers*. Journal of Polymer Science Part B: Polymer Physics, 1996. **34**(5): p. 799-819. <https://doi.org/10.1002/polb.1996.900>.
 32. Wiberg, K.B. and K.E. Laidig, *Barriers to rotation adjacent to double bonds. 3. The carbon-oxygen barrier in formic acid, methyl formate, acetic acid, and methyl acetate. The origin of ester and amide resonance*. Journal of the American Chemical Society, 1987. **109**(20): p. 5935-5943. <https://doi.org/10.1021/ja00254a006>.
 33. Acree, W. and J.S. Chickos, *Phase Transition Enthalpy Measurements of Organic and Organometallic Compounds and Ionic Liquids. Sublimation, Vaporization, and Fusion Enthalpies from 1880 to 2015. Part 2. C11–C192*. Journal of Physical and Chemical Reference Data, 2017. **46**(1): p. 013104. <https://doi.org/10.1063/1.4970519>
 34. Chickos, J.S. and G. Nichols, *Simple Relationships for the Estimation of Melting Temperatures of Homologous Series*. Journal of Chemical & Engineering Data, 2001. **46**(3): p. 562-573. <https://doi.org/10.1021/jc0002235>
 35. Raghunanan, L. and S.S. Narine, *Influence of structure on chemical and thermal stability of aliphatic diesters*. The Journal of Physical Chemistry B, 2013. **117**(47): p. 14754-14762. <https://doi.org/10.1021/jp409062k>.

36. Abes, M. and S.S. Narine, *Crystallization and phase behavior of fatty acid esters of 1,3-propanediol: I: Pure systems*. Chemistry and Physics of Lipids, 2007. **149**(1): p. 14-27. <https://doi.org/10.1016/j.chemphyslip.2007.05.001>.
37. Cabus, S., K. Bogaerts, J. Van Mechelen, M. Smet, and B. Goderis, *Monotropic Polymorphism in Ester-Based Phase Change Materials from Fatty Acids and 1,4-Butanediol*. Crystal Growth & Design, 2013. **13**(8): p. 3438-3446. <https://doi.org/10.1021/cg400339z>.
38. Ravotti, R., O. Fellmann, L.J. Fischer, J. Worlitschek, and A. Stamatiou, *Investigation of the Thermal Properties of Diesters from Methanol, 1-Pentanol, and 1-Decanol as Sustainable Phase Change Materials*. Materials, 2020. **13**(4): p. 810. <https://doi.org/10.3390/ma13040810>.
39. Raghunanan, L. and S.S. Narine, *Engineering Green Lubricants I: Optimizing Thermal and Flow Properties of Linear Diesters Derived from Vegetable Oils*. ACS Sustainable Chemistry & Engineering, 2016. **4**(3): p. 686-692. <https://doi.org/10.1021/acssuschemeng.5b01644>.
40. Sasanuma, Y., Y. Nonaka, and Y. Yamaguchi, *Conformational characteristics and configurational properties of poly(ethylene succinate) and poly(butylene succinate) and structure–property–function relationships of representative biodegradable polyesters*. Polymer, 2015. **56**: p. 327-339. <https://doi.org/10.1016/j.polymer.2014.11.003>.
41. Godwin , A.D. and G. Claudius, *Polymer compositions comprising terephthalates*. June 24, 2010, ExxonMobil Chemical Patents Inc. (Baytown, TX): United States.
42. H., W.J. and F.S. A., *Biodegradable packaging film*. June 30, 2008, Kimberly-Clark Worldwide, Inc. (Neenah, WI): United States.
43. Shi, B. and W.H. James, *Film formed from a blend of biodegradable aliphatic-aromatic copolyesters*. Jun 18, 2009, Kimberly-Clark Worldwide, Inc (Neenah, WI): United States.
44. P., N.G., *Lithium complex grease thickener and high dropping point thickened grease*. July 12, 1988, Pennzoil Products Company (Houston, TX): United States.
45. Keoshkerian , B., V.M. Farrugia, J. Eliyahu, G. Sisler, B.A. Esther, and S.V. Drappel, *Phase change ink containing polyester for improved image robustness*. 2014, Xerox Corporation (Norwalk, CT): United States.
46. D, M.B., Y.D. J, and M.E. J, *Ketal esters compounds and uses thereof*. 2017, GFBiochemicals Limited: United States.
47. Marangoni, A.G. and L.H. Wesdorp, *Structure and Properties of Fat Crystal Networks, Second Edition*. Second ed. 2012, New York, USA: Taylor & Francis.
48. Bouzidi, L., S. Li, and S. Narine, *Lubricating and Waxy Esters. VI. Effect of Symmetry about Ester on Crystallization of Linear Monoester Isomers*. Symmetry, 2014. **6**(3): p. 655. <https://doi.org/10.3390/sym6030655>.
49. Boz, E., K.B. Wagener, A. Ghosal, R. Fu, and R.G. Alamo, *Synthesis and Crystallization of Precision ADMET Polyolefins Containing Halogens*. Macromolecules, 2006. **39**(13): p. 4437-4447. <https://doi.org/10.1021/ma0605088>.
50. Gaines, T.W., E.B. Trigg, K.I. Winey, and K.B. Wagener, *High Melting Precision Sulfone Polyethylenes Synthesized by ADMET Chemistry*. Macromolecular

- Chemistry and Physics, 2016. **217**(21): p. 2351-2359.<http://doi.org/10.1002/macp.201600118>.
51. Ghotra, B.S., S.D. Dyal, and S.S. Narine, *Lipid shortenings: a review*. Food Research International, 2002. **35**(10): p. 1015-1048.[https://doi.org/10.1016/S0963-9969\(02\)00163-1](https://doi.org/10.1016/S0963-9969(02)00163-1).
 52. Heym, F., B.J.M. Etzold, C. Kern, and A. Jess, *An improved method to measure the rate of vaporisation and thermal decomposition of high boiling organic and ionic liquids by thermogravimetical analysis*. Phys. Chem. Chem. Phys., 2010. **12**(38): p. 12089-12100.<http://dx.doi.org/10.1039/C0CP00097C>.
 53. Jia, F., S. Wei Guo, F. Qun Chao, and Z. Yi, *A detailed bond stretch model of thermal decomposition*. Mater. Sci. Eng. C, 2014. **62**(1): p. 012020.<http://dx.doi.org/10.1039/C1SM06234D>.
 54. Yalkowsky, S.H. and D. Alantary, *Estimation of Melting Points of Organics*. Journal of Pharmaceutical Sciences, 2018. **107**(5): p. 1211-1227.<https://doi.org/10.1016/j.xphs.2017.12.013>.
 55. Zhang, X.-x., Y.-f. Fan, X.-m. Tao, and K.-l. Yick, *Crystallization and prevention of supercooling of microencapsulated n-alkanes*. Journal of Colloid and Interface Science, 2005. **281**(2): p. 299-306.<https://doi.org/10.1016/j.jcis.2004.08.046>.
 56. Kalnæs, S.E. and B.P. Jelle, *Phase change materials and products for building applications: A state-of-the-art review and future research opportunities*. Energy Buildings, 2015. **94**: p. 150-176.<https://doi.org/10.1016/j.enbuild.2015.02.023>.
 57. Vrbancich, J. and G.L.D. Ritchie, *Quadrupole moments of benzene, hexafluorobenzene and other non-dipolar aromatic molecules*. Journal of the Chemical Society, Faraday Transactions 2: Molecular and Chemical Physics, 1980. **76**(0): p. 648-659.<https://doi.org/10.1039/F29807600648>.
 58. Battaglia, M.R., A.D. Buckingham, and J.H. Williams, *The electric quadrupole moments of benzene and hexafluorobenzene*. Chemical Physics Letters, 1981. **78**(3): p. 421-423.[https://doi.org/10.1016/0009-2614\(81\)85228-1](https://doi.org/10.1016/0009-2614(81)85228-1).
 59. Pauling, L. and J. Sherman, *The Nature of the Chemical Bond. VI. The Calculation from Thermochemical Data of the Energy of Resonance of Molecules Among Several Electronic Structures*. The Journal of Chemical Physics, 1933. **1**(8): p. 606-617.<https://doi.org/10.1063/1.1749335>.
 60. Etzkorn, F.A., *Green Chemistry: Principles and Case Studies*. 2019: Royal Society of Chemistry.
 61. Daubeny, R.D.P., C.W. Bunn, C.J. Brown, and W.L. Bragg, *The crystal structure of polyethylene terephthalate*. Proceedings of the Royal Society of London. Series A. Mathematical and Physical Sciences, 1954. **226**(1167): p. 531-542.<https://doi.org/10.1098/rspa.1954.0273>.
 62. Lautenschlaeger, P., J. Brickmann, J. Van Ruiten, and R.J. Meier, *Conformations and rotational barriers of aromatic polyesters*. Macromolecules, 1991. **24**(6): p. 1284-1292.<https://doi.org/10.1021/ma00006a012>.
 63. Coussensa, B., K. Pierloot, and R.J. Meier, *Conformations and rotational barriers of aromatic polyesters: Part II. Rotational barriers in parahydroxybenzoic acid, polyethylene terephthalate, and small aromatic moieties*. Journal of Molecular

- Structure: THEOCHEM, 1992. **259**: p. 331-344.[https://doi.org/10.1016/0166-1280\(92\)87023-S](https://doi.org/10.1016/0166-1280(92)87023-S).
64. Contakes, S.M., *Host-Guest Chemistry and π - π stacking interactions*. 2021.
 65. Tasaki, M., H. Yamamoto, T. Yoshioka, M. Hanesaka, T.H. Ninh, K. Tashiro, H.J. Jeon, K.B. Choi, H.S. Jeong, H.H. Song, and M.H. Ree, *Crystal structure analyses of arylate polyesters with long methylene segments and their model compounds on the basis of 2-D X-ray diffractions and infrared progression bands*. *Polymer*, 2014. **55**(5): p. 1228-1248.<https://doi.org/10.1016/j.polymer.2014.01.024>.
 66. Pendas, A., S. Shaik, J.J. Novoa, A. Gavezzotti, P. Popelier, J. Contreras-Garcia, E. Arunan, R. Gobetto, A. Bacchi, and P. Politzer, *Intermolecular Interactions in Crystals: Fundamentals of Crystal Engineering*. 2017: Royal Society of Chemistry.
 67. Fu, X.-X., J.-F. Li, and R.-Q. Zhang, *Strong Orbital Interaction in pi-pi Stacking System*. arXiv: Atomic and Molecular Clusters 2016.
 68. Tyagi, O.S., H.S. Bisht, and A.K. Chatterjee, *Phase Transition, Conformational Disorder, and Chain Packing in Crystalline Long-Chain Symmetrical Alkyl Ethers and Symmetrical Alkenes*. *The Journal of Physical Chemistry B*, 2004. **108**(9): p. 3010-3016.<https://doi.org/10.1021/jp027565x>.
 69. Bouzidi, L., M. Boodhoo, K.L. Humphrey, and S.S. Narine, *Use of first and second derivatives to accurately determine key parameters of DSC thermographs in lipid crystallization studies*. *Thermochimica Acta*, 2005. **439**(1): p. 94-102.<https://doi.org/10.1016/j.tca.2005.09.013>.
 70. Klein, D.R., *Organic Chemistry*. 3rd Edition ed. 2017, New York, United States: Wiley.
 71. Carey, F.A. and R.J. Sundberg, *Advanced Organic Chemistry: Part A: Structure and Mechanisms*. 3 ed. 2000: Springer Science & Business Media, 2000.
 72. Scudder, P.H., *Electron Flow in Organic Chemistry: A Decision-Based Guide to Organic Mechanisms*. 2nd Edition ed. 2013: Wiley. 448.
 73. Clayden, J., N. Greeves, and S. Warren, *Organic Chemistry*. Second ed. 2012, New York, USA: Oxford university.

3 Chapter 3 Phase behavior of Monosulfones: Use of High Polarity Sulfonyl Groups to Improve the Thermal Properties of lipid-based materials for PCM applications

3.1 Introduction

Phase change materials (PCM) are characterized by large latent heats during the thermal phase transitions and therefore can be used for the storage and release of thermal energy [1]. PCMs are used to optimize the energy management of buildings [2], in textiles of clothing for better comfort [3], the recovery of waste heat [4], medical hot-cold therapies [5], solar heating systems and greenhouses, and as protective shielding in heat-releasing high-performance electronic equipment [6]. A wide variety of PCMs which exploit solid-liquid phase transitions are available and used in different energy storage applications [7]. These materials are selected based on their melting point, enthalpy of fusion, and thermal conductivity. It is also desirable for such materials to melt congruently, crystallize with minimum supercooling, and be thermally/chemically stable, nontoxic, noncorrosive, green and inexpensive [8]. The lack of one or more of these properties is why organic compounds such as sugars, sugar alcohols and urea are not used in thermal energy storage (TES) applications [9]. Many types of lipid-based compounds have been investigated as potential PCMs. In this regard, fatty acids, their eutectic mixtures, and fatty acid derivatives, such as esters, have received considerable attention [10-17]. For example, mono and diesters have been reported to circumvent typical fatty acid weaknesses such as corrosiveness, poor odor and sublimation during heating while maintaining high latent heat, narrow melting ranges and minimum requirements for super cooling. These compounds are proven to be thermally stable withstanding numerous thermal cycles without loss of performance. Saturated aliphatic lipid-

based oleochemical carbonates [18], alcohols [18], monoamides [19, 20] and ethers [21] have also been studied as low-temperature PCM alternatives to paraffin wax and salt hydrates.

The main shortcoming of current lipid-based PCMs is that they melt at a relatively low temperatures (generally between 25-80 °C), which limits their application in TES systems [8]. Higher temperature lipid-based PCMs can be achieved in principle by increasing the molecular weight through longer saturated fatty chains. However, even long chain (< 38 carbons) lipid based-organic compounds such as fatty acids, fatty amines, fatty alcohols, ethers, esters and monoamides have melting temperatures that are limited to typically around 80 °C [21]. Further, the available chain length for lipid-based PCM syntheses is limited to the most abundant naturally occurring fatty acid, i.e., C₁₈ and its derivatives. The incorporation of polar functional groups within the linear saturated fatty chains can be exploited to increase the intermolecular interactions and consequently the phase change temperature [22, 23]. For instance, 1,6-hexamethylene dioctadecyl diamide possesses a melting temperature of 65 °C which higher than octadecane amide which has the same fatty chain but only one amide functional group [41]. The introduction of functional groups with stronger dipole moments into the fatty chain is expected to further increase the net intermolecular attraction and achieve PCMs with higher phase change temperatures. The sulfonyl functional group is here investigated as an interesting candidate which may be used to achieve lipid-based high melting PCMs.

Sulfones (R₂S=O₂) are known to be the most stable and inert class of organosulfur compounds since the sulfur valence shell is fully occupied and is therefore in the highest possible oxidation state. The central sulfur atom of the sulfones is bonded to two terminal oxygen atoms and two carbon atoms linked to alkyl or aryl R-groups substituents [24]. The net permanent dipole is generated from the two highly electronegative oxygen atoms drawing the electrons away from

the sulfur atom, making it highly electron deficient. The dipole moment generated is known to create four positive and two strongly negative sites. The presence of these positive and negative sites promotes intermolecular electrostatic attractions between the opposite charges on the sulfonyl group [25].

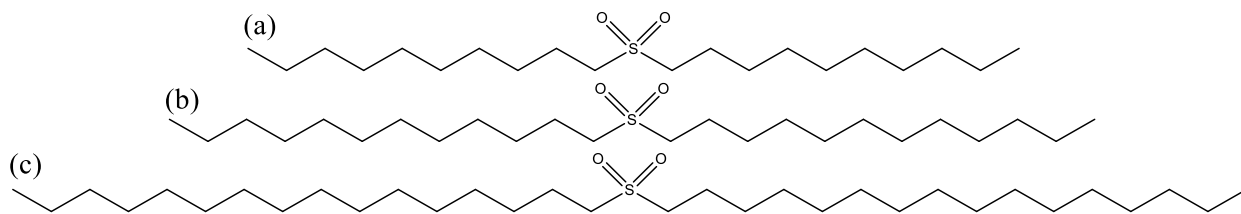
The sulfonyl group is known to have a larger dipole moment compared to the carboxylic, ether, alcohol, ester, ketone, and amide groups. The large dipole moment facilitates intermolecular interactions namely sulfonyl-sulfonyl interactions [25, 26] and hydrogen bonding between the sulfonyl group and adjacent α -hydrogens [27]. The sulfones typically have stronger intermolecular attractions which lead to higher phase change temperatures and enthalpies compared to, for example, esters and amides [25, 28]. For instance, the latent heat of paraffin increased by 25 J/g upon sulfonation due to the formation of hydrogen bonds between sulfonic acid groups [29]. The branched alkyl sulfones are acknowledged as excellent plasticizers [30] while the more complex sulfone molecules are known to possess numerous biological properties[31]. The high thermo-oxidative stability of the biphenylsulfonyl group has been exploited for the preparation of rigid thermoplastic polysulfone polymers [32].

To the best of our knowledge, no research has been conducted on the potential of sulfones for use in PCM applications. Also, systematic thermal and crystallographic information is not available for saturated aliphatic sulfones – knowledge which would help in the design of PCMs based on lipid-derived sulfones.

In the present study, three symmetrical saturated aliphatic sulfones (a) 1-(decylsulfonyl) decane (10-SO₂-10), (b) 1-(dodecylsulfonyl) dodecane (12-SO₂-12) and (c) 1-(octadecylsulfonyl) octadecane (18-SO₂-18) (**Scheme 3-1**) were synthesized and their crystal structure, kinetics of

crystallization and melting and thermal degradation behavior studied in detail. The study was targeted at (i) examining the effect of the sulfonyl group on the crystallization structure and thermal properties of straight chain fatty compounds; (ii) investigating the effect of saturated fatty chain length on the crystal packing and thermal properties of aliphatic sulfones; (iii) evaluating saturated aliphatic sulfones as PCMs for TES applications.

The sulfones were synthesized via the oxidation of n-alkyl sulfides with hydrogen peroxide and confirmed using proton Nuclear Magnetic Resonance (^1H NMR), Fourier Transform Infrared Spectroscopy (FTIR) and Electrospray Ionization Mass Spectrometry (ESI-MS). The thermal stability and thermal transition properties of the sulfones were investigated using Thermogravimetric Analysis (TGA) and Differential Scanning Calorimetry (DSC), respectively. Their crystal structures were elucidated using powder X-ray diffraction (XRD).



Scheme 3-1. Structure of the lipid-based sulfones (n-SO₂-n) synthesized in this work. (a) 10-SO₂-10, (b) 12-SO₂-12 and (c) 18-SO₂-18.

3.2 Materials & Methods

3.2.1 Materials

All materials were purchased from Sigma-Aldrich, Oakville, Ontario Canada and used as received. The purity of decyl sulfide (10-S-10), dodecyl sulfide (12-S-12) and octadecyl sulfide (18-S-18) were higher than 96 %. 30 % hydrogen peroxide (H_2O_2) and glacial acetic acid (AcOH) (99 % purity) were used as the oxidant and catalyst, respectively. Purity of dichloromethane (DCM), anhydrous ethanol (EtOH) and magnesium sulfate was higher than 99 %. All chemicals were used as provided.

3.2.2 Synthesis of the sulfones

The three sulfones ($n\text{-SO}_2\text{-n}$, $n = 10, 12$ and 18) were synthesized via the solvent-free oxidation of the respective fatty sulfides [$n\text{-S-n}$; decyl sulfide ($n=10$), dodecyl sulfide ($n=12$) and octadecyl sulfide ($n=18$)] with H_2O_2 and AcOH. In brief, 4 g (1 M equiv.) of $n\text{-S-n}$ was added to a 25 mL round bottom flask equipped with a reflux condenser placed in an oil bath set to the melting point of the corresponding sulfide. Once the sulfide was melted, 8 mL (2.5 M equiv.) of 30 % H_2O_2 was added dropwise followed by 2 mL of AcOH and the mixture was stirred for a total of 4 h at 550 rpm. The reaction temperature was increased by 20-30 °C to melt the precipitated crystals so as to keep the reaction mixture in the liquid state. After four hours, the reaction was stopped and cooled to room temperature. The obtained white solid was filtered and washed with distilled water (100 mL $\times 10$) and cold anhydrous EtOH (25 mL $\times 2$). The crude $n\text{-SO}_2\text{-n}$ was dissolved in DCM and dried over anhydrous MgSO_4 . The DCM was subsequently removed by rotary evaporation at 60 °C under reduced pressure at a spinning rate of 100 rpm. Next, the product was vacuum filtered and recrystallized from hot anhydrous EtOH (20 mL). Finally, the

n-SO₂-n was filtered and dried in a vacuum oven for 24 hours at 65 °C. Each reaction was run once. The average purity and standard deviation for all the sulfones is $> 96 \pm 1.5 \%$.

3.2.3 Characterization methods

3.2.3.1 Fourier Transform Infrared Spectroscopy (FTIR)

ATR-FTIR spectra were collected using a Thermo Scientific Nicolet 380 FTIR spectrometer (Thermo Electron Scientific Instruments LLC, USA) with 64 scans collected for each sample over a range of 400 to 4000 cm⁻¹ at a spectral resolution of 1 cm⁻¹.

3.2.3.2 Proton nuclear magnetic resonance (¹H NMR)

Molecular structures were confirmed by ¹H NMR recorded on a Varian Unity-INOVA at 499.695 MHz in CDCl₃ (Agilent Technologies, Santa Clara, CA, USA) with a 1 s relaxation delay. The spectra were processed with ACD Labs NMR Processor, version 12.01.

3.2.3.3 Electrospray Ionization - Mass Spectrometry (ESI-MS)

Mass spectra were collected on an API 3000 triple quadrupole Thermo QExactive Orbitrap mass spectrometer (Thermo Fischer Scientific, San Jose, CA) equipped with an electron ionspray source (ESI) in the positive ion mode. Samples (1 ppm wt/vol) were prepared using CHCl₃:MeOH 70:30 (v/v) (HPLC grade; VWR, Mississauga ON, Canada) and analyzed at a resolution of 17500.

3.2.3.4 Thermogravimetric analysis (TGA)

Thermogravimetric analysis was performed on a TGA Q500 (TA Instruments, Newcastle, DE, USA). Samples (10-15 mg) were heated on a platinum pan from room temperature to 600 °C at a rate of 10 °C/min under a nitrogen flow of 60.0 mL/min. The thermal stability of the sulfones

was characterized by the onset temperature of degradation (T_{ON}) determined at 5 % of weight loss. The DTG and its peak temperature (T_D) were used to assess the weight loss mechanism. The TGA measurements were performed in triplicates. The reported TGA values are the mean and standard deviations of these replicates.

3.2.3.5 Differential Scanning Calorimetry (DSC)

The thermal transition properties of the sulfones were measured using a Q200 DSC (TA Instruments, Newcastle, DE, USA) equipped with a refrigerated cooling system. Samples were processed in hermetic aluminum pans. Each sample (4-6 mg) was equilibrated at 150 °C for 10 min to erase the thermal history, then cooled at a prescribed rate (20 and 5 °C/min) down to -90 °C, where it was held isothermally for 10 min and subsequently heated to 150 °C at 10 °C/min. Additionally, cooling was carried out at 0.1 °C/min within a restricted temperature range. In this case the sulfones were cooled to 30 °C below their melting temperatures as cooling further was observed to not provide different results or extra information in terms of phase structure and composition. The DSC measurements were performed at least in triplicates. The reported DSC values are the mean and standard deviations of these replicates.

3.2.3.6 X-Ray Diffraction (XRD)

A Panalytical Empyrean X-ray diffractometer (XRD) equipped with Cu-K α radiation ($\lambda = 0.1542$ nm, 45 kV and 40 mA) and a PIXcel^{3D} detector (PANalytical B.V., Lelyweg, The Netherlands) was used to elucidate the crystal structure of the sulfones. In order to allow for comparison, each sample was crystallized following the DSC crystallization protocols (20, 5 and 0.1 °C/min) in a temperature-controlled stage (Linkam LS 350, Linkam Scientific Instruments, Tadworth, Surrey, UK). Additionally, the samples prepared in the 0.1 °C/min cooling

experiments were reanalyzed after 4 months of storage at room temperature. The crystallized samples were loaded into #50 glass capillary tubes (Hampton Research, California USA) and measured at room temperature. The XRD patterns were recorded between 0.2° and 70° (2θ) in 0.013° steps, with 200 s intervals. The procedure was automated and controlled by the PANalytical's Data Collector (V 3.0c) software.

3.3 Results

3.3.1 Chemical characterization and confirmation of the synthesized compounds

The structures of the sulfones prepared in this work were confirmed from FTIR, ^1H NMR, and ESI-MS. **Figure 3-1a** and **b** show ^1H NMR and FTIR spectra, respectively of 12-S-12 and 12-SO₂-12 - representatives of the present sulfides and sulfones, respectively. The ^1H NMR and ESI-MS data are summarized in **Table 3-1**.

Figure 3-1a shows the FTIR of 12-S-12 and 12-SO₂-12 representatives of the sulfides and sulfones. The five characteristic absorbance wave bands of the aliphatic sulfone are indicated with arrows in **Figure 3-1a** for 12-SO₂-12. As expected, the sp_3 C-H stretching of the C₁₂ methylene chain showed in the wavebands $2850\text{-}3000\text{ cm}^{-1}$ (v in **Figure 3-1a**) and the medium methylene C-H bending absorption peak occurred at 1464 cm^{-1} (iv in **Figure 3-1a**). Moreover, the weak C-S stretching was found at $710\text{-}766\text{ cm}^{-1}$ in both 12-S-12 and 12-SO₂-12 (i in **Figure 3-1a**). The strong symmetrical and asymmetrical O=S=O stretching vibrations were observed at $1077\text{-}1159\text{ cm}^{-1}$ (ii in **Figure 3-1a**) and $1212\text{-}1334\text{ cm}^{-1}$ (iii in **Figure 3-1a**) respectively, confirming the formation of the sulfonyl groups. The absence of the peaks at $1070\text{-}1030\text{ cm}^{-1}$ of the intermediate sulfoxide group (S=O), which forms prior to the sulfonyl group, confirms the completion of the reaction.

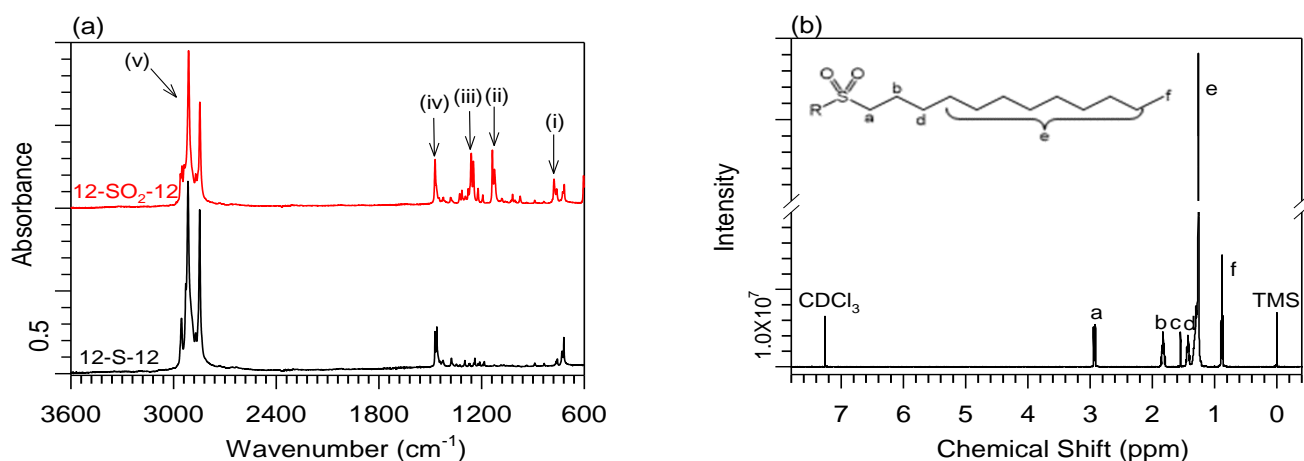


Figure 3-1. (a) FTIR spectra of 12-S-12 and 12-SO₂-12, (i) C-S stretch, (ii) O=S=O sym. stretch, (iii) O=S=O asym stretch, (iv) C-H bending and (v) sp³ C-H stretching; (b) ¹H NMR spectrum of 12-SO₂-12.

Table 3-1. Chemical name, ¹H NMR shifts, and ESI-MS results of the sulfones.

Chemical name	¹ H NMR (δ ppm)	ESI-MS
1-(Decyl sulfonyl) decane (10-SO ₂ -10)	-CH ₃ δ 0.87-0.90 (t, 6H), -CH ₂ - δ 1.26-1.31 (m, 24H), -SO ₂ -CH ₂ - δ 2.92-2.95 (t, 4H), -SO ₂ -CH ₂ -CH ₂ - δ 1.80-1.86 (p, 4H), -SO ₂ -CH ₂ -CH ₂ -CH ₂ - δ 1.41-1.46 (p, 4H)	Monoisotopic Mass = 346.3 g/mol Mass observed [M + Na] ⁺ = 369.3 m/z
1-(Dodecyl sulfonyl) dodecane (12-SO ₂ -12)	-CH ₃ δ 0.87-0.89 (t, 6H), -CH ₂ - δ 1.26-1.31 (m, 32H), -SO ₂ -CH ₂ - δ 2.92-2.95 (t, 4H), -SO ₂ -CH ₂ -CH ₂ - δ 1.80-1.86 (p, 4H), -SO ₂ -CH ₂ -CH ₂ -CH ₂ - δ 1.4-1.45 (p, 4H)	Monoisotopic Mass = 402.4 g/mol Mass observed [M + Na] ⁺ = 425.3 m/z
1-(Octadecyl sulfonyl) octadecane (18-SO ₂ -18)	-CH ₃ δ 0.88-0.90 (t, 6H), -CH ₂ - δ 1.26-1.32 (m, 56H), -SO ₂ -CH ₂ - δ 2.92-2.96 (t, 4H), -SO ₂ -CH ₂ -CH ₂ - δ 1.80-1.87 (p, 4H), -SO ₂ -CH ₂ -CH ₂ -CH ₂ - δ 1.41-1.47 (p, 4H)	Monoisotopic Mass = 570.5 g/mol Mass observed [M + Na] ⁺ = 593.5 m/z

The MS results presented in **Table 3-1** confirm the molecular masses of the sulfones. The ¹H NMR spectra showed all the characteristic protons of the sulfones (labeled a, b, d, e and f in

Figure 3-1b). The protons characteristic of the sulfonyl group were presented at 2.94 ppm (peak a) and 1.83 ppm (peak b) and the spanned methylene chain length bracketed in the molecular structure was presented at 1.26-1.31 ppm (peak e). The terminal methyl protons is confirmed at 0.88 ppm (peak f) the protons on the third carbon atom adjacent to the sulfonyl group at 1.44 ppm (peak d). Peak “c” at 1.55 ppm is from the water present in the CDCl_3 . The purity of the sulfones based on the ratio of the calculated and theoretical methyl protons is higher than 95 %.

3.3.2 Thermal stability

The results of the TGA experiments are represented in **Figure 3-2a** with the weight loss (TGA) and TGA derivative (DTG) curves of 12-SO₂-12 shown. The variation of the onset of degradation (T_{ON}) as determined at 5 % weight loss, and the DTG peak temperature (T_D) versus the number of fatty carbons are presented in **Figure 3-2b**. Errors bars are the calculated standard deviations from at least 3 runs.

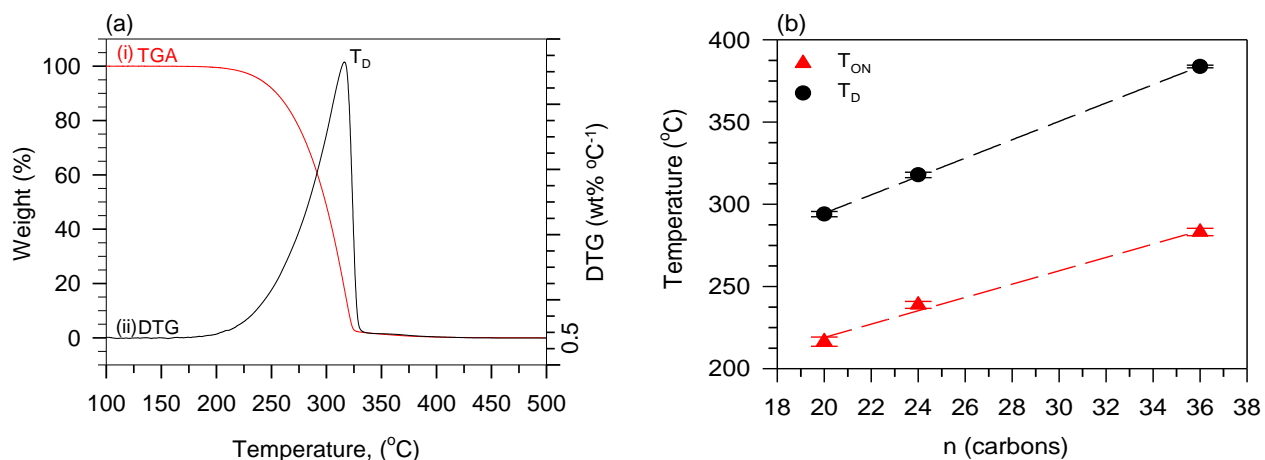


Figure 3-2. (a) TGA and DTG weight loss curves of 12-SO₂-12, (b) 5 % and weight loss temperatures of the sulfones. Dashed lines in (b) are guides for the eye.

The DTG of the sulfones (**Figure 3-2a**) presented asymmetrical shapes typical of materials undergoing weight loss predominantly by evaporation [33]. The apparent linear increase of T_{ON} with chain length (**Figure 3-2b**) indicates a direct correlation between the onset of degradation and fatty acid chain length and hence molecular mass, consistent with the increasing activation energy required to bring the larger molecules into the gaseous state [34]. The almost parallel trend followed by T_D confirms this analysis. The maximum rate of weight loss for the sulfones decreases linearly with the size of the sulfones, also consistent with the mass effect. The rate values measured at T_D versus fatty chain length are provided in *Fig. S1 in the Supporting information (SI)*.

3.3.3 Phase change properties of the sulfones

The DSC cooling and heating traces for the sulfones are presented in **Figure 3-3a** and **b**, respectively, and the corresponding thermal transition data are presented in **Table 3-2**.

Table 3-2. Crystallization and melting results of the sulfones under the 20.0, 5.0 and 0.1 C/min cooling protocols. Standard deviation is > 0.3 °C for the temperatures and > 8 J/g for the enthalpies.

Cooling rate	20.0 °C/min		5.0 °C/min		0.1 °C/min	
	T_{cl} (°C)	ΔH_{cl} (J/g)	T_{cl} (°C)	ΔH_{cl} (J/g)	T_{cl} (°C)	ΔH_{cl} (J/g)
Crystallization results						
10-SO ₂ -10	82.2	208	84.0	215	85.4	205
12-SO ₂ -12	89.3	218	91.1	220	93.4	214
18-SO ₂ -18	98.5	227	103	235	105.1	220
Melting results						
	T_{ml} (°C)	ΔH_{ml} (J/g)	T_{ml} (°C)	ΔH_{ml} (J/g)	T_{ml} (°C)	ΔH_{ml} (J/g)
10-SO ₂ -10	88.8	204	89.7	203	88.9	196
12-SO ₂ -12	96.2	210	96.6	205	96.8	201
18-SO ₂ -18	109.1	218	109.1	223	108.4	219

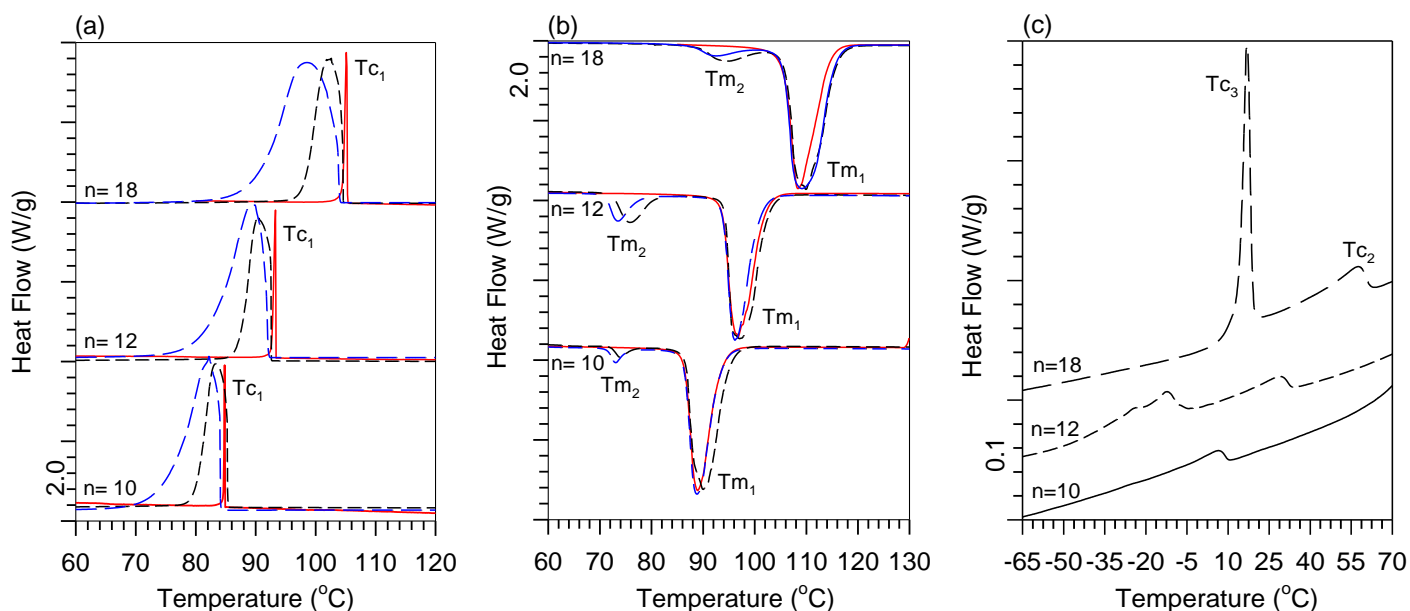


Figure 3-3. (a) crystallization and (b) melting thermograms of the sulfones cooled at 0.1 (red), 5 (black) and 20 °C/min (blue). (c) Zoom into the low temperature regions of the crystallization thermograms of the sulfones cooled at 5 °C/min.

The crystallization of the sulfones is dominated by a strong exotherm (T_{c1} , **Figure 3-3a**) followed by two small crystallization events (**Figure 3-3c**), which make up between 2 to 5 % of the total enthalpy, depending on the size of the molecule and the cooling rate. The heating traces show a single endotherm for the samples run at 0.1 °C/min and two endotherms in the case of those run at 5 and 20 °C/min (T_{m1} and T_{m2} in **Figure 3-3b**). In all cases T_{c1} is close to T_{m1} (5 °C in the case of the samples run at 5 °C/min, for example) indicating that they are closely associated. They are in fact crystallization and melting traces, respectively, of the same phase. The small T_{m2} is associated to the solid-solid transformation of the low temperature metastable phases of the system. These will not be discussed further as they are negligible and inconsequential for the functionality of the materials in TES applications.

The bulk of the crystallization as determined by the width of T_{cl} is complete in less than 1 min in all the cooling experiments (0.1 C/min, 5.0 C/min, 20 C/min). The corresponding melting peak (T_{m1} in **Figure 3-3b**) is also as narrow. The span of crystallization and melting is an important criterion when selecting PCMs since the phase change span is indicative of the ability of a material to efficiently release latent heat at the peak temperature. The sharpness of the crystallization and melting peaks indicates the ability of the material to rapidly release and absorb heat which is important for the performance of TES systems [35]. The sulfones showed a small level of supercooling which is also a desirable property for the storage and release of heat at a fixed temperature.

Figure 3-4a presents the crystallization and melting temperatures (T_{cl}, T_{m1}), and **Figure 3-4b** the enthalpies of crystallization and melting ($\Delta H_{cl}, \Delta H_{m1}$) obtained in the 5 °C/min experiments. Errors bars are standard deviation of at least three runs. One can detect visually in **Figure 3-4a-b** the tendency of T_{cl} , T_{m1} , ΔH_{cl} and ΔH_{m1} to increase towards a plateau as the fatty chain length increases. This is explained by the combination of the increase of dispersion forces between the fatty chains and mass transfer limitations with increasing carbon number.

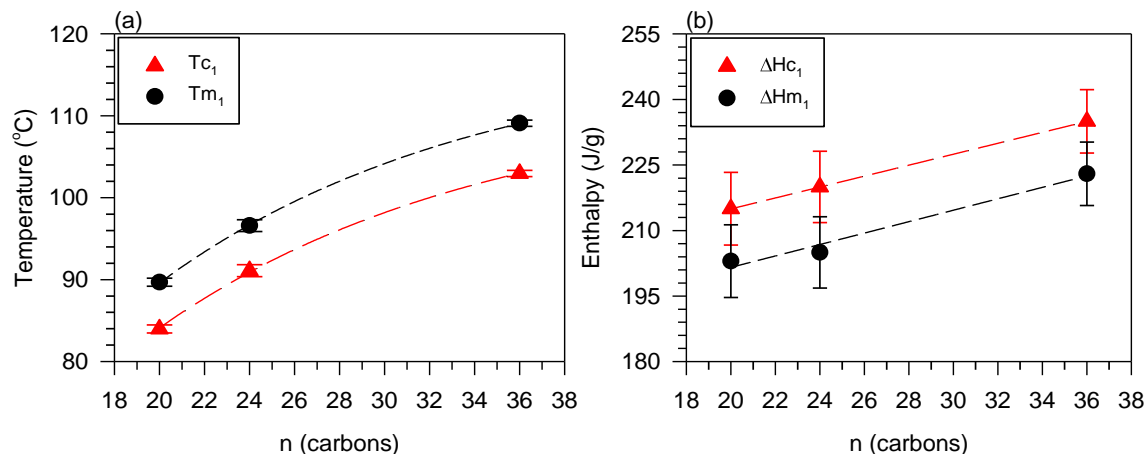


Figure 3-4. Variation of the characteristics of the main crystallization and melting peaks; (a) Temperature (T_{cl} , T_{ml}), (b) enthalpy (ΔH_{cl} , ΔH_{ml}). *Dashed lines are guides for the eye.*

The crystallization data indicate minor kinetic effects. For example, only a small difference (< 3 °C) was recorded for T_{cl} between the very slow cooling (0.1 °C/min) and the fast cooling (20 °C/min) experiments. The melting peak temperature (T_{ml}) was not altered and the enthalpy of melting (ΔH_{ml}) not significantly affected by the crystallization protocol, indicating the absence of kinetic effects. In fact, the dominant crystal phases achieved by the sulfones at all cooling rates are the most stable phases attainable by such thermal protocols.

The crystallization and melting temperatures displayed by the present sulfones for 10-SO₂-10, 12-SO₂-12, and 18-SO₂-18 are: (T_{cl}) = 84, 91 and 103 °C, respectively, and (T_{ml}) = 90, 97, and 109 °C, respectively. The range of phase change temperatures is practically extended by ~ 20 °C. The phase change enthalpies are rather high (196 – 235 J/g) and competitive with commercial salt hydrates [8]. The thermal transition data collected here is promising for the extending and diversifying of the range of current medium temperature lipid based PCMs.

3.3.4 Crystal structure elucidation

The XRD data provide information on the cross-sectional packing of the fatty chain through the Bragg's d-spacings. The Bragg's short d-spacing data are used to distinguish the crystal subcell structure. The Bragg's long d-spacing data allows access to information on the packing of the molecules along the direction normal [36]. XRD data are typically presented in two 2θ -regions: the wide-angle scattering region (WAXD) and the small-angle scattering region (SAXD). For

convenience, we refer to the $2\theta = [1 - 16]^\circ$ range as the SAXD region and to the $[16 - 26]^\circ$ range as the WAXD region.

There are three well-known polymorphic forms that occur in triacylglycerols (TAG), fatty acids, esters and amides: the alpha (α), beta prime (β') and beta (β) polymorphs. These crystal forms generally increase in crystal stability, melting point and density [37]. The least stable α -polymorph fatty chains packs in a hexagonal subcell. This form is characterized by a very strong reflection at 4.1-4.2 Å. The β' -polymorph commonly possesses an orthorhombic subcell arrangement and is characterized with two reflections at 3.8 Å and 4.2 Å, whereas the β -polymorph ordinarily packs in a triclinic (or monoclinic, if the angles α and γ are 90°) parallel subcell and is characterized with strong reflections at 3.7 Å, 3.8 Å and 4.6 Å along with other small peaks [38]. Additionally, there also exists the metastable gamma (γ) polymorph which has a pseudo-orthorhombic subcell packing. The γ -polymorph normally forms through the transformation of the unstable α -polymorph upon heating and can itself irreversibly transform into the more stable β' -and β - polymorphs when cooled further [39]. The γ -polymorph exhibits strong reflections at 3.9 Å and 4.8 Å and medium reflections at 3.6 Å, 4.3 Å and 4.5 Å. The γ -form has been observed for TAGs such as 1,3-distearoyl-2-oleoyl-sn-glycerol (SOS), and oleic acid [40, 41].

3.3.4.1 SAXD results

The SAXD patterns of 10-SO₂-10, 12-SO₂-12 and 18-SO₂-18 are presented in **Figure 3-5a-c**, respectively. The SAXD data (d-spacing and Miller indices, angle of tilt, stacking length) are provided in *Table S1* in the *SI*. **Figure 3-5d** shows the theoretical molecular length of the sulfones and the layer thickness obtained from XRD (experimental stacking length or ESL) as a

function of chain length. The theoretical molecular length is calculated using standard bond lengths and bond angles.

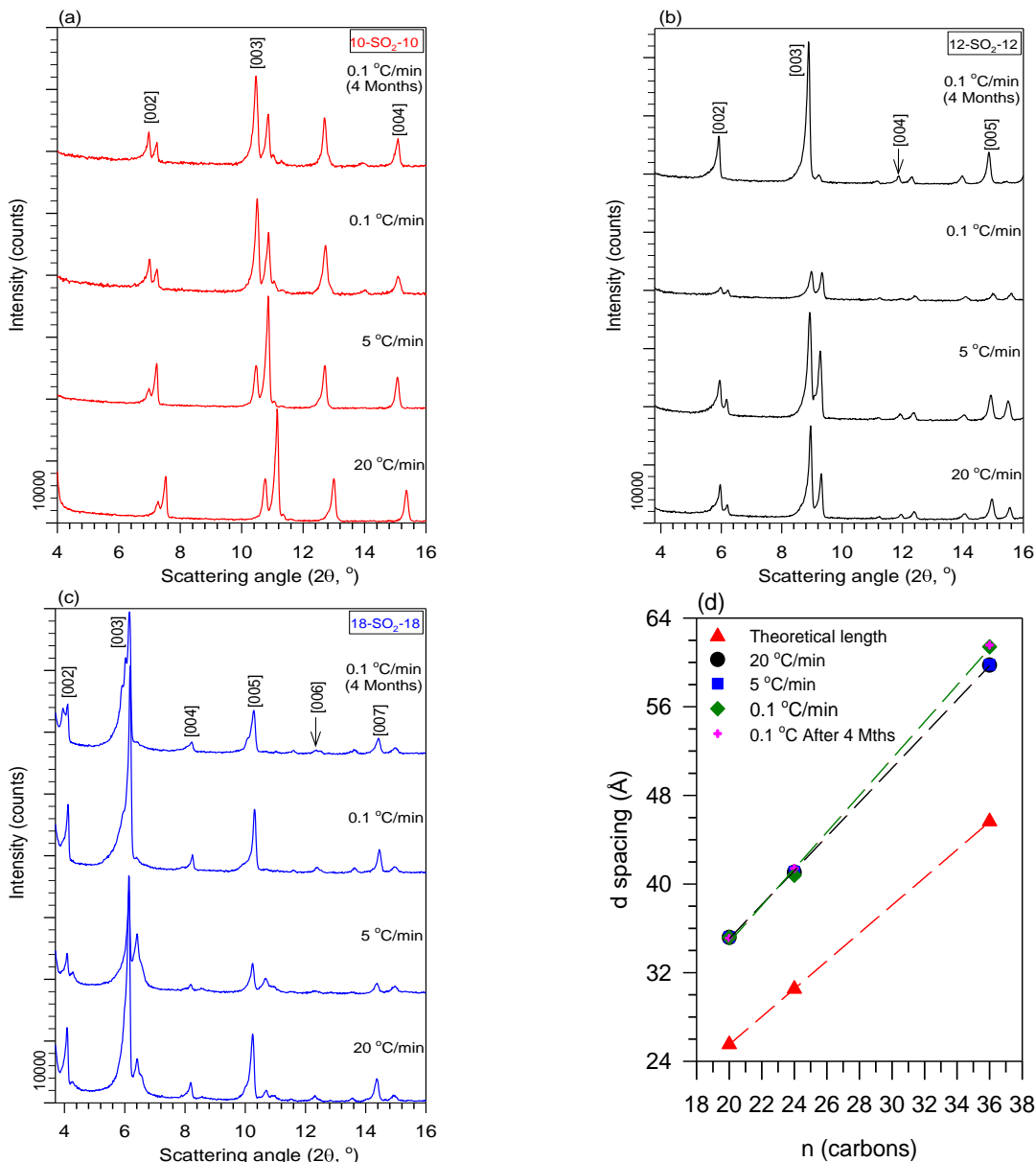


Figure 3-5. SAXD spectra of the sulfones crystals with labelled miller indices (001). (a) 10-SO₂-10, (b) 12-SO₂-12, and (c) 18-SO₂-18. Cooling rates are labelled as 20, 5, 0.1 and, 0.1 °C/min after 4 months. (d) shows the effect of cooling rates on the sulfones ESL.

The fundamental [001] reflection and its following 6 harmonics were observed for both the perpendicular and parallel contributions to the stacking of the sulfones (**Figure 3-5a-c** and *Table S.1 in SI*). The angle of tilt measured for the three sulfones was $\sim 46^\circ$ in all cases, indicating the same methyl-end structure. The SAXD data (**Figure 3-5a-d**) show that the overall molecular stacking structure is not affected by cooling rate nor by long storage at room temperature. However, one can notice a 1.6 Å increase in the ESL of the 18-SO₂-18 sample when cooled very slowly (0.1 °C/min) compared to those cooled more rapidly (20 and 5 °C/min, **Figure 3-5d**), indicating a subtle molecular reorganization along the perpendicular direction. **Figure 3-5d** also reveals that the ESL deviates more from the theoretical length for the larger sulfones.

The packing structure as elucidated by the SAXD data is presented in **Figure 3-6a-c** for 10-SO₂-10, 12-SO₂-12, and 18-SO₂-18 respectively. The data are consistent with a single molecular packing configuration in which single molecules arrange in the layer with the sulfonyl groups sliding past each other. For a distance between two layers approximately equal to the length of a C-C bond (1.5 Å), the adjacent sulfonyl groups are approximately 3.5 Å away from each other for 10-SO₂-10 (**Figure 3-6a**) and 3.7 Å for 12-SO₂-12 (**Figure 3-6b**). For 18-SO₂-18 the adjacent sulfonyl groups are 5.5 Å further from each other (**Figure 3-6c**). This increasing distance between adjacent sulfonyl groups arises from the increasing effect of the dispersion forces between fatty chains with increasing methylene chain electronic density. Therefore, sulfones with longer fatty chain possess stronger dispersion forces and weaker sulfonyl-sulfonyl ($S^{\delta+} \cdots O^{\delta-}$) attractions. The packing arrangement of the sulfones as revealed by the SAXD data (see **Figure 3-6a-c**) is the result of the optimization of these intermolecular attractions. The decrease in the attraction between adjacent sulfonyl groups is in part responsible for the tendency to

plateau observed for the melting point (T_{m1}) and enthalpy of melting (ΔH_{m1}) (see **Figure 3-6a-**

b).

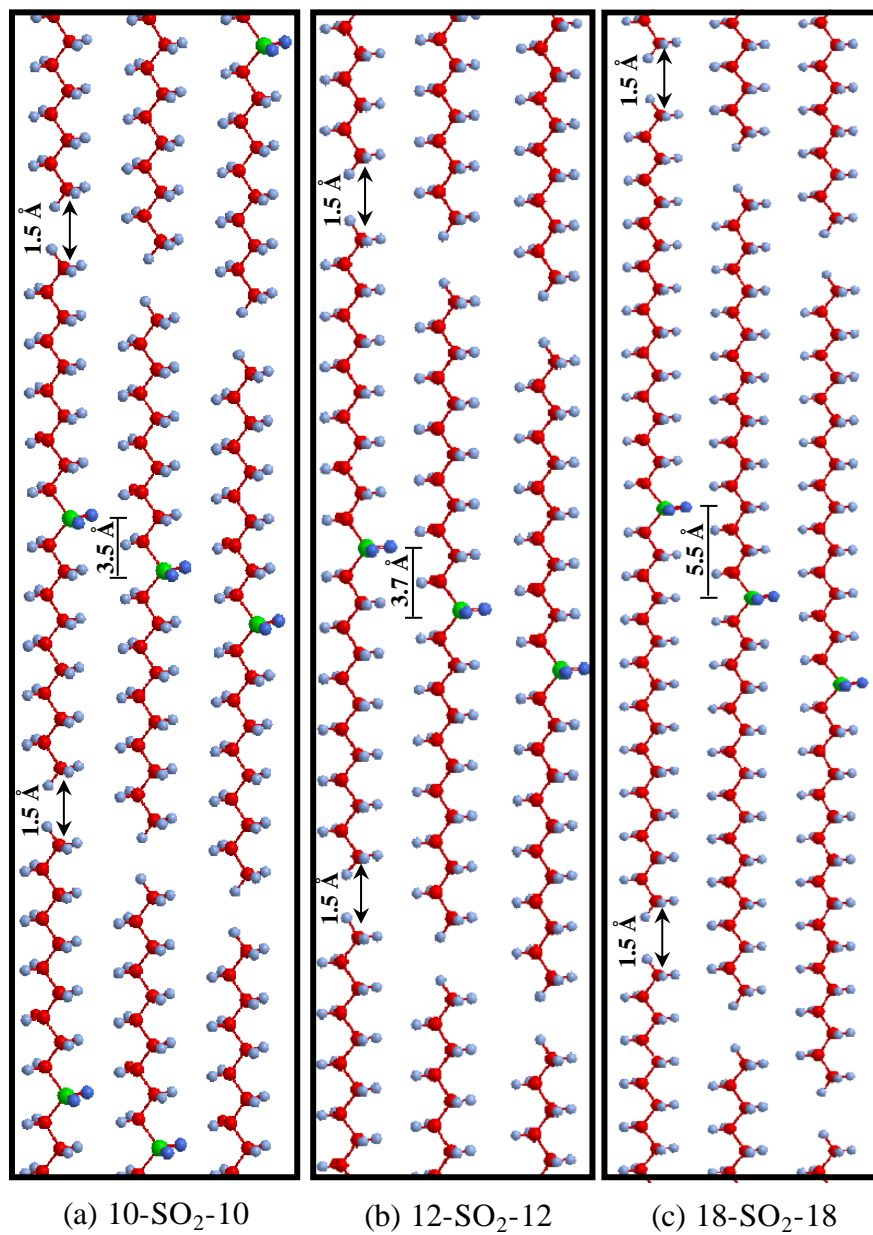


Figure 3-6. XRD long-range c-axis stacking of (a) 10-SO₂-10, (b) 12-SO₂-12, and 18-SO₂-18.

The sulfonyl group (sulfur (yellow) and oxygens (blue)) is shown at the center of the molecule.

3.3.4.2 WAXD results

The WAXD patterns of 10-SO₂-10, 12-SO₂-12 and 18-SO₂-18 are presented in **Figure 3-7a-c** respectively. The phase structures obtained from the WAXD at the different cooling rates are presented in **Table 3-3**. The reported Miller indices and corresponding crystal form identification are mined from the literature [27, 42, 43]. The crystal phase behavior of the sulfones was interpreted from the WAXD Bragg's d-spacings.

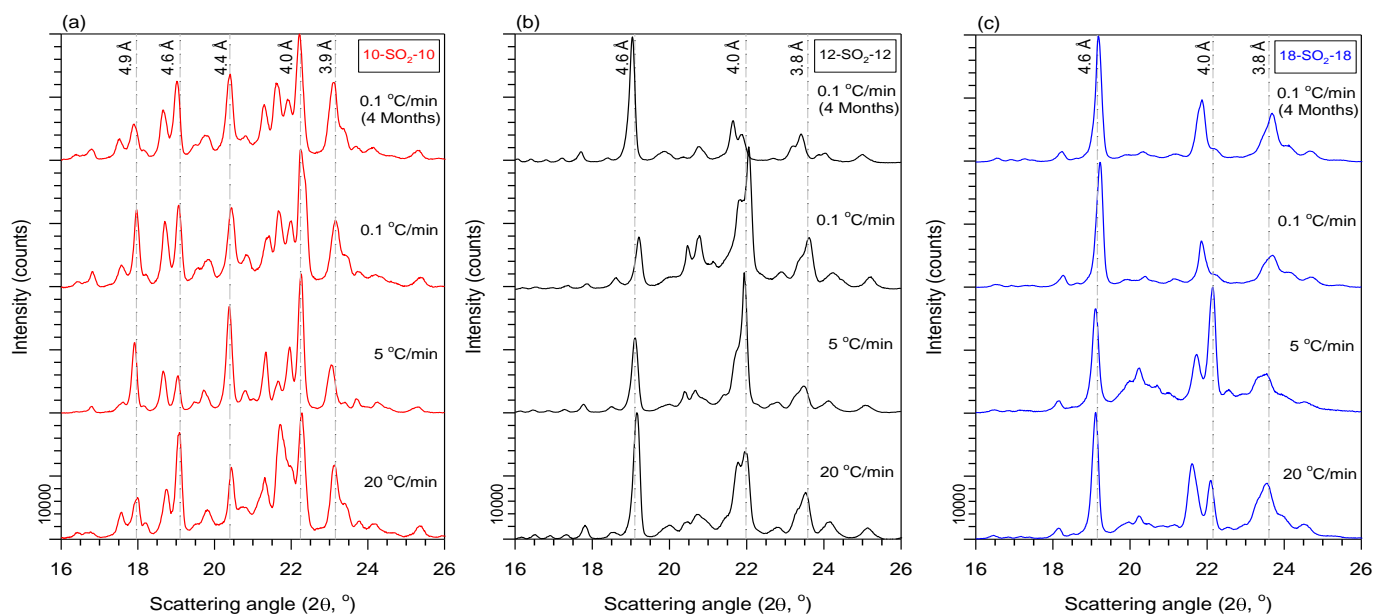


Figure 3-7. WAXD patterns of (a) 10-SO₂-10, (b) 12-SO₂-12, and (c) 18-SO₂-18. The d-spacing values are shown on top of the peaks (vertical lines are guides for the eye).

The thermal treatment is reported on top of the right wing of each pattern (cooling at 20, 5, and 0.1 °C/min and after 4 months at room temperature for the sample cooled at 0.1 °C/min).

Table 3-3. Phase composition of the sulfones and melting temperatures at the various cooling protocols.

Sulfones	20 °C/min	5 °C/min	0.1 °C/min	4 months at 0.1 °C/min
10-SO ₂ -10	γ $T_{m1} = 89$ °C	γ $T_{m1} = 90$ °C	γ $T_{m1} = 90$ °C	γ
12-SO ₂ -12	β $T_{m1} = 96$ °C	β $T_{m1} = 97$ °C	β $T_{m1} = 97$ °C	β
18-SO ₂ -18	β $T_{m1} = 109$ °C	β $T_{m1} = 109$ °C	β $T_{m1} = 109$ °C	β

From **Figure 3-7c** the 18-SO₂-18 WAXD patterns exhibit strong and sharp reflections at 4.6 Å and 4.0 Å and a relatively broad reflection at 3.8 Å. These reflections correspond to the 010, 020 and 200 planes respectively of the thermodynamically stable β -polymorph. This crystal form is therefore associated with T_{cl} (n= 18 in **Figure 3-3a**) whereby the 18-SO₂-18 molecules are tightly packed in the triclinic parallel subcell structure. Correspondingly the melting point $T_{m1} = 109$ °C and enthalpy of melting $\Delta H_{m1} = 223$ J/g (n= 18 in **Figure 3-3a**) are associated with the melting of this β -phase. The cross-sectional packing of the 18-SO₂-18 β -polymorph shown in **Figure 3-8** outlines how the molecules are arranged into the triclinic subcell.

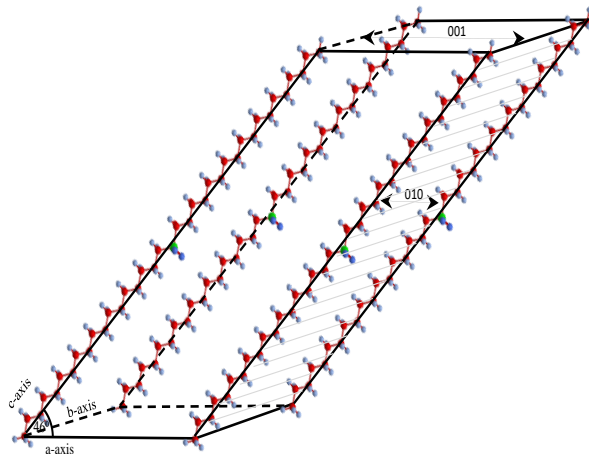


Figure 3-8. Cross-sectional packing of the 18-SO₂-18 polymorph in the triclinic subcell. The shaded region represents the 010 planes containing the sulfonyl groups.

There is a slight tightening (0.03 Å) of the 010 plane at 4.6 Å (**Figure 3-7c**) for the slow cooled 18-SO₂-18. Additionally, a subtle feature can be observed in the WAXD (**Figure 3-7c**) whereby the reflection at 4.0 Å, attributed to the 020 family of planes, is present when fast-cooled (20 and 5 °C/min) but absent when slow-cooled (0.1 °C/min). This indicates a dramatic change in the electronic distribution in this plane. The disappearance of the 020 reflection is associated with the disposition of the oxygen atoms, which comprise the 020 plane, in a way that maximizes the electronic density and extinction of its reflection. This is facilitated via the “face-to-face” configuration of the sulfonyl groups within the stacking unit which results in high electronic densities when the sulfonyl groups are close together and decreased electronic density when the sulfonyl groups “slip” past each other along the c-axis (**Figure 3-8**). The latter is promoted by the slowest cooling only. The “slippage” of the sulfonyl groups of 18-SO₂-18 is also observed from the SAXD with the increase of the ESL as shown in **Figure 3-5d**. The configuration was confirmed after 4 months at room temperature.

The WAXD of 12-SO₂-12 provided similar general crystal structure signatures. It also crystallized in the β -form at all cooling rates and lost the 020 reflection when subjected to isothermal storage for 4 months after crystallization at 0.1 °C/min (**Figure 3-7b**). However, in this case one also observes the weakening of the 010 reflections (4.6 Å peak in **Figure 3-7b**) and the growing of the 020 reflection (at 4.1 Å in **Figure 3-7b**) as the cooling rate is decreased from 20 to 0.1 °C/min, indicating a growing tendency of the sulfone molecules to approach each other along the a-axis (**Figure 3-8**) and of the electronic density between oxygen planes to decrease.

The WAXD of 12-SO₂-12 taken after 4 months of isothermal storage at room temperature recovered the intensity of the 010 reflection and lost the 020-reflection indicating a full relaxation to the configuration where the sulfonyl groups are close but past each other, similar to the configuration of 18-SO₂-18. This suggests that this configuration for the β -form of these two sulfones is the most stable accessible by the non-isothermal and isothermal crystallization protocols used. The β -phase of 12-SO₂-12 is characterized by a melting point of 97 °C and an enthalpy of melting of 205 J/g.

The WAXD of 10-SO₂-10 presented three strong and sharp reflections at 4, 4.4 and 4.9 Å and a medium reflection at 3.8 Å which were independent of cooling rate (**Figure 3-7a**). These peaks are indicative of the γ -form which is a loosely packed pseudo-orthorhombic subcell structure typically documented for fatty acids such as oleic acid [40] and TAGs [39]. The WAXD data of the 10-SO₂-10 sample did not change upon storage of the sample for 4 months at room temperature. Thus, the γ was the only form detected in 10-SO₂-10 regardless of cooling rate and storage and therefore can be considered the most stable phase recorded so far for this compound. The melting temperature of the γ -phase is 90 °C and its enthalpy of melting is 201 J/g.

3.4 Discussion

In this section, the thermal stability and thermal transition properties of the sulfones are compared against those of a variety of analogous linear saturated organic PCMs mined from the literature. The compounds include alkanes (R), fatty acids (R-COOH), fatty alcohols (R-OH), symmetric monoesters (R-COO-R), monoamides (R-CONH-R), ethers (R-O-R), aliphatic diesters and diamides. The influence of the functional groups and molecular geometry is captured and compared to the sulfones' properties and those of monofunctional structures and difunctional structures having similar total chain length. The thermal properties of the PCMs cited here are provided in the *SI* in *Table S2*.

3.4.1 Thermal stability

Figure 3-9a-b show the onset of degradation (T_{ON}) and maximum derivative weight loss temperature (T_D) of the sulfones compared with those of a range of organic compounds mined from the literature [17, 44-48].

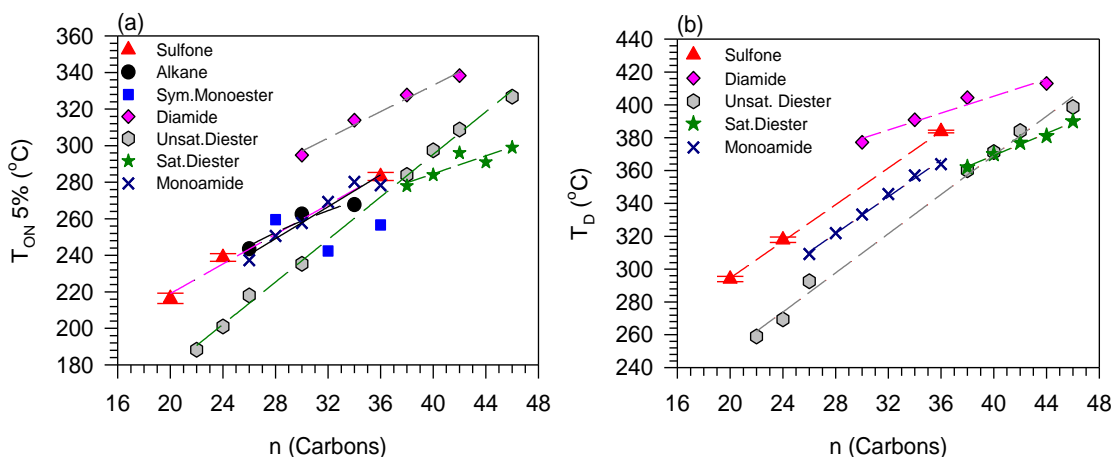


Figure 3-9. (a) Onset of weight loss (T_{ON}) as determined at 5 % weight loss and (b) maximum derivative weight loss temperature (T_D) of the sulfones compared with other PCMs mined from the literature.

Notwithstanding a plateauing effect, **Figure 3-9a** shows that T_{ON} of the sulfones (▲) falls into the same apparent linear curve which is followed by the alkanes (●) and monoamides (✕). At least in the available range, T_{ON} of the larger saturated diesters (★ in **Figure 3-9a**) appear to follow a gentler slope (m) compared to the sulfones (3.5 °C versus 5 °C per carbon, respectively) indicating a lower thermal stability. This is further backed by the variation of T_D which linear dependence on chain length shows a marked difference in slope, i.e., 5.6 °C per carbon for the sulfones versus 3.8 °C per carbon for the saturated diesters (▲ and ★ in **Figure 3-9b**, respectively). T_{ON} and T_D of the unsaturated diesters (◉ in **Figure 3-9a-b**) are also below those of the sulfones for any given chain length. These data show, that overall, the thermal stability of the sulfones is higher than that of alkanes, saturated monoesters and saturated and unsaturated diesters; underlining the higher relative contribution of the polar sulfonyl groups to the intermolecular interactions.

The thermal stability data for monoamides [49] and diamides also show trends similar with the sulfones (✕ and ◆ in **Figure 3-9a-b**). The higher thermal stability of the diamides is attributed to the larger number of hydrogen bonds, a total of 4 bonds per molecule, [50] compared to the 2 bonds per molecule formed by the one sulfur group. The high thermal stability observed for the sulfones, monoamides and diamides reflects some degree of short-range order in the liquid state due to the sulfonyl-sulfonyl and hydrogen bonding interactions respectively, which would require an increase in the kinetic energy of the molecules prior to evaporation [51]. In contrast the alkanes and esters have no strong intermolecular interactions in the liquid state other than weak dispersion forces [50].

3.4.2 Phase change temperature

The melting temperatures (T_{m1}) of the sulfones (\blacktriangle) are compared with those of the symmetric monoesters (\bullet) [44-46], monoamides (\blacksquare) [19, 20], alkanes (\blacklozenge) [52], fatty acids (\ominus); [53], fatty ethers (\star), fatty alcohols (\blacklozenge) [21], diesters (\times) [17] and diamides (\times) [47]. The data is represented in **Figure 3-10**. The characteristic functional group of the monoesters, monoamides and fatty ethers is in the center of the molecule whereas the carboxylic group of the fatty acids and the hydroxyl group of the fatty alcohols are located on a terminal carbon atom. All of the molecules are saturated.

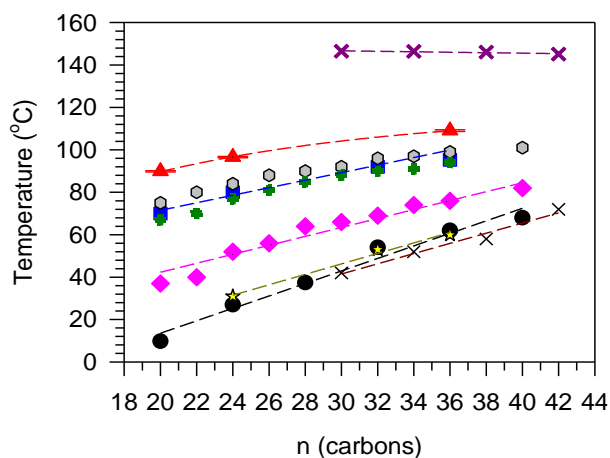


Figure 3-10. T_{m1} of the present sulfones and selected organic compounds mined from the literature. Symbols: sulfones (\blacktriangle); monoesters (\bullet); monoamides (\blacksquare); alkanes (\blacklozenge); carboxylic acids (\ominus); ethers (\star); alcohols (\blacklozenge); diamides (\times); and diesters (\times).

3.4.2.1 Influence of the hydrocarbon chain on the phase change temperature

It is apparent from **Figure 3-10** that the melting temperatures of each series of compounds increase with increasing methylene chain length and tend to plateau regardless of the functional group type. The tendency to plateau at large chain lengths is attributed to energy and mass

transfer limitations. This trend in melting temperature is well known to arise from the increasing Van der Waals forces between the fatty chains as a result of increasing chain length [50]. The main Van der Waals force that occurs between the long fatty chains are the London dispersion forces [54]. The dispersion forces occur when the electron clouds of the fatty chains are distorted and generates temporary dipoles that cause the chains to be more attracted to each other and are the basis of the formation of closely packed lattice arrangements [55].

3.4.2.2 Influence of functional group on the phase change temperature

The almost parallel curves of **Figure 3-10** describing the melting temperature of the different series reveal the effect of the functional groups on the phase change temperature of organic compounds. Except for the diamides, the sulfones have the highest melting temperatures followed by the carboxylic acids, monoamides, fatty alcohols, alkanes, monoesters, ethers and finally diesters. The higher T_m s of the sulfones compared to all of the compounds with only one functional group is attributable to their strong sulfonyl-sulfonyl attractions [56]. The sulfonyl group is the most polar of the series with a dipole moment of 4.5 Debye (D) [25] followed by the amide (3.8 D), ketone (2.8 D), ester (1.7 D), hydroxyl (1.5 D) and carboxyl (1.7 D) groups [57] (see *Table S3* and *Fig. S2 in SI*). Due to its larger dipole moment, the sulfonyl group result in stronger intermolecular attractions compared to the amide, carboxylic, ester, ether and hydroxyl functional groups [58]. Also, hydrogen bonding between the electronegative sulfonyl oxygens and adjacent Lewis acidic α -hydrogens is possible, similar to what was reported for polysulfones [27].

T_m of the monoesters, diesters and ethers (\times , \star and \bullet respectively in **Figure 3-10**) practically lie on the same curve and is the lowest. The alkanes (\blacklozenge in **Figure 3-10**) melt at temperatures

~13 °C higher relatively to the monoesters, diesters and ethers. This is attributed to the combined effects of the flexibility (C-O-C and O-C=O), bulkiness and weak attraction power of the ether or ester groups presence in the center of the molecule which limit the formation of close packed structures contrary to the alkanes in which such hindrance is missing [59].

The diamides possess significantly higher T_m compared to the sulfones. For example, T_m of 18-SO₂-18 is ~109 °C and T_m of 1,6-hexamethylene dioctadecyl diamide (18-2-18) is ~ 146 °C. It is obvious that the doubling of the high polarity functional group is instrumental in setting such high phase change temperature. Furthermore, one can notice that T_m of the reported diamides (✕ in **Figure 3-10**) is practically independent of fatty chain length (~145 ± 2 °C), which stresses the dominance of the hydrogen bond contributions over the other contributions brought by the fatty chains. In the case of the diesters of 1, 6-diol [17] (✕ in **Figure 3-10**), the melting temperatures are as low and show a similar trend as the monoesters and ethers, which indicates the dominance of the fatty chain contributions over the ester functional groups.

The knowledge gathered from **Figure 3-10** suggests that higher phase change temperatures can be achieved by incorporating one or more polar functional groups in lipid based molecular architectures without the drawback of mass limitation, at least where these effects are not overwhelming, such as probably with C₁₀ - C₁₈ chains.

3.4.3 Phase change enthalpy

Figure 3-11 compares the enthalpy of melting (ΔH_{ml}) of the sulfones with other PCMs found in the literature [17, 21, 44-47, 52] as a function of total chain length. All the molecules are saturated. The characteristic functional group of the sulfones (▲); monoesters (●); diesters (⊕),

monoamides (✕), diamides (☆) and ethers (◇) is in the center of the molecule whereas the hydroxyl group of the fatty alcohols (⊖) is located on a terminal carbon atom.

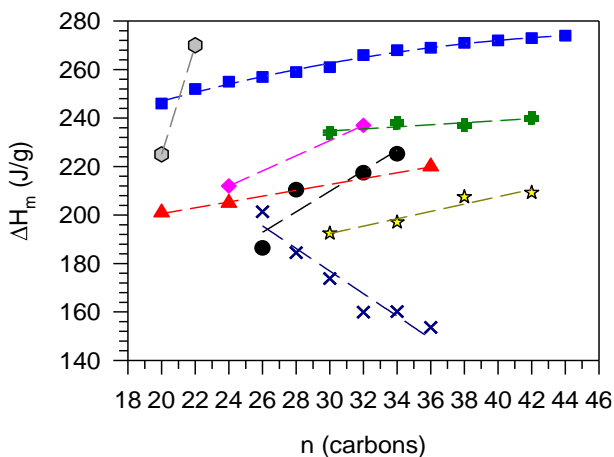


Figure 3-11. Enthalpy of melting (ΔH_{m1}) of the sulfones with organic PCMs: sulfones (▲); monoesters (●); alkanes (■); ethers (◇); alcohols (⊖); diamides (☆); diesters (◼); and monoamides (✕).

With the exception of the monoamides, the melting enthalpy for each series of organic PCMs in **Figure 3-11** increases with increasing chain length and plateau similarly to what was observed for their melting point (**Figure 3.10**) as a result of the combined effects of increasing attractive dispersion forces and mass transfer limitations associated with the increasing chain length. The even carbon alkanes (■ in **Figure 3-11**) demonstrate the highest enthalpy due to the better long-range crystal lattice packing arrangements facilitated by the maximum attraction between their methylene chains, increasing the crystal density (molecules per unit cell) and therefore, the phase change enthalpy [50].

The higher melting enthalpy of the alkane compared to the cases where a functional group is present is due to a combination of the various factors which contribute to the packing

arrangement of the molecules in crystal structures, particularly the geometry of the molecules, the size and specific interaction strength of the functional group [29, 50]. For compounds with polar functional groups, such as the amide, hydroxyl and sulfonyl groups the close packing requirements are known to be less compelling [55]. This is so because, unlike the dispersion forces, the attraction between the highly polar functional groups is directional and favors a particular packing orientation. As a result, the most energetically favorable arrangement that the molecule form may not be the best arrangement for achieving high enthalpy of fusion [50, 55]. The disrupting role of the functional group can be as strong as to prevent any stable phase from forming is illustrated by 10-SO₂-10 which formed the metastable γ -polymorph regardless of crystallization and/storage conditions.

The case of the monoamides which melting enthalpy even decreases with increasing chain length (negative slope in **Figure 3-11** of -4.2 J/g/carbon) is an extreme example where on top of the above effects, the hydrogen bond strength is decreased by the increase in the separation distance between the amide without any compensation by the added van der Waals [49].

The effect of increasing chain length on the phase change enthalpy is much stronger in ethers, monoesters and diesters than in sulfones, diesters, and diamides alkanes (see apparent slopes in **Figure 3-11**) because the former contain weak hydrogen bonding donor and acceptor atoms and therefore do not readily form hydrogen bonds which leaves the long-range dispersion forces as the main intermolecular interactions that determines the phase change enthalpy. In the case of the sulfones, the positive slope of their enthalpy versus n curve (▲ in **Figure 3-11**) indicates that both the sulfonyl-sulfonyl interactions and dispersion forces contribute to the total intermolecular forces and consequently to the phase change enthalpy. The similar apparent slope of the (★ in **Figure 3-11**) indicate that the diamides benefit from the added dispersion forces almost in the

same manner as the sulfones confirming the roles of their strong hydrogen bonding and dispersion forces in the determination of the phase change enthalpy [50].

The comparison of linear saturated diesters and diamides (✚ and ✨ in **Figure 3-11**) with the sulfones highlights the effect of doubling functional groups. As shown, the melting enthalpies of the sulfones lie between those of the diesters and diamides. Even though the diamides have higher melting temperatures than the sulfones (**Figure 3-10**) due to the presence of the reinforced hydrogen bonds, their melting enthalpies are slightly lower. In contrast, the diesters which have lower melting temperatures than the sulfones and diamides, possess higher melting enthalpies. Both the sulfone and the diamides are highly polar molecules with significant directional intermolecular attractions that favor particular packing orientations which are not the best arrangement for achieving highest melting enthalpy (as discussed earlier in this section). The larger polarity of the sulfonyl functional group compared to the amide functional group (4.5 D versus 3.8 D respectively) imparts increased directionality to its molecular arrangement that makes the close packing requirements compelling but provides less attraction strength than the two amide groups. Unlike the sulfones and the diamides the diesters do not possess hydrogen bonding and therefore do not experience strong directionality requirements. As a result, the dispersion forces are dominant, facilitating the formation of close packing arrangements which result in higher energy storage enthalpies than in the sulfones and diamides.

3.5 Conclusion

Three lipid-based sulfones were synthesized in high purities and yields from lipid-based sulfide feedstocks via a solvent-free oxidative synthesis route. All sulfones crystallized in a dominant single crystal phase and small very low temperature phases unsequential for PCM

functionality. Sulfones with the longer fatty chain length; ie. 18-SO₂-18 and the 12-SO₂-12, crystallized in the thermodynamically stable β -polymorph form whereas 10-SO₂-10 crystallized in the γ -polymorph. The sulfones presented relatively higher phase change temperatures, competitive phase change enthalpies and thermal stabilities, compared to the existing lipid-based PCMs comprising one functional group.

The sulfones displayed sharp phase transitions with negligible supercooling. Their phase change temperatures range between 90 and 109 °C and their phase change enthalpies are higher than 200 J/g which qualifies them for use in numerous medium temperature TES applications. The renewability of the feedstock and the solvent and catalyst free routes to obtain them further make the sulfone material very attractive choices for TES applications.

The incorporation of highly polar sulfonyl groups in fatty chains was demonstrated as a possible mean to achieve improved PCMs with thermal properties that are suitable for latent heat TES; especially higher phase change temperatures than what currently exist. It remains to be demonstrated if multiple sulfonyl functional groups can further increase the phase change temperatures and if there is a limiting number for such an increase as is the case for the increase of the number of carbons in the aliphatic chain.

3.6 References

1. A.K. Pandey, et al., *Novel approaches and recent developments on potential applications of phase change materials in solar energy*. *Renew. Sust. Energ. Rev.* 82.(2018) 281-323. <https://doi.org/10.1016/j.rser.2017.09.043>
2. Z. Zhou, et al., *Phase change materials for solar thermal energy storage in residential buildings in cold climate*. *Renew. Sust. Energ. Rev.* 48.(2015) 692-703. <https://doi.org/10.1016/j.rser.2015.04.048>

3. N. Sarier and E. Onder, *Organic phase change materials and their textile applications: An overview*. *Thermochim. Acta.* 540.(2012) 7-60. <https://doi.org/10.1016/j.tca.2012.04.013>
4. Y. Ammar, et al., *Low grade thermal energy sources and uses from the process industry in the UK*. *Appl. Energ.* 89.(2012) 3-20. <https://doi.org/10.1016/j.apenergy.2011.06.003>
5. A. Mishra, A. Shukla, and A. Sharma, *Latent heat storage through phase change materials*. *Resonance.* 20.(2015) 532-541. 10.1007/s12045-015-0212-5
6. PhaseChangeMaterialsReport. *Advanced Phase Change Material (PCM) Market by Type (Organic, Inorganic & Bio-based) and Application (Building & Construction, HVAC, Shipping & Packaging, Cold Chain, Thermal Energy Storage (TES), Textile, and Electronics)*. 2015 [cited 2019 10 March]; Available from: <http://www.marketsandmarkets.com/Market-Reports/advanced-phase-change-material-pcm-market-1087.html>.
7. W. Su, J. Darkwa, and G. Kokogiannakis, *Review of solid–liquid phase change materials and their encapsulation technologies*. *Renew. Sust. Energ. Rev.* 48.(2015) 373-391. <http://dx.doi.org/10.1016/j.rser.2015.04.044>
8. L.F. Cabeza, et al., *Materials used as PCM in thermal energy storage in buildings: A review*. *Renew. Sust. Energ. Rev.* 15.(2011) 1675-1695. <http://dx.doi.org/10.1016/j.rser.2010.11.018>
9. D. Haillot, et al., *Thermal analysis of phase change materials in the temperature range 120–150°C*. *Thermochim. Acta.* 513.(2011) 49-59. <https://doi.org/10.1016/j.tca.2010.11.011>
10. S. Kahwaji and M.A. White, *Prediction of the properties of eutectic fatty acid phase change materials*. *Thermochim. Acta.* 660.(2018) 94-100. <https://doi.org/10.1016/j.tca.2017.12.024>
11. X.L. Huang, et al., *Novel phase change materials based on fatty acid eutectics and triallyl isocyanurate composites for thermal energy storage*. *J. Appl. Polym. Sci.* 134.(2017) 44866-n/a. Artn 44866 10.1002/App.44866
12. Y. Yuan, Zhang, N., Tao, W., Cao, X. and He, Y., *Fatty acids as phase change materials: a review*. *Renew. Sust. Energ. Rev.* 29.(2014) 482-498. DOI 10.1016/j.rser.2013.08.107
13. G.J. Suppes, M.J. Goff, and S. Lopes, *Latent heat characteristics of fatty acid derivatives pursuant phase change material applications*. *Chem. Eng. Sci.* 58.(2003) 1751-1763. [https://doi.org/10.1016/S0009-2509\(03\)00006-X](https://doi.org/10.1016/S0009-2509(03)00006-X)
14. D. Rozanna, et al., *Fatty Acids as Phase Change Materials (PCMs) for Thermal Energy Storage: A Review*. *Int. J. Green Energy.* 1.(2005) 495-513. 10.1081/ge-200038722

15. C. Alkan and A. Sari, *Fatty acid/poly(methyl methacrylate) (PMMA) blends as form-stable phase change materials for latent heat thermal energy storage*. Sol. Energy. 82.(2008) 118-124. <http://dx.doi.org/10.1016/j.solener.2007.07.001>
16. M.M. Kenisarin, *Thermophysical properties of some organic phase change materials for latent heat storage. A review*. Sol. Energy. 107.(2014) 553-575. <https://doi.org/10.1016/j.solener.2014.05.001>
17. M.C. Floros and S.S. Narine, *Latent heat storage using renewable saturated diesters as phase change materials*. Energy. 115.(2016) 924-930. 10.1016/j.energy.2016.09.085
18. J.A. Kenar, *Latent heat characteristics of biobased oleochemical carbonates as potential phase change materials*. Sol Energy Mater Sol Cells. 94.(2010) 1697-1703. <https://doi.org/10.1016/j.solmat.2010.05.031>
19. Y. Yoshioka and K. Tashiro, *Structural Changes in Phase Transitions of Nylon Model Compounds. 1. Transition Behavior of Model Compounds of R-NHCO-R' Type*. J. Phys. Chem. 107.(2003) 11835-11842. 10.1021/jp0224160
20. R. Stewart, *Thermally-responsive materials and devices comprising such materials*. US 7,875,207 B2., 2011.
21. T. Hasl and I. Jiricek, *The Prediction of Heat Storage Properties by the Study of Structural Effect on Organic Phase Change Materials*. Energy Procedia. 46.(2014) 301-309. <https://doi.org/10.1016/j.egypro.2014.01.186>
22. R.J.C. Brown and R.F.C. Brown, *Melting Point and Molecular Symmetry*. J. Chem. Educ. 77.(2000) 724. 10.1021/ed077p724
23. S.H. Yalkowsky, *Carnelley's Rule and the Prediction of Melting Point*. J. Pharm. Sci. 103.(2014) 2629-2634. <https://doi.org/10.1002/jps.24034>
24. J. Clayden, N. Greeves, and S. Warren, *Organic Chemistry*, OUP Oxford, 2012.
25. T. Clark, et al., *Why are dimethyl sulfoxide and dimethyl sulfone such good solvents?* J. Mol. Model. 14.(2008) 689-697. 10.1007/s00894-008-0279-y
26. L. Vandermeeren, T. Leyssens, and D. Peeters, *Theoretical study of the properties of sulfone and sulfoxide functional groups*. J. Mol. Struc-Theochem. 804.(2007) 1-8. <https://doi.org/10.1016/j.theochem.2006.10.006>
27. T.W. Gaines, et al., *High Melting Precision Sulfone Polyethylenes Synthesized by ADMET Chemistry*. Macromol. Chem. Phys. 217.(2016) 2351-2359. doi:10.1002/macp.201600118
28. E. Denehy, J.M. White, and S.J. Williams, *Electronic Structure of the Sulfonyl and Phosphonyl Groups: A Computational and Crystallographic Study*. Inorg. Chem. 46.(2007) 8871-8886. 10.1021/ic700687t

29. C. Alkan, *Enthalpy of melting and solidification of sulfonated paraffins as phase change materials for thermal energy storage*. *Thermochim. Acta.* 451.(2006) 126-130. <https://doi.org/10.1016/j.tca.2006.09.010>
30. C. Gibbs, *Plasticizers-Compounds containing sulfur bound to oxygen*. US150327A., 1937.
31. A. Irshad and Shagufta, *Sulfones: An important class of organic compounds with diverse biological activities*. *J. Pharm. Pharm. Sci.* 7.(2015)
32. C. Dizman, A.M. Tasdelen, and Y. Yagci, *Recent advances in the preparation of functionalized polysulfones*. *Polym Int.* 62.(2013) 991-1007. doi:10.1002/pi.4525
33. F. Heym, et al., *An improved method to measure the rate of vaporisation and thermal decomposition of high boiling organic and ionic liquids by thermogravimetric analysis*. *Phys. Chem. Chem. Phys.* 12.(2010) 12089-12100. 10.1039/c0cp00097c
34. F. Jia, et al., *A detailed bond stretch model of thermal decomposition*. *Mater. Sci. Eng. C.* 62.(2014) 012020.
35. S.E. Kalnæs and B.P. Jelle, *Phase change materials and products for building applications: A state-of-the-art review and future research opportunities*. *Energ Buildings.* 94.(2015) 150-176. <https://doi.org/10.1016/j.enbuild.2015.02.023>
36. A.G. Marangoni, et al., *Structure and functionality of edible fats*. *Soft Matter.* 8.(2012) 1275-1300.
37. B.S. Ghotra, S.D. Dyal, and S.S. Narine, *Lipid shortenings: a review*. *Food Res. Int.* 35.(2002) 1015-1048. [https://doi.org/10.1016/S0963-9969\(02\)00163-1](https://doi.org/10.1016/S0963-9969(02)00163-1)
38. A.G. Marangoni and L.H. Wesdorp, *Structure and Properties of Fat Crystal Networks, Second Edition*, Taylor & Francis, 2012.
39. K. Sato, *Crystallization behaviour of fats and lipids - a review*. *Chem. Eng. Sci.* 56.(2001) 2255-2265. [https://doi.org/10.1016/S0009-2509\(00\)00458-9](https://doi.org/10.1016/S0009-2509(00)00458-9)
40. F. Kaneko, et al., *Structure and Crystallization Behavior of the β Phase of Oleic Acid*. *J. Phys. Chem. B.* 101.(1997) 1803-1809. 10.1021/jp963400a
41. E. Ikeda, et al., *Phase Behavior of a Binary Mixture of 1,3-Dipalmitoyl-2-oleoyl-sn-glycerol and 1,3-Dioleoyl-2-palmitoyl-sn-glycerol in n-Dodecane Solution*. *J. Phys. Chem. B.* 114.(2010) 10961-10969. 10.1021/jp101821c
42. L. Bouzidi, S. Li, and S. Narine, *Lubricating and Waxy Esters. VI. Effect of Symmetry about Ester on Crystallization of Linear Monoester Isomers*. *Symmetry.* 6.(2014) 655.
43. E. Boz, et al., *Synthesis and Crystallization of Precision ADMET Polyolefins Containing Halogens*. *Macromolecules.* 39.(2006) 4437-4447. 10.1021/ma0605088

44. A.A. Aydın, *High-chain fatty acid esters of 1-octadecanol as novel organic phase change materials and mathematical correlations for estimating the thermal properties of higher fatty acid esters' homologous series*. Sol. Energy Mater. Sol Cells. 113.(2013) 44-51. <https://doi.org/10.1016/j.solmat.2013.01.024>
45. A.A. Aydın and A. Aydın, *High-chain fatty acid esters of 1-hexadecanol for low temperature thermal energy storage with phase change materials*. Sol. Energy Mater. Sol. Cells. 96.(2012) 93-100. <http://dx.doi.org/10.1016/j.solmat.2011.09.013>
46. A.A. Aydın and H. Okutan, *High-chain fatty acid esters of myristyl alcohol with even carbon number: Novel organic phase change materials for thermal energy storage—1*. Sol. Energy. Mater. Sol. Cells. 95.(2011) 2752-2762. <http://dx.doi.org/10.1016/j.solmat.2011.04.015>
47. M.C. Floros, et al., *Lipid derived diamide phase change materials for high temperature thermal energy storage*. Sol. Energy 139.(2016) 23-28. <https://doi.org/10.1016/j.solener.2016.09.032>
48. L. Raghunanan, M.C. Floros, and S.S. Narine, *Thermal stability of renewable diesters as phase change materials*. Thermochim. Acta. 644.(2016) 61-68. <https://doi.org/10.1016/j.tca.2016.10.009>
49. K.D. Poopalam, et al., *Lipid-derived Monoamide as Phase Change Energy Storage Materials* Sol. Energy Mater. Sol. Cells. 2019) Unpublished results
50. S.H. Yalkowsky and D. Alantary, *Estimation of Melting Points of Organics*. J. Pharm. Sci. 107.(2018) 1211-1227. <https://doi.org/10.1016/j.xphs.2017.12.013>
51. B. Lian and S.H. Yalkowsky, *Molecular Geometry and Melting Point Related Properties*. Ind. Eng. Chem. Res. 51.(2012) 16750-16754. 10.1021/ie302574y
52. A. Sharma, et al., *Review on thermal energy storage with phase change materials and applications*. Renew. Sust. Energ. Rev. 13.(2009) 318-345. <http://dx.doi.org/10.1016/j.rser.2007.10.005>
53. F. Huq, *Why the lower-membered alkanolic acids are infinitely soluble in water whereas the higher-membered ones have a very low solubility in water? A molecular modeling analysis*. Asian J. Chem. 17.(2005) 1001-1012.
54. J.N. Israelachvili, *Intermolecular and Surface Forces*, Elsevier Science, 2011.
55. A. Gavezzotti and H. Flack *Crystal Packing-Theromdynamics and kinetics*. International Union of Crystallography Commission on Crystallographic Teachin, 2005.
56. T.J. Deming, *Functional Modification of Thioether Groups in Peptides, Polypeptides, and Proteins*. Bioconjug. Chem. 28.(2017) 691-700. 10.1021/acs.bioconjchem.6b00696
57. V.I. Minkin, *Dipole Moments in Organic Chemistry*, Springer US, 2012.

58. J.F. Casteel and P.G. Sears, *Dielectric constants, viscosities, and related physical properties of 10 liquid sulfoxides and sulfones at several temperatures*. J. Chem. Eng. Data. 19.(1974) 196-200. 10.1021/je60062a001
59. R. Ravotti, et al., *Analysis of Bio-Based Fatty Esters PCM's Thermal Properties and Investigation of Trends in Relation to Chemical Structures*. Appl. Sci. 9.(2019) 10.3390/app9020225

4 Chapter 4 Effect of Pendant Sulfide and Sulfonyl groups on the Thermal, Flow and Antioxidative Properties of Lipid Based Aliphatic Monoesters

4.1 Introduction

Environmental and sustainability concerns are driving research efforts to develop environmentally friendly biodegradable lubricants to replace those derived from petroleum [1]. Vegetable oils are considered a feedstock of choice as they are abundant, renewable, non-toxic, non-volatile and highly biodegradable [2-5]. In their commonly available form, almost all vegetable oils have limited use as lubricants because they are composed of ~90 % triacylglycerols (TAGs) which display inherent disadvantages such as poor cold-flow performance, poor thermo-oxidative stability and limited viscosity [6]. TAGs, however, are relatively easy to derivatize and transform into compounds that may mitigate these limitations.

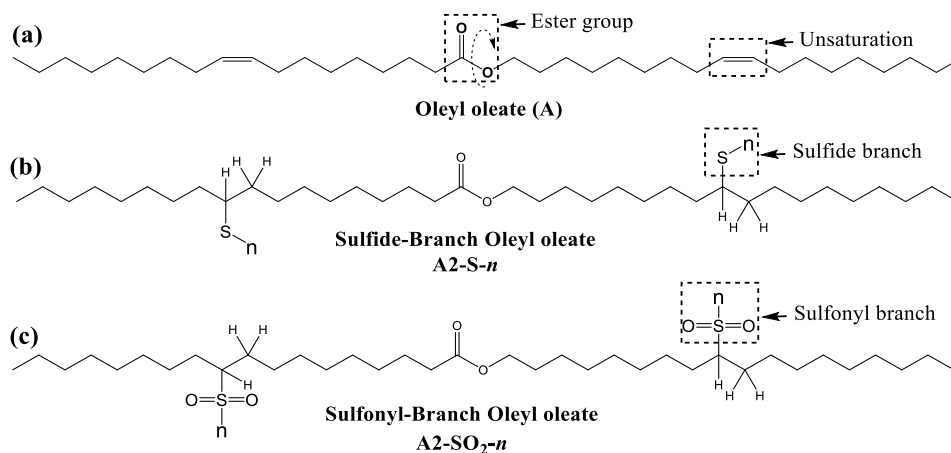
Ester lubricants prepared from unsaturated fatty acids and their derivatives are widely studied and used since they present properties similar to well-established mineral and synthetic lubricants [4, 7, 8]. The naturally abundant oleic acid [9-11] and its widely available and inexpensive derivative oleyl oleate (octadec-9-enyl octadec-9-enoate) are common precursors of many existing biolubricants [12]. Ester materials are usually branched at the C=C double bonds with hydrocarbon chains to mitigate oxidation susceptibility and early crystallization [13-16]. For example, unsaturated monoesters [17-20], unsaturated diacid diesters [21-24] and unsaturated diol diesters [25, 26] present onset of crystallization (T_{on}^c) between -30 °C and 20 °C and viscosity between 10 mPa.S and 40 mPa.S; whereas, branched ester lubricants present T_{on}^c as low as -55 °C and viscosity ranging from 100 mPa.s to 500 mPa.s [17, 18, 25-32].

Further improvements in lubrication properties are possible with novel designs of ester compounds. This can be achieved by incorporation of functional groups which confer specific interactions and conformations or by creating novel molecular architectures that promote advantageous transformation paths and phase behaviors. Sulfur is one of the abundant elements with several unique chemical properties which if appropriately positioned in the molecule can enhance the lubricant properties of ester compounds. Sulfur is a p-block element in group VI (atomic number 16) with a relatively large atomic radius (1.05 Å), compared to oxygen for example (0.66 Å). Consequently, sulfur is expected to distort molecular arrangements in which it is present considerably more compared to oxygen. This bulkiness is expected to obstruct crystallization, particularly if sulfur is present in branched groups. Sulfur is slightly more electronegative than carbon and less electronegative than oxygen. As a result, sulfur forms thermally stable bonds similar to carbon [33]. The C–S bond is slightly polar and slightly weaker than the C–C bond (362 kJ/mol vs. 376 kJ/mol) [34]. Unlike oxygen which can mainly exist in –1 and –2 oxidation states in organic compounds like esters, sulfur can exist in oxidation states ranging from –2 to +6 and can have coordination numbers of 0 to 7 via 3D orbitals [34]. This facilitates the further modification of the sulfur atom to create bulkier functional groups with different polarities such as sulfoxide, sulfonyl, sulfonic and sulfonate groups.

High polarity sulfur-containing sulfonyl and sulfonic groups have been demonstrated to impart anticorrosive properties [35-40]. Additionally, sulfur groups with low oxidation states (–2) like thiols and sulfides impart antioxidant properties to certain complex molecular branched structures such as zinc dialkyl dithiophosphate (ZDDP) and its derivatives [41-43].

The present work investigates sulfide and sulfonyl branched oleyl oleate monoester for use as lubricants. Four sulfide (A2-S-*n*) and four sulfonyl (A2-SO₂-*n*) branched oleyl oleate monoesters

of different branch chain lengths ($n = 2, 3, 4, 6$) were prepared from oleyl oleate (A) and examined for viscosity and flow behavior, phase transition, crystal growth and thermal and oxidative stability. The structures of oleyl oleate and its sulfide and sulfonyl branched monoesters are shown in **Scheme 4-1**. To the best of our knowledge, these compounds have not been previously investigated for use as lubricants.



Scheme 4-1. (a) Oleyl oleate (A)-curved arrow denotes the rotation of ester group, (b) sulfide (A2-S- n) and (c) sulfonyl (A2-SO₂- n) doubly branched monoesters. S and SO₂: sulfide and sulfonyl functional groups, respectively and n : length of the branched carbon chain.

The sulfide (A2-S- n) and sulfonyl (A2-SO₂- n) branched oleyl oleate monoesters ($n = 2, 3, 4, 6$) were synthesized via robust thiolene chemistry. Unlike the epoxidation/ring-opening route, which is typically used to prepare ester branched lubricants and which produces mixtures of molecules with varying degrees of branching in the crude, some of which may be undesirable, thiolene synthesis does not yield unwanted byproducts [44-56]. Thiolene chemistry yields uniquely numbered branched molecules in the crude. When the C=C bond is in a terminal position in the fatty chain, thiolene addition mainly yields branched products at the end of the

chain (anti-Markownikoff branched-products) [57]. When the C=C bond is internal, the sulfide branch groups can be added to either side of the bond, forming 1:1 ratio of positional isomers [34].

The molecular structure and purity of the compounds synthesized for this work were confirmed using proton Nuclear Magnetic Resonance ($^1\text{H-NMR}$) and Electrospray Ionization Mass Spectrometry (ESI-MS). Their viscosity and flow behavior, thermal phase transition and oxidative stability, thermal stability were determined using rotational rheometry, differential scanning calorimetry (DSC) and thermogravimetric analysis (TGA), respectively. Polarized light microscopy (PLM) was used to monitor crystallization under the same conditions as the DSC. The PLM characteristic temperatures such as the temperature at which crystallites appear were compared to the DSC characteristic temperatures such as T_{on}^c . The properties of the present compounds were compared with those of esters analogs [18, 25-30], and those of synthetic and mineral oils [58, 59]. The antioxidant properties of sulfide and sulfonyl branched oleyl oleate monoesters are discussed and compared to analogous lubricants and common antioxidant additives [60-64].

4.2 Materials & Methods

4.2.1 Materials

The reagents (dichloromethane (DCM), azobisisobutyronitrile (AIBN), anhydrous ethanol, magnesium sulfate, ethane thiol, propane thiol, butane thiol, pentane thiol, hexane thiol, oleic acid and oleyl alcohol with purity higher than 99 %) were purchased from Sigma-Aldrich, Oakville, Ontario Canada, and used as received. HPLC grade chloroform and methanol were

purchased from VWR, Mississauga ON, Canada. Hydrogen peroxide (30 %, H₂O₂), glacial acetic acid (AcOH) (both 99 % purity) were used as the oxidant and catalyst, respectively.

4.2.2 Preparation of Oleyl Oleate Monoesters

Oleyl oleate was prepared from a neat Fischer esterification reaction of oleic acid and oleyl alcohol (1:1 mole ratio) catalyzed by hydrochloric acid. Oleic acid, oleyl alcohol and hydrochloric acid was added into a 500mL round bottom flask. The esterification reaction was carried out under vacuum at 140 °C for 2 hours at a stirring rate of 500rpm and the formation of the oleyl oleate was monitored by TLC using 1:9 ethyl acetate/hexane solvent system. After reaction completion, the crude oleyl oleate was washed with distilled water in a 500 mL separating funnel until all the hydrochloric acid was removed and stopped when the pH was neutral. The oleyl oleate obtained was placed in a vacuum oven at 60 °C for 24 hours to remove residual water.

4.2.3 Preparation of Sulfide-Branched Oleyl Oleate Monoesters (A2-S-n)

Oleyl oleate was added into a 250 mL three-neck round bottom flask followed by 100 mL CHCl₃ and swirled until completely dissolved. Next, alkane thiol of selected chain length ($n = 2, 3, 4$ & 6) was added to the mixture along with AIBN (3 wt.% vs. oleyl oleate). The reaction was carried out for 12 hours at 85 °C with a stirring rate of 1000 rpm. CHCl₃ and excess alkane thiol were removed by rotor evaporation to obtain the crude sulfide-branched oleyl oleate monoesters (A2-S- n).

4.2.4 Preparation of Sulfonyl-Branched Oleyl Oleate Monoesters (A2-SO₂-n)

Sulfonyl-branched oleyl oleate monoesters (A2-SO₂-n) were synthesized via solvent-free oxidation of sulfide-branched oleyl oleate monoesters (A2-S-n). In brief, a measured amount of A2-S-n was added to a 25 mL round bottom flask equipped with a reflux condenser placed in an oil bath set to 60 °C. 30 % H₂O₂ was added dropwise followed by AcOH and the mixture was stirred at 550 rpm for 4 hours after which the reaction was stopped and cooled to room temperature. The obtained colorless liquid was washed with distilled water (100 mL × 10) to remove unreacted H₂O₂ and AcOH catalyst. A2-SO₂-n were dried in a vacuum oven for 24 hours at 65 °C.

Each reaction was performed once for oleyl oleate, sulfide and sulfonyl-branched oleyl oleate monoesters. The purity of the synthesized compounds was higher than 90 %. The purity of oleyl oleate was determined based on the ratio of the calculated and theoretical methyl protons. The purity of sulfide and sulfonyl-branched oleyl oleate monoesters was determined based on the ratio of the calculated and theoretical pendant group methyl protons.

4.3 Characterization Methods

4.3.1 Proton Nuclear Magnetic Resonance (¹H-NMR)

The structures of the synthesized compounds were confirmed by ¹H-NMR recorded on a Varian Unity-INOVA at 499.695 MHz in CDCl₃ (Agilent Technologies, Santa Clara, CA, USA) with 1s recycle delay and the spectra were processed with ACD Labs NMR Processor, version 12.01.

4.3.2 *Electrospray Ionization - Mass Spectrometry (ESI-MS)*

Mass spectra were collected on an API 3000 triple quadrupole Thermo QExactive Orbitrap mass spectrometer (Thermo Fischer Scientific, San Jose, CA) equipped with an Electron Spray Ionization source (ESI) in the positive ion mode. Samples (1 ppm wt./v) were prepared using chloroform:methanol 70:30 (v/v) and analyzed at a resolution of 140,000.

4.3.3 *Viscosity and Flow Behavior*

Viscosity and flow behavior were determined on a computer controlled AR2000ex rheometer (TA Instruments, DE, U.S.A.) using a standard 40 mm 2° steel cone geometry (SIN 511406.901, TA Instruments) under an air bearing pressure of 27psi. Temperature control was achieved by Peltier Plate (AR Series, TA Instruments) with an accuracy of 0.1 °C. The shear rate–shear stress experiments were performed with increasing and decreasing shear rate using the continuous ramp procedure. The viscosity versus temperature data was collected using the constant temperature rate method. The sample was quickly heated to 110 °C and equilibrated at that temperature for 5min then cooled at a constant rate (1.0 and 3.0 °C/min). Sampling points were recorded every 1 °C.

The shear rate - shear stress curves were fitted with the Herschel–Bulkley equation (*Equation 1*), a model commonly used to describe the general behavior of materials characterized by yield stress.

$$\tau = \tau_0 + k\dot{\gamma}^n \quad \text{Equation 1}$$

τ : shear stress, $\dot{\gamma}$: shear rate, τ_0 : the yield stress below which there is no flow, k : consistency index, and n : flow index. n depends on the constitutive properties of the material. For

Newtonian fluids, $n = 1$ and $k = \eta$ is the fluid viscosity. For shear-thickening fluids, $n > 1$ and for shear-thinning fluids, $n < 1$.

The experimental viscosity-temperature data were analyzed using a generalized form of the Van Velzen equation (GvVE, *Equation 2*).

$$\ln(\nu) = A\left(-1 + \frac{1}{T^m}\right) \quad \text{Equation 2}$$

The GvVE fits yield physically meaningful parameters: A relates directly to the magnitude of the viscosity of the liquid and exponent m relates to the complexity of the molecule, similar to the parameters of the Andrade and generalized Andrade models from which it is derived [65].

4.3.4 Differential Scanning Calorimetry (DSC)

The thermal transition behavior and oxidative stability were determined using a Q200 DSC (TA Instruments, Newcastle, DE, USA) equipped with a refrigerated cooling system. The DSC instrument was calibrated with pure indium.

4.3.4.1 Thermal Transition Behavior

The samples (4-6 mg) were processed in hermetic aluminum pans. The sample was equilibrated at 50 °C for 10 min to erase the thermal history, then cooled at 5 °C/min down to -90 °C where it was held isothermally for 10min, and finally heated from -90 to 150 °C at 10 °C/min. Cooling rates of 0.1 and 20 °C/min were also used to study the effect of kinetics.

4.3.4.2 Oxidative Stability

The oxidative stability of the compounds was determined according to ASTM E 2009 [54, 66] using dry air instead of oxygen atmosphere. The sample (4-6 mg) was placed in an open aluminum pan and airflow was maintained at 50 mL/min. The cell temperature was raised to 250 °C at 10 °C/min. The onset temperature of oxidation (T_{on}^{ox}) was determined at the intersection of the signal baseline and the tangent of the steepest segment (highest slope) of the oxidation exotherm i.e., when a rapid increase in the rate of oxidation is observed.

4.3.4.3 Oxidation Induction Time

The oxidation induction time (OIT) is typically determined from a DSC heating cycle as the period where no change in heat flow signal occurs [67]. A protocol used for polymers [68] was used to determine OIT of the present lipid-based materials. Nitrogen atmosphere is used to heat the sample until the offset of melting (T_{off}^m) than switched to dry air while the heating rate is maintained at 5 °C/min. The time taken from when the gas is switched from nitrogen to dry air (i.e., at T_{off}^m) to the onset of oxidation (T_{on}^{ox}) i.e., when the sample starts to oxidize, is taken as the OIT.

4.3.5 Thermogravimetric Analysis (TGA)

Thermogravimetric analysis (TGA) was performed on a TGA Q500 (TA Instruments, Newcastle, DE, USA). The sample (10-15 mg) was heated on a platinum pan from 25 °C to 600 °C at 10°C/min under a nitrogen flow of 60.0 mL/min. The thermal stability of the compounds was characterized by the onset temperature of mass loss taken at 10 % w/w following the typical protocol used to determine the thermal stability of polymers. This point is of practical

importance as it is typically where the material starts to lose its inherent physical properties. The derivative of the TGA (DTG) was also used to determine the temperature of maximum rate of degradation (T_D).

4.3.6 Polarized Light Microscopy (PLM)

A Leica DM2500P (Leica Microsystems, Wetzlar, Germany) fitted with a Leica DFC420C digital camera was used for the microstructure studies. A Linkam LS 350 temperature-controlled stage (Linkam Scientific Instruments, Tadworth, Surrey, UK) fitted to the PLM was used to thermally condition the samples. A small droplet of the sample was carefully pressed between a preheated glass slide and coverslip ensuring a uniform thin layer. The sample was melted at 50 °C for 10 °C/min to erase crystal memory then cooled down to -90 °C at 1 °C/min which ensures suitable monitoring of the crystallization progress. Temperature resolved images were taken at 100× magnification during cooling using the PLM's automatic multi-time image capture feature. The temperature at which the first growth centers observed as “black spots” is recorded as the induction temperature of crystallization (T_{ind}).

4.4 Results and Discussion

4.4.1 Synthesis and Structural Characterization

Sulfide branched oleyl oleate monoesters was prepared from oleyl oleate using thiolene addition. Sulfonyl branched oleyl oleate monoesters was obtained by oxidation of sulfide branched oleyl oleate monoesters with H₂O₂. The synthesis route of sulfide and sulfonyl branched oleyl oleate monoesters is provided in **Scheme 4-2**.

4.4.2 Thermal Stability

All TGA and DTG curves are provided in *SI* in *Fig S.2*. TGA curves of A2-S-3 and A2-SO₂-3, representative of sulfide and sulfonyl branched oleyl oleate monoesters are shown in **Figure 4-1a**. The TGA curve of oleyl oleate (A) is also included in **Figure 4-1a** for comparison. The 10% w/w mass loss and T_D of the sulfide and sulfonyl branched oleyl oleate monoesters series and oleyl oleate (A) are shown in **Figure 4-1b**. Overall, A2-S-*n* and A2-SO₂-*n* presented similar TGA profiles with final mass conversions that reached at least 99.9% at ~420°C. The shape of the DTG curves is typical of a single-stage mass loss mechanism dominated by evaporation [69].

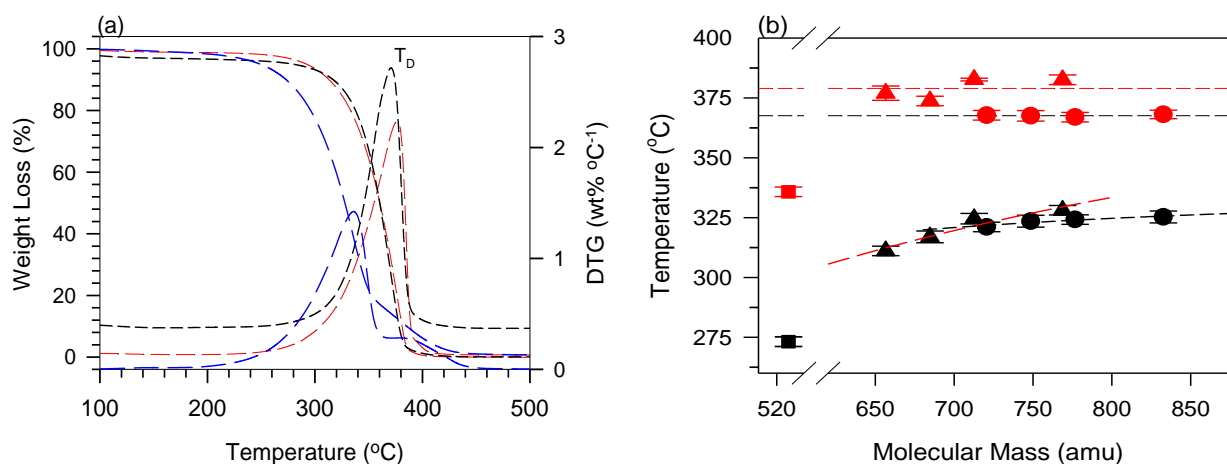


Figure 4-1. (a) TGA and DTG curves of A2-S-3 (red dashed lines), A2-SO₂-3 (black dashed lines) and oleyl oleate (blue dashed lines) (b) 10 % w/w mass loss versus molecular mass of versus molecular mass of A2-S-*n* (▲), A2-SO₂-*n* (●) and oleyl oleate (■).and T_D A2-S-*n* (▲), A2-SO₂-*n* (●) and oleyl oleate (■).

As shown in **Figure 4-1a**, 10% w/w mass loss increases with molecular mass and seems to follow linear trends, which however are more likely linear segments of the exponential growth to

a maximum curve that is commonly observed for hydrocarbons [70]. 10 % w/w mass loss for both series was high and averages 322 ± 5 °C (**Figure 4-1b**) indicating similar activation energies required to evaporate the molecules [71] despite a 64amu difference in molecular mass from the extra two oxygen atoms on the sulfonyl groups.

Although the differences between A2-S-*n* and A2-SO₂-*n* are not significant from a practical perspective, a smaller 10 % w/w mass loss rate of change is observed for A2-SO₂-*n* (0.03 ± 0.01 °C/amu vs. 0.15 ± 0.03 °C/amu) which is the manifestation of the extra steric hindrance introduced by the bulkier sulfonyl group and extra weakening of the sulfonyl-sulfonyl attractions due to increasing separation distance between the adjacent sulfonyl groups.

The difference in T_b between the A2-S-*n* and A2-SO₂-*n* series (379 ± 2 °C and 368 ± 2 °C, respectively) is attributable to the differences in intermolecular forces that persist in the liquid state until evaporation. The lower T_b observed for A2-SO₂-*n* is due to higher repulsion of the sulfonyl groups with increasing kinetic energy. This results in weaker attractions that help to more effectively overcome the attractive potential energy of the other molecules which leads to higher evaporation rates. Overall, it can be seen that inclusion of the sulfide and sulfonyl branched groups on the oleyl oleate backbone increase its 10 % w/w mass loss from 270 °C to 322 ± 5 °C and T_b values from 337 °C to as high as 379 ± 2 °C.

4.4.3 Thermal Transition Behavior

The cooling and heating DSC thermograms of all sulfide and sulfonyl branched oleyl oleate monoesters are provided in the SI in Fig S.3 a-b and 3c-d, respectively. The corresponding crystallization and melting results of oleyl oleate, sulfide and sulfonyl branched oleyl oleate monoesters are presented in **Table 4-1**. As illustrated with the examples of the cooling and

heating thermograms of A2-S-3, A2-SO₂-3 and oleyl oleate shown in **Figure 4-2a** and **b**, respectively, the branching of oleyl oleate with sulfide and sulfonyl groups altered its phase transition behavior by shifting and suppressing crystallization and melting signals.

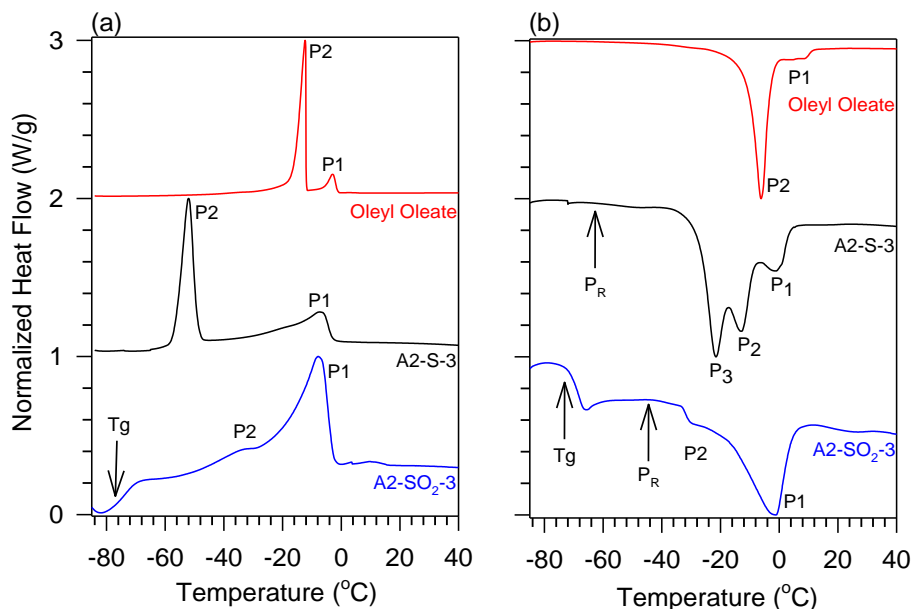


Figure 4-2. (a) Cooling and (b) Heating thermograms (both at 5 °C/min) of oleyl oleate, A2-S-3 and A2-SO₂-3. P_1 , P_2 : main peaks of crystallization or melting, P_R : recrystallization peak, T_g : glass transition temperature.

Table 4-1. DSC crystallization and melting results for oleyl oleate, sulfide and sulfonyl branched oleyl oleate monoesters. Average standard deviation is ± 0.5 °C for the temperatures and ± 5 J/g for the enthalpies. The molar enthalpy (kJ/mol) is also reported in bracket.

DSC Data – Cooling Cycle (5 °C/min)						
Compound	T_{ON}	$T_c P_1$	$T_c P_2$	T_{OFF}	T_g	ΔH_c
Oleyl oleate monoester						
A	-1.3 ± 0.5	-2.9 ± 0.5	-12.3 ± 0.5	-16.1 ± 0.5	-	144 ± 2.5 (76.6 ± 1.3)
Sulfide Branched Oleyl Oleate Monoesters						

A2-S2	-5.9±0.6	-12.5±0	-56.6±0.1	-66.2±0.0	-	52±2.5 (34±1.6)
A2-S3	-3.1±0.1	-7.5±0.1	-52.1±0.1	-69.1±0.3	-	80±4.4 (55±3.0)
A2-S4	-7.4±0.6	-14.2±0.1	-57.9±0.1	-62.3±0.5	-	55±5.7 (39±4.1)
A2-S6	-7.2±0.8	-13.6±1.1	-61.2±1.3	-66.0±3.5	-	56±4.8 (43±3.7)
Mean	-5.9±0.5	-11.9±0.4	-56.9±0.4	-65.7±1.0	-	61±4.3 (43±3.1)
Sulfonyl Branched Oleyl Oleate Monoesters						
A2-SO ₂ -2	-7.4±0.3	-15.5±0.7	-34.1±0.2	-30.9±1.2	-70.9±2.8	13±0.6 (9±0.4)
A2-SO ₂ -3	-2.5±0.4	-7.6±0.3	-32.1±0.7	-20.6±0.7	-72.9±1.2	18±1.4 (13±1.1)
A2-SO ₂ -4	-10.8±0.1	-18.4±0.1	-32.1±0.6	-39.6±2.5	-75.2±0.5	6±0.1 (5±0.1)
A2-SO ₂ -6	-5.9±0.5	-11.4±0.7	-33.1±0.8	-24.1±1.1	-75.0±0.1	17±0.6 (15±0.5)
Mean	-6.7±0.3	-13.2±0.4	-32.8±0.6	-28.3±1.4	-73.3±1.1	14±0.7 (10±0.5)
DSC Data – Heating Cycle (5°C/min)						
	T_{ON}	T_m P ₁	T_m P ₂	T_{OFF}	T_g	ΔH_m
Oleyl oleate monoester						
A	-10±0.5	-6.2±0.5	8.5±0.5	11.4±0.5	-	143±3.0 (76±1.6)
Sulfide Branched Oleyl Oleate Monoesters						
A2-S2	-65.7±0.0	-16.2±0	-54.7±0.0	-5.6±0	-	70±2.5 (46±1.6)
A2-S3	-61.1±0.1	-13.0±0.2	-21.6±0.1	3.5±0.1	-	85±4.4 (58±3.0)
A2-S4	-41.9±0.1	-9.4±0.3	-34.2±0.4	-1.0±0.1	-	62±3.3 (44±2.4)
A2-S6	-75.9±3.8	-7.8±0.8	-30.0±0.8	0.3±0.8	-	61±0.8 (47±0.6)
Mean	-61.6±1.0	-11.6±0.3	-35.2±0.3	2.6±1.0	-	70±2.7 (49±1.9)
Sulfonyl Branched Oleyl Oleate Monoesters						
A2-SO ₂ -2	-40.1±2.7	-6.5±0.8	-30.1±0.7	2.2±0.6	-66.2±2.3	17±1.5 (12±1.1)
A2-SO ₂ -3	-18.7±1.3	-1.0±0.2	-30.2±0.3	4.4±0.2	-67.6±0.5	23±0.3 (17±0.2)
A2-SO ₂ -4	-37.4±0.1	-8.4±0.8	-35.9±0.1	-0.9±0.0	-70.5±0.2	6±2.5 (5±1.9)
A2-SO ₂ -6	-45.2±1.0	-3.2±0.3	-35.4±0.5	2.6±0.2	-70.1±0.1	14±1.0 (12±0.8)
Mean	-35.2±1.3	-4.8±0.5	32.7±0.4	2.6±1.0	-68.6±0.8	15±1.3 (11±1.0)

The phase transformation path of the sulfide branched oleyl oleate monoesters show similarity with oleyl oleate in that they crystallized through mainly two crystallization exotherms (P_1 and P_2 in **Figure 4-2a**) mirrored by corresponding endotherms during heating (**Figure 4-2b**). The branching of oleyl oleate with sulfide groups did not significantly change the onset of crystallization. However as shown in **Table 4-1**, the enthalpy of sulfide branched oleyl oleate monoesters were lower compared to the oleyl oleate base monoester (mean value of 43 ± 3.1 kJ/mol compared to 77 ± 1.3 kJ/mol). Moreover, the sulfonyl branched oleyl oleate monoesters have much lower mean enthalpy (10 ± 0.5 kJ/mol) than the oleyl oleate base ester and sulfide branched oleyl oleate monoesters (See **Table 4-1**). Also, sulfonyl branched oleyl oleate monoesters presented glass transitions at -75 °C (See **Table 4-1**), whereas oleyl oleate and sulfide branched oleyl oleate monoesters did not. Both the sulfide and sulfonyl branched oleyl oleate monoesters presented recrystallization mediated by melt upon heating (P_R at -60 °C and -45 °C in **Figure 4-2b**, respectively).

For both sulfide and sulfonyl branched oleyl oleate monoesters, the length of the branched hydrocarbon chain ($n = 2$ to 6) had little effect on the crystallization and melting transition path and transition parameters. The difference in phase transition behavior between the sulfide and the sulfonyl monoesters can be chiefly attributed to the large difference in bulkiness of the functional groups and extent of intermolecular interactions that they contribute.

According to Gibbs free energy at the phase transition ($T_m = \Delta H / \Delta S$) [72], the fact that transition onset and peak temperatures were not significantly affected by branched hydrocarbon chain length indicates that the difference in enthalpy is driven by entropy considerations. The size and conformation of the sulfonyl pendant groups introduce much larger numbers of conformational

arrangements than the sulfide pendant groups. The lower onset of crystallization of the sulfonyl branched oleyl oleate monoesters compared to oleyl oleate and sulfide branched oleyl oleate monoesters is attributable to the sulfonyl-sulfonyl repulsions and geometry of the sulfonyl branches which offset the van der Waals and dipole-dipole attractions. The dense oxygen electronic clouds on the sulfonyl groups tend to repel each other upon supercooling. XRD studies on saturated aliphatic monosulfones showed that adjacent sulfonyl groups repel each other and separate by as much as 5Å in the crystal phase [73].

The glass transition observed in the sulfonyl-branched oleyl oleate monoesters is explained by the presence of the bulky, inflexible and polar sulfonyl groups. At low temperature, sulfonyl-sulfonyl interaction becomes effective enough to arrange the molecules but so slowly that they cannot adequately order configurations in the available time allowed by the cooling rate and hence lead to the formation of a glass rather than a crystal [74].

4.4.4 PLM Observations

PLM images obtained for A2-S-3 and A2-SO₂-3 when cooled from 50 °C down to -90 °C at 1 °C/min are shown in **Figure 4-3a**. As shown in **Figure 4-3a**, sulfonyl and sulfide branched monoesters crystallized in the same manner but nucleated and achieved different final number of crystallites and maximum crystallization at different temperatures. Both materials started with a burst of a small number of growth centers (at induction temperature T_{ind}) that remained homogeneously dispersed and did not significantly grow until a lower temperature (the growth temperature T_{Gr}) at which they slowly start to form small rods and eventually dendrites homogeneously dispersed on the PLM slide view window.

The PLM slide and coverslip constrains how the crystallites grow and can be different from when allowed to grow from the bulk melt; the PLM study was carried out for comparison purposes under common conditions. It allowed to determine differences in crystallization propensity and is not entirely indicative of what would happen when crystallized from the bulk melt.

T_{Ind} and T_{Gr} of A2-S-3 are -5 °C and -47 °C, respectively. A2-S-3 crystallites achieved final size at about -56 °C. The crystallites however remained small ($9.4 \pm 1.6 \mu\text{m}^2$) and occupied only a small fraction of the slide view window area estimated between 25 % to 30 % of the total view window area. T_{Ind} and T_{Gr} of A2-SO₂-3 are -3 °C and -47 °C, respectively. Similarly, A2-SO₂-3 crystallites also remained small ($7.9 \pm 1.2 \mu\text{m}^2$) and occupied a slide surface area estimated between 5 % to 10 % of the total slide view window area.

Secondary nucleation occurred at -56 °C, in A2-S-3 and at T_g for A2-SO₂-3 concomitant with the growth of the existing crystallites suggesting sporadic nucleation that is kinetically driven [75]. The secondary crystallites are formed in the melt where the fragments of crystallites from growing crystallites becomes new growth centers [76].

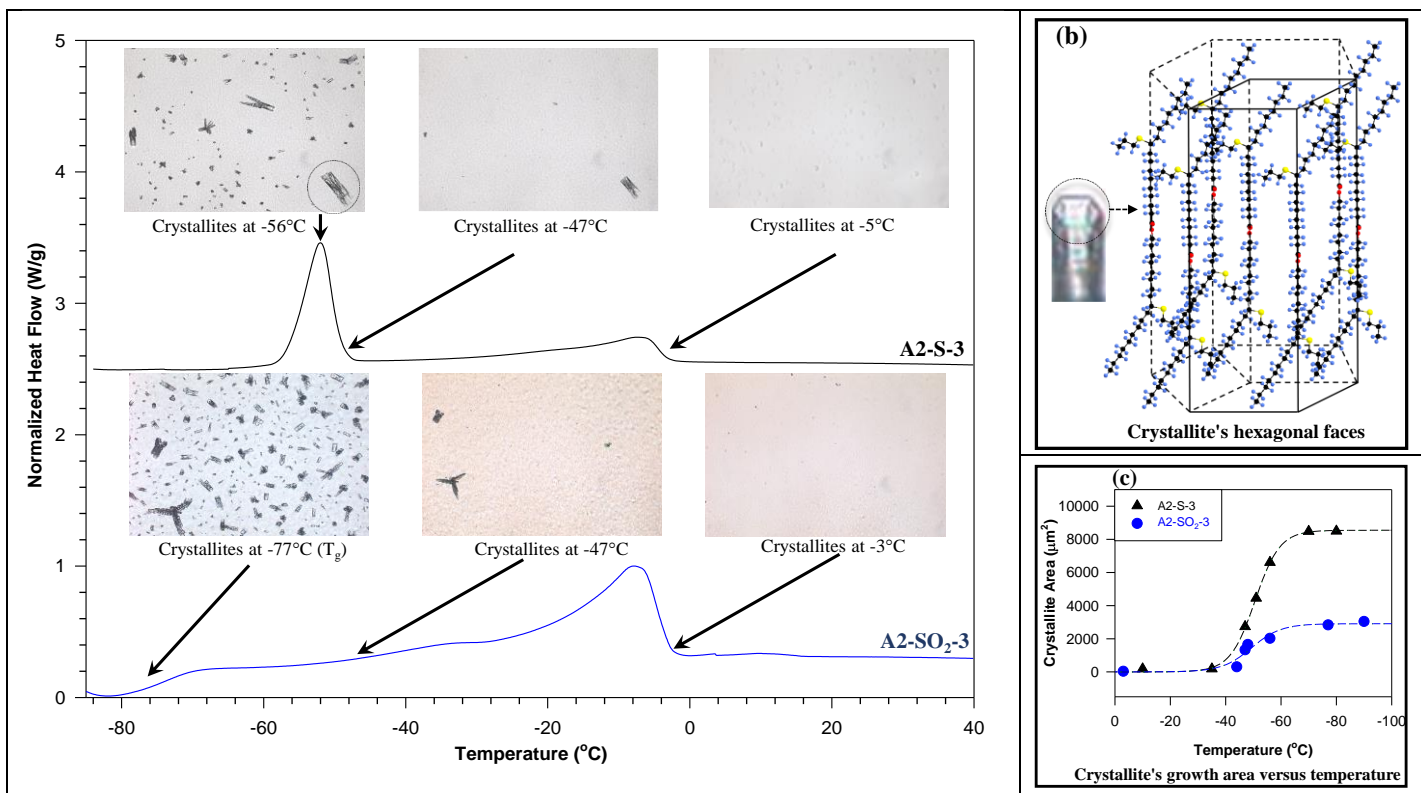


Figure 4-3. (a) Correlation of data from DSC cooling thermograms of A2-S-3 and A2-SO₂-3 with PLM observations at selected temperatures, (b) zoom into a crystallite hexagonal face and representation of associated α -polymorph, and (c) progression in crystallite size as determined by area versus temperature (dashed lines are fits to a sigmoidal function, Equation 3).

As shown in **Figure 4-3a**, the PLM data are consistent with the DSC results. In both A2-S-3 and A2-SO₂-3, the appearance of the first crystallites corresponds with the DSC onset of crystallization. The crystallites size increased steadily to reach a maximum at about the peak temperature of the second exotherm (P_2 , the most intense peak).

The rod-like crystallites observed in both A2-S-3 and A2-SO₂-3 PLM presented perfect hexagonal faces which indicate α -polymorphs. An example of such a face is shown in **Figure**

4-3b in the PLM of A2-S-3 sample taken at -56 °C. The crystallization of the lowest stability α - phases is consistent with the very poor and low temperature crystallization of these molecules.

The progression in crystallite size as determined by area versus temperature for A2-S-3 and A2-SO₂-3 is shown in **Figure 4-3c**. Both data is fitted to sigmoidal functions (*Equation 3*; $R^2 > 0.9950$).

$$f = \frac{A}{(1 + \exp(-\frac{x - x_0}{b}))} \quad \text{Equation 3}$$

Equation 3 adequately describes the crystallization process. Beside T_{md} which is provided by the first data point, the growth function allows the determination of T_{Gr} through onset temperature of growth, determined for example at the intersection of the baseline with the tangent at the inflection point, and maximum size that the crystallites achieve under the cooling rates through the plateau that is achieved (parameter A). The function also provides information on the rate of growth through the parameter b which indicates how far the inflection point is from the initial region of shallow slope. Parameter A and b are shown in **Table 4-2**.

Table 4-2. Parameter A and b of the sigmoidal function for A-S-3 and A2-SO₂-3.

Compound	Parameter A	Parameter b
A2-SO ₂ -3	3106±150μm ²	11.6±2.7°C
A2-S-3	8550±82.6μm ²	4.5±0.2°C

The inflection points of the curve for A2-SO₂-3 with $b = 11.6 \pm 2.7$ °C lies much further from the initial region of shallow slope than that of A2-S-3 which b is 4.5 ± 0.2 °C indicating a slower

growth rate (ratio 0.4). The tangents' ratio at the inflection points is estimated at 0.3 further confirming that A2-S-3 crystallites grows much faster than A2-SO₂-3 crystallites. The large difference in final crystallites size between A2-SO₂-3 and A2-S-3 as indicated by parameter A (3106±150 μm² and 8550±82.6 μm², respectively, i.e, 3:1) indicates that much larger limitations are imposed on growing surface by the bulky sulfonyl groups than the sulfide groups.

The difference in growth rate and crystal size between A2-SO₂-3 and A2-S-3 can be explained by the chemical natures of the sulfide and sulfonyl groups and their influence on the crystallization process. After growth centers form upon supercooling, molecules in the bulk melt are diffused onto the surface of the growing crystallite at a rate dictated by mass transfer consideration. The sulfonyl groups are not only bulkier than the sulfide groups but are also repulsive which adds to the difficulty of being in the appropriate configuration to attach to the growing surface. Additionally, as the temperature decreases the viscosity of A2-SO₂-3 increases more than that of A2-S-3 which causes a larger slowdown of molecular diffusion. The slowing down of the molecular diffusion process by sulfonyl groups in A2-SO₂-3 upon further supercooling is due to the entropy decreases without the molecules crystallizing until lower temperature is attained [76, 77].

4.4.5 Flow Behavior and Viscosity

4.4.5.1 Shear Stress- Shear Rate and Flow Behavior

The shear stress - shear rate data of the sulfide and sulfonyl branched oleyl oleate monoesters are provided in the SI in Fig S3. All compounds presented shear stress - shear rate curves which when fitted to the Herschel-Bulkley model (*Equation 1*, $R^2 \geq 0.9999$) yielded a power index $n = 1.000 \pm 0.001$ and yield stress values of less than 0.02 ± 0.02 Pa.s indicating Newtonian flow

behaviors. This is illustrated in **Figure 4-4** with the data obtained at 40°C for A2-S-3 and A2-SO₂-3.

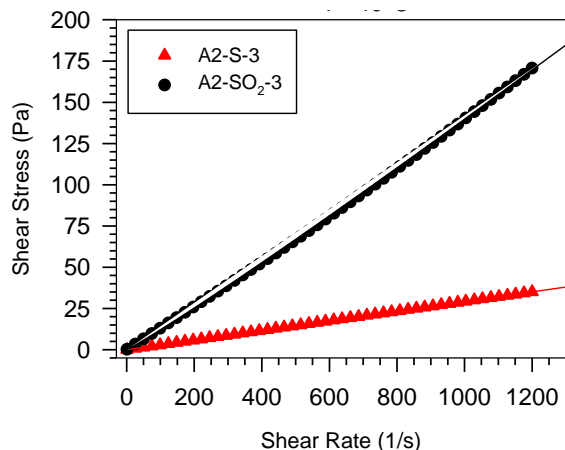


Figure 4-4. Shear stress - shear rate curves obtained at 40 °C for A2-S-3 and A2-SO₂-3. Solid lines are fits to the Herschel-Bulkley model (*Equation 1*).

4.4.5.2 Viscosity Versus Temperature Relationships

For any given temperature, viscosity of the sulfonyl-branched oleyl oleate monoesters was higher than that of the sulfide-branched oleyl oleate monoesters and oleyl oleate. As shown in **Figure 4-5a**, the sulfide and sulfonyl-branched oleyl oleate monoesters series are grouped in two distinct collections of viscosity versus temperature curves which all decrease with temperature following a typical exponential trend. The difference in viscosity ($\Delta\nu$) between them also decreases with temperature following a typical exponential trend (**Figure 4-5b**).

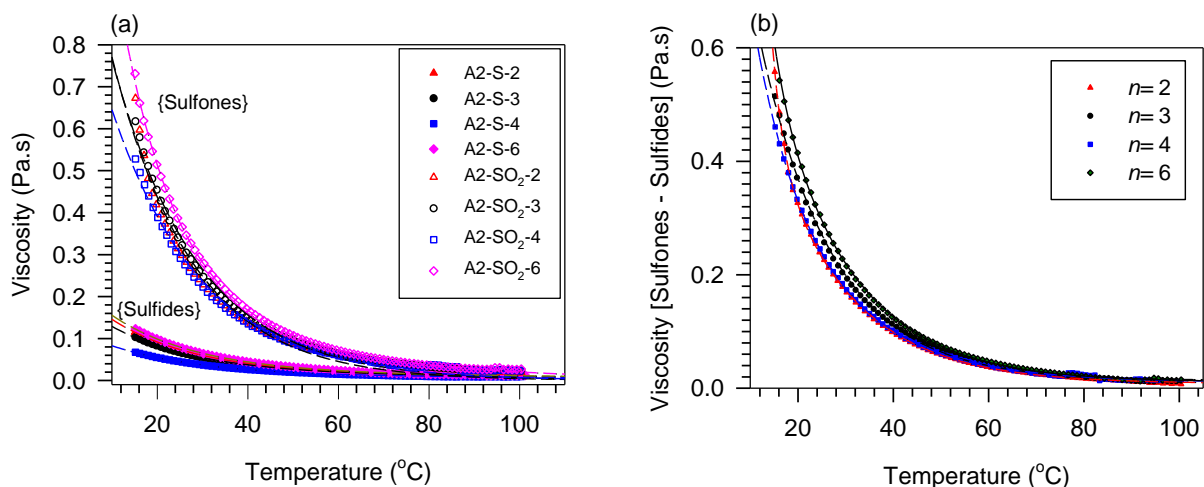


Figure 4-5. Viscosity versus temperature curves of (a) sulfide (filled) and sulfonyl (unfilled) branched oleyl oleate monoesters. (b) viscosity difference between the sulfonyl and sulfide branched oleyl oleate monoesters ($\Delta\nu$) versus temperature for $n=2 - 6$.

As shown in **Figure 4-5b**, $\Delta\nu$ versus temperature curves are practically independent of n . Overall, viscosity of sulfonyl branched oleyl oleate monoesters series is larger than sulfide branched oleyl oleate monoesters by 8 times at 20 °C, 4 times at 40 °C and 2 times at 100 °C. This suggests that contribution of the CH₂ units to the viscosity do not depend on the type of functional group.

For each series and for any given temperature, viscosity versus chain length present a flat minimum at $n = 4$. The example of viscosity at 40 °C of the sulfide and sulfonyl branched oleyl oleate monoesters is shown in **Figure 4-6a**. The difference in viscosity ($\Delta\nu$) versus n is consistently linear. This trend is illustrated in **Figure 4-6b** for $T= 25$ °C, 40 °C and 90 °C. As expected, the slope of these lines (m in **Figure 4-6b**) consistently decreases with increasing temperature. The presence of the flat minimum in the viscosity versus n curves and linear increase of $\Delta\nu$ versus n , indicates that although the CH₂ units add equally to the viscosity in

both sulfide and sulfonyl branched oleyl oleate monoesters, internal configuration involving geometry (bulkiness) and polarity effects determine the overall magnitude of the viscosity. These data suggest that the contribution of the hydrocarbon chain effect prevails only when n is higher than 4 carbons.

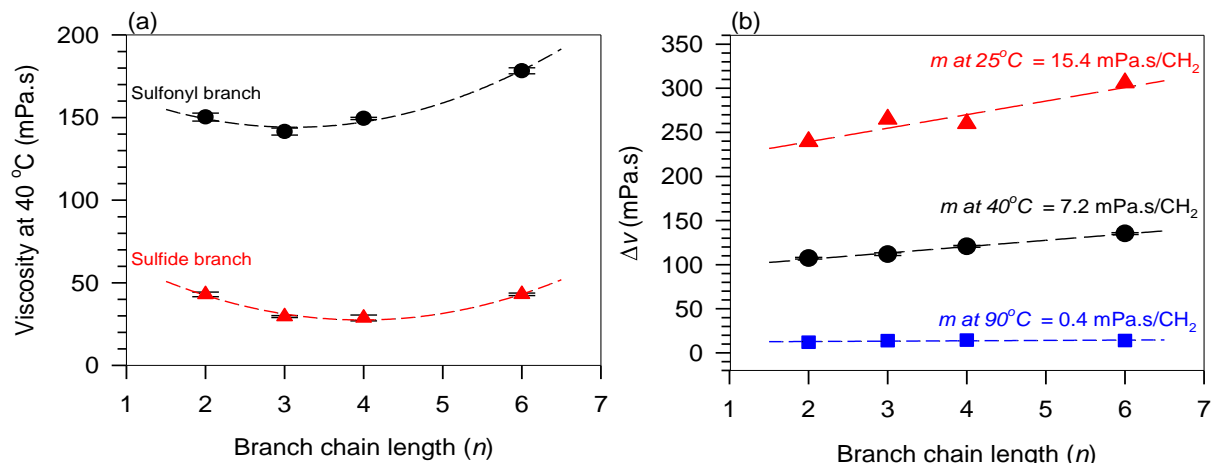


Figure 4-6. (a) Viscosity at 40°C of the sulfide and sulfonyl branched oleyl oleate monoesters versus branch chain length (n). Dashed line are guides for the eyes. (b) Difference in viscosity between sulfonyl branch and sulfide functional group (ΔV) taken at 25 °C, 40 °C and 90 °C. Error bars are standard deviation of three replicates.

The Generalized van Velzen model (GvVE, Equation 1) provided good fits to the viscosity versus temperature data for all sulfide and sulfonyl branched oleyl oleate monoesters with $R^2 > 0.9998$ and residuals $< 0.25\%$. The results of the fit (parameters A and exponent m) are provided in **Figure 4-7**.

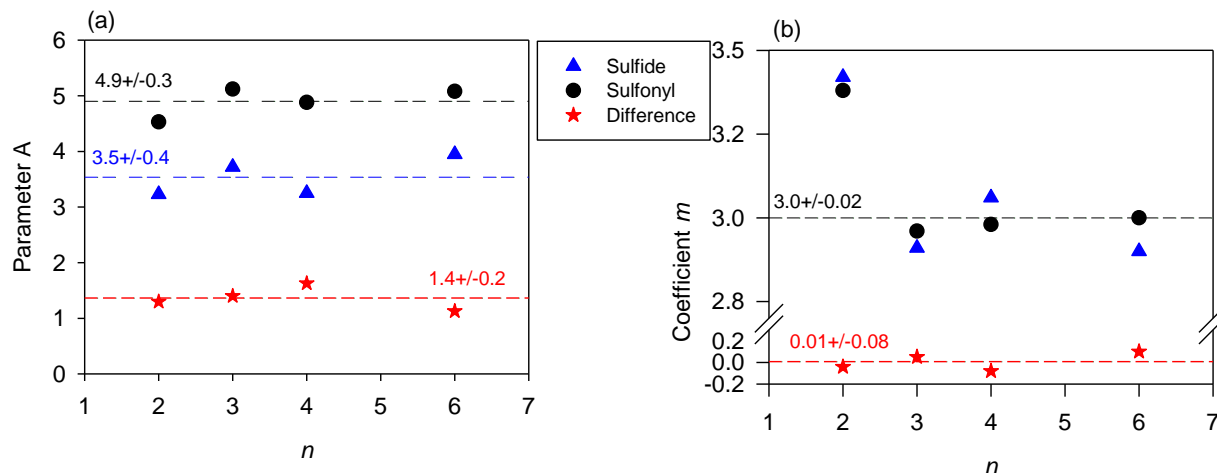


Figure 4-7. Parameters of the fit of sulfide and sulfonyl branched oleyl oleate monoesters to the GvVE versus branch chain length n (a) parameter A , (b) coefficient m .

As shown in **Figure 4-7a**, parameter A for sulfonyl branched oleyl oleate monoester is higher than that of the sulfide branched oleyl oleate monoesters confirming the overall difference in viscosity magnitude. Importantly, there is no significant difference in A among the compounds of the same series indicating that essentially similar factors drive the level of viscosity that can be attained in each series. The coefficient m on the other hand is similar in both series. Overall, the difference in m between the two series is less than the uncertainty of the fit (calculated standard deviation of less than 0.02). There is however a dip in m from 3.4 ± 0.02 to 3.0 ± 0.02 when the ester is branched with more than $n = 2$. These data suggest a jump in conformation complexity at $n = 2$.

The viscosity in the temperature region where it was measured (0-100°C, i.e., liquid state) is dictated predominately by molecular size and conformation and intermolecular force constants and is affected by the number of external degrees of freedom per molecule excited in the state [78]. The significant difference in the shape of the two molecules and the stronger sulfonyl

permanent dipoles (4.4D [79]) which provide extra persistent sulfonyl-sulfonyl intermolecular attraction in the liquid state are therefore the main contributors to the difference in viscosity between the two series.

The GvVE data suggest that the complexity of the molecule relevant to viscosity is only related to chain length not functional group size. The difference in magnitude would be therefore due to the large dipole moments on the sulfonyl groups and their persistent interaction in the liquid state.

The GvVE parameters obtained here can be used to accurately determine the viscosity of any sulfide and sulfonyl branched oleyl oleate monoesters without actual measurement, which would be a powerful screening tool before eventual synthesis of the materials. The extent of branch chain length at which the constant A and m determined would be valid is subject of further experimental work which is out of the scope of the present work.

4.4.6 Oxidative Stability

The oxidative stability curves obtained under dry air (DSC heating thermograms at 10 °C/min) of sulfide and sulfonyl branched oleyl oleate monoesters and corresponding data are provided *in SI* in *Fig SI.3* and *Table SI.2*, respectively.

The oxidative stability curves of oleyl oleate (A), ester branched oleyl oleate (A4-C-3), sulfide branched oleyl oleate (A2-S-3) and sulfonyl branched oleyl oleate (A2-SO₂-3) are shown in **Figure 4-8**. The onset temperature of oxidation (T_{on}^{ox}) is indicated in **Figure 4-8** by arrows. The molecular structures of the compound corresponding to each oxidative stability curves are

provided in the right panel of **Figure 4-8** to assist in the discussion. The protons susceptible to oxidations are highlighted in blue and yellow boxes on the molecular structures.

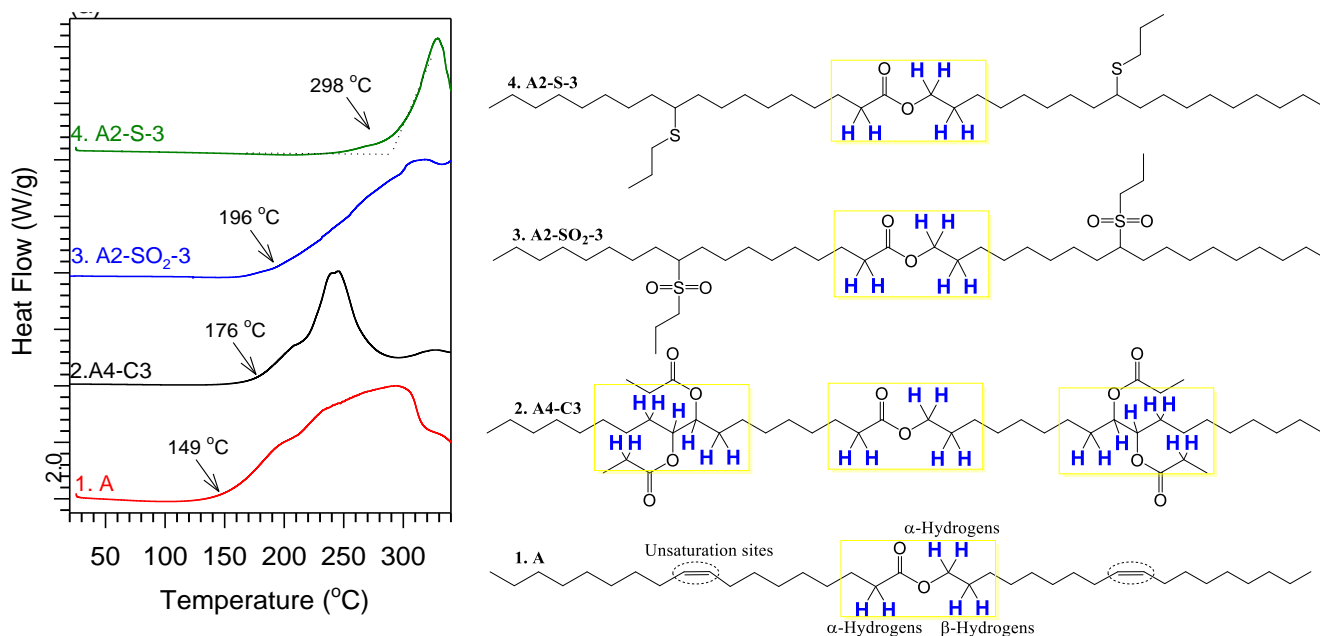


Figure 4-8. DSC heating (10°C/min) thermograms at of oleyl oleate (A), ester branched oleyl oleate (A4-C-3), sulfonyl branched oleyl oleate (A2-SO₂-3) and sulfide branched oleyl oleate (A2-S-3). Onset temperatures of oxidation (T_{on}^{ox}) are indicated by arrows. Right panel: molecular structures of above compounds with protons prone to oxidation highlighted in blue and yellow boxes.

Figure 4-8 indicates that the oxidative stability is improved by branching through the elimination of the double bonds and introduction of functional groups capable of mitigating oxidation. A4-C-3 which has four ester pendant chains (Compound 2 in **Figure 4-8**) increased oleyl oleate T_{on}^{ox} by 27 °C. This is attributable to the elimination of the ester pendant group at the site of branching. T_{on}^{ox} of A2-S-3 (298±2 °C) and A2-SO₂-3 (196±2 °C) are respectively 149 °C and 47 °C higher than T_{on}^{ox} of oleyl oleate and higher than that of A4-C-3 by 12 °C and 115 °C,

respectively. This indicates that the functional groups significantly contributes to the oxidation stability. If one considers that the increase in T_{on}^{ox} A4-C-3 compared to oleyl oleate is due to the removal of the ester groups at the site of branching, then in a first approximation, the sulfide pendant group would be responsible for an added 88 °C. The significant increase in the oxidative stability due to the sulfide's pendant groups is attributable to its ability to mitigate chain propagation by decomposing reactive hydroperoxides generated at the initiation stage of oxidation [41].

In general, the most detrimental reaction to the properties of ester lubricants is high-temperature oxidation with peroxy radicals [80]. The oxidation of ester lubricants with hydroperoxides proceeds like in other organic compounds through a free radical chain mechanism which can be described in terms of initiation, propagation, and termination processes [80]. Hydroperoxides typically react at the following reactive sites associated with the ester groups: α -hydrogens on the alkoxy carbon moiety and at the α and β hydrogens on the acyl moiety [81]. These sites are highlighted (yellow boxes) in the right panel of **Figure 4-8**. Sulfide groups are known to convert hydroperoxides to non-radical derivatives relatively rapidly [82]. This reaction removes hydroperoxides as they are formed, and thus mitigate oxidation [83, 84].

The typical solution to prevent oxidation of commercial base oil is by antioxidant additives such as Zinc dialkyldithiophosphate (ZDDP) and butylated hydroxytoluene (BHT). These well-known and universally used antioxidant additives operate through similar mechanisms to prevent oxidative degradation [85]. **Table 4-3** shows the antioxidant inhibition performance measured by the OIT of some of the various antioxidants used in commercial lubrication formulations compared to the OIT of the present sulfide and sulfonyl branched oleyl oleate monoesters. The

ranking of **Table 4-3** from the highest to the lowest is a measure of the relative inhibition strength of the different lubricant formulations. However, because the OITs were determined at different oxidation processing conditions such as different heating rate and isothermal processing, the ranking of **Table 4-3** is only indicative. At this time, there is no official method that would allow a more consistent determination of OIT.

Table 4-3. Oxidation induction time (OIT) of various sulfide-based and commercial antioxidants used in lubrication formulation from largest to smallest.

	Additives	wt % (w/w)	Base Oil	OIT (min)	Refs
1.	ZDDP	2 %	Hexadecane mineral oil	214	[86]
2.	ZDDP	1 %	Hexadecane mineral oil	205	[86]
3.	AO1	3 %	Trimethylolpropane trioleate	100	[87]
4.	ZDDP	0 %	Hexadecane mineral oil	96	[86]
5.	Hexadecane thiol	1 %	10W50 engine oil	94	[43]
6.	Hexadecane thiol	1 %	10W50 engine oil	89	[43]
7.	Hexadecane thiol	1 %	10W50 engine oil	86	[43]
8.	BHT	3 %	Trimethylolpropane trioleate	75	[87]
9.	--	--	A2-S-3	62	<i>This work</i>
10.	Hexadecane thiol	0 %	10W50 engine oil	61	[43]
11.	AO1	1.5 %	Trimethylolpropane trioleate	60	[87]
12.	ZDDP	1 %	Hexadecane/20%-methyl oleate	52	[86]
13.	dibutyl sulfide	0.5 %	Poly- α -olefin	49	[42]
14.	BHT	1.5 %	Trimethylolpropane trioleate	40	[87]
15.	--	--	A2-SO ₂ -3	37	<i>This work</i>
16.	AO1	0.5 %	Trimethylolpropane trioleate	36	[87]
17.	--	--	Oleyl oleate (A)	30	<i>This work</i>
18.	Irganox 1076	3 %	Trimethylolpropane trioleate	30	[87]
19.	Irganox 1076	0.5 %	Trimethylolpropane trioleate	22	[87]
20.	BHT	0.5 %	Trimethylolpropane trioleate	21	[87]
21.	Irganox 1076	1.5 %	Trimethylolpropane trioleate	21	[87]
22.	BHT	0 %	Trimethylolpropane trioleate	20	[87]
23.	ZDDP	0 %	Hexadecane/20%-methyl oleate	15	[86]
24.	Dodecyl sulfide	10 %	Naphthenic mineral oil	14	[88]

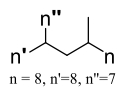
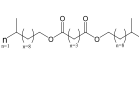
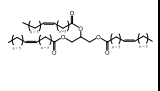
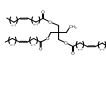
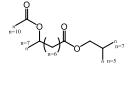
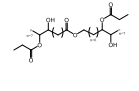
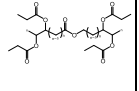
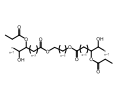
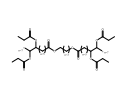
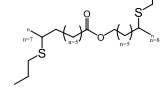
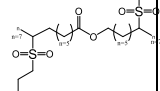
The OIT of the sulfide-branched oleyl oleate monoesters is 62 min. This value is relatively significant compared to other sulfide-based molecules and commercial antioxidants. It ranks 9th

among the formulations listed in **Table 4-3** and is about 30 % of the best listed commercial formulation (2 % w/w ZDDP in hexadecane mineral oil) and compares well with the 3 % BHT in trimethylolpropane trioleate formulation. The advantage of the present sulfide-branched oleyl oleate monoesters over sulfide additives is that their propensity to prevent oxidization-is carried by the molecules of the base oil itself, which would assist in the extra cost and possible hazards of additives.

4.4.7 Comparison Of Oleyl Oleate, Sulfide and Sulfonyl Branched Oleyl Oleate Monoesters with Mineral Oils and Biobased Lubricants.

Table 4-4 compare the pour point (PP) and viscosity of A2-S-3 and A2-SO₂-3 (representatives of A2-S-*n* and A2-SO₂-*n*) with typical commercial mineral oil, common synthetic lubricants (poly alkyl olefins (PAOs) and isoalkyl adipate) and select high-performance biolubricants mined from the literature [58, 59]. The flow properties of soybean oil, trioleate trimethylolpropane, estolides as well as jojoba-like monoesters (JLEM) and jojoba-like diester studied by our research group [25, 27] are also included in **Table 4-4**. The molecular structures of the listed materials such as total carbon chain length, unsaturation sites, functional group flexibility and polarity and number and position of branch chain on the backbone are included in the table to explain the differences in lubricant functionality including the flow properties.

Table 4-4. Comparison of flow properties of select commercial lubricants and biolubricants of similar carbon chain length.

Lubricant	Mineral Oil	PAO	Di i-C13 adipate	Soybean Oil	TMP	Estolide	JLEM 1	JLEM 2	JLED 1	JLED 2	A2-S-3	A2-SO ₂ -3
Reference	[59]	[58, 59]	[59]	[59]	[89]	[90]	[25, 27]	[25, 27]	[28]	[29]	<i>(This work)</i>	<i>(This work)</i>
Molecular structure												
Total carbon chain length ^a		21	32	39	39	31	36	36	42	42	36	36
Pour point ^b (°C)	-21	-63	-54	-9	-55	-45	-57 (T _g)	-73 (T _g)	-64 (T _g)	-73 (T _g)	-10	-73 (T _g)
Viscosity mPa.s @40°C	71	17	27	32	46	47	391	130	338	162	35	145

TMP: Trimethylpropane esters

PAO: Poly alkyl olefins

^aNumber of carbon atoms contained in the longest linear segment.

^bASTM derived values for the last temperature at which a liquid will flow.

The data presented in **Table 4-4** indicate that protruding branched groups are effective in suppressing crystallization. Branching an aliphatic chain backbone with a minimum of two internal protruding chains was sufficient to drive crystallization to below -50 °C. The flexibility of the ester functional group introduces high degrees of freedom which decrease the energy barrier to rotation [78] and thereby lowering crystallinity and inducing glass transitions at low temperature. The flexible C-O bond of ester groups combines with the branched chains to promote gel-like soft matter instead of crystals.

The viscosity is influenced by total carbon chain length and presence of functional group in the molecular structures. **Table 4-4** indicates the weak dispersion forces of compounds with only hydrocarbon structure impart the lowest viscosity (for example PAO has a viscosity of 17 mPa.s). The molecules with only ester or sulfide functional groups such as Di i-C13 adipate (27 mPa.s), soybean oil (32 mPa.s), trioleate trimethylol propane (46 mPa.s), estoloids (47 mPa.s) and sulfide branched oleyl oleate monoesters (35mPa.s) have slightly higher but still low viscosity because of low polarity [91]. Molecules with hydroxyl (JLEM and JLED with free OH groups) and sulfonyl groups (A2-SO₂-3) have higher viscosities because they form strong dipole-dipole interaction that persist in the liquid state.

JLEMs which have two free hydroxyl group present a viscosity ~3 times higher than A2-SO₂-3 which has two sulfonyl groups (391 mPa.s and 145 mPa.s, respectively). Although the sulfonyl group has a stronger dipole moment (4.4 D) [92] than the hydroxyl group (1.7 D) it imparted a lower viscosity to the molecule because of stark differences in the geometry and electronic structure of the groups. Contrary to the small hydroxyl groups of JLEMs which efficiently form a strong hydrogen bond network, the sulfonyl group has a

bulky geometry and a dense oxygen electron cloud which generates sulfonyl-sulfonyl repulsion and therefore much weaker intermolecular attractions.

4.5 Conclusion

Novel compounds suitable for potential use as biolubricants synthesized by branching oleyl oleate with sulfide and sulfonyl groups were prepared using thiolene chemistry. The internal nature of the sites of functionalization enabled the formation of protuberant sulfide and sulfonyl branch groups which altered phase behavior and benefiting critical lubricant properties. The branching suppressed crystallization and increased viscosity owing to the combined effects of increased mass, steric hindrances and functional groups attractions. The sulfonyl-branched oleyl oleate monoesters were more effective in suppressing crystallization, effectively inducing glass transitions at temperatures as low as $-73\text{ }^{\circ}\text{C}$ and significantly increasing viscosity. The sulfide-branched oleyl oleate monoesters also improved oleyl oleate in suppressing crystallization and increasing viscosity but not as much as the sulfonyl-branched oleyl oleate monoesters. sulfide-branched oleyl oleate monoesters imparted higher inherent oxidation stability reflected in an increase of $149\text{ }^{\circ}\text{C}$ in onset of oxidation compared to oleyl oleate. Overall, the sulfide and sulfonyl branched oleyl oleate monoesters of this work presented useful thermal transition and viscosity profiles which are better than mineral oils, making them suitable alternatives for use in lubricant formulations.

4.6 References

1. Shah, R., M. Woydt, and S. Zhang, *The Economic and Environmental Significance of Sustainable Lubricants*. Lubricants, 2021. **9**(2): p. 21.<https://doi.org/10.3390/lubricants9020021>.
2. Salih, N. and J. Salimon, *A Review on eco-friendly green biolubricants from renewable and sustainable plant oil sources*. Biointerface Res. Appl. Chem, 2021. **11**(5): p. 13303-13327.<https://doi.org/10.33263/BRIAC115.1330313327>.
3. Deliverable, N., *Knowledge Based Bio-based Products' Pre-Standardization*. 2015.<https://www.biobasedeconomy.eu/app/uploads/sites/2/2017/03/Public-report-on-horizontal-standard-for-bio-based-carbon-content-determination.pdf>.
4. Erhan, S.Z., B.K. Sharma, Z. Liu, and A. Adhvaryu, *Lubricant base stock potential of chemically modified vegetable oils*. Journal of Agricultural and Food Chemistry, 2008. **56**(19): p. 8919-8925.<https://doi.org/10.1021/jf801463d>.
5. Arnsek, A. and J. Vizintin, *Scuffing load capacity of rapeseed-based oils (c)*. Lubrication Engineering, 1999. **55**(8): p. 11-18. ISSN: 0024-7154.
6. Salih, N. and J. Salimon, *A Review on New Trends, Challenges and Prospects of Ecofriendly Friendly Green Food-Grade Biolubricants*. 2021. **12**(1): p. 1185-1207.<https://doi.org/10.33263/BRIAC121.11851207>.
7. Sharma, B.K., Z. Liu, A. Adhvaryu, and S.Z. Erhan, *One-pot synthesis of chemically modified vegetable oils*. Journal of Agricultural and Food Chemistry, 2008. **56**(9): p. 3049-3056.<https://doi.org/10.1021/jf073070z>.
8. Wu, H.P., S. Jiang, Y.Y. Xu, and J.Z. Chen, *Preparation of bio-lubricating base oils from rapeseed oil*. Gao Xiao Hua Xue Gong Cheng Xue Bao/Journal of Chemical Engineering of Chinese Universities, 2009. **23**(1): p. 116-121.
9. Kinney, A.J., *Development Of Genetically Engineered Soybean Oils For Food Applications*. Journal of Food Lipids, 1996. **3**(4): p. 273-292.<https://doi.org/10.1111/j.1745-4522.1996.tb00074.x>.
10. Ghazani, S.M. and A.G. Marangoni, *Healthy Fats and Oils*, in *Reference Module in Food Science*. 2016, Elsevier: <https://doi.org/10.1016/B978-0-08-100596-5.00100-1>.
11. Al-Bachir, M. and H. Sahloul, *Fatty acid profile of olive oil extracted from irradiated and non-irradiated olive fruits*. International Journal of Food Properties, 2017. **20**(11): p. 2550-2558.<https://doi.org/10.1080/10942912.2016.1243557>.

12. Alibaba. *High Quality Oleyl Oleate; CAS:3687-45-4; Best Price from China, Factory Hot sale Fast Delivery.* 2021; Available from: https://www.alibaba.com/product-detail/High-Quality-Oleyl-Oleate-CAS-3687_1600121399286.html?spm=a2700.galleryofferlist.normal_offer.d_title.62191151mZvVOO.
13. Zainal, N.A., N.W.M. Zulkifli, M. Gulzar, and H.H. Masjuki, *A review on the chemistry, production, and technological potential of bio-based lubricants.* Renewable and Sustainable Energy Reviews, 2018. **82**: p. 80-102. <https://doi.org/10.1016/j.rser.2017.09.004>.
14. Salimon, J., B.M. Abdullah, and N. Salih, *Optimization of the oxirane ring opening reaction in biolubricant base oil production.* Arabian Journal of Chemistry, 2016. **9**: p. S1053-S1058. <https://doi.org/10.1016/j.arabjc.2011.11.002>.
15. Mudhaffar, B. and J. Salimon, *Epoxidation of vegetable oils and fatty acids: catalysts, methods and advantages.* Journal of Applied Sciences, 2010. **10**(15): p. 1545-1553. doi <https://dx.doi.org/10.3923/jas.2010.1545.1553>.
16. Saurabh, T., M. Patnaik, S. Bhagt, and V. Renge, *Epoxidation of vegetable oils: a review.* Int. J. Adv. Eng. Technol, 2011. **2**(4): p. 491-501. E-ISSN 0976-3945.
17. Bouzidi, L., S. Li, S. Di Biase, S.Q. Rizvi, and S.S. Narine, *Lubricating and waxy esters, I. Synthesis, crystallization, and melt behavior of linear monoesters.* Chemistry and Physics of Lipids, 2012. **165**(1): p. 38-50. <https://doi.org/10.1016/j.chemphyslip.2011.11.003>.
18. Bouzidi, L., S. Li, S. Di Biase, S.Q. Rizvi, and S.S. Narine, *Lubricating and waxy esters. 4. Synthesis, crystallization behavior, melt behavior, and flow behavior of linear monoesters incorporating 9-Decenol and 9-Decenoic acid.* Industrial & Engineering Chemistry Research, 2013. **52**(7): p. 2740-2749.
19. Rodrigues Jr, J.d.A., F.d.P. Cardoso, E.R. Lachter, L.R. Estevão, E. Lima, and R.S. Nascimento, *Correlating chemical structure and physical properties of vegetable oil esters.* Journal of the American Oil Chemists' Society, 2006. **83**(4): p. 353-357. <https://doi.org/10.1007/s11746-006-1212-0>.
20. Allen, C.A.W., K.C. Watts, R.G. Ackman, and M.J. Pegg, *Predicting the viscosity of biodiesel fuels from their fatty acid ester composition.* Fuel, 1999. **78**(11): p. 1319-1326. [https://doi.org/10.1016/S0016-2361\(99\)00059-9](https://doi.org/10.1016/S0016-2361(99)00059-9).
21. Salimon, J., W. Abdo, N. Salih, A. Yarmo, and D. Derawi, *Lubricity and Tribological Properties of Dicarboxylic Acid and Oleyl Alcohol Based Esters.* Sains Malaysia, 2015. **44**: p. 405-412. <http://dx.doi.org/10.17576/jsm-2015-4403-12>.
22. Yasa, S.R., S. Cheguru, S. Krishnasamy, P.V. Korlipara, A.K. Rajak, V.J.I.c. Penumarthy, and products, *Synthesis of 10-undecenoic acid based C22-dimer acid*

- esters and their evaluation as potential lubricant basestocks*. 2017. **103**: p. 141-151.<https://doi.org/10.1016/j.indcrop.2017.04.005>.
23. Ahmed, W.A., J. Salimon, and M.A. Yarmo, *Lubricity Characterizations of Sebacic Acid Based Ester*. International Journal on Advanced Science, Engineering and Information Technology, 2014. **4**(1): p. 1-6.<http://dx.doi.org/10.18517/ijaseit.4.1.355>.
 24. Ahmed, W.A., A. Yarmo, N. Salih, M.D. Derawi, M.R. Yusop, and J. Salimon, *Synthesis and Lubricity Properties Analysis of Branched Dicarboxylate Esters Based Lubricant*. Malaysian Journal of Analytical Sciences, 2015. **19**(1): p. 106-117.https://www.ukm.my/mjas/v19_n1/pdf/Waled_19_1_13.pdf.
 25. Narine, S., S. Li, A. Mahdevari, L. Bouzidi, S.A. DiBiase, and S.Q. Rizvi, *Patent - Esters for use as a base stock and in lubricant applications*. 2014, <https://patents.google.com/patent/WO2012109653A1/en>.
 26. Raghunanan, L. and S.S. Narine, *Engineering Green Lubricants I: Optimizing Thermal and Flow Properties of Linear Diesters Derived from Vegetable Oils*. ACS Sustainable Chemistry & Engineering, 2016. **4**(3): p. 686-692.<https://doi.org/10.1021/acssuschemeng.5b01644>.
 27. Li, S., L. Bouzidi, and S.S. Narine, *Lubricating and Waxy Esters, V: Synthesis, Crystallization, and Melt and Flow Behaviors of Branched Monoesters Incorporating 9-Decenol and 9-Decenoic Acid*. Industrial & Engineering Chemistry Research, 2014. **53**(31): p. 12339-12354.<https://doi.org/10.1021/ie5014844>.
 28. Li, S., L. Bouzidi, and S.S. Narine, *Lubricating and Waxy Esters. 6. Synthesis and Physical Properties of (E)-Didec-9-enyl Octadec-9-enedioate and Branched Derivatives*. Industrial & Engineering Chemistry Research, 2014. **53**(51): p. 20044-20055.<https://doi.org/10.1021/ie502776s>.
 29. Raghunanan, L. and S.S. Narine, *Branched Biobased Diesters with Exceptional Low Temperature and Flow Properties for Use in Lubricant Formulations*. ACS Sustainable Chemistry & Engineering, 2016. **4**(5): p. 2542-2549.<https://doi.org/10.1021/acssuschemeng.5b01686>.
 30. Raghunanan, L. and S.S. Narine, *Engineering Green Lubricants II: Thermal Transition and Flow Properties of Vegetable Oil-Derived Diesters*. ACS Sustainable Chemistry & Engineering, 2016. **4**(3): p. 693-700.<https://doi.org/10.1021/acssuschemeng.5b01708>.
 31. Bouzidi, L., S. Li, S. Di Biase, S. Q. Rizvi, P. Dawson, and S. Narine, *Lubricating and Waxy Esters II: Synthesis, Crystallization, and Melt Behavior of Branched Monoesters*. 2012. **51**: p. 14892–14902.<https://doi.org/10.1021/ie3016472>.

32. Raghunanan, L. and S.S. Narine, *Engineering Green Lubricants IV: Influence of Structure on the Thermal Behavior of Linear and Branched Aliphatic Fatty Acid-Derived Diesters*. ACS Sustainable Chemistry & Engineering, 2016. **4**(9): p. 4868-4874.<https://doi.org/10.1021/acssuschemeng.6b01144>.
33. Waterhouse, A.L., G.L. Sacks, and D.W. Jeffery, *Understanding Wine Chemistry*. 2016: Wiley: <https://books.google.ca/books?id=xd5QDAAAQBAJ>.
34. Clayden, J., N. Greeves, and S. Warren, *Organic Chemistry*. 2012: OUP Oxford: <https://books.google.com/books?id=G3wUe-2e-4MC>.
35. Kenisarin, M.M., *Thermophysical properties of some organic phase change materials for latent heat storage. A review*. Solar Energy, 2014. **107**: p. 553-575.<https://doi.org/10.1016/j.solener.2014.05.001>.
36. Schäfer, V., A. Pauli, and A. Fessenbecker, *Patent - Corrosion Protection Additives Based On Epoxides*. 2017, <https://patents.google.com/patent/US5368776A/en>.
37. Johnson, D., *Lubricants for Turbine Engines*. 2016.doi <https://dx.doi.org/10.5772/62394>.
38. Ganiyu, S.A. and S.A. Lateef, *Review of adsorptive desulfurization process: Overview of the non-carbonaceous materials, mechanism and synthesis strategies*. Fuel, 2021. **294**: p. 120273.<https://doi.org/10.1016/j.fuel.2021.120273>.
39. Xing, H., P. Hu, S. Li, Y. Zuo, J. Han, X. Hua, K. Wang, F. Yang, P. Feng, and T. Chang, *Adsorption and diffusion of oxygen on metal surfaces studied by first-principle study: A review*. Journal of Materials Science & Technology, 2021. **62**: p. 180-194.<https://doi.org/10.1016/j.jmst.2020.04.063>.
40. Karmakar, G., P. Ghosh, and B. Sharma, *Chemically Modifying Vegetable Oils to Prepare Green Lubricants*. Lubricants, 2017. **5**(4): p. 44.<https://doi.org/10.3390/lubricants5040044>.
41. Soleimani, M., L. Dehabadi, L. Wilson, and L. Tabil, *Antioxidants Classification and Applications in Lubricants*. 2018.<http://dx.doi.org/10.5772/intechopen.72621>.
42. Amat, S., Z. Braham, Y. Le Dréau, J. Kister, and N. Dupuy, *Simulated aging of lubricant oils by chemometric treatment of infrared spectra: Potential antioxidant properties of sulfur structures*. Talanta, 2013. **107**: p. 219-224.<https://doi.org/10.1016/j.talanta.2012.12.051>.
43. Chen, R.-Y., P.-H. Tung, B. Laiwang, H.-J. Liaw, and C.-M. Shu, *Oxidation and thermal stability analysis of hexadecyl mercaptan added to engine oil*. Journal of Thermal Analysis and Calorimetry, 2021.<https://doi.org/10.1007/s10973-021-10792-5>.

44. Kade, M.J., D.J. Burke, and C.J. Hawker, *The power of thiol-ene chemistry*. Journal of Polymer Science Part A: Polymer Chemistry, 2010. **48**(4): p. 743-750.<https://doi.org/10.1002/pola.23824>.
45. Northrop, B.H. and R.N. Coffey, *Thiol-ene click chemistry: Computational and kinetic analysis of the influence of alkene functionality*. Journal of the American Chemical Society, 2012. **134**(33): p. 13804-13817.<https://doi.org/10.1021/ja305441d>.
46. Bantchev, G.B., J.A. Kenar, G. Biresaw, and M.G. Han, *Free Radical Addition of Butanethiol to Vegetable Oil Double Bonds*. Journal of Agricultural and Food Chemistry, 2009. **57**(4): p. 1282-1290.<https://doi.org/10.1021/jf802774g>.
47. Biresaw, G., G.B. Bantchev, and S.C. Cermak, *Tribological properties of vegetable oils modified by reaction with butanethiol*. Tribology Letters, 2011. **43**(1): p. 17-32.<https://doi.org/10.1007/s11249-011-9780-z>.
48. Arukali, S., P.K. V., and P.R.B. N., *Tribology and oxidation studies of fatty acid sulfide derivatives synthesized via thiol-ene "Click" additions*. European Journal of Lipid Science and Technology, 2016. **118**(3): p. 495-502.<https://doi.org/10.1002/ejlt.201500119>.
49. F., W.J., F. Shashi, W. Dimuthu, C. Zhigang, and W.D. C., *Synthesis of Soybean Oil-Based Thiol Oligomers*. ChemSusChem, 2011. **4**(8): p. 1135-1142.<https://doi.org/10.1002/cssc.201100071>.
50. Ionescu, M., D. Radojčić, X. Wan, Z.S. Petrović, and T.A. Upshaw, *Functionalized vegetable oils as precursors for polymers by thiol-ene reaction*. European Polymer Journal, 2015. **67**: p. 439-448.<https://doi.org/10.1016/j.eurpolymj.2014.12.037>.
51. Zhao, Y.H., S. Hupin, L. Lecamp, D. Vuluga, C. Afonso, F. Burel, and C. Loutelier-Bourhis, *Thiol-ene chemistry of vegetable oils and their derivatives under UV and air: a model study by using infrared spectroscopy and mass spectrometry*. RSC Advances, 2017. **7**(6): p. 3343-3352.<http://dx.doi.org/10.1039/C6RA25633C>.
52. Montero de Espinosa, L. and M.A.R. Meier, *Plant oils: The perfect renewable resource for polymer science?!* European Polymer Journal, 2011. **47**(5): p. 837-852.<https://doi.org/10.1016/j.eurpolymj.2010.11.020>.
53. Desroches, M., S. Caillol, V. Lapinte, R. Auvergne, and B. Boutevin, *Synthesis of Biobased Polyols by Thiol-Ene Coupling from Vegetable Oils*. Macromolecules, 2011. **44**(8): p. 2489-2500.<https://doi.org/10.1021/ma102884w>.
54. Sammaiah, A., K.V. Padmaja, and R.B.N. Prasad, *Tribology and oxidation studies of fatty acid sulfide derivatives synthesized via thiol-ene "Click" additions*.

- European Journal of Lipid Science and Technology, 2016. **118**(3): p. 495-502.<https://doi.org/10.1002/ejlt.201500119>.
55. TÜRÜNÇ, O. and M.A. Meier, *Fatty acid derived monomers and related polymers via thiol-ene (click) additions*. Macromolecular rapid communications, 2010. **31**(20): p. 1822-1826.<https://doi.org/10.1002/marc.201000291>.
56. Samuelsson, J., M. Jonsson, T. Brinck, and M. Johansson, *Thiol-ene coupling reaction of fatty acid monomers*. Journal of Polymer Science Part A: Polymer Chemistry, 2004. **42**(24): p. 6346-6352.<https://doi.org/10.1002/pola.20468>.
57. Griesbaum, K., *Problems and possibilities of the free-radical addition of thiols to unsaturated compounds*. Angewandte Chemie International Edition in English, 1970. **9**(4): p. 273-287.<https://doi.org/10.1002/anie.197002731>.
58. Zolper, T., Z. Li, C. Chen, M. Jungk, T. Marks, Y.-W. Chung, and Q. Wang, *Lubrication properties of polyalphaolefin and polysiloxane lubricants: Molecular structure-tribology relationships*. Tribology letters, 2012. **48**(3): p. 355-365.<https://doi.org/10.1007/s11249-012-0030-9>.
59. Erhan, S.Z. and S. Asadauskas, *Lubricant basestocks from vegetable oils. Industrial crops and products*, 2000. **11**(2-3): p. 277-282.[https://doi.org/10.1016/S0926-6690\(99\)00061-8](https://doi.org/10.1016/S0926-6690(99)00061-8).
60. Spikes, H., *The history and mechanisms of ZDDP*. Tribology letters, 2004. **17**(3): p. 469-489.<https://doi.org/10.1023/B:TRIL.0000044495.26882.b5>.
61. Barnes, A.M., K.D. Bartle, and V.R.A. Thibon, *A review of zinc dialkyldithiophosphates (ZDDPS): characterisation and role in the lubricating oil*. Tribology International, 2001. **34**(6): p. 389-395.[https://doi.org/10.1016/S0301-679X\(01\)00028-7](https://doi.org/10.1016/S0301-679X(01)00028-7).
62. Armstrong, D., E. Ferrari, K. Roberts, and D. Adams, *An investigation into the molecular stability of zinc di-alkyl-di-thiophosphates (ZDDPs) in relation to their use as anti-wear and anti-corrosion additives in lubricating oils*. Wear, 1997. **208**(1-2): p. 138-146.[https://doi.org/10.1016/S0043-1648\(96\)07332-2](https://doi.org/10.1016/S0043-1648(96)07332-2).
63. Luiz, J.F. and H. Spikes, *Tribofilm formation, friction and wear-reducing properties of some phosphorus-containing antiwear additives*. Tribology Letters, 2020. **68**(3): p. 1-24.<https://doi.org/10.1007/s11249-020-01315-8>.
64. Thersleff, T., I.Z. Jenei, S. Budnyk, N. Dörr, and A. Slabon, *Structure and Formation of Soot Particles from Tribofilm Decomposition Under Real Engine Conditions*. 2020.<https://doi.org/10.26434/chemrxiv.12927533.v1>.
65. Harris, K.R., *Temperature and pressure dependence of the viscosities of 2-ethylhexyl benzoate, bis (2-ethylhexyl) phthalate, 2, 6, 10, 15, 19, 23-hexamethyltetracosane (squalane), and diisodecyl phthalate*. Journal of Chemical

- & Engineering Data, 2009. **54**(9): p. 2729-2738.<https://doi.org/10.1021/je900284z>.
66. Standard, A., *Standard Test Method for Oxidation Onset Temperature of Hydrocarbons by Differential Scanning Calorimetry*, in ASTM International, West Conshohocken, PA. 2002 <https://www.astm.org/e2009-02.html>.
 67. Šimon, P., *Induction periods: theory and applications*. Journal of Thermal Analysis and Calorimetry, 2006. **84**(1): p. 263-270.<https://doi.org/10.1007/s10973-005-7204-z>.
 68. Saldaña, M. and S. Martínez-Monteagudo, *Oxidative stability of fats and oils measured by differential scanning calorimetry for food and industrial applications*. Appl calorim a wide context-differ scanning calorimetry, isothermal titration calorim microcalorim, 2013.<http://dx.doi.org/10.5772/54486>.
 69. Heym, F., B.J.M. Etzold, C. Kern, and A. Jess, *An improved method to measure the rate of vaporisation and thermal decomposition of high boiling organic and ionic liquids by thermogravimetric analysis*. Phys. Chem. Chem. Phys., 2010. **12**(38): p. 12089-12100.<http://dx.doi.org/10.1039/C0CP00097C>.
 70. ToolBox, E., *Hydrocarbons, Alcohols and Acids - Boiling points*. 2017 https://www.engineeringtoolbox.com/melting-boiling-temperature-hydrocarbons-alkane-alkene-benzene-aromatic-alcohol-acid-naphthalene-d_1940.html
 71. Jia, F., S. Wei Guo, F. Qun Chao, and Z. Yi, *A detailed bond stretch model of thermal decomposition*. Mater. Sci. Eng. C, 2014. **62**(1): p. 012020.<http://dx.doi.org/10.1039/C1SM06234D>.
 72. Yalkowsky, S.H. and D. Alantary, *Estimation of Melting Points of Organics*. Journal of Pharmaceutical Sciences, 2018. **107**(5): p. 1211-1227.<https://doi.org/10.1016/j.xphs.2017.12.013>.
 73. Soodoo, N., L. Raghunanan, L. Bouzidi, S.K. Yeong, and S.S. Narine, *Phase behaviour of monosulfones: A case study for the incorporation of high polarity sulfonyl groups for dramatically improve of the thermal properties of lipid-based materials for PCM applications*. Solar Energy Materials and Solar Cells, 2019. **201**: p. 110115.<https://doi.org/10.1016/j.solmat.2019.110115>.
 74. Stillinger, F.H. and P. Debenedetti, *Supercooled liquids and the glass transition*. Nature, 2001. **410**: p. 259-267.<https://doi.org/10.1038/35065704>.
 75. Marangoni, A.G., *Kinetic analysis of food systems*. 2017: Springer <http://dx.doi.org/10.1007/978-3-319-51292-1>.
 76. Ghotra, B.S., S.D. Dyal, and S.S. Narine, *Lipid shortenings: a review*. Food Research International, 2002. **35**(10): p. 1015-1048.[https://doi.org/10.1016/S0963-9969\(02\)00163-1](https://doi.org/10.1016/S0963-9969(02)00163-1).

77. Abiad, M., M. Carvajal, and O. Campanella, *A review on methods and theories to describe the glass transition phenomenon: applications in food and pharmaceutical products*. Food engineering reviews, 2009. **1**(2): p. 105-132.<https://doi.org/10.1007/s12393-009-9009-1>.
78. Bondi, A., *Viscosity and Molecular Structure*, in *Rheology Theory and Applications*, F.R. Eiriche, Editor. 1967, Academic Press: New Lork and London. p. 1-83 <https://doi.org/10.1016/B978-1-4832-2941-6.50007-6>.
79. Deming, T.J., *Functional modification of thioether groups in peptides, polypeptides, and proteins*. Bioconjug Chem, 2017. **28**(3): p. 691-700.<https://doi.org/10.1021/acs.bioconjchem.6b00696>.
80. Frankel, E.N., *Chapter 1 - Free radical oxidation*, in *Lipid Oxidation (Second Edition)*, E.N. Frankel, Editor. 2012, Woodhead Publishing. p. 15-24 <https://doi.org/10.1533/9780857097927.15>.
81. Smith, J.R.L., E. Nagatomi, and D.J. Waddington, *The autoxidation of simple esters: Towards an understanding of the chemistry of degradation of polyol esters used as lubricants*. Journal of the Japan Petroleum Institute, 2003. **46**(1): p. 1-14.<https://doi.org/10.1627/jpi.46.1>.
82. Rubinshtein, I.A. and E.P. Sobolev, *Antioxidant properties of organic sulfur compounds and criteria for evaluating these properties*. Chemistry and Technology of Fuels and Oils, 1965. **1**(1): p. 59-64.<https://doi.org/10.1007/BF00717842>.
83. Denison, G.H. and P.C. Condit, *Oxidation of Lubricating Oils*. Industrial & Engineering Chemistry, 1945. **37**(11): p. 1102-1108.<https://doi.org/10.1021/ie50431a025>.
84. Hawkins, W. and H. Sautter, *Synergistic antioxidant combinations. Mechanism of stabilization with organo-sulfur compounds*. Journal of Polymer Science Part A: General Papers, 1963. **1**(11): p. 3499-3509.<https://doi.org/10.1002/pol.1963.100011119>.
85. Willermet, P.A., D.P. Dailey, R.O. Carter, P.J. Schmitz, and W. Zhu, *Mechanism of formation of antiwear films from zinc dialkyldithiophosphates*. Tribology International, 1995. **28**(3): p. 177-187.[https://doi.org/10.1016/0301-679X\(95\)98965-G](https://doi.org/10.1016/0301-679X(95)98965-G).
86. Wang, J., T. He, C. Song, X. Li, and B. Chen, *Engine Oil Degradation Induced by Biodiesel: Effect of Methyl Oleate on the Performance of Zinc Dialkyldithiophosphate*. ACS omega, 2019. **4**(14): p. 16166-16170.<https://doi.org/10.1021/acsomega.9b02353>.
87. Nath, A.R., W.A. Yehye, N.W.M. Zulkifli, and M.R. Johan, *Ester of thiolated butylated hydroxytoluene: Potential antioxidant for synthetic lubricant oil*.

- Thermochemica Acta, 2018. **670**: p. 7-12. <https://doi.org/10.1016/j.tca.2018.09.021>.
88. Qiu, C., S. Han, X. Cheng, and T. Ren, *Determining the antioxidant activities of organic sulfides by rotary bomb oxidation test and pressurized differential scanning calorimetry*. Thermochemica Acta, 2006. **447**(1): p. 36-40. <https://doi.org/10.1016/j.tca.2006.01.014>.
89. Samidin, S., N. Salih, and J. Salimon, *Synthesis and Characterization of Trimethylolpropane Based Esters as Green Biolubricant Basestock*. Biointerface Research in Applied Chemistry, 2021. **11**(5): p. 13638-13651. <http://dx.doi.org/10.33263/BRIAC115.1363813651>.
90. Cermak, S.C., J.W. Bredsguard, K.L. Roth, T. Thompson, K.A. Feken, T.A. Isbell, and R.E. Murray, *Synthesis and physical properties of new coco-oleic estolide branched esters*. Industrial Crops and Products, 2015. **74**: p. 171-177. <https://doi.org/10.1016/j.indcrop.2015.05.011>.
91. Soodoo, N., K.D. Poopalam, L. Bouzidi, and S.S. Narine, *Fundamental structure-function relationships in vegetable oil based phase change materials: A critical review*. Journal of Energy Storage, 2022. **51**: p. 104355. <https://doi.org/10.1016/j.est.2022.104355>.
92. Soodoo, N., L. Raghunanan, L. Bouzidi, and S. Narine, *Phase behavior of monosulfones: Use of high polarity sulfonyl groups to improve the thermal properties of lipid-based materials for PCM applications*. Solar Energy Materials and Solar Cells, 2019. **201**: p. 110115. <https://doi.org/10.1016/j.solmat.2019.110115>.

5 Conclusions

This thesis presents the study of novel phase change materials (PCMs) and lubricants derived from vegetable oil (VO) and select functional groups. The goal was to combine the advantageous characteristics of both the renewable feedstock and the functional groups to make industrially relevant materials. Two series of PCMs were investigated: (1) terephthalate diesters (n-TA-n) with fatty chains $n = 12, 14, 16$ and 18 and (2) monosulfones (n-SO₂-n) with $n = 10, 12,$ and 18 . The lubricant study involved two series of sulfur based compounds: (1) sulfide and (2) sulfonyl branched oleyl oleate monoesters. All the compounds were investigated for thermal degradation and thermal transition behavior. The crystal structure of the PCMs and flow behavior and oxidative stability of the lubricants were also investigated. The PCMs are intended for thermal energy storage (TES) applications and lubricants as base oils for automotive, industrial and specialized applications.

All the objectives of the thesis have been met and the hypotheses addressed.

5.1 Conclusion for the PCMs Study: Monosulfones and Terephthalate Diesters

A literature review of VO-based PCMs comprising more than 200 compounds in which predictive structure-function relationships were suggested based on the studies reviewed were published as part of the thesis. This work helps towards a comprehensive understanding of the phase behavior of VO PCMs and identifies research gaps to be further explored.

The study of the VO-based PCMs revealed predictive trends between the structures (ester groups, hydrocarbon chains and functional groups) and phase change properties including temperature, enthalpy and entropy (T_m , ΔH_m , ΔS_m , and T_{ON}). The free Gibbs energy at the transition was used to explain the magnitude of thermal transition parameters in light of the

competition between entropic and enthalpic effects. A conclusion was asserted that any attempt to model a phase change parameter should take into consideration all the interactions and configuration factors including dispersion and dipole-dipole forces, group size, molecular mass, symmetry, and flexibility.

5.1.1 Objectives and Hypotheses Achieved

Did the fatty chains, benzene group and sulfonyl group influence (i) thermal stability, (ii) thermal transition behavior and (iii) crystal packing?

5.1.1.1 Influence of the Fatty Chains, Sulfonyl and Benzene Group on Thermal Stability

The onset of mass loss (T_{ON}) for terephthalate diesters and monosulfones increased with molecular mass following exponential rise to a maximum function (**Figure 5-1**).

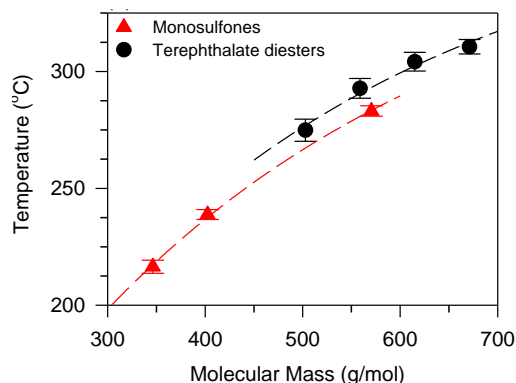


Figure 5-1. T_{ON} versus molecular mass for monosulfones (▲) and terephthalate diesters (●).

For the monosulfones, T_{ON} increased exponentially from 216 °C for 10-SO₂-10 to 289 °C for 18-SO₂-18 and for the terephthalate diesters from 275 °C for 12-TA-12 to 310 °C for 18-TA-18. This predictive relationship between molecular mass and thermal stability is explained by the incremental contribution of the CH₂ units of the fatty chains to T_{ON} . The parameters of the fit were similar for both curves indicating a similar effect of mass on thermal stability. The T_{ON} curve of the terephthalate diesters lies about 10 °C above that of the monosulfones (**Figure 5-1**)

indicating that the benzene group is more effective in improving thermal stability than sulfonyl-group due to its higher mass.

5.1.1.2 Influence of the Fatty Chains, Sulfonyl and Benzene Group on Thermal Transition

The monosulfones crystallized in one main crystal phase upon cooling and presented a small solid-solid phase transition before melting upon heating. The terephthalate diesters presented a single exotherm upon cooling mirrored by an endotherm upon heating indicating a single crystal phase. T_m versus fatty chain length (n) of both the monosulfones and terephthalate diesters followed an exponential rise to a maximum function with similar fit parameters (**Figure 5-2**).

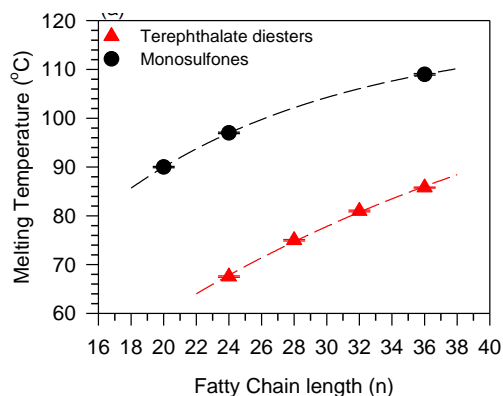


Figure 5-2. T_m versus fatty chain length (n) of terephthalate diesters and monosulfones.

For any given chain length, T_m of the monosulfones is 30 °C higher than that of the terephthalate diesters. This large difference in melting point is attributable to the larger sulfonyl-sulfonyl attractions compared to the terephthalate diesters π - π attractions and the smaller entropy due to the much more limited mobility of the sulfonyl group compared to the benzene group which is linked to the fatty chain by ester groups. T_m of the monosulfones is higher than that of VO-based monofunctional PCMs such as fatty acids, fatty alcohols, esters, fatty ethers, fatty carbonates, fatty amines, amides and alkanes which have T_m up to 80 °C [1] and diesters (77 °C)[2] but lower than diamides which have T_m as high as 140 °C [3].

ΔH_m of the monosulfones and terephthalate diesters with fatty chain length of ≤ 28 carbons is practically the same averaging 208 ± 5 J/g and those with fatty chain length ≥ 32 carbons have ΔH_m between 220 to 256 J/g attributable to the competition between the effects of dispersion forces, group-group interactions bulkiness and conformation arrangement. Because of the bulky nature of their functional groups, the monosulfones and terephthalate diesters presented ΔH_m comparable to other monofunctional such as fatty acids, fatty alcohols, esters, fatty ethers, fatty carbonates, fatty amines, amides, alkanes, and difunctional PCMs such as diamides and diesters, and sugar esters [1]. T_{ON} of monosulfones is 2 times higher than their T_m and that of the terephthalate diesters is 3.5 times higher which ensures a high margin of working safety before degradation.

5.1.1.3 Influence of Sulfonyl and Benzene Group on Crystal Packing Behavior

The XRD data collected for the monosulfones and terephthalate diesters indicated a single crystal phase in which the molecules arrange in layers with the functional groups (sulfonyl or benzene) parallel to each other. The analysis of the SAXD data of the monosulfones and terephthalate diesters indicates that the bulky sulfonyl groups are not oriented uniformly in the crystal lattice whereas the planar benzene group positions itself uniformly in the crystal lattice as hypothesized.

The monosulfone with the shortest fatty chain ($n= 10$) crystallized in the loosely packed γ -polymorph and those with longer fatty chain ($n= 12$ and 18) in the highest thermodynamic β -form. The terephthalate diesters crystallized in a tighter β -form regardless of fatty chain length. The analysis of the main WAXD reflections indicated that terephthalate diesters crystallized in a tighter β -form than the monosulfones.

5.2 Conclusion for Sulfide and Sulfonyl Branched Oleyl Oleate Monoesters Lubricants

5.2.1 Objectives and Hypotheses Achieved

Did the sulfide and sulfonyl pendant groups influence: (i) flow type and viscosity (ii) thermal transition behavior, (iii) thermal stability, (iv) oxidative stability and (v) crystal growth?

5.2.1.1 Influence of Sulfide and Sulfonyl Pendant Group on Viscosity and Flow Type

The addition of sulfide and sulfonyl pendant groups to oleyl oleate affected its flow behavior as hypothesized. Oleyl oleate viscosity increased from 16 mPa.s to a mean of 48mPa.s with the addition of the sulfide pendant groups and 150 mPa.s with the sulfonyl pendant groups. The viscosity did not significantly vary with chain length of the pendant chain. The 32 mPa.s difference between the two functional groups indicates the effect of polarity on viscosity.

The application of the Herschel-Bulkley model (Equation 1) to the shear stress - shear rate data of the sulfide and sulfonyl branched oleyl oleate monoesters indicated Newtonian behavior for all the compounds. This type of fluid is suitable for automotive applications [4].

5.2.1.2 Influence of Sulfide and Sulfonyl Pendant Group on Thermal Transition Behavior

The crystallization temperature and enthalpy were not affected by pendant chain length. The sulfonyl group was more effective in depressing the crystallization temperature and enthalpy than the sulfide group because of its larger size. The sulfide and sulfonyl pendant groups decreased the enthalpy of oleyl oleate from 144J/g to a mean enthalpy of 60J/g and 15J/g, respectively. the temperature of crystallization of oleyl oleate was also decreased as hypothesized. The sulfide and sulfonyl pendant groups shifted oleyl oleate main crystallization peak from -12.3°C to mean values of -56°C and -47°C, respectively. Furthermore, the bulkier sulfonyl pendant groups induced glass transitions at temperatures as low as -74°C.

5.2.1.3 Influence of Sulfide and Sulfonyl Pendant Group on Thermal Stability

Sulfide and sulfonyl branched oleyl oleate monoesters as well as oleyl oleate base ester presented similar TGA profiles indicating similar degradation mechanisms, probably dominated by evaporation. T_{ON} of mass loss for both sulfide and sulfonyl branched oleyl oleate monoesters increased with molecular mass similarly to what is observed in hydrocarbons. Contrary to the hypothesis that the high polarity sulfonyl groups would provide higher T_{ON} than the low polarity sulfide groups, no significant difference was observed between T_{ON} of the sulfide and sulfonyl branched oleyl oleate monoesters.

5.2.1.4 Influence of Sulfide and Sulfonyl Pendant Group on Oxidative Stability

The sulfide and sulfonyl pendant groups beneficially affected the oleyl oleate oxidative stability as hypothesized. They increased the oxidation onset (T_{on}^{ox}) of oleyl oleate from 149 °C to 196 °C and 298 °C, respectively. The improvement of the oxidation stability by the sulfonyl pendant group is due to removal of the double bond by branching. The high T_{on}^{ox} achieved by the sulfide pendant groups is attributable to the removal of the double bond and its inherent ability to prevent chain propagation by decomposing hydroperoxides generated at the initiation stage of oxidation [5].

5.2.1.5 Influence of Sulfide and Sulfonyl Pendant Group on microstructure and Crystal Growth

The PLM of the sulfide and sulfonyl branched oleyl oleate monoesters correlated well with the DSC results. The first appearance of the smallest crystallites occurred at the DSC crystallization onset temperatures which are -5 °C and -3 °C for the sulfide and sulfonyl branched oleyl oleate monoesters. The sulfonyl branched oleyl oleate monoesters showed a smaller crystal growth rate

and smaller final size of the crystals than the sulfide branched oleyl oleate monoesters. The difference in growth rate and crystal size can be explained by the chemical natures of the sulfide and sulfonyl pendant groups and their influence on the crystallization process. After the growth centers form upon supercooling, molecules in the bulk melt are diffused onto the surface of the growing crystallite at a rate dictated by mass transfer consideration. The sulfonyl groups are not only bulkier than the sulfide groups but are also repulsive which adds to the difficulty of being in the appropriate configuration to attach to the crystallites' growing surface.

5.3 Challenges and Future Perspectives

5.3.1 Challenges and Perspectives with the VO Feedstock

5.3.1.1 Cost, Supply and Food Chain

VO is a feedstock of choice because it is renewable and relatively abundant. Currently most VO-based materials use edible varieties such as soybean, sunflower, rapeseed, or palm oil. A larger scale usage of these materials may interfere with the food supply and may cause severe shortages, unaffordable prices and social unrest. The current global annual supply of VO is ~209 million metric tons and is mostly used for consumption [6]. Currently, PCMs and lubricants utilize ~40 million metric tons of crude oil [7, 8], a quantity that cannot be replaced in any significant part by current VO production. Furthermore, VO price is prohibitive compared to crude oil. The price of crude soybean oil for example (~1700/metric ton) is almost double that of crude oil (888 USD/metric ton) [9]. Some of the directions suggested to tackle the food supply problem include the increase in the production of VOs and non-edible crops and the use of other oil producing organisms [10, 11]. The cultivation of non-edible oils, such as jojoba oil, karanja

oil, jatropha oil, and castor oil, has increased over the last few years [12]. Microalgae have also emerged as a viable source due to its high oil content which can reach over 70 % in some cases.

5.3.1.2 Cost of Derivatization and Transformation into Useable Materials

From the VO feedstock to the useable material, multiple synthetic routes and purification steps are needed. The cost of the physical and chemical refining to remove undesirable molecules such as free fatty acids, phospholipids, waxes, aldehydes and ketones to obtain pure TAGs adds to the cost of derivatization necessary to obtain useful ester structures such as fatty acids. The price of fatty acids for example (~\$2661-3300/metric ton) is almost double of VOs [13].

The scientific community is currently working on novel derivatization, transformation and purification processes to improve efficiency in the synthesis of VO-based lubricants [14, 15]. There are also efforts to improve on the synthetic routes and purification steps currently used to produce VO-based materials. Several authors [16] reported on the use of mechanochemical treatments, microwaves, or ultrasound to improve process yields under mild reaction conditions. Over the last few years, the use of enzymatic processes has emerged as an alternative to obtain precursors or even lubricants at low reaction temperatures [17].

5.3.1.3 Consumer Acceptance

Consumer acceptance of VO-based materials including PCMs and lubricants is a major concern mainly related to performance and cost. VO-based PCMs and lubricants are approximately two-to-three times more expensive than petroleum-based counterparts. Additionally, the environmental benefits, particularly those related to renewability, carbon footprint and end of life need to be popularized. To solve this problem more sustainable formulations should be developed in many fields, such as engine oils, hydraulic oils, and compressor oils.

5.3.2 Challenges and Perspectives for VO-based PCMs and Lubricants

5.3.2.1 VO-based PCMs

There are several research directions from a structure-property perspective to further improve the thermophysical properties of VO-based PCMs. These are related to (i) design of functional molecular architectures and (ii) development of more effective external performance enhancement techniques. The major challenges involved in these directions and potential solutions to overcome these challenges are:

(i) New Molecular Architectures

There exists the possibility of achieving VO-based organometallic PCMs with superior thermal properties using coordination chemistry principles [18, 19]. Carefully designed coordination complexes between thermally conductive transition metals such as Fe, Cu, and Zn (κ values between 80- 400 W/m.K) with VO-based ligands such as carboxylic acid or amide functional groups could provide a powerful platform to explore specific factors that contribute to thermal conductivity and energy storage density of VO-based organometallic PCMs. Moreover, unlike conventional organic and inorganic PCMs, the structure of organometallic PCMs can be controlled through rational ligand design and directional coordination bonds to tailor the crystal lattice dimensionality and strength of covalent and noncovalent interactions within a solid in a predictable fashion.

(ii) Performance Enhancement Techniques

VO-based PCMs are known to have an inherently low thermal conductivity and leak during phase transition in open TES systems. The solutions to address these problems, such as the use of thermal conductivity additives [20-22] and microencapsulation techniques [23, 24] have yielded

some good results but are still not sufficiently tested with VO-based PCMs [20]. Investigating the thermal conductivity of VO-PCMs can lead to insights into their heat transport mechanism and limitations which would lead to possible solutions and tangible improvements. Microencapsulated VO-based PCMs can greatly extend the heat transfer surface area and improve on the efficiency of thermal performance.

High conductivity porous composites, nanocomposites structures and nano additives may be effective means to improve VO-based PCMs for TES applications. The preparation of these materials would be multifaceted and the ensuing phase behavior very complex. All aspects related to these materials as well as the techniques used to make them need careful investigation in order to determine their phase behavior and structure-function relationships. Understanding the fundamental mechanisms driving the behavior of these materials and interactions at play would be instrumental in finding means to adjust the preparation processes for select molecular systems for optimal phase structure and performance.

5.3.2.2 VO-based Ester Lubricants

The sulfide and sulfonyl branched oleyl oleate monoesters of this work demonstrated excellent low temperature and flow performance as well as high thermal and oxidative stability. The branching of monoesters with polar functional groups may represent the next generation of superior commercial lipid-based lubricants. In fact, rough estimates on the production costs of the oleyl oleate monoesters and the sulfide and sulfonyl branched oleyl oleate monoesters (*Appendix B*) show that the unbranched oleyl oleate would cost ~USD 1.04/lb and the sulfide and sulfonyl branched oleyl oleate monoesters would cost ~ USD 1.07/lb to produce.

The use of functional groups in VO-based lubricants remains an area for future investigation and optimization. The results obtained with the sulfide and sulfonyl pendant groups invite to study

other pendant groups (such as phosphate, amide, ether and carbonate groups). Also, instead of using oleyl oleate monoester backbone, other unsaturated backbones such as diesters and triesters can be used to create new VO-based ester lubricants which might have improved viscosity and cold-flow performance. To take these materials from the laboratory to the market, it is imperative to determine their tribological properties which determine lubricant properties such as friction coefficient and wear performance, and hydrolytic and oxidative stability which influence the shelf and use life.

5.4 References

1. Soodoo, N., et al., *Fundamental structure-function relationships in vegetable oil based phase change materials: A critical review*. Journal of Energy Storage, 2022. **51**: p. 104355.
2. Floros, M.C. and S.S. Narine, *Latent heat storage using renewable saturated diesters as phase change materials*. Energy, 2016. **115**: p. 924-930.
3. Poopalam, K.D., et al., *The anomalous behaviour of aliphatic fatty diamides: Chain length and hydrogen bonding interactions*. Solar Energy Materials and Solar Cells, 2019. **201**: p. 110056.
4. Jang, J.Y. and M.M. Khonsari, *Lubrication with a Newtonian Fluid*, in *Encyclopedia of Tribology*, Q.J. Wang and Y.-W. Chung, Editors. 2013, Springer US: Boston, MA. p. 2142-2146.
5. Soleimani, M., et al., *Antioxidants Classification and Applications in Lubricants*. 2018.
6. ExpertMarketResearch, *Global Vegetable Oil Market*. 2022.
7. MaximizeMarketResearch, *Global Lubricant Market: Industry Analysis and Forecast (2021-2027) by Type, Fluid Type, and Region*. 2021.
8. ExpertMarketResearch, *Global Advanced Phase Change Materials Market Outlook*. 2022.
9. MarketInsider, *Price of oil (Brent Crude and WTI)*. 2022.
10. Galloway, R., *Market demand and outlook*, in *High Oleic Oils*. 2022, Elsevier. p. 261-274.
11. Almasi, S., et al., *A review on bio-lubricant production from non-edible oil-bearing biomass resources in Iran: Recent progress and perspectives*. Journal of Cleaner Production, 2021. **290**: p. 125830.
12. D'Ambrosio, V., E. Scelsi, and C. Pastore, *Non-edible Oils for Biodiesel Production: State of the Art and Future Perspectives*. Biodiesel Production: Feedstocks, Catalysts, and Technologies, 2022: p. 49-66.
13. Hásl, T., et al., *Cost/Performance Analysis of Commercial-Grade Organic Phase-Change Materials for Low-Temperature Heat Storage*. Energies, 2020. **13**(1): p. 5.

14. Naji, S.Z., C.T. Tye, and A.A. Abd, *State of the art of vegetable oil transformation into biofuels using catalytic cracking technology: Recent trends and future perspectives*. Process Biochemistry, 2021. **109**: p. 148-168.
15. Belousov, A.S., et al., *Recent advances in sustainable production and catalytic transformations of fatty acid methyl esters*. Sustainable Energy & Fuels, 2021.
16. Qadeer, M.U., et al., *Review of biodiesel synthesis technologies, current trends, yield influencing factors and economical analysis of supercritical process*. Journal of Cleaner Production, 2021. **309**: p. 127388.
17. Vilas Bôas, R.N. and H.F. de Castro, *A review of synthesis of esters with aromatic, emulsifying, and lubricant properties by biotransformation using lipases*. Biotechnology and Bioengineering, 2022.
18. Butler, K.T., et al., *Organised chaos: entropy in hybrid inorganic–organic systems and other materials*. Chemical science, 2016. **7**(10): p. 6316-6324.
19. Yaghi, O.M., et al., *Reticular synthesis and the design of new materials*. Nature, 2003. **423**(6941): p. 705-714.
20. Tao, Y.B. and Y.-L. He, *A review of phase change material and performance enhancement method for latent heat storage system*. Renewable and Sustainable Energy Reviews, 2018. **93**: p. 245-259.
21. Nazir, H., et al., *Recent developments in phase change materials for energy storage applications: A review*. International Journal of Heat and Mass Transfer, 2019. **129**: p. 491-523.
22. Kalnæs, S.E. and B.P. Jelle, *Phase change materials and products for building applications: A state-of-the-art review and future research opportunities*. Energy and Buildings, 2015. **94**: p. 150-176.
23. Khan, Z., Z. Khan, and A. Ghafoor, *A review of performance enhancement of PCM based latent heat storage system within the context of materials, thermal stability and compatibility*. Energy Conversion and Management, 2016. **115**: p. 132-158.
24. Umair, M.M., et al., *Novel strategies and supporting materials applied to shape-stabilize organic phase change materials for thermal energy storage—A review*. Applied Energy, 2019. **235**: p. 846-873.

6 Appendix 1

6.1 Fundamental Structure-Function Relationships in Vegetable Oil Based Phase Change Materials: A Critical Review

6.1.1 Abstract

Vegetable oils (VOs) are one of the most promising renewable sources of phase change materials (PCMs). Although several studies have been published, there are no comprehensive reviews of VO-based PCMs or the structure-property relationships governing their thermal behavior. This critical review systematically organizes the published literature on VO-based PCMs focusing on the role that structural elements play in the establishment of thermal properties relevant to thermal energy storage (TES). Thermal properties such as thermal stability, phase change temperature, enthalpy, entropy and thermal conductivity are the functional parameters examined within the context of structure. The empirical correlations between structure and thermal functionality of the PCMs are assembled in predictive relationships, drawing a unified picture of the rules that govern their phase behavior. Relationships such as the effect of fatty chain length, number and types of functional groups, symmetry, and isomerism on the molecule's thermal properties were explored. Phase change temperatures and enthalpies of linear saturated PCMs with monofunctional group follow exponential rise to maximum functions while the entropy increases linearly with increasing carbon chain length. The ranges for phase change temperature, enthalpy, entropy, thermal stability, and thermal conductivity for all the VO-based PCMs in this work were -100–300°C, 90–270J/g, 100–500J/mol/K, 95–350°C and 0.1–0.4W/mK respectively. The gathered knowledge is critically discussed to provide directions for future PCM research and development.

Keywords:

Vegetable oil (VO); Phase change material (PCM); Latent heat thermal energy storage (LHTES);
Structure-property relationships; Intermolecular interaction

6.1.2 Chemical nomenclature and list of abbreviations

Class of PCMs	Scheme #	Figure #	Generalized Chemical Formula	Value of R
Even alkanes	Scheme 0-1	Figure 0-1	$C_R H_{2R+2}$	Even R= 2 to 390
Odd alkanes			$C_R H_{2R+2}$	Odd R= 1 to 43
Even saturated acids			$C_R H_{2R+1} COOH$	Even R= 2 to 46
Odd saturated acids			$C_R H_{2R+1} COOH$	Odd R= 1 to 35
Saturated alcohols			$C_R H_{2R+1} OH$	R= 1 to 50
Saturated amines			$C_R H_{2R+1} NH_2$	R= 1 to 22
Saturated monoamides			$C_{R-1} H_{2R-1} (CONH) C_{R'} H_{2R'+1}$	R and R' = 1 to 36
Saturated monoesters			$C_{R-1} H_{2R-1} (CO_2) C_{R'} H_{2R'+1}$	R and R' = 1 to 36
Saturated monosulfones			$C_R H_{2R+1} (SO_2) C_{R'} H_{2R'+1}$	R and R' = 1 to 36
Saturated ethers			$C_R H_{2R+1} (O) C_{R'} H_{2R'+1}$	R and R' = 1 to 36
Saturated carbonates			$C_R H_{2R+1} (CO_3) C_{R'} H_{2R'+1}$	R and R' = 1 to 36
Asymmetrical monoesters			Figure 0-3	$C_{R-1} H_{2R-1} (CO_2) C_{R'} H_{2R'+1}$
Saturated diamides		Figure 0-4	$C_{R-1} H_{2R-1} (CONHC_R'' H_{2R}'' CONH) C_{R'-1} H_{2R'-1}$	R = R' = 12-18, R''=2-10
Saturated diesters			$C_{R-1} H_{2R-1} (CO_2 C_R'' H_{2R}'' CO_2) C_{R'-1} H_{2R'-1}$	R = R' = 12-18, R''=2-10
Glycerol esters		Scheme 0-3	Figure 0-5	$C_3 H_5 O_3 (C_R H_{2R+1})_3$
Erythritol esters	$C_4 H_6 O_4 (C_R H_{2R+1})_4$			R = 12, 14, 16 & 18
Xylitol esters	$C_5 H_7 O_5 (C_R H_{2R+1})_5$			R = 12, 14, 16 & 18
Galactitol esters	$C_6 H_8 O_6 (C_R H_{2R+1})_6$			R = 12, 14, 16 & 18
Mannitol esters	$C_6 H_8 O_6 (C_R H_{2R+1})_6$			R = 12, 14, 16 & 18

List of abbreviations	
TES	Thermal Energy Storage
LHTES	Latent Heat Thermal Energy Storage
VOs	Vegetable Oils
TAGs	Triacylglycerols
PCMs	Phase Change Materials
NMR	Nuclear Magnetic Resonance
DSC	Differential Scanning calorimetry
XRD	Xray Diffraction
MW	Molecular Weight
HVAC	Heating, Ventilation, And Air Conditioning
T_m	Melting Temperature
T_c	Crystallization Temperature
ΔH_m	Melting Enthalpy
ΔS_m	Melting Entropy
κ	Thermal Conductivity
T_{ON}	Onset Temperature
n_s	Melting Point Singularity
R^2	Coefficient of Correlation
n_0	Characteristic Carbon Number
SI	Supporting Information
ΔG	Gibbs Free Energy
$\alpha_{\Delta S}$	Rate Of Change Of ΔS_m
β	Beta Polymorph
β'	Beta Prime Polymorph
D	Debye
m	Spacer Chain Length
R	Length of Carbon Chain
C–O	Alkoxy Moiety
–COO–	Ester Group
–CONH–	Amide Group
–COOH	Carboxylic Group
–OH	Hydroxyl Group
–SO ₂ –	Sulfonyl Group
–CH ₂ –	Methylene Unit

6.1.3 Introduction

The finite nature of fossil fuel reserves, rapid increase in energy consumption and growing environmental concerns about greenhouse gas emissions are drivers of a worldwide search for

new sources of energy and development of materials and methods which would enable the effective and efficient utilization of energy. The storage of energy is a key challenge within this broader effort. Energy storage, particularly from intermittent sources such as solar and wind, has been the focus of extensive research in the last decades. The capture, concentration and reuse of waste energy is a key aspect of the energy storage endeavor as it relates to vast amounts and holds immense potential for increased efficiencies both in industrial and domestic applications. Thermal energy is by far the most generated and transported type of energy [1, 2]. The development of materials and systems which would enable economical, environmentally responsible and facile thermal energy storage (TES) in a wide variety of modern applications is therefore a pivotal aspect of the energy storage challenge.

There are three common ways to store thermal energy: conversion to thermochemical energy and as sensible and latent heat [1]. Regardless of the method used to store thermal energy, materials are always a key component. In thermochemical energy storage, thermal energy is stored and released by reversible chemical reactions [3]. In sensible heat storage, the energy is used to change the temperature of a storage medium (usually solid or liquid) without phase change. The amount of stored sensible heat in a material depends on its heat capacity and thermal diffusivity (the rate at which the heat can be released and extracted) [4]. Latent heat thermal energy storage (LHTES) involves the heat absorbed or released by a material during a phase transition process in which the phase change temperature remains constant. The materials used in LHTES are called phase change materials (PCMs) [5]. Although latent heat can be achieved through any change of state of matter (solid, liquid, gas), the solid-liquid phase change is the most practical for thermal energy storage. The typical solid-liquid PCMs store 5 to 14 times the heat per unit volume than conventional sensible heat storage materials such as water or granite [1]. The

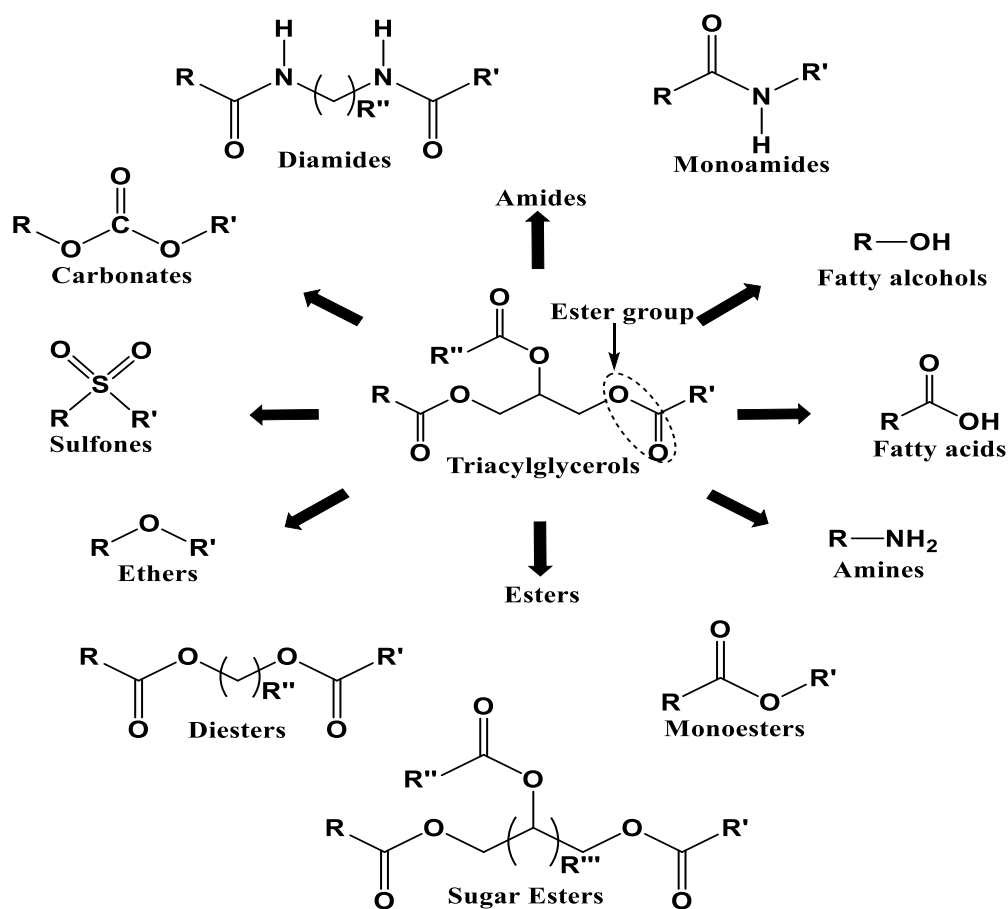
research in solid-liquid PCMs target as high energy storage and release density as possible on melting and solidifying at specific narrow temperature ranges. The contribution of the sensible heat to the storage capacity of a PCM is typically omitted as it is negligible over the temperature range of the phase change process.

A large selection of PCMs which exploit the solid-liquid phase transition are used in a variety of TES applications [6-15]. The current applications of PCMs are discussed in *Section 8*. PCMs are typically selected based on their thermal stability, melting point, latent heat of fusion and thermal conductivity. It is desirable for these materials to melt congruently, crystallize with minimum supercooling, be thermally and chemically stable, non-toxic, non-corrosive, green and inexpensive [16].

Vegetable oils (VOs) constitute an attractive renewable and sustainable feedstock to make PCMs. VO-based PCMs can potentially replace the petroleum-based and inorganic salt hydrate PCMs in many TES applications. The triacylglycerols (TAGs), which are the main components of VOs, in their unmodified state do not deliver all the required qualities for direct use as PCMs. The TAGs which consist of three fatty acids esterified to a glycerol backbone are subject to large supercooling effects and demonstrate polymorphism, typically making their phase change broad and incongruent [1, 17, 18]. However, TAGs are exemplary feedstock for the synthesis of functional PCMs because of the simplicity of the derivatization of their ester functional groups and unsaturation sites and the relatively inert nature of their saturated hydrocarbon chains.

Several classes of compounds have been derived from TAGs and used as PCMs. Fatty acids and their eutectic mixtures [19-25], fatty alcohols [26-30], fatty carbonates [26], fatty ethers [31], fatty amines [31] mono- sulfones [32], mono- di- and sugar- esters [33-37], mono- and diamides

[38-40] have been extensively studied for TES applications. The general structures of different classes of compounds derivatized from TAGs are shown in **Scheme 0-1**. These compounds generally present high phase change enthalpies, narrow melting ranges and minimum requirements for supercooling. Moreover, they have been shown to be thermally stable, withstanding numerous thermal cycles without loss of performance.



Scheme 0-1. Saturated organic phase change materials derived from triacylglycerols (TAGs). (R, R' and R'' denotes the number of carbon atoms in the aliphatic chains)

The present work reviews the research conducted on VO-based PCMs for LHTES applications. The experimental thermal data of the VO-based PCMs mined from the literature are melting/

crystallization temperatures (T_m/T_c), enthalpy of fusion (ΔH_m), thermal stability (T_{ON}) and thermal conductivity (κ). The entropy of fusion (ΔS_m) was calculated using free Gibbs energy at the transition (T_m and ΔH_m in Equation 2 - see Section 3). These data are tabulated in Table S.1 provided in the Supporting Information (SI). In the following, VO-based PCMs are simply referred to as PCMs for brevity.

This review compiles and systematically organizes the thermal properties of VO-based PCMs. The transition parameters such as T_m , ΔH_m and ΔS_m are linked to molecular structure features such as fatty chain length, functional group symmetry and isomerism to reveal any trends. These trends are evaluated, and predictive modelling performed to suggest the best molecular architectures which would improve thermal heat storage and release of VO-based PCMs.

6.1.4 Methodology

The data are systematically compiled to elucidate the influence of molecular structure on the phase change properties. T_m , ΔH_m , ΔS_m , T_{ON} and κ data are presented in figures according to particular PCMs' structural features to allow for the comprehensive but clear visualization of the structure-property trends and to capture the related predictive relationships, if any, through empirical equations. Linear and exponential functions were found to correctly describe the variation of the data as a function of specific structural parameters and to predict trends of select physical properties.

Section 3 briefly summarizes the typical synthesis routes to make VO-based PCMs from fatty acids and their derivatives. The thermodynamic equation expressing the change in the Gibbs free energy (ΔG) is presented in Section 4 to allow for a fundamental understanding of the relationship between molecular structure and PCM thermodynamic properties and eventually

direct an informed selection of optimal PCM structural architectures. The thermal phase change behavior, thermal stability and thermal conductivity are reviewed in three broad sections (5, 6 and 7, respectively). The thermal phase change behavior was discussed in four subsections based on particular PCMs' structural feature to reveal the role of: (5.1) the functional groups and hydrocarbon chain using monofunctional PCM, (5.2) symmetry using linear saturated monoesters, (5.3) two functional group using diesters and diamides and (5.4) branching and isomerism using sugar esters. In section 6, the onset temperature of degradation (T_{ON}) was discussed in terms of molecular mass (6.1), type and number of functional groups (6.2), and branching (6.3). In section 7, the thermal conductivity (κ) was discussed in terms of hydrocarbon chain length and number of hydrogen bonds sites. The current applications of PCMs are discussed in *Section 8* and a conclusion with perspective and directions for future research on VO-based PCMs is presented in *Section 9*.

6.1.5 Derivatization of TAGs to produce PCMs

VO-based PCMs are typically synthesized from fatty acids and their derivatives. The TAGs are hydrogenated and consequently hydrolyzed with either an acid, base or enzymatic catalyst to obtain linear saturated fatty acids [41, 42]. Fatty alcohols are synthesized by reduction of the carboxylic group on the fatty acids to a hydroxyl group using a reducing agent such as sodium borohydride or with a copper catalyst under high temperature and pressure [43].

Esters are synthesized via the reaction of suitable alcohol with (i) a fatty acid through an esterification reaction [44] or (ii) with an ester through transesterification [45]. Fatty amines are commonly prepared through the nitrile process: the fatty acid is reacted with ammonia under metal oxide catalyst to form a fatty nitrile and subsequently hydrogenated with Rainey-Nickel

catalyst to produce the fatty amine [42]. Fatty amides are synthesized from fatty acid and suitable amine by the amidation reaction [44]. Fatty carbonates are synthesized from carbonate interchange reaction using fatty alcohol and trialkyl carbonate with n-dibutyltin catalyst [17]. The standard route for the preparation of fatty ethers is through the Williamson ether synthesis via the reaction of fatty alcohol with fatty halide under a base catalyst [46]. Thioetherification of a fatty halide with a fatty thiol produces a fatty sulfide which is then further oxidized with hydrogen peroxide to fatty sulfones [32, 47].

6.1.6 Gibb's free energy of the phase change

The melting point (T_m) and melting enthalpy (ΔH_m) of a PCM are two main thermodynamic properties that are used for the selection of a PCM for TES applications. T_m is the temperature at which a PCM changes phase from the solid to the liquid state and ΔH_m is the heat absorbed by a specific quantity of the PCM to undergo the solid to liquid phase transition.

An understanding of the relationship between molecular structure and these thermodynamic properties would allow for an informed selection of PCMs. By determining how and at what level a certain molecular block contributes to ΔH_m and/or T_m , it is possible to define the classes of PCMs that hold the most promise for TES applications. The problem is somehow simplified in the case of VO-based PCMs as they are typically comprised of linear saturated hydrocarbon chains (principally saturated fatty acids and/or fatty alcohols) and a finite number of functional groups.

The thermodynamic equation expressing the change in the Gibbs free energy (ΔG) at constant temperature can be used to predict key trends in the phase change parameters based on the

structure of the PCM. The Gibbs free energy (ΔG) at constant T_m during the solid-liquid transition is expressed as a function of the enthalpy (ΔH_m) and the entropy of fusion (ΔS_m):

$$\Delta G_m = \Delta H_m - T\Delta S_m \quad \text{Equation 1}$$

At T_m the PCM is at solid-liquid phase equilibrium, and $\Delta G_m = 0$, giving:

$$T_m = \frac{\Delta H_m}{\Delta S_m} \quad \text{Equation 2}$$

ΔH_m depends on the magnitude of the attractive intermolecular forces in the crystal and the melt phase [48]. The change in entropy when melting the PCM is positive and depends on the molecular configuration [49]. These parameters are affected by the molecular geometry (geometry of the fatty chains and functional groups in the case of VO-based PCMs), which determines how easily the molecules can arrange in stable crystal structures.

6.1.6.1 Structural elements driving the phase change temperature and enthalpy

The hydrocarbon chains (principally saturated fatty acids and fatty alcohols) and diverse functional groups, such as ester ($-\text{COO}-$), amide ($-\text{CONH}-$), carboxylic ($-\text{COOH}$), hydroxyl ($-\text{OH}$), and sulfonyl ($-\text{SO}_2-$) groups can be arranged in versatile and diverse molecular architectures to make PCMs. The main van der Waals forces that exist in VO-based compounds are London dispersion forces between the hydrocarbon chains and dipole-dipole forces (*e.g.* hydrogen bonding) between functional groups [48]. The phase change ΔH_m and T_m can be principally adjusted by varying (i) the length of the hydrocarbon chain, (ii) the type and number of the functional groups and (iii) the overall molecular configuration.

Equation 2 teaches that for a molecule with a given (fixed) ΔS_m , any increase in dispersion forces brought by the methylene ($-\text{CH}_2-$) units of the hydrocarbon chain will increase both ΔH_m and T_m . Similarly, incorporating polar functional groups in the fatty chain would contribute to the intermolecular attractions. The functional groups such as hydroxyl, amide, and carboxylic groups possess permanent dipoles which can form hydrogen bonds, and the polar sulfonyl groups which undergo sulfonyl-sulfonyl interactions would increase ΔH_m and T_m .

6.1.6.2 Structural elements driving the phase change entropy (ΔS_m)

ΔS_m varies with the hydrocarbon chain length and the type of functional groups contained in the PCM molecule and is affected by the molecular configuration. The PCM molecule is confined in several ways within the crystal lattice and is restricted in its conformation as well as in its intermolecular distance and orientation with respect to its nearest neighbor molecules. Upon melting, these restrictions become relaxed, and the molecule can exist in a greater number of arrangements (microstates), number of positions and conformations. It is this increased disorder relative to the solid-state that determines the excess in ΔH_m . ΔS_m is determined by the way the molecules are unpacked from the crystal lattice in the first place [48]. It is therefore tied to the quality of the packing, i.e., polymorphism, that is achieved in the solid state (degree of order or conversely degree of disorder) and the subsequent unpacking into the liquid state. The amount of disorder involved in the phase transition is dictated by molecular symmetry, molecular flexibility, odd-even effect, and the type and number of functional groups and branched groups, which also are the parameters that determine the thermodynamic phase change parameters. Increasing the rotational symmetry of a molecule increases its probability of being in the proper orientation for uniform packing into the crystal lattice. The flexibility of a molecule increases with longer fatty chains and with easily rotatable functional groups such as the ester group. The

flexible molecules are less likely to crystallize compared to rigid molecules because the molecules are less likely to be in the proper conformation for incorporation into the crystal lattice and thus have higher conformational entropy [48].

Equation 2 establishes that larger ΔS_m is required to achieve the same T_m with higher ΔH_m . Typically, when a structure is changed, the molecular configuration is changed and so is ΔS_m . General trends show that a gain in ΔH_m is concomitant with an increase in ΔS_m . For example, increasing hydrocarbon chain length is known to increase ΔS_m because longer chains can secure more degrees of freedom in the liquid phase, which increase the entropy gain [50, 51].

6.1.7 Thermal phase change behaviour

6.1.7.1 Linear saturated PCMs with monofunctional group

T_m and ΔH_m data available for saturated aliphatic PCMs (C₈-C₄₀) comprising one functional group are presented in **Figure 0-1a** and b, respectively. Data were sourced from [1, 27-36, 38, 50, 52-87]. The data for alkanes are included in the figures and serve as a baseline for the aliphatic chains comprising functional groups. T_m of the alkanes which are available for C₁ to C₄₀₀ provides a maximum T_m (132°C [88, 89]) that is achievable by dispersion forces alone, given the absence of functional groups.

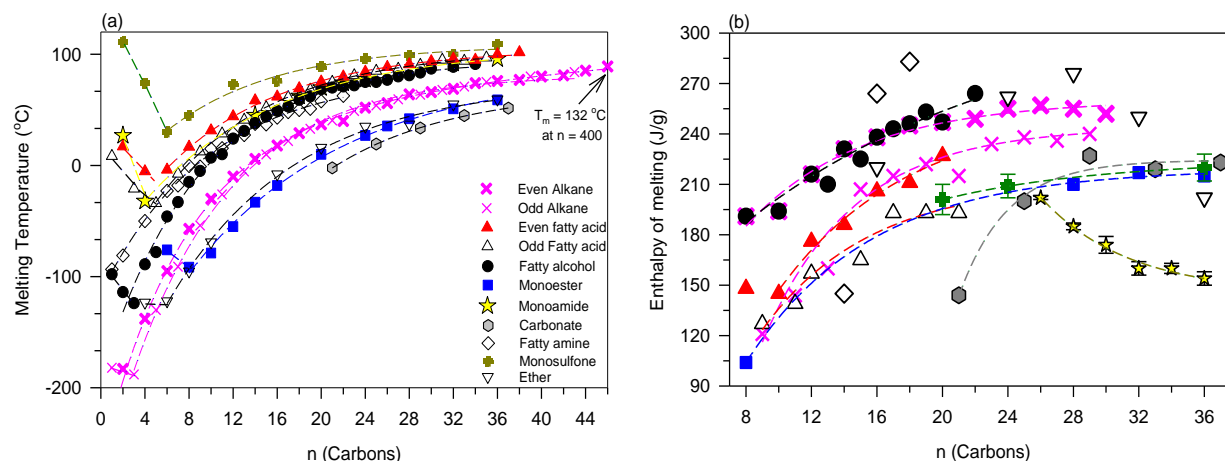


Figure 0-1. (a) T_m and (b) ΔH_m of linear saturated PCMs with one functional group versus total carbons atoms (n), *Dashed lines are guides for the eyes.*

6.1.7.2 Effect of Total Hydrocarbon Chain Length (n)

As shown in **Figure 0-1a**, T_m of the linear saturated monofunctional PCMs first decreases to a minimum before regularly increasing with chain length. The position of the minimum (singularity n_s) depends on the parity of the molecule and the type of functional group. For any given functional group, n_s of the odd molecules is one (01) carbon smaller than for the even molecules. It is lowest for the alkanes and highest for the sulfones ($n_s = 0$ for the alkanes and 6 for the monosulfones) increasing with increasing polarity and hydrogen bonding strength. This is attributed to the increasing strength of the contribution of the functional group to the intermolecular interaction coupled with the higher crystal stability that the small molecules achieve compared to the larger, disorder prone molecules. Above the singularity n_s , T_m versus total carbons curves (**Figure 0-1a**) are all well described by an exponential rise to a maximum function (*Equation 3*; $R^2 \geq 0.9840$).

$$f(n) = y_0 + a(1 - \exp(-n/n_0)) \quad \text{Equation 3}$$

Also, except the monoamides, ΔH_m of these PCMs (**Figure 0-1b**) follows the same function ($R^2 \geq 0.9655$). The fit parameters for the data in **Figure 0-1a-b** are given in **Table 0-1**. There is not enough ΔH_m data points for fatty amines and ethers to perform a good fit.

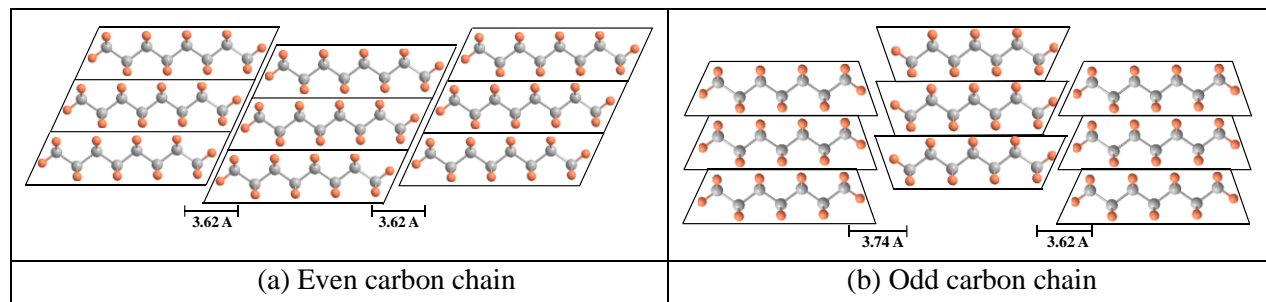
Table 0-1. Fit parameters for the exponential rise to a maximum function for the series of linear PCMs. (Equation 3)

PCM series	R^2		y_0		a		n_0	
	T_m	ΔH_m	T_m	ΔH_m	T_m	ΔH_m	T_m	ΔH_m
even alkanes	0.9983	0.9683	-267.5	25.6	284.5	234.7	7.2	7.0
odd alkanes	0.9986	0.9873	-287.1	-394.2	368.6	638.3	9.2	5.6
even fatty acids	0.9976	0.9829	-84.4	-124.3	189.2	379.2	10.6	7.9
odd fatty acids	0.9995	0.9673	-119.3	-137.3	223.0	349.0	10.2	6.5
fatty alcohols	0.9927	0.9673	-189.8	108.1	284.6	208.4	8.8	16.7
monoesters	0.9970	0.9989	-235.3	-112.1	321.0	331.4	14.2	7.6
monoamides	0.9996	0.9870	-85.8	145.3	191.2	7433.0	12.1	5.3
carbonates	0.9998	0.9802	-397.5	-91686.0	466.0	91910.5	11.1	3.0
fatty amines	0.9962	-	-114.8	-	197.2	-	9.8	-
monosulfones	0.9838	1.0000	-33.9	34.5	142.1	189.9	9.8	9.6
ethers	0.9976	-	-258.5	-	332.5	-	11.6	-

The exponential trend is due to the increase of the attractive dispersion forces tempered by mass transfer limitations [90, 91]. The plateaus observed for the T_m of monofunctional PCMs are all well below T_m achieved by the large alkanes (132°C), indicating the adverse influence of the conformation of the bulky functional groups. The characteristic carbon number (n_0 in **Table 0-1**) obtained from the exponential fit, which is ~14 for the monoesters and about either 10 or 11 for all the others, indicates that increasing the size of the fatty moieties beyond the longest most abundant naturally occurring fatty acids (C18) does not significantly increase T_m . Above twenty (20) -CH₂- units is the size at which the T_m of this type of materials is reported to generally begin to add little practical marginal increase and to plateau [51, 89]. The use of the size of the

hydrocarbon chain as a structural element to improve the phase change temperature and enthalpy of these PCMs is therefore practically limited to this range of fatty chain length.

T_m as well as ΔH_m of the even alkanes and fatty acids are larger than those of their odd counterparts. A typical example is shown in **Figure 0-1b** for alkanes (odd (×) even (×)) and fatty acids ((odd (△) even (▲)). For example, the C18 alkane and C18 fatty acid have ΔH_m of 245 and 210J/g, respectively, while the C17 alkane and C17 fatty acid counterpart have is 215 and 185J/g, respectively. The odd/even effect is explained by the variation in crystal packing densities due to the subtle difference in the inter-atomic distance between the terminal methyl groups of neighboring chains as shown in **Scheme 0-2** [92].



Scheme 0-2. Schematic representation of the two-dimensional projection for the packing of (a) even numbered and (b) odd numbered alkanes.

The shape of an even alkane can be described in the plane of the carbon skeleton as a parallelogram and that of an odd alkane as a trapezoid (**Scheme 0-2**) [92]. When going from odd alkane to even alkane via addition of $-\text{CH}_2-$ group, the molecule chain length increases by an increment of 1.26\AA and its area increases by similar proportions. Such a packing leads to a monotonic increase in the density because the parallelogram and a trapezoid have the same area with the same length of the center line and height. However, the terminal methyl groups situated opposite to each other try to adapt to the low energy staggered conformation as may be seen

from **Scheme 0-2** [92]. Thus, the columns of the parallelograms are shifted with respect to each other so as to achieve the staggered arrangement of methyl groups. A similar shift is possible in the trapezoid pattern but only on one side; on the other side the shift results in longer distances ($\sim 3.74\text{\AA}$ in **Scheme 0-2b**) and the methyl groups are not really situated opposite to each other. Thus, the even alkanes have optimal intermolecular contacts at both ends, whereas the odd alkanes possess these at one end, and at the other end the distances are longer [54]. This leads to a less dense packing for the odd alkanes and as a consequence, to relatively lower T_m and ΔH_m , as observed in **Figure 0-1a-b**, due to lower dispersion forces [92, 93].

6.1.7.3 *Effect of the Functional Group*

The PCMs with polar functional groups such as amine, hydroxyl, amide, and carboxyl are capable of forming hydrogen bonds and sulfonyl groups are capable of forming sulfonyl-sulfonyl interactions between opposite charges of their permanent dipoles [94] which allows for strong secondary intermolecular attractions. The polarity which is quantified by the estimated dipole moment of the electronegative bonds (**Table 0-2** and **Figure 0-2**) can be used to gauge the scope of the contribution of the functional group to the intermolecular forces [95, 96]. These estimates are based on the experimentally determined dipole moments of alkane compounds with the shortest carbon chains (R and $R' = \text{CH}_3$) where the moments are essentially fixed by the functional groups [97-102].

Table 0-2. Estimated dipole moments (Debye, D) for main functional groups and comparison of T_m for PCMs with three representative fixed carbon chain (C_{20} , C_{28} and C_{38}).

‘*’ functional groups capable of dipole-dipole intermolecular interaction with each other

Rank	Functional group	Dipole moment (D)	T_m C ₂₀ carbon chain (°C)	T_m C ₂₈ carbon chain (°C)	T_m C ₃₈ carbon chain (°C)
1	Alkane (R)	0	37	64	76
2	Carbonate (R-CO ₃ -R')	0.91	-2.2	33.7	51.6
3	Ether (R-O-R')	0.95	16	37	59.5
4	Amine (R-NH ₂) *	1.2	57.8	-	-
5	Hydroxyl (R-OH) *	1.7	68.5	81	-
6	Ester (R-COO-R')	1.74	10	37	59.5
7	Carboxyl (R-COOH) *	1.78	75.4	90.9	99.9
8	Amide (R-CONH-R') *	3.76	70	-	96
9	Sulfonyl (R-SO ₂ -R') *	4.4	89	99	109

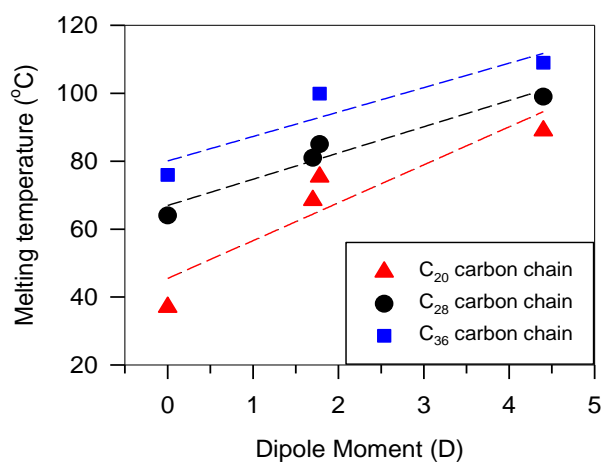


Figure 0-2. Relationship between dipole moment and T_m for PCMs with three fixed carbon chain (C₂₀, C₂₈ and C₃₈) and polar functional group capable of forming dipole-dipole intermolecular interaction between each other (* in **Table 0-1**). *Dashed lines are guide for the eyes only.*

6.1.7.3.1 Melting point (T_m)

Figure 0-1a and **Table 0-2** reveal a hierarchy in T_m based on the type of the functional group, i.e., the strength of the extra forces from the polarity and the conformation that it imposes on the

molecule. For any given carbon number, T_m of the fatty carbonates (●) is the lowest followed by the monoesters (■) and fatty ethers (▽) all below T_m of the alkanes (✕). T_m of the fatty amines (◇) and fatty alcohols (●) are just above the alkanes, closely followed by the monoamides (★), the fatty acids (▲) and the monosulfones (+) which show the highest T_m . This hierarchy is driven by the strength of the intermolecular forces provided by the dipole moments of the functional groups (**Figure 0-2**) and the contribution to the entropy of fusion of the specific conformation that the functional group imposes on the molecule.

Overall, T_m of the PCMs with functional groups which do not readily form hydrogen bonds such as fatty ethers (▽), fatty carbonates (●) and monoesters (■) are lower compared to those which forms dipole-dipole intermolecular interaction such as the fatty alcohols (●), fatty acids (▲), monoamides (★) and monosulfones (+). The ether, carbonate, and ester functional groups do not readily form hydrogen bonds since their molecules lack hydrogen bond donor atoms. The primary forces contributing to their T_m are the dispersion forces from the $-\text{CH}_2-$ units. **Table 0-2** shows for fixed carbon chain length, the fatty ethers (▽), monoesters (■) and fatty carbonates (●) have even lower T_m than the alkanes (✕) and is attributed to the flexibility of the alkoxy moiety (C–O) on their functional group, which increases the lattice vibration via a larger number of degrees of freedom [88, 103].

6.1.7.3.2 Enthalpy of melting (ΔH_m)

The analysis of the contribution to ΔH_m is more complex than the examination of T_m above, as it involves the conjunction of the polar attractions and steric hindrances of the functional group. ΔH_m of the fatty alcohols (●) is practically superimposed to that of the even alkanes, whereas ΔH_m of the fatty acids (▲) although not perfectly, aligns well with the odd alkanes in the high

carbon number range. ΔH_m of the fatty carbonates (●) also follows an exponential rise to a maximum with values that are ~30 J/g lower than the odd alkanes. This difference in ΔH_m arises from the electronic repulsion and C–O flexibility of the carbonate group which prevents the molecules from stacking as tightly as the alkanes.

ΔH_m of the monosulfones is at the level of the large fatty carbonates, which is much less than that of the other PCMs despite bearing strong dipolar intermolecular forces. In both cases, it is the steric repulsion provided by the functional groups that primarily affects the crystal structure and the entropy of fusion.

Noticeably, and contrary to what was observed for their T_m (**Figure 0-1a**), ΔH_m of the monoamides follows an apparent exponential decrease with total carbon (★ in **Figure 0-1b**). This trend reveals a decrease in the hydrogen bond strength and increasing regions of heterogeneity in the crystalline solid [38]. Crystallographic studies conducted on the monoamides showed that the crystal packing efficiency decreases with increasing chain length, explaining the lower ΔH_m . XRD as well as NMR analysis also revealed a continuous decrease of the hydrogen bond strength with increasing chain length which results in the lowering of the overall intermolecular attraction [38, 48]. ΔH_m of the monosulfones (✚) did not suffer a similar decrease because of the much stronger polar contribution. As indicated by XRD, these forces have been able to maintain the highest stability crystalline packing despite the increasing steric hindrance [32, 47].

6.1.8 Effect of Symmetry – Case of the Monoesters PCMs

Linear saturated monoesters hold great potential as economical PCMs for low temperature applications [33-35, 50, 66-72]. This is because their T_m can be easily fine-tuned almost

anywhere between -20°C and 60°C by simply altering the length of the fatty acid (R) and / or fatty alcohol (R'). To visualize the effect of each moiety T_m is presented in two series: (1) fixed fatty alcohol chain with varying fatty acid chain (**Figure 0-3a-b**) and (2) fixed fatty acid chain with varying fatty alcohol chain (**Figure 0-3c**). The monoesters with short-chain alcohols (R' = 1, 2, 3, & 4) are presented in **Figure 0-3a** and those with long-chain alcohols (i.e. R' = 5, 10, 14, 16, & 18) are presented in **Figure 0-3b**. T_m of the monoesters with fixed fatty acid chain (i.e. R = 12, 14, 16 & 18) versus alcohol chain length (R' = 1, 2, 3, 4, 5, 10, 14, 16, & 18) is presented in **Figure 0-3c**. **Figure 0-3d** presents the available ΔH_m data of all the monoesters.

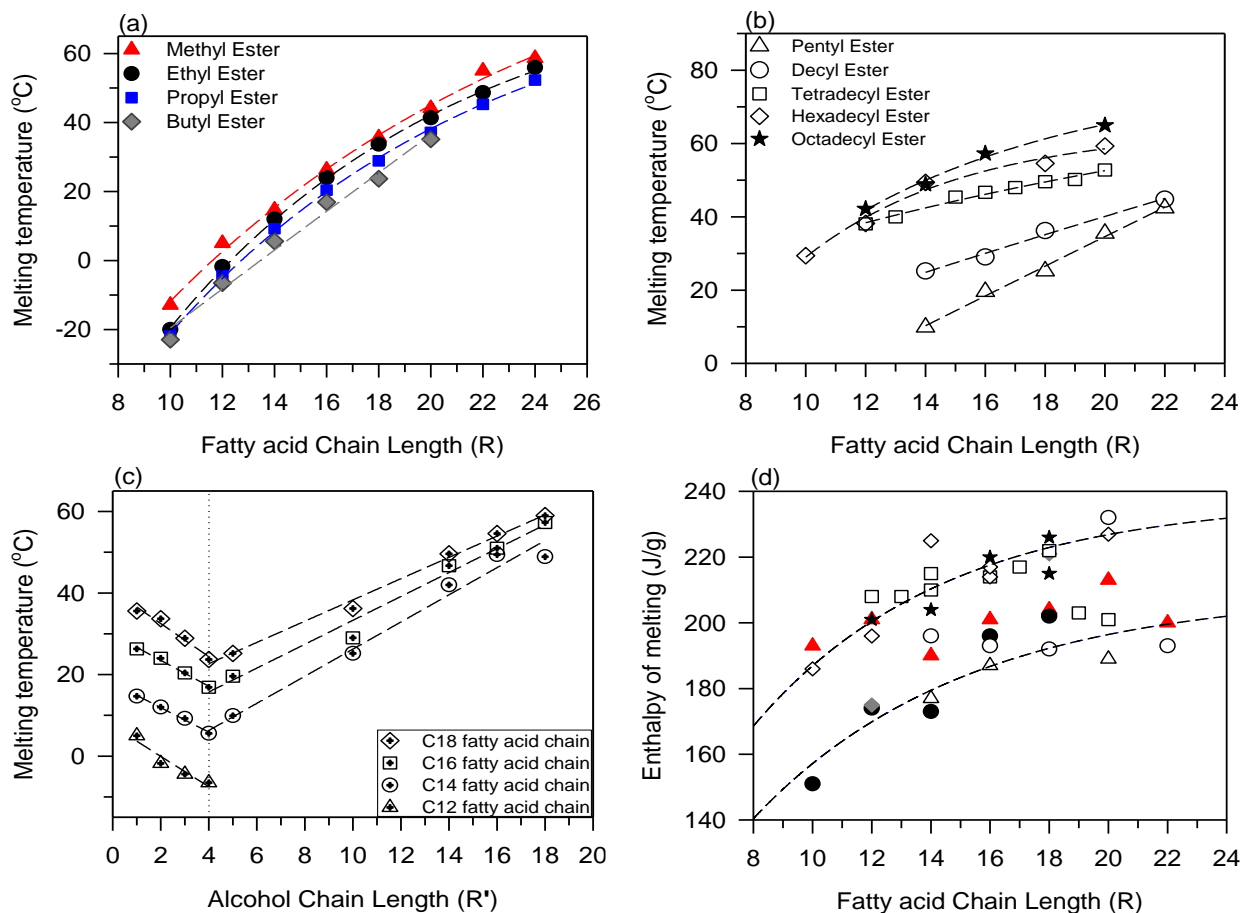


Figure 0-3. (a) T_m versus fatty acid chain length of monoesters with (a) C₁-C₄ alcohol, (b) C₅-C₁₈ alcohol, (c) T_m of monoesters with fixed fatty acid chain (C₁₂-C₁₈) versus alcohol chain length and (d) ΔH_m of monoesters versus fatty acid chain length. *Dashed lines are guide for the eyes.*

As shown in **Figure 0-3a-b**, T_m versus fatty acid chain length of the monoesters follows the typical exponential rise to a maximum (*Equation 3*; fit parameters are given in **Table 0-3**). The rate of change of T_m as quantified by the characteristic number of fatty acid carbons is the same regardless of fatty alcohol size ($n_0 = 13 \pm 2$ in **Table 0-3**) indicating similar structural effects. For any given fatty alcohol, the monoesters of the series shown in **Figure 0-3a** gain $\sim 6^\circ\text{C}$ in T_m for each carbon added to the fatty acid chain moiety (i.e., from methyl (\blacktriangle), ethyl (\bullet), propyl (\blacksquare) to butyl (\blacklozenge) monoesters). For the monoesters of the series shown in **Figure 0-3b** this gain averages $\sim 4^\circ\text{C}$ per fatty acid carbon (from pentyl (\triangle), decyl (\circ), tetradecyl (\square), hexadecyl (\diamond), and octadecyl monoester).

Table 0-3. Parameters of the fit to an exponential rise to a maximum function (*Equation 3*) of T_m of asymmetric monoesters versus total carbons curves (**Figure 0-3a-b**).

Asymmetric Monoesters	R^2	y_0	a	n_0
Methyl Esters (C1)	0.99	-134.4	243.3	15.6
Ethyl Esters (C2)	0.99	-219.1	304.3	11.2
Propyl Esters (C3)	0.99	-219.5	305.6	12.3
Butyl Esters (C4)	0.99	-228.8	310.3	12.8
Average				13.0\pm1.9
Pentyl esters (C5)	0.97	-89.1	364.6	59.5
Decyl esters (C10)	0.99	-61.3	214.4	46.7
Tetradecyl esters (C14)	0.99	-349.7	412.3	9.2
Hexadecyl esters (C16)	0.98	-4257.0	4321.1	5.4
Octadecyl esters (C18)	0.99	-1393.6	1472.9	8.2

6.1.8.1 Effect of fatty alcohol chain length on T_m

Figure 0-3c shows a minimum in T_m at the alcohol chain length = 4. Both segments seem to follow straight lines, but this is probably due to the small data set as the trend should plateau as is typically the case for all linear hydrocarbons. Note that T_m of the monoesters experiences a

similar rate of change with alcohol chain length on the decreasing and increasing segments (slopes = -3.0 and 3.5 , respectively).

This trend is the result of the alcohol chain position relative to the ester functional group. The alkoxy moiety of the $\text{O}-\text{C}=\text{O}$ ester bond rotates more freely and provides flexibility to the alcohol chain which increases the vibrations with chain length [72, 88]. Two competing effects take place when the length of the alcohol chain is increased: (i) it allows for more dispersion forces and (ii) induces stronger lattice vibrations. The trend observed for the alcohol chain length until $R'=4$ (decreasing T_m in **Figure 0-3c**) is attributed to the weak dispersion forces and increasing vibrations and consequent weakening of the crystal lattice network. At longer alcohol chains of ≥ 5 (Increasing T_m in **Figure 0-3c**), the effect of dispersion forces overwhelms the effect of the ester group flexibility which increases T_m . This observation supports Carnelley's melting point rule which states that molecules with higher molecular symmetry tend to have higher T_m [49].

6.1.8.2 Effect of fatty chain length on ΔH_m

Although no clear trends are observed in the ΔH_m of the monoesters variation as a function of total fatty chain length (**Figure 0-3d**), probably due to the complexity of the structural effects and the large uncertainty on the published values, one can detect overall gradual increases tending to plateaus at large number of carbons similar to what was observed for the other PCMs (**Figure 0-3b**). One can divide the ΔH_m data of **Figure 0-3d** in two clusters that follow an exponential rise to a maximum function (*Equation 3*). The fitting attempts shown in **Figure 0-3d** as dashed lines delimit a high ΔH_m group around the decyl (\circ), hexadecyl (\diamond) and octadecyl (\star) esters and a low ΔH_m group around the methyl (\blacktriangle), ethyl (\bullet) and pentyl (\triangle) esters. ΔH_m

of the monoesters of the low value group lay between 150J/g and 190J/g and the high value group lay between 190J/g and 230J/g. A discussion of these variations in detail in terms of dispersion forces, functional group contributions, conformation and mass transfer limitations similar to what was done for the other PCMs can only be general given the wide dispersion of the data.

6.1.9 Diesters and Diamides PCMs

The thermal properties of the symmetrical diesters and diamides (R–R''–R') shown in **Scheme 0-1** have been studied in detail as PCMs [34, 36, 38-40, 104, 105]. The inter-functional groups aliphatic chain which length is denoted “R''” in the above nomenclature (shown in **Scheme 0-1**) is referred to as ‘spacer chain’ to conveniently and better visualize the central position of this important segment of the molecules with two functional groups. T_m and ΔH_m of diesters and diamides are presented as a function of spacer chain length (R'') in **Figure 0-4a-b**, respectively.

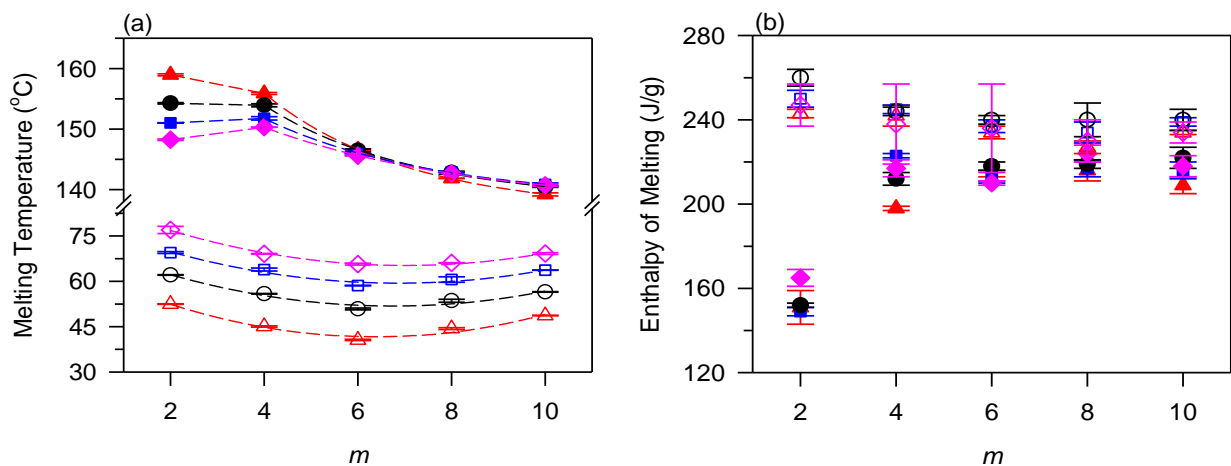


Figure 0-4. (a) T_m and (b) ΔH_m of the symmetrical diesters and diamides versus spacer chain length (R'') (symbols Δ & \blacktriangle : R & R' = 11; \circ & \bullet : R & R' = 13; \square & \blacksquare : R & R' = 15; \diamond & \blacklozenge : R & R' = 17; unfilled: diesters and filled: diamides). Error bars represent the standard deviations of three runs. *Dashed lines are guides for the eye.*

6.1.9.1 Effect of spacer chain and hydrocarbon chain on T_m and ΔH_m

T_m of the diamides (filled symbols in **Figure 0-4a**) is about 75°C higher than that of the diesters (unfilled symbols in **Figure 0-4a**) highlighting the significance of the hydrogen bond contributions. In both cases, as the size of the spacer chain increases, an overall decrease in T_m is observed despite the increase in hydrocarbon chain length (**Figure 0-4a**). In the case of the diamides, this behavior is explained by the weakening of the hydrogen bond strength with the increase of the spacer chain length. The decrease in hydrogen bond strength with increasing spacer size was documented by NMR and confirmed by XRD with the subsequent increases in the intermolecular distance comprising the hydrogen bond layer [106].

The T_m of the diesters versus diol chain spacer length (R'') curves present a minimum at $R'' = 6$ (for R & $R' = 17$, T_m minimum = 67°C) attributed to the competition between the dispersion forces and the intramolecular steric repulsion of the electron clouds between the ester groups [107]. The ester groups experience intramolecular steric repulsions which distort the diol chain and degrade the crystal packing allowing for smaller intermolecular stabilization arrangements. For $R'' < 6$, the distortions lower T_m in a manner that is not compensated by the contribution of the added methylene ($-\text{CH}_2-$) units to the spacer chain length. For the longer spacer chain diols ($R'' > 6$), the intramolecular repulsions are small and insufficient to compensate for the added spacer $-\text{CH}_2-$ units.

Figure 0-4b illustrates the similarities and stark differences of the effect of the spacer chain length on the phase change enthalpy of molecules which form hydrogen bonds (diamides), and those which do not (diesters). ΔH_m of the PCMs having $R'' \geq 4$ spacer is virtually constant for both diesters and diamides series. The $R'' = 2$ diamides present a much lower ΔH_m due to amide

group steric repulsions, which force the molecule to assume a higher energy conformation [106]. The diamide molecules with the higher energy conformation at $m = 2$ stacks less efficiently in their crystal lattice [106] thus decrease the total intermolecular interaction as reflected in the ΔH_m . ΔH_m of the diesters ($\sim 230\text{J/g}$) and ΔH_m of the diamides with $R'' \geq 4$ ($\sim 220\text{J/g}$) remained constant because as the ester/amide groups move further from each other, the ester/amide groups steric repulsion becomes less and assume a similar packing arrangement (β -form). Overall, ΔH_m of the diesters is slightly higher than the diamides because of closer stacking in their crystal lattice.

6.1.9.2 Comparison of PCMs with difunctional vs. monofunctional groups

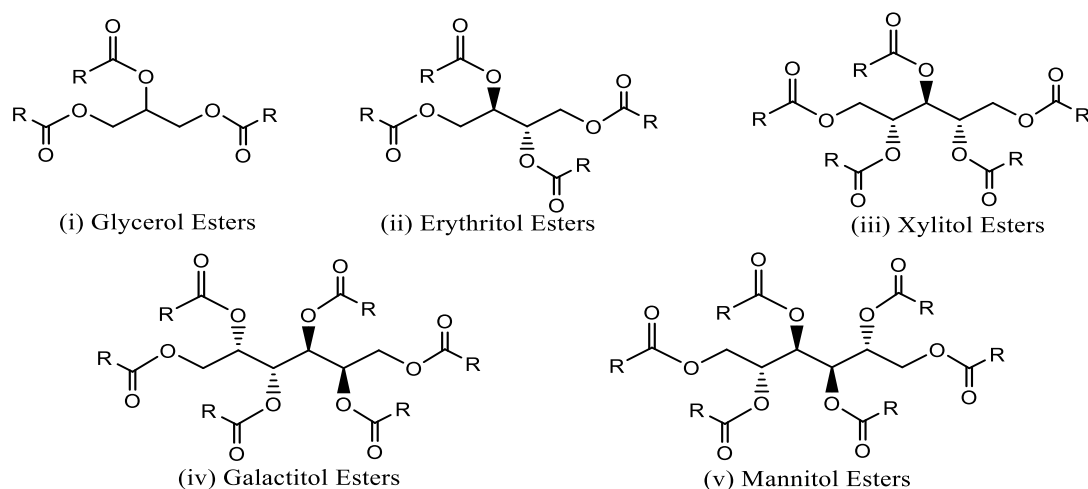
The comparison of the thermal properties of the linear saturated diesters and diamides with the linear saturated monoesters and monoamides [38] show the extent and limits to the TES effectiveness of added functional groups in PCMs. For the same number of carbon; T_m of the diamide 14-8-14 is 143°C and the monoamide 18-18 is 96°C which is larger by 47°C . Likewise, ΔH_m of 14-8-14 and 18-18 is 217J/g and 196J/g respectively. The increase in T_m and ΔH_m is attributed (in the case of the amide PCMs) to the increase of the number of hydrogen bonds. In the presence of two amide functional groups, a maximum of four hydrogen bonds is formed between adjacent diamide molecules in the crystal lattice instead of two formed by monoamides.

On the contrary for the same number of carbons, the diester; 14-8-14 has a lower T_m (59°C) with higher ΔH_m (234J/g) compared to the monoester; 18-18 which has a T_m of 54°C and ΔH_m of 215J/g . The high ΔH_m is attributable to the presence of dispersion forces between hydrocarbon chains. However, the lower T_m of the diesters is due to the increased crystal lattice vibration

associated with the presence of the two flexible ester functional groups and the symmetry effect as discussed for the asymmetrical monoesters under *Section 4.2*.

6.1.10 Sugar Esters PCMs – Effect of Branching and Isomerism on TES

T_m and ΔH_m of the sugar esters derived from: glycerol, erythritol, xylitol, galactitol, and mannitol [82-86] are presented in **Figure 0-5a** and b, respectively, as a function of total number of total carbons. The molecular structures of these sugar esters are presented in **Scheme 0-3**. The wedge-and-dash projection is used in the scheme to visualize the plane in which the hydrocarbon chains are positioned.



Scheme 0-3. Wedge-and-dash projection molecular structures of the sugar esters. The solid and dash wedges represent the hydrocarbon chains that are coming out and going into the plane, respectively. R = 11, 13, 15 and 17 for molecules in the sugar alcohol series.

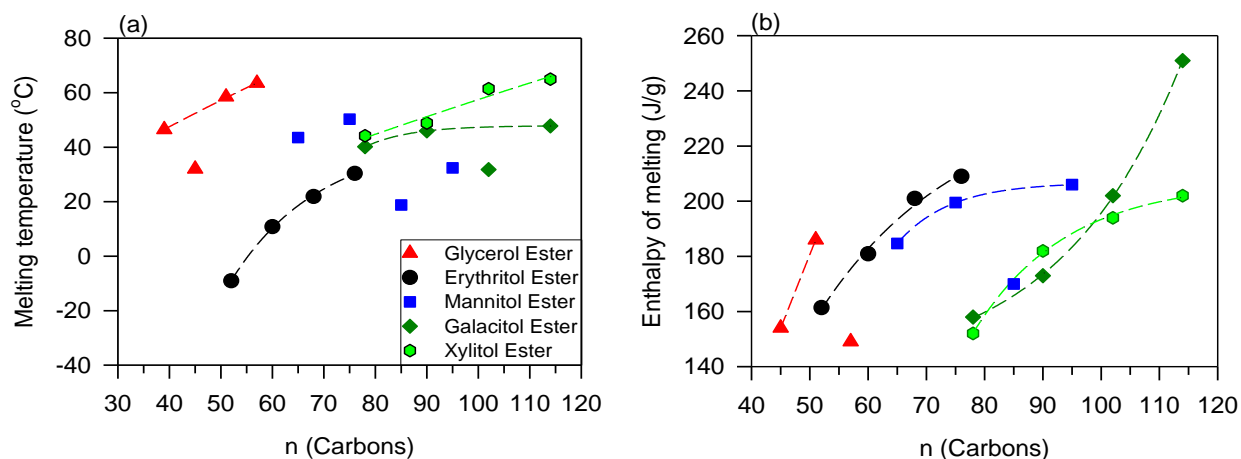


Figure 0-5. (a) T_m and (b) ΔH_m of the sugar esters versus total carbons (n). Symbols: (\blacktriangle) glycerol, (\bullet) erythritol, (\blacksquare) xylitol, (\blacklozenge) galacitol and (\blacklozenge) mannitol. Dashed lines are guides for the eye.

Overall and for similar geometrical configuration, the larger sugar esters have larger T_m and ΔH_m . In general, T_m and ΔH_m versus total carbons for each series of sugar esters seem to follow the typical exponential rise to a maximum trend common to hydrocarbons. The erythritol esters (\bullet) and mannitol esters (\blacklozenge) may be the best examples for illustrating that trend. Although the trends are unmistakable, there are not sufficient data to draw satisfactory quantitative and predictive relationships for these materials.

6.1.10.1 Effect of branching and chain length

All the sugar ester PCMs synthesized so far present T_m below 70°C and ΔH_m in the range 140-210J/g (Figure 0-5a-b). T_m and ΔH_m of these compounds are considered low relative to the linear saturated mono- and difunctional PCMs (example: paraffin, diesters, and diamides). These low values can be explained by the steric hindrances associated with the long hydrocarbon chains protruding in various directions from the sugar alcohol backbone (solid/dash wedges in Scheme 0-3) highlighting the importance of the geometrical configuration. The protruding hydrocarbon

chains limit their close packing arrangement in the crystal lattice thereby reducing the intermolecular interactions which are necessary to increase T_m and ΔH_m [48].

The presence of protuberant conformations adversely affects T_m . The importance of the branched hydrocarbon chain length on T_m is revealed in **Figure 0-5a**. Glycerol trimyristate (\blacktriangle at $n = 45$ in **Figure 0-5a**) which has relatively longer hydrocarbon chains than glycerol trilaurate (\blacktriangle at $n = 39$ in **Figure 0-5a**) possess lower T_m most likely due to its lower stability crystal packing arrangement in the crystal lattice. Likewise, in the case of xylitol esters (\blacksquare in **Figure 0-5a**) for example, one can notice the much lower T_m of the 85 and 95 carbon compound (xylitol pentapalmitate; 19°C and xylitol pentastearate; 32°C) compared to the 65 and 75 carbon compounds (xylitol pentalaurate; 44°C and xylitol pentamyristate; 50°C). Galactitol hexapalmitate, which has 12 carbons more than galactitol hexamyristate has a much lower T_m (32°C vs 46°C). These compounds do not perfectly follow the exponential trend most likely because their molecular geometry favors the formation of lower stability polymorphs. The three other galactitol esters of **Figure 0-5a** seem to fit into an exponential trend like the erythritols.

6.1.10.2 Effect of isomerism

The importance of the geometrical configuration of the sugar esters in setting the thermodynamic properties relevant to TES is further stressed in the stark differences shown by the isomers. The galactitol and mannitol esters (compound *iv* and *v* in **Scheme 0-3**, respectively) are isomers, i.e., they both have identical molecular formulas but distinct molecular structures. The difference between these two structures is the directions in which the hydrocarbon chains are protruding from the sugar alcohol backbone. **Scheme 0-3** shows that for the mannitol esters (compound *iv*), one pair of the hydrocarbon chain is going into the plane (dash wedges) while another pair is

protruding out of the plane (solid wedges), whereas; two of the hydrocarbon chains of the mannitol esters (compound ν) located in the center of the molecule (solid wedges) are protruding out of the plane while the two adjacent hydrocarbon chain (dash-wedge) next to them are behind the plane. The variation of T_m and ΔH_m versus hydrocarbon chain length of galactitol (◆) and mannitol (●) esters are quite distinct. For example, ΔH_m of galactitol hexastearate is 50J/g higher than mannitol hexastearate ($n = 114$, ◆ and ● in **Figure 0-5b**, respectively) which indicates that it packs more efficiently.

6.1.11 Entropy of fusion (ΔS_m) of linear saturated functional PCMs

The relationship between ΔS_m and hydrocarbon chain length is well known and is typically explained by flexibility considerations. The flexible sp^3 C-C bond in the hydrocarbon chains has the tendency to align in the *trans*- linear conformation to maximize the dispersion forces in the melt [48]. The entire chain conforms in segments of four $-CH_2-$ units in either the stable *trans*-conformation or in the unstable eclipsed high energy conformation. The probability of the hydrocarbon chain to adopt the stable low energy *trans*-conformation is 33.3%. With the increase of hydrocarbon chain length, the number of eclipsed conformations and available microstates during the transition increases, thereby increasing the disorder. The contribution of the functional groups to ΔS_m is typically attributed to conformational hindrances. **Figure 0-5a-b** presents ΔS_m of the PCMs as a function of total carbons.

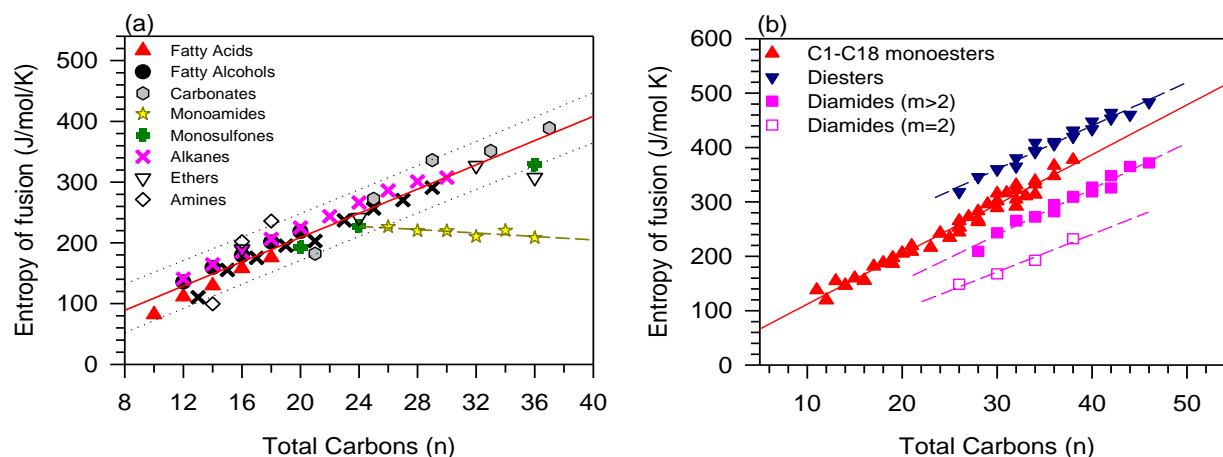


Figure 0-6. Molar entropy of melting (ΔS_m) versus total carbons: (a) linear saturated monofunctional PCMs, (b) monoesters; diesters; and diamides (spacer chain (m)). *Dashed lines are fits of the data to straight lines.*

Except for the monoamides (\star), ΔS_m of all the PCMs increase linearly with hydrocarbon chain length (**Figure 0-6a-b**). Generally, ΔS_m of all the monofunctional PCMs are comprised in the 95% prediction band of the fit of the whole set to a straight line (**Figure 0-6a**, $R^2 > 0.9349$). Such increase of the entropy of fusion with chain length is also common for saturated aliphatic monoesters, alkanes, alkenes, alkynes, alkanols, alkanethiols, alkanamines, nitroalkanes, chloroalkanes, bromoalkanes and iodoalkanes [93, 108].

The overall slope or rate of change of ΔS_m ($\alpha_{\Delta S}$) is $9.8 \pm 0.4 \text{ J/mol/K}$ per $-\text{CH}_2-$ unit. This value accounts for the contribution of the hydrocarbon chain flexibility which predominantly drives the disorder and for the averaged functional groups' conformational effects. The increasing disorder is explained by the proportional increase in degrees of freedom in the melt and probability of possible microstates introduced by the flexibility of the fatty chains. This increases the number of ways the thermal energy can be dispersed within the molecule [48].

ΔS_m data of each category of PCM follows a particular straight line with notable differences in rate of change ($\alpha_{\Delta S}$). A plot of $\alpha_{\Delta S}$ versus individual categories is presented in **Figure 0-7**. The $\alpha_{\Delta S}$ versus PCM type plot shows a well-defined hierarchization of the contribution of the functional groups to the “disorder” indicating definite and distinct contributions of each functional group.

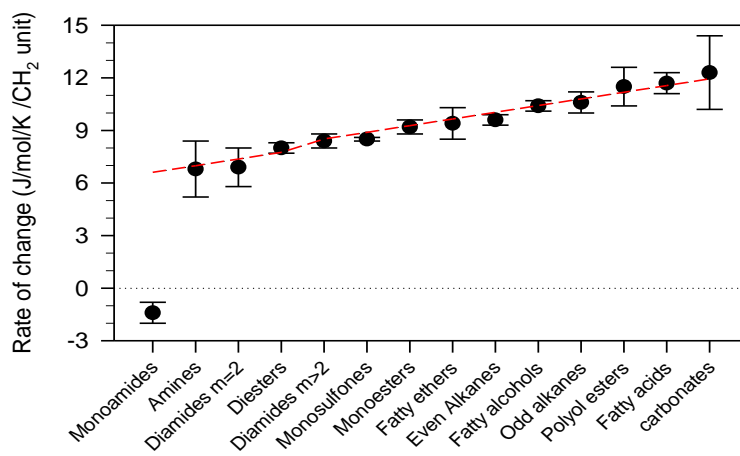


Figure 0-7. Rate of change in ΔS_m of the individual categories of PCM. *Dashed line is a guide for the eye.*

The rate at which the “disorder” tends to increase is highest for the fatty carbonates (12.3J/mol/K/CH₂) and lowest for the fatty amines (6.8J/mol/K/CH₂). These data show that although the “transition disorder” is overall driven by the size of the fatty chains through the flexibility of the molecule during the phase change and is tuned by conformation considerations which result from the functional group’s geometry and polar / hydrogen bond interactions.

The case of the monoamides (★ in **Figure 0-6a**) is interesting as it shows a negative rate of change (-1.4J/mol/K/CH₂). This tendency to order highlights the role of polymorphism in setting the entropy of fusion of PCMs. While the increase in chain length provides more degrees of

freedom in the melt, it may modify the polymorphism of the initial state (crystal state) [38]. The contribution of the change in polymorphism can be strong enough such as in the diamides, to even reverse the tendency from “disordering” to “ordering” [38]. Recall that ΔS_m is the increase in entropy in the transition from an organized crystalline solid to the disorganized structure of a liquid. The XRD analysis of monoamides revealed that as the chain length increases, the less stable β' phase grew at the detriment of the stable β -phase which was the only form detected for the shortest compound [46]. In the monoamides, the effect of polymorphism is strong enough to offset the increase in melt entropy and even slightly lower the entropy of fusion [38]. The difference in rate of change of the entropy of fusion between the monoamides and the other monofunctional PCMs (difference of $\sim 11\text{J/mol/K/CH}_2$) may be used to quantify the part of “disorder” that is introduced to the solid state (crystal) by each added $-\text{CH}_2-$ unit before the thermal transition. This value may be used to estimate the contribution to the entropy of fusion due to polymorphism.

The complex sugar ester structures present a higher ΔS_m than any other category of PCMs (reported values vary between 365 to 1390J/mol/K [82-86]) but generally follow the same linear trend (*Fig. S5 in SI.*, $R^2 = 0.9283$). These non-linear compounds comprise flexible hydrocarbon chains and ester functional groups in complex conformations. They are also subject to high polymorphism. Their overall ΔS_m rate of change is high ($\alpha_{\Delta S} = 11.5\text{J/mol/K/CH}_2$) but lower than that of fatty acids and carbonates, indicating intricate competition between flexibility, conformation and polymorphism effects. Unfortunately, given the available data and current understanding of these materials, it is difficult to determine which part of the change in entropy is driven by flexibility, conformation, or polymorphism.

Although much more complex relationships are probably at play, a simple scale for ranking the “disorder” tendency of the PCMs can be outlined relative to the maximum rate achieved by the carbonates ($\alpha_{\Delta S} = 12.3\text{J/mol/K/CH}_2$). When reported in percentages of this maximum, the rate of change in ΔS_m indicates five (05) groups of PCMs with statistically indistinguishable disordering rate (plot is not shown). These are in order of increasing tendency to disorder: (1) amines, diamides $R'' = 2$ ($56 \pm 1\%$); (2) diesters, diamides $R'' > 2$, monosulfones ($67 \pm 2\%$); (3) monoesters, fatty ethers, even alkanes ($76 \pm 2\%$); (4) fatty alcohols, odd alkanes ($85 \pm 1\%$), (5) sugar esters, fatty acids, fatty carbonates ($96 \pm 3\%$).

6.1.11.1 Enthalpy – Entropy Correlation

The correlation between molar entropy of melting and molar enthalpy of melting are presented in **Figure 0-8** for the PCMs. Data are sourced from [1, 27-36, 38, 50, 52-86].

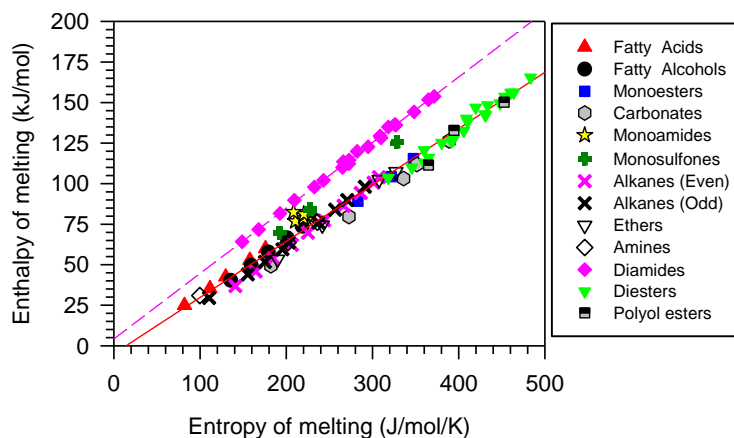


Figure 0-8. Correlation between Molar entropy of melting versus molar enthalpy of melting of the PCMs. *Dashed lines are fits of the data to straight lines.*

Practically, except the amide, the entropy and enthalpy of melting of the PCMs correlate very well (**Figure 0-8**, $R^2 > 0.9744$). This indicates the balance between the disorder (ΔS_m) and the

forces holding the molecules in the crystal lattice (ΔH_m). This means that overall, the same entropy changes bring the same latent heat during the transition at the respective melting temperatures. Note that the correlation line crosses the enthalpy axis below zero which indicates that for small changes in entropy this is no longer the case. The cluster in the entropy and enthalpy data observed for the monoamide (★ in **Figure 0-8**) is related to the strong effect of polymorphism which positively affects the transition order. The diamide entropy and enthalpy correlation line (◆ in **Figure 0-8**, $R^2 = 0.9991$) lies above the general correlation line indicating that for a similar amount of entropy, the enthalpy is larger. This can be explained by the extra attractions provided by the hydrogen bonds. Note that this effect becomes larger as the entropy increases (slopes: 0.35 vs 0.40 in **Figure 0-8**).

6.1.12 Thermal Stability

Thermal stability of PCMs is typically determined by thermogravimetric analysis (TGA). The goal is to understand how temperature affects the degradation of the PCM prior to utilization in TES systems. PCMs thermal stability is typically indicated by the onset temperature of mass loss (T_{ON}). Unlike the readily available T_m and ΔH_m data, the thermal stability data of VO-based PCMs is limited because thermal degradation and cycling analysis studies are time consuming and generally carried out scarcely by researchers in academia. Nevertheless, the available thermal stability data gathered in this work provide valid conclusions on how VO PCM's molecular structure, particularly molecular mass, functional groups and branch groups influence thermal stability.

The available thermal stability data for VO-based PCMs comprising a variety of functional groups mined from the literature includes fatty acids [27, 35, 57, 58], fatty alcohols [27, 30, 61,

64], monoesters [33-35, 50, 66, 69, 70, 72], diesters [34, 36], sugar esters [82-86], fatty carbonates [26], monoamides [38], diamides [38, 40], monosulfones [32], and alkanes [1, 53-56]. The majority of the PCMs are reported to undergo weight loss in a single stage where evaporation is the predominant mechanism.

6.1.12.1 Effect of molecular mass

The analysis of the TGA of the PCMs indicates that the main structural parameter influencing mass loss is molecular mass. The functional group and branching are noted to play a role whereas symmetry, chain length mismatch and the configuration seem to not affect mass loss. T_{ON} of saturated aliphatic monofunctional, difunctional and multifunctional PCMs are presented in **Figure 0-9a-b**, respectively, as a function of molecular mass.

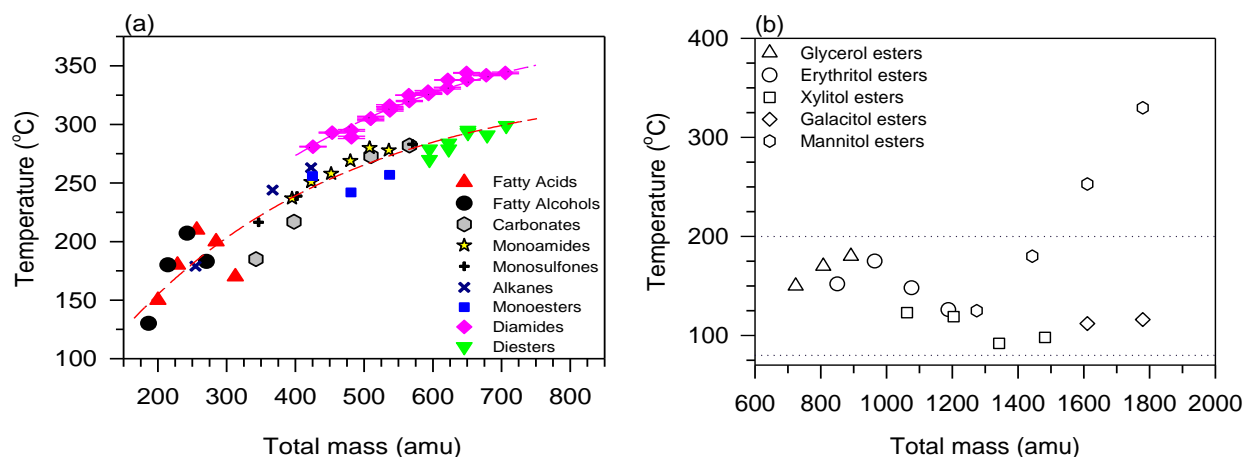


Figure 0-9. Onset of degradation (T_{ON}) of (a) monofunctional and difunctional PCMs and (b) branched multifunctional sugar ester PCMs. *Dashed lines are guides for the eye.*

Although scattered in a 20°C band, the T_{ON} data of all the monofunctional PCMs increases with molecular mass and plateaus following an apparent exponential rise to a maximum function (Equation 3, $R^2 = 0.9280$, **Figure 0-9a**) regardless of the type of functional group. The exponential curves and plateau describe the gradual resistance of the molecules to evaporate as

the molecular mass increases. The trend is consistent with the increase of activation energy required to bring the molecules into the gaseous state subsequent to the increase in molecular surface area and dispersion forces between the fatty chains [37, 109].

6.1.12.2 Effect of the functional group

As noted above, there is a confidence band of $\sim 20^\circ\text{C}$ for T_{ON} of monofunctional compounds which does not allow for evidence of the effect of one particular functional group. Note that even T_{ON} of the highly polar monoamides and monosulfones fall inside the confidence band. Furthermore, T_{ON} of the linear saturated diesters continues the trend of the monofunctional PCMs. Significant deviations from the general trend are only observed for the diamides (\blacklozenge ; **Figure 0-9a**). For similar molecular mass T_{ON} of the diamides are larger than that of the monofunctional PCMs and diesters by ~ 25 to 50°C . The effect of the functional group is observed in the diamides because of the increased hydrogen bonds which remain effective in the liquid state, making evaporation much more difficult than in esters which do not possess such hydrogen bonds.

Each diamide molecule has two amide groups with two electron pair donor and electron pair acceptor atoms. Therefore, one diamide molecule can form a maximum of four hydrogen bonds with two adjacently parallel diamide molecules that are coplanar to form a reinforced intermolecular hydrogen bond network [48]. A higher number of hydrogen bonds increases intermolecular attraction which increases thermal stability because of enhanced hydrogen bonds strength [48].

T_{ON} of the diesters and diamides follow gentle rises to plateaus reminiscent of what is observed for T_m and ΔH_m for which this secondary force plays a major role alongside mass and energy

transfer limitations. Note that the T_{ON} curve of the diamides is above and parallel to that of the diesters which points to the same contribution of the intermolecular interactions to the thermal stability of the molecules regardless of hydrocarbon chain length.

6.1.12.3 Effect of branched groups

T_{ON} of the sugar esters presented in **Figure 0-9b** are between 80-200°C despite having large molecular masses. Overall, T_{ON} does not exceed 220°C except for Mannitol hexapalmitate and Mannitol hexastearate which record 253°C and 330°C, respectively (**Figure 0-9b**). The sugar esters degrade at lower temperatures compared to monoesters, monoamides, monosulfones, diesters and diamides. Compared to the saturated aliphatic monofunctional and difunctional PCMs, molecular mass is not a main determinant of thermal stability for these complex branched structures. For example, T_{ON} of the linear saturated diamide: ditetradecanamide is approximately 2.5 times higher than that of the branched sugar ester: erythritol tetrastearate (320°C and 126°C, respectively) for half the molecular mass (MW 566g/mol and 1188g/mol, respectively). The thermal stability (low T_{ON} values) of the sugar esters is in fact driven by the chain branching. The branched groups are hindering efficient close packing arrangements and thus reduce the strength of the intermolecular interaction thereby creating weaker crystal structures with larger crystal defects. A similar effect of branching on boiling points was also observed for the linear and branched alkanes [110]. The branched groups protruding off the sugar alcohol backbone are quite long with chain lengths ranging from 14Å for C12 fatty branched group up to 21Å for C18 fatty branched group. The multiple branched groups with 14-21Å prevent the molecules from forming densely packed crystals which influences dispersion force and detrimentally affects thermal stability. The onset temperature of mass loss ranges from 80-200°C in accordance with

increasing branch size (14-21Å) despite having significantly high molecular mass (750-1800g/mol).

6.1.13 Thermal Conductivity

Thermal conductivity measures the rate at which heat passes through a PCM across a temperature gradient via conduction. PCMs with higher thermal conductivity conduct more heat than those with lower conductivity for a given temperature. Thermal conductivity of organic and salt hydrates are between 0.2 to 0.5W/mK [111], which is considered low to charge and discharge of the latent heat during the phase change. In the melt, heat is transmitted mainly by convection and is influenced by viscosity [112]. Also, in all cases and as expected, the thermal conductivity in the solid crystal state is higher than in the liquid state [113, 114].

Thermal conductivity of PCMs is important to quantify as it influences the time required to complete the phase change. However, the heat transport mechanism is a complex process because as the PCM undergo phase change the thermal conductivity is affected by the solid-liquid phase boundary [115]. Unlike in metals where heat transport is dominated by free electrons, the heat transport mechanism in VO-based PCMs occurs mainly by phonons since the electrons are involved in covalent bonds and they are few free electrons for use as conduction carriers [116, 117]. A phonon is a unit of vibrational energy that arises from oscillating atoms within the PCM's crystal lattice and its transmission is influenced by the phonon velocity, specific heat capacity and mean free path [115]. The stronger the phonon transmission in a PCM, the greater its ability to conduct heat and the higher thermal conductivity. However, the phonon transmission is known to be obstructed in organic PCMs via phonon scattering which shift or

reverse the direction of energy transport and is the fundamental reason for their low thermal conductivity [118].

6.1.13.1 Crystal structure and thermal conductivity correlation

From the analysis of the data, a direct correlation between organic PCMs crystal structure and thermal conductivity can be drawn; that is PCM molecules which pack in a more thermodynamically stable crystalline arrangement have inherently higher thermal conductivity [119]. Moreover, the strength of hydrogen bonding present in the crystal lattice network appears as the most important determinant of thermal conductivity in these materials [119]. The thermal conductivity is available for the following PCMs: fatty acids [23, 62], fatty alcohols [27, 30, 61, 64], monoesters [70, 73, 74], sugar-esters [82-86], sugar alcohols [120-122] diamides [38] and alkanes [1, 52-56] (included for comparison) are discussed in this section as a function of total number of carbons and total number hydrogen bonds in order to have better insight of the structural parameters that affect their κ -values.

6.1.13.2 Effect of hydrogen bond

The sugar alcohols which can form eight (08) to twelve (12) hydrogen bonds present the highest κ values (0.8-1.4W/mK) [120-122] and the alkanes and esters which do not form hydrogen bonds the lowest (~ 0.2 W/mK) [1, 52-56, 70, 73, 74]. The thermal conductivity of the diamides [38] which can form four (04) hydrogen bonds per molecule is higher than that of the fatty acids and fatty alcohols which can form two (02) hydrogen bonds [27, 30, 61, 64]. The thermal conductivity of the available PCMs versus total number of carbons and number of hydrogen bonds is shown in **Figure 0-10a** and b, respectively. As can be seen thermal conductivity did not show any predictive trend with total number of carbons (**Figure 0-10a**). The thermal

conductivity measured in the solid-state at room temperature for the PCMs, alkanes, and sugar alcohols fit in an apparent sigmoidal curve as a function of the number of hydrogen bonds (Figure 0-10b).

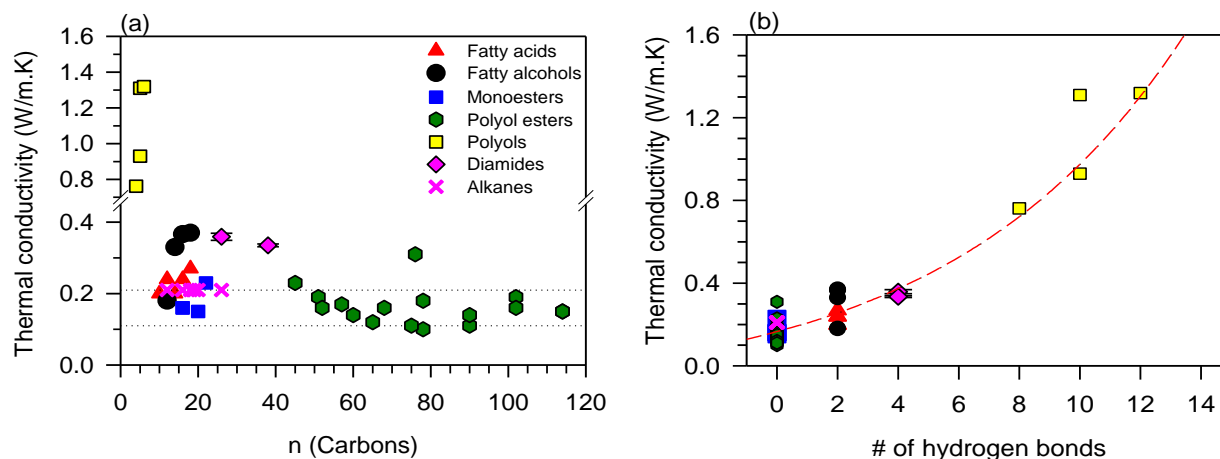


Figure 0-10. Thermal conductivity of PCMs mined from the literature measured at room temperature versus (a) total number of carbons (n); and (b) total number of hydrogen bonds per molecule. Dashed lines are guides for the eyes.

In principle, polar compounds exhibit stronger intermolecular interaction and therefore better heat conduction [123]. The network of hydroxyl groups allows stronger lattice vibrations at a higher frequency, which leads to higher heat conduction by the phonons [121, 123]. The effect of hydrogen bonding is best illustrated with the significant drop in the thermal conductivity after the esterification of the hydroxyl groups of sugar alcohols with fatty acids. The esterification eliminates the hydrogen bonds in the crystal and produces lesser ordered crystalline structures with severely limited heat transport (the sugar esters; ● in Figure 0-10a).

The κ values of the sugar alcohols is more than three times that of the diamides. For example, κ of mannitol and 12-2-12 diamide are 1.319W/mK [121] and 0.359 W/mK [38], respectively, commensurate with their ratio of hydroxyl groups per molecule. Also, the highly rigid crystalline

structures of sugar alcohols with much lower carbon numbers (C₄-C₆) has a much stronger hydrogen bond network that contributes to higher rate of heat transfer compared to the long diamides molecules (C₂₆ and C₃₈) which have looser hydrogen bond networks because of the separation between the amide functional groups.

The disposition of the hydrogen bonds in the molecule is instrumental in the stability of the crystal and hence the thermal conductivity. The effect of hydrogen bond conformation on thermal conductivity is illustrated with the examples of xylitol and l-arabitol. Both have 10 hydrogen bonds, but the κ value of L-arabitol is much lower than xylitol (0.93W/mK vs. 1.31W/mK [121]) due to the less favorable disposition of the hydroxyl groups to optimal packing. Contrary to xylitol where they are distributed intermittently on both side of the backbone, the hydroxyl groups in L-arabitol are adjacent causing large electrostatic repulsions that destabilize the crystalline structure and decrease the strength of the hydrogen bonds and network [124].

6.1.14 Applications of VO-based PCMs

VO-based PCMs are developed as a renewable alternative to PCMs produced from petroleum and salt hydrates. The environmental, safety and social benefits of using VO-based PCMs are significantly greater than paraffin. Besides, many VO-based PCMs are food-grade, thus are not harmful if ingested. A wide range of biodegradable VO-based PCMs with melting temperature at below ambient temperature up to 160°C and high latent heat (150-220J/g) is available for use in various TES applications.

PCMs are currently incorporated in the form of pure or eutectic mixtures in buildings wallboards and building materials, e.g., gypsum powders, concrete, plaster slabs, and polyurethane foams to reduce the temperature fluctuation range and improve the comfort of the indoor environment in buildings as well as for efficient thermal management [125-129]. They also find application in solar thermal energy for water heating systems [13, 130-132], solar cooker [11, 133] and industrial and consumer waste heat recovery system [130] and solar thermal energy storage in photovoltaic modules [12, 134].

One of the most promising PCM applications is in heating, ventilation, and air conditioning (HVAC) [135]. The working temperatures for PCMs in these applications (typically between 7 and 20°C) are readily achievable. The potential PCM market for HVAC is considerable as the amounts of energy involved are very large. For comparison, the amount of energy consumed in HVAC and water heating in the US is the same as that burned in gasoline engines [135].

PCMs are used in small scale applications like industrial and consumer electronics and devices for temperature regulation during operations [132, 136]. PCMs also find utility in food and beverages, e.g. (i) keeping food warm during delivery, example pizza at ~65°C [137] and (ii) and bringing the temperature of beverages such as coffee or tea down from the brewing temperature (80-90°C) to safe drinking levels (50-70°C) and maintaining it for an extended period of time [36].

Other applications of PCMs are in the (i) textile industry, e.g. vest to cool outdoor workers in the summer, and PCM coated fabrics, gloves, and socks to keep warm during winter, (ii) temperature-controlled packaging to protect temperature sensitives goods and (iii) containers that

maintain temperature for extended period during shipping of food, beverages, medicines, blood samples and donor organ [130, 131, 138].

6.1.15 Challenges and Future Trends

They are several research directions from a structure-property perspective to further improve the thermophysical properties of VO-based PCMs. These are related to (i) building new molecular architectures and (ii) developing more effective external performance enhancement techniques. The major challenges involved in these directions and potential solutions to overcome these challenges are:

(i) New molecular architectures

The analysis of the thermal properties of more than 200 VO-based PCMs in this review indicates that current molecular architectures have inherent limitations that prevent from achieving energy storage densities higher than 300J/g and working temperatures higher than 200°C. The main barrier to achieving higher T_m and ΔH_m is mainly due to the intrinsically high entropy associated with the flexibility of the fatty chains and functional groups which are present in all VO-based PCM molecular architectures.

The challenge is therefore to design molecular architectures with structural features that increase ΔH_m and T_m without increasing the entropy. Theoretically, it is possible to mitigate to some extent the degree of freedom of the fatty chains by inserting multiple polar functional groups (eg. Amide, sulfonyl, carboxylic, hydroxyl) in the linear fatty chains. Additionally, as our research group has found in a recent work (submitted to *Solar Energy Material and Solar Cells* [139]) one can use aromatic groups such as benzene to include planar segments in the PCM molecular architectures in order to decrease rotatability of the functional group and stabilize the fatty acid

moieties. Planar groups and others to be tested may also decrease interstitial defects in the crystal structure and provide larger surface areas that would increase the attractions including dispersion forces while significantly lowering the entropy of fusion.

There exists the possibility of achieving VO-based organometallic PCMs with superior thermal properties using coordination chemistry principles [140, 141]. Carefully designed coordination complexes between thermally conductive transition metals such as Fe, Cu, and Zn (κ values between 80- 400W/m.K) with VO-based ligands such as carboxylic acid or amide functional groups could provide a powerful platform to explore specific factors that contribute to thermal conductivity, energy storage density and entropy of VO-based organometallic PCMs. Moreover, unlike conventional organic and inorganic PCMs, the structure of organometallic PCMs can be controlled through rational ligand design and directional coordination bonds to tailor the crystal lattice dimensionality, entropy, and strength of covalent and noncovalent interactions within a solid in a predictable fashion. This approach was carried out in a recent study from McGillicuddy et. al [142]) on a series of divalent metal amide coordination complexes featuring extended hydrogen bond networks where melting points between 80-200°C and ΔH_m values ranging between 300 and 350J/g were achieved. McGillicuddy et. al [142] were able to demonstrate the potential of manipulating the order-disorder phase transitions in organometallic PCMs to benefit phase change properties for TES applications. They showed the significance of high densities of coordination bonds and hydrogen bonds to achieving high energy storage density. They were also able to show how metal-dependent changes to the local coordination environment during melting impact the entropy and enthalpy of organometallic PCMs. However, since low molecular weight ligands namely acetamide and N-methylurea were used, these complexes are likely to undergo decomposition over time after multiple thermal cycling.

Organometallic PCMs may require a relatively more complex synthetic process which would increase cost but this would be cost effective if functionality is sufficiently improved. Also, if successful, economies of scale and/or niche uses would render them economically viable. Nonetheless, the fundamental knowledge that would be gathered would be invaluable to the advancement of the understanding of materials for TES.

(ii) Performance enhancement techniques

VO-based PCMs are known to have an inherently low thermal conductivity (see *Section 7*) and leak during phase transition in open TES systems. The solutions to address these problems, such as the use of thermal conductivity additives [128, 143, 144] and microencapsulation techniques [132, 145] have bore some good results but are still not sufficiently tested with VO-based PCMs [143]. Investigating the thermal conductivity of VO-PCMs can lead to insights on their heat transport mechanism and limitations which would lead to possible solutions and tangible improvements. Microencapsulated VO-based PCMs can greatly extend the heat transfer surface area and improve on the efficiency of thermal performance. Currently, due to fabrication problems, microencapsulation is used for low-temperature PCMs including VO-based PCMs such as fatty acids [146]. The development of encapsulation methods suitable for high-temperature VO-based PCMs may help improve on the currently available medium temperature VO-based PCMs. This would add to improvements which would be obtained with structural changes such as in diamides where high hydrogen bonding between the amine groups and carbonyl groups imparted a 75% higher thermal conductivity than the best of alkanes, fatty acids and monoesters [38].

Among several possibilities already tested on other organic PCMs [14, 147-150], high conductivity porous composites, nanocomposites structures and nano additives may be effective

means to improve VO-based PCMs for TES applications. The preparation of these materials would be multifaceted and the ensuing phase behavior very complex. All aspects related to these materials as well techniques used to make them need careful investigation in order to determine their phase behavior and structure-function relationships. Understanding the fundamental mechanisms driving the behavior of these materials and interactions at play would be instrumental in finding means to adjust the preparation processes for select molecular systems for optimal phase structure and performance.

In the engineering side of TES applications, cascaded techniques, where PCMs with different working temperatures are used in cascade, are shown to improve the uniformity of the heat transfer process [143]. This aspect although seemingly obvious is very complex as its effect depends on PCM ratios and thermal properties such as melting temperature, melting enthalpy and thermal conductivity. The judicious selection and careful arrangement of the PCMs are critical in the performance of the TES system. Studies of selection and matching criteria of cascaded PCM systems including VO-based PCMs for cascaded latent heat storage systems may be one of future research topics.

6.1.16 Conclusion

The present work critically reviews more than 200 VO-based PCMs intended for thermal energy storage technology for both domestic and industrial applications. VO-based PCMs are a renewable, and eco-friendly alternative to traditional paraffin wax PCMs. The range of VO-based PCMs is rapidly extending and includes fatty acids and alcohols, carbonates, sulfones, amines, ethers, monoesters, diesters, sugar esters, monoamides and diamides. Analysis of their published melting temperature, enthalpy, entropy, thermal stability, and conductivity in relation

to molecular structure, particularly the hydrocarbon chains and functional groups, uncovered notable trends between molecular structure and phase change properties. For instance, the monofunctional PCMs and alkanes T_m and ΔH_m follows exponential rise to maximum functions with increasing fatty chain length. Predictive structure-function relationships, especially the thermal properties, have been confirmed or established for these PCMs. Importantly, insights on how to model the key thermal transition parameters such as temperature, enthalpy and entropy were gained. For example, the central role of the entropy of fusion has been made evident and conclusion was asserted that any attempt to model any phase change parameter should take into consideration not only the flexibility of the molecule but also symmetry, polarity and polymorphism.

Overall, linear saturated VO-based PCMs with polar monofunctional groups such as fatty acids, alcohols, amines, amides and sulfones present higher T_m than those with no functional groups like the alkanes, esters, carbonates and ethers. With regards to ΔH_m , the alkanes and compounds with small functional groups such as alcohols, amines and ethers have relatively higher ΔH_m than those with bulky functional groups such as carbonates, monoamides, monosulfones and fatty acids because they can more closely pack and maximize dispersion forces. Furthermore, geometry and conformation considerations increase the entropy of fusion and thereby lowering the transition enthalpy. VO-based PCMs with difunctional groups such as the diamides have increased polarity and are capable of forming more hydrogen bonds which significantly increase T_m (up to 160°C) compared to their monofunctional group counterparts and much lower than diesters counterparts (T_m up to 78°C). Because of similar entropy consideration, diamides present slightly lower ΔH_m (~220J/g) relative to diesters counterparts (~240J/g).

Thermal stability of VO-based PCMs with monofunctional groups increases exponentially with fatty chain length regardless of the type of functional group present. High polarity difunctional PCMs such as diamides present significantly higher thermal stability compared to diesters because reinforced hydrogen bonds between the functional groups significantly contribute to thermal stability.

Thermal conductivity of the linear saturated VO-based PCMs like alkanes and fatty acids, fatty alcohols, monoesters are low and in the range of 0.1-0.4W/mK. A notable increase in thermal conductivity with increasing number of hydrogen bonds was observed in VO PCMs. Diamides, fatty acid and fatty alcohols and sugar alcohols present relatively higher thermal conductivity (~0.4-1.4W/mK) compared to alkanes and esters which do not form hydrogen bonds (~0.2W/mK). This is due to the network of hydrogen bonds which allow stronger lattice vibrations at higher frequency which leads to higher phonon heat conduction.

Linear saturated VO-based PCMs with polar monofunctional groups that form intermolecular interactions (such as fatty acids, alcohols, amines, amides and sulfones) are suitable for applications in solar thermal energy storage (TES) in water heating systems, solar TES in photovoltaic modules, temperature-controlled packages and containers to protect temperature-sensitive goods and storage of industrial and consumer waste heat recovery systems. VO-based PCMs with functional groups incapable of forming intermolecular interactions (such as alkanes and fatty esters, carbonates and ethers) are suitable for applications in building materials such as wallboards and in clothing textiles to thermally regulate comfort temperatures.

The new insights developed in the present work can be used to advance our current knowledge of structure-property relationships and help improve PCMs through targeted material design and process modelling.

6.1.17 Acknowledgment

The authors would like to acknowledge the financial support of Natural Sciences and Engineering Research Council of Canada (NSERC), Northwater Capital, Grain Farmers of Ontario, Greater Peterborough Area Economic Development Corporation (GPA-EDC), Industry Canada, Trent University and Malaysian Palm Oil Board.

6.1.18 References

1. Sharma, S.D. and K. Sagara, *Latent Heat Storage Materials and Systems: A Review*. International Journal of Green Energy, 2005. **2**(1): p. 1-56.<http://doi.org/10.1081/ge-200051299>.
2. Sarbu, I. and C. Sebarchievici, *A comprehensive review of thermal energy storage*. Sustainability, 2018. **10**(1): p. 191.<https://doi.org/10.3390/su10010191>.
3. Prieto, C., P. Cooper, A.I. Fernández, and L.F. Cabeza, *Review of technology: Thermochemical energy storage for concentrated solar power plants*. Renewable and Sustainable Energy Reviews, 2016. **60**: p. 909-929.<https://doi.org/10.1016/j.rser.2015.12.364>.
4. Lugolole, R., A. Mawire, K.A. Lentswe, D. Okello, and K. Nyeinga, *Thermal performance comparison of three sensible heat thermal energy storage systems during charging cycles*. Sustainable Energy Technologies and Assessments, 2018. **30**: p. 37-51.<https://doi.org/10.1016/j.seta.2018.09.002>.
5. Mehling, H. and L.F. Cabeza, *Phase Change Materials and Their Basic Properties*. Thermal Energy Storage for Sustainable Energy Consumption, 2007: p. 257-277.https://doi.org/10.1007/978-1-4020-5290-3_17.
6. Su, W., J. Darkwa, and G. Kokogiannakis, *Review of solid–liquid phase change materials and their encapsulation technologies*. Renew Sust Energ Rev, 2015. **48**: p. 373-391.<http://dx.doi.org/10.1016/j.rser.2015.04.044>.
7. Zhou, Z., Z. Zhang, J. Zuo, K. Huang, and L. Zhang, *Phase change materials for solar thermal energy storage in residential buildings in cold climate*. Renew Sust Energ Rev, 2015. **48**: p. 692-703.<https://doi.org/10.1016/j.rser.2015.04.048>.
8. Sarier, N. and E. Onder, *Organic phase change materials and their textile applications: An overview*. Thermochim Acta, 2012. **540**: p. 7-60.<https://doi.org/10.1016/j.tca.2012.04.013>.
9. Ammar, Y., S. Joyce, R. Norman, Y. Wang, and A.P. Roskilly, *Low grade thermal energy sources and uses from the process industry in the UK*. Applied Energy, 2012. **89**(1): p. 3-20.<https://doi.org/10.1016/j.apenergy.2011.06.003>.
10. Mishra, A., A. Shukla, and A. Sharma, *Latent heat storage through phase change materials*. Resonance, 2015. **20**(6): p. 532-541.<https://doi.org/10.1007/s12045-015-0212-5>.
11. Buddhi, D. and L. Sahoo, *Solar cooker with latent heat storage: design and experimental testing*. Energy Conversion and Management, 1997. **38**(5): p. 493-498.[https://doi.org/10.1016/S0196-8904\(96\)00066-0](https://doi.org/10.1016/S0196-8904(96)00066-0).
12. Borri, E., G. Zsembinszki, and L.F. Cabeza, *Recent developments of thermal energy storage applications in the built environment: A bibliometric analysis and systematic review*. Applied Thermal Engineering, 2021. **189**: p. 116666.<https://doi.org/10.1016/j.applthermaleng.2021.116666>.
13. Singh, P., R.K. Sharma, A.K. Ansu, R. Goyal, A. Sari, and V.V. Tyagi, *A comprehensive review on development of eutectic organic phase change materials and their composites for low and medium range thermal energy storage*

- applications*. Solar Energy Materials and Solar Cells, 2021. **223**: p. 110955.<https://doi.org/10.1016/j.solmat.2020.110955>.
14. Al-Ahmed, A., M.A.J. Mazumder, B. Salhi, A. Sari, M. Afzaal, and F.A. Al-Sulaiman, *Effects of carbon-based fillers on thermal properties of fatty acids and their eutectics as phase change materials used for thermal energy storage: A Review*. Journal of Energy Storage, 2021. **35**: p. 102329.<https://doi.org/10.1016/j.est.2021.102329>.
 15. Sari, A. and A. Biçer, *Thermal energy storage properties and thermal reliability of some fatty acid esters/building material composites as novel form-stable PCMs*. Solar Energy Materials and Solar Cells, 2012. **101**: p. 114-122.<https://doi.org/10.1016/j.solmat.2012.02.026>.
 16. Cabeza, L.F., A. Castell, C. Barreneche, A. de Gracia, and A.I. Fernández, *Materials used as PCM in thermal energy storage in buildings: A review*. Renew Sust Energ Rev, 2011. **15**(3): p. 1675-1695.<http://dx.doi.org/10.1016/j.rser.2010.11.018>.
 17. Kenar, J.A., G. Knothe, and A.L. Copes, *Synthesis and characterization of dialkyl carbonates prepared from mid-, long-chain, and guerbet alcohols*. Journal of the American Oil Chemists' Society, 2004. **81**(3): p. 285-291.<https://doi.org/10.1007/s11746-004-0897-4>.
 18. Zhang, C., T.F. Garrison, S.A. Madbouly, and M.R. Kessler, *Recent advances in vegetable oil-based polymers and their composites*. Progress in Polymer Science, 2017. **71**: p. 91-143.<https://doi.org/10.1016/j.progpolymsci.2016.12.009>.
 19. Kahwaji, S. and M.A. White, *Prediction of the properties of eutectic fatty acid phase change materials*. Thermochim. Acta, 2018. **660**: p. 94-100.<https://doi.org/10.1016/j.tca.2017.12.024>.
 20. Huang, X.L., J. Guo, J. He, Y.M. Gong, D. Wang, and Z.Y. Song, *Novel phase change materials based on fatty acid eutectics and triallyl isocyanurate composites for thermal energy storage*. J. Appl. Polym. Sci., 2017. **134**(27): p. 44866.<http://doi.org/10.1002/app.44866>.
 21. Yuan, Y., Zhang, N., Tao, W., Cao, X. and He, Y., *Fatty acids as phase change materials: a review*. Renew Sust Energ Rev, 2014. **29**: p. 482-498.<http://doi.org/10.1016/j.rser.2013.08.107>.
 22. Suppes, G.J., M.J. Goff, and S. Lopes, *Latent heat characteristics of fatty acid derivatives pursuant phase change material applications*. Chem Eng Sci, 2003. **58**(9): p. 1751-1763.[https://doi.org/10.1016/S0009-2509\(03\)00006-X](https://doi.org/10.1016/S0009-2509(03)00006-X).
 23. Rozanna, D., T.G. Chuah, A. Salmiah, T.S.Y. Choong, and M. Sa'ari, *Fatty Acids as Phase Change Materials (PCMs) for Thermal Energy Storage: A Review*. Int. J. Green Energy, 2005. **1**(4): p. 495-513.<https://doi.org/10.1081/GE-200038722>.
 24. Alkan, C. and A. Sari, *Fatty acid/poly(methyl methacrylate) (PMMA) blends as form-stable phase change materials for latent heat thermal energy storage*. Sol Energy, 2008. **82**(2): p. 118-124.<http://dx.doi.org/10.1016/j.solener.2007.07.001>.
 25. Kenisarin, M.M., *Thermophysical properties of some organic phase change materials for latent heat storage. A review*. Sol Energy, 2014. **107**: p. 553-575.<https://doi.org/10.1016/j.solener.2014.05.001>.

26. Kenar, J.A., *Latent heat characteristics of biobased oleochemical carbonates as potential phase change materials*. *Solar Energy Mater Sol Cells*, 2010. **94**(10): p. 1697-1703.<http://doi.org/10.1016/j.solmat.2010.05.031>.
27. Kumar, R., S. Vyas, and A. Dixit, *Fatty acids/1-dodecanol binary eutectic phase change materials for low temperature solar thermal applications: Design, development and thermal analysis*. *Solar Energy*, 2017. **155**: p. 1373-1379.<https://doi.org/10.1016/j.solener.2017.07.082>.
28. van Miltenburg, J.C., H.A.J. Oonk, and L. Ventola, *Heat Capacities and Derived Thermodynamic Functions of 1-Octadecanol, 1-Nonadecanol, 1-Eicosanol, and 1-Docosanol between 10 K and 370 K*. *Journal of Chemical & Engineering Data*, 2001. **46**(1): p. 90-97.<https://doi.org/10.1021/je000048s>.
29. van Miltenburg, J.C., G.J.K. van den Berg, and M. Ramirez, *Heat Capacities and Derived Thermodynamic Functions of 1-Dodecanol and 1-Tridecanol between 10 K and 370 K and Heat Capacities of 1-Pentadecanol and 1-Heptadecanol between 300 K and 380 K and Correlations for the Heat Capacity and the Entropy of Liquid n-Alcohols*. *Journal of Chemical & Engineering Data*, 2003. **48**(1): p. 36-43.<http://doi.org/10.1021/je025524o>.
30. Zeng, J.L., Y.Y. Liu, Z.X. Cao, J. Zhang, Z.H. Zhang, L.X. Sun, and F. Xu, *Thermal conductivity enhancement of MWNTs on the PANI/tetradecanol form-stable PCM*. *Journal of Thermal Analysis and Calorimetry*, 2008. **91**(2): p. 443-446.<http://doi.org/10.1007/s10973-007-8545-2>.
31. Hasl, T. and I. Jiricek, *The Prediction of Heat Storage Properties by the Study of Structural Effect on Organic Phase Change Materials*. *Energy Procedia*, 2014. **46**: p. 301-309.<https://doi.org/10.1016/j.egypro.2014.01.186>.
32. Soodoo, N., L. Raghunanan, L. Bouzidi, and S. Narine, *Phase behavior of monosulfones: Use of high polarity sulfonyl groups to improve the thermal properties of lipid-based materials for PCM applications*. *Solar Energy Materials and Solar Cells*, 2019. **201**: p. 110115.<https://doi.org/10.1016/j.solmat.2019.110115>.
33. Alper Aydın, A., *High-chain fatty acid esters of 1-octadecanol as novel organic phase change materials and mathematical correlations for estimating the thermal properties of higher fatty acid esters' homologous series*. *Solar Energy Materials and Solar Cells*, 2013. **113**: p. 44-51.<https://doi.org/10.1016/j.solmat.2013.01.024>.
34. Aydın, A.A. and A. Aydın, *High-chain fatty acid esters of 1-hexadecanol for low temperature thermal energy storage with phase change materials*. *Solar Energy Materials and Solar Cells*, 2012. **96**: p. 93-100.<http://dx.doi.org/10.1016/j.solmat.2011.09.013>.
35. Aydın, A.A. and H. Okutan, *High-chain fatty acid esters of myristyl alcohol with odd carbon number: Novel organic phase change materials for thermal energy storage—2*. *Solar Energy Materials and Solar Cells*, 2011. **95**(8): p. 2417-2423.<https://doi.org/10.1016/j.solmat.2011.04.018>.
36. Floros, M.C. and S.S. Narine, *Latent heat storage using renewable saturated diesters as phase change materials*. *Energy*, 2016. **115**: p. 924-930.<https://doi.org/10.1016/j.energy.2016.09.085>.

37. Raghunanan, L. and S.S. Narine, *Influence of structure on chemical and thermal stability of aliphatic diesters*. The Journal of Physical Chemistry B, 2013. **117**(47): p. 14754-14762. <https://doi.org/10.1021/jp409062k>.
38. Poopalam, K.D., L. Raghunanan, L. Bouzidi, S.K. Yeong, and S.S. Narine, *Lipid-derived monoamide as phase change energy storage materials*. International Journal of Energy Research, 2019. **0**(0). <https://doi.org/10.1002/er.4711>.
39. Poopalam, K.D., L. Raghunanan, L. Bouzidi, S.K. Yeong, and S.S. Narine, *Aliphatic fatty diamide as renewable phase change materials for thermal energy storage*. Journal of Energy Storage, 2021. **42**: p. 102934. <https://doi.org/10.1016/j.est.2021.102934>.
40. Floros, M.C., K.L. Kaller, K.D. Poopalam, and S.S. Narine, *Lipid derived diamide phase change materials for high temperature thermal energy storage*. Solar Energy, 2016. **139**: p. 23-28. <https://doi.org/10.1016/j.solener.2016.09.032>.
41. Knothe, G. and J.T.P. Derksen, *Recent Developments in the Synthesis of Fatty Acid Derivatives*. 1999: Taylor & Francis.
42. Foley, P., A. Kermanshahi pour, E.S. Beach, and J.B. Zimmerman, *Derivation and synthesis of renewable surfactants*. Chemical Society Reviews, 2012. **41**(4): p. 1499-1518. <https://doi.org/10.1039/c1cs15217c>.
43. Kushairi, A., S.K. Loh, I. Azman, E. Hishamuddin, M. Ong-Abdullah, Z. Izuddin, G. Razmah, S. Sundram, and G.K.A. Parveez, *Oil palm economic performance in Malaysia and R&D progress in 2017*. Journal of Oil Palm Research, 2018. **30**(2): p. 163-195. <https://doi.org/10.21894/jopr.2018.0030>.
44. Gunstone, F., *The Chemistry of Oils and Fats: Sources, Composition, Properties and Uses*. 2009: Wiley.
45. Xia, Y. and R.C. Larock, *Vegetable oil-based polymeric materials: synthesis, properties, and applications*. Green Chemistry, 2010. **12**(11): p. 1893-1909. <http://doi.org/10.1039/c0gc00264j>.
46. Williamson, A., *XLV. Theory of ætherification*. The London, Edinburgh, and Dublin Philosophical Magazine and Journal of Science, 1850. **37**(251): p. 350-356. <https://doi.org/10.1080/14786445008646627>.
47. Kazemi, M., H. Kohzadi, and O. Abdi, *Alkylation of thiols in green mediums*. J. Mater. Environ. Sci, 2015. **6**: p. 1451-1456. ISSN: 2028-2508.
48. Yalkowsky, S.H. and D. Alantary, *Estimation of melting points of organics*. Journal of pharmaceutical sciences, 2018. **107**(5): p. 1211-1227. <https://doi.org/10.1016/j.xphs.2017.12.013>.
49. Yalkowsky, S.H., *Carnelley's Rule and the Prediction of Melting Point*. Journal of Pharmaceutical Sciences, 2014. **103**(9): p. 2629-2634. <https://doi.org/10.1002/jps.24034>.
50. Ravotti, R., O. Fellmann, N. Lardon, L. Fischer, A. Stamatiou, and J. Worlitschek, *Synthesis and Investigation of Thermal Properties of Highly Pure Carboxylic Fatty Esters to Be Used as PCM*. Applied Sciences, 2018. **8**(7): p. 1069. <https://doi.org/10.3390/app8071069>.

51. Acree, W. and J.S. Chickos, *Phase transition enthalpy measurements of organic and organometallic compounds and ionic liquids. Sublimation, vaporization, and fusion enthalpies from 1880 to 2015. Part 2. C11–C192*. Journal of Physical and Chemical Reference Data, 2017. **46**(1): p. 013104.<http://doi.org/10.1063/1.4970519>.
52. Watanabe, H. and D.J. Seong, *The Thermal Conductivity and Thermal Diffusivity of Liquid n-Alkanes: C_nH_{2n+2} (n=5 to 10) and Toluene*. International Journal of Thermophysics, 2002. **23**(2): p. 337-356.<http://doi.org/10.1023/a:1015158401299>.
53. Wang, X. and T. Zhao, *Effects of parameters of the shell formation process on the performance of microencapsulated phase change materials based on melamine-formaldehyde*. Textile Research Journal, 2016. **87**(15): p. 1848-1859.<http://doi.org/10.1177/0040517516659382>.
54. Peng, H., D. Zhang, X. Ling, Y. Li, Y. Wang, Q. Yu, X. She, Y. Li, and Y. Ding, *n-Alkanes phase change materials and their microencapsulation for thermal energy storage: A critical review*. Energy & Fuels, 2018. **32**(7): p. 7262-7293.<http://doi.org/10.1021/acs.energyfuels.8b01347>.
55. Karaipekli, A., A. Biçer, A. Sarı, and V.V. Tyagi, *Thermal characteristics of expanded perlite/paraffin composite phase change material with enhanced thermal conductivity using carbon nanotubes*. Energy Conversion and Management, 2017. **134**: p. 373-381.<https://doi.org/10.1016/j.enconman.2016.12.053>.
56. Yu, S., X. Wang, and D. Wu, *Microencapsulation of n-octadecane phase change material with calcium carbonate shell for enhancement of thermal conductivity and serving durability: Synthesis, microstructure, and performance evaluation*. Applied Energy, 2014. **114**: p. 632-643.<https://doi.org/10.1016/j.apenergy.2013.10.029>.
57. Rozanna, D., T.G. Chuah, A. Salmiah, T.S.Y. Choong, and M. Sa'ari, *Fatty Acids as Phase Change Materials (PCMs) for Thermal Energy Storage: A Review*. International Journal of Green Energy, 2005. **1**(4): p. 495-513.<https://doi.org/10.1081/GE-200038722>.
58. Şahan, N. and H. Paksoy, *Developing microencapsulated 12-hydroxystearic acid (HSA) for phase change material use*. International Journal of Energy Research, 2018. **42**(10): p. 3351-3360.<http://doi.org/10.1002/er.4090>.
59. Akhiani, A.R., M. Mehrali, S. Tahan Latibari, M. Mehrali, T.M.I. Mahlia, E. Sadeghinezhad, and H.S.C. Metselaar, *One-step preparation of form-stable phase change material through self-assembly of fatty acid and graphene*. The Journal of Physical Chemistry C, 2015. **119**(40): p. 22787-22796.<http://doi.org/10.1021/acs.jpcc.5b06089>.
60. Dao, T.D. and H.M. Jeong, *A Pickering emulsion route to a stearic acid/graphene core-shell composite phase change material*. Carbon, 2016. **99**: p. 49-57.<https://doi.org/10.1016/j.carbon.2015.12.009>.
61. Chen, Z., J. Wang, F. Yu, Z. Zhang, and X. Gao, *Preparation and properties of graphene oxide-modified poly(melamine-formaldehyde) microcapsules containing phase change material n-dodecanol for thermal energy storage*. Journal of

- Materials Chemistry A, 2015. **3**(21): p. 11624-11630.<https://doi.org/10.1039/c5ta01852h>.
62. Bayram, Ü., S. Aksöz, and N. Maraşlı, *Temperature dependency of thermal conductivity of solid phases for fatty acids*. Journal of Thermal Analysis and Calorimetry, 2014. **118**(1): p. 311-321.<https://doi.org/10.1007/s10973-014-3968-Z>.
 63. Mosselman, C., J. Mourik, and H. Dekker, *Enthalpies of phase change and heat capacities of some long-chain alcohols. Adiabatic semi-microcalorimeter for studies of polymorphism*. The Journal of Chemical Thermodynamics, 1974. **6**(5): p. 477-487.[https://doi.org/10.1016/0021-9614\(74\)90009-3](https://doi.org/10.1016/0021-9614(74)90009-3).
 64. Xing, J., Z. Tan, Q. Shi, B. Tong, S. Wang, and Y. Li, *Heat capacity and thermodynamic properties of 1-hexadecanol*. Journal of Thermal Analysis and Calorimetry, 2008. **92**(2): p. 375-380.<http://doi.org/10.1007/s10973-007-8955-1>.
 65. Sedunov, B. and I. Brondz, *The Zigzag Progression of Melting and Triple Point Properties of n-Alkanes, n-Alcohols, n-Alkanoic Amines and n-Alkanoic Acids*. Voice of the Publisher, 2017. **3**(01): p. 1.<https://doi.org/10.4236/vp.2017.31001>
 66. Nikolić, R., M. Marinović-Cincović, S. Gadžurić, and I.J. Zsigrai, *New materials for solar thermal storage—solid/liquid transitions in fatty acid esters*. Solar Energy Materials and Solar Cells, 2003. **79**(3): p. 285-292.[https://doi.org/10.1016/S0927-0248\(02\)00412-9](https://doi.org/10.1016/S0927-0248(02)00412-9).
 67. van Bommel, M.J., H.A.J. Oonk, and J.C. van Miltenburg, *Heat Capacity Measurements of 13 Methyl Esters of n-Carboxylic Acids from Methyl Octanoate to Methyl Eicosanoate between 5 K and 350 K*. Journal of Chemical & Engineering Data, 2004. **49**(4): p. 1036-1042.10.1021/je0499364.
 68. Agafonova, L.E., R.M. Varushchenko, A.I. Druzhinina, O.V. Polyakova, and Y.S. Kolesov, *Heat capacity, saturation vapor pressure, and thermodynamic functions of ethyl esters of C3–C5 and C18 carboxylic acids*. Russian Journal of Physical Chemistry A, 2011. **85**(9): p. 1516.<https://doi.org/10.1134/s0036024411090020>.
 69. Stamatiou, A., M. Obermeyer, L.J. Fischer, P. Schuetz, and J. Worlitschek, *Investigation of unbranched, saturated, carboxylic esters as phase change materials*. Renewable Energy, 2017. **108**: p. 401-409.<https://doi.org/10.1016/j.renene.2017.02.056>.
 70. Sarı, A., A. Biçer, and A. Karaipekli, *Synthesis, characterization, thermal properties of a series of stearic acid esters as novel solid–liquid phase change materials*. Materials Letters, 2009. **63**(13-14): p. 1213-1216.<https://doi.org/10.1016/j.matlet.2009.02.045>.
 71. Robustillo, M.D., D.F. Barbosa, A.J.d.A. Meirelles, and P.d.A.P. Filho, *Solid–liquid equilibrium in ternary mixtures of ethyl oleate, ethyl laurate and ethyl palmitate*. Fluid Phase Equilibria, 2013. **339**: p. 58-66.<https://doi.org/10.1016/j.fluid.2012.11.030>.
 72. Ravotti, R., O. Fellmann, N. Lardon, J.L. Fischer, A. Stamatiou, and J. Worlitschek, *Analysis of bio-based fatty esters PCM's thermal properties and investigation of trends in relation to chemical structures*. Applied Sciences, 2019. **9**(2).<http://doi.org/10.3390/app9020225>.

73. Ma, L., C. Guo, R. Ou, Q. Wang, and L. Li, *Synthesis and characterization of the n-butyl palmitate as an organic phase change material*. Journal of Thermal Analysis and Calorimetry, 2019. **136**(5): p. 2033-2039.<https://doi.org/10.1007/s10973-018-7846-y>.
74. Wang, G., J. Fan, X. Wang, F. Song, Q. Wang, and L. Zhang, *Measurement on the thermal conductivity of five saturated fatty acid ethyl esters components of biodiesel*. Fluid Phase Equilibria, 2018. **473**: p. 106-111.<https://doi.org/10.1016/j.fluid.2018.06.004>.
75. Kenar, J.A., *Latent heat characteristics of biobased oleochemical carbonates as potential phase change materials*. Solar Energy Materials and Solar Cells, 2010. **94**(10): p. 1697-1703.<https://doi.org/10.1016/j.solmat.2010.05.031>.
76. *Lubricants for plastic working of metals*. 1982, Kao Soap Co., Ltd., Japan . p. 9 pp.
77. Talvitie, Y., *n-Decylseries*. Ann. acad. sci. Fennicae, 1927. **26A**(Copyright (C) 2019 American Chemical Society (ACS). All Rights Reserved.): p. 1-94.
78. Aikawa, H., S. Tago, K. Umetsu, N. Haginiwa, and N. Asao, *Gold-catalyzed substitution reaction with ortho-alkynylbenzoic acid alkyl ester as an efficient alkylating agent*. Tetrahedron, 2009. **65**(9): p. 1774-1784.<https://doi.org/10.1016/j.tet.2008.12.033>.
79. Perron, R. and C. Paquot, *The preparation and physical properties of symmetrical ethers derived from alcohols contained in fatty substances*. Compt. rend., 1950. **231**(Copyright (C) 2019 American Chemical Society (ACS). All Rights Reserved.): p. 237-8.
80. Senderens, J.-B., *Preparation of ethers in the aliphatic series*. Compt. rend., 1925. **181**(Copyright (C) 2019 American Chemical Society (ACS). All Rights Reserved.): p. 698-700.
81. Castells, J., D. Grandes, M. Moreno-Manas, and A. Virgili, *Bouveault-Blanc reductions of sulfonic acid esters. Carbon-oxygen vs. oxygen-sulfur cleavage*. An. Quim., 1976. **72**(Copyright (C) 2019 American Chemical Society (ACS). All Rights Reserved.): p. 74-5.
82. Sari, A., A. Biçer, A. Karaipekli, C. Alkan, and A. Karadag, *Synthesis, thermal energy storage properties and thermal reliability of some fatty acid esters with glycerol as novel solid–liquid phase change materials*. Solar Energy Materials and Solar Cells, 2010. **94**(10): p. 1711-1715.<https://doi.org/10.1016/j.solmat.2010.05.033>.
83. Sari, A., R. Eroglu, A. Biçer, and A. Karaipekli, *Synthesis and Thermal Energy Storage Properties of Erythritol Tetrastearate and Erythritol Tetrapalmitate*. Chemical Engineering & Technology, 2011. **34**(1): p. 87-92.<http://doi.org/10.1002/ceat.201000306>.
84. Sari, A., A. Biçer, Ö. Lafçı, and M. Ceylan, *Galactitol hexa stearate and galactitol hexa palmitate as novel solid–liquid phase change materials for thermal energy storage*. Solar Energy, 2011. **85**(9): p. 2061-2071.<https://doi.org/10.1016/j.solener.2011.05.014>.

85. Biçer, A. and A. Sarı, *Synthesis and thermal energy storage properties of xylitol pentastearate and xylitol pentapalmitate as novel solid–liquid PCMs*. *Solar Energy Materials and Solar Cells*, 2012. **102**: p. 125-130.<https://doi.org/10.1016/j.solmat.2012.03.014>.
86. Sari, A., *Thermal energy storage properties of mannitol–fatty acid esters as novel organic solid–liquid phase change materials*. *Energy Conversion and Management*, 2012. **64**: p. 68-78.<https://doi.org/10.1016/j.enconman.2012.07.003>.
87. Sharma, R.K., P. Ganesan, V.V. Tyagi, H.S.C. Metselaar, and S.C. Sandaran, *Developments in organic solid–liquid phase change materials and their applications in thermal energy storage*. *Energy Conversion and Management*, 2015. **95**: p. 193-228.<https://doi.org/10.1016/j.enconman.2015.01.084>.
88. Bunn, C.W., *The melting points of chain polymers*. *Journal of Polymer Science Part B: Polymer Physics*, 1996. **34**(5): p. 799-819.<http://doi.org/10.1002/polb.1996.900>.
89. Chickos, J.S. and G. Nichols, *Simple relationships for the estimation of melting temperatures of homologous series*. *Journal of Chemical & Engineering Data*, 2001. **46**(3): p. 562-573.<http://doi.org/10.1021/je0002235>.
90. Yalkowsky, S.H. and D. Alantary, *Estimation of Melting Points of Organics*. *J Pharm Sci*, 2018. **107**(5): p. 1211-1227.<https://doi.org/10.1016/j.xphs.2017.12.013>.
91. A. Gavezzotti and H. Flack. *Crystal Packing-Thermodynamics and kinetics*. International Union of Crystallography Commission on Crystallographic Teaching 2005 03-01-2019 (accessed 3 March 2019)]; Available from: <https://www.iucr.org/data/assets/pdf/0006/14964/21.pdf>.
92. Boese, R., H.-C. Weiss, and D. Bläser, *The melting point alternation in the short-chain n-alkanes: Single-crystal X-Ray analyses of propane at 30 K and of n-butane to n-nonane at 90 K*. *Angewandte Chemie International Edition*, 1999. **38**(7): p. 988-992.[http://doi.org/10.1002/\(sici\)1521-3773\(19990401\)38:7<988::aid-anie988>3.0.co;2-0](http://doi.org/10.1002/(sici)1521-3773(19990401)38:7<988::aid-anie988>3.0.co;2-0).
93. Costa, J.C.S., A. Mendes, and L.M.N.B.F. Santos, *Chain length dependence of the thermodynamic properties of n-alkanes and their monosubstituted derivatives*. *Journal of Chemical & Engineering Data*, 2018. **63**(1): p. 1-20.<http://doi.org/10.1021/acs.jced.7b00837>.
94. Deming, T.J., *Functional modification of thioether groups in peptides, polypeptides, and proteins*. *Bioconjug Chem*, 2017. **28**(3): p. 691-700.<https://doi.org/10.1021/acs.bioconjchem.6b00696>.
95. Ouellette, R.J. and J.D. Rawn, *1 - Structure and Bonding in Organic Compounds*, in *Organic Chemistry (Second Edition)*, R.J. Ouellette and J.D. Rawn, Editors. 2018, Academic Press. p. 1-30.
96. Vladimir I. Minkin, Osip A. Osipov, and Y.A. Zhdanov, *Dipole moments in organic chemistry*. 2012, Springer, Boston, MA, USA: Springer Science & Business Media.

97. Nelson Jr, R.D., D.R. Lide Jr, and A.A. Maryott, *Selected values of electric dipole moments for molecules in the gas phase*. 1967, National Standard Reference Data System.
98. Marks, M., J. Thompson, and G. Krishnan, *An experimental study of die attach polymer bleedout in ceramic packages*. *Thin Solid Films*, 1994. **252**: p. 54-60.[https://doi.org/10.1016/0040-6090\(94\)90825-7](https://doi.org/10.1016/0040-6090(94)90825-7).
99. Wang, F., N. Zhao, F. Xiao, W. Wei, and Y. Sun. *The Design and Simulation of the Synthesis of Dimethyl Carbonate and the Product Separation Process Plant*. 2012.
100. Durig, J.R., Y. Jin, H. Phan, J. Liu, and D.T. Durig, *Far-Infrared Spectra, Conformational Stability, Barriers to Internal Rotation, Ab Initio Calculations, r0 Structural Parameters, and Vibrational Assignment of Ethyl Methyl Ether*. *Structural Chemistry*, 2002. **13**(1): p. 1-26.<https://doi.org/10.1023/A:1013410428690>.
101. Krisher, L.C. and E. Saegbarth, *Microwave Spectrum of Acetic Acid, CH₃COOH and CD₃COOH*. *The Journal of Chemical Physics*, 1971. **54**(11): p. 4553-4558.<https://doi.org/10.1063/1.1674721>.
102. Clark, T., J.S. Murray, P. Lane, and P. Politzer, *Why are dimethyl sulfoxide and dimethyl sulfone such good solvents?* *Journal of Molecular Modeling*, 2008. **14**(8): p. 689-697.<https://doi.org/10.1007/s00894-008-0279-y>.
103. Ravotti, R., O. Fellmann, N. Lardon, J.L. Fischer, A. Stamatiou, and J. Worlitschek, *Analysis of Bio-Based Fatty Esters PCM's Thermal Properties and Investigation of Trends in Relation to Chemical Structures*. *Appl Sci*, 2019. **9**(2).<http://doi.org/10.3390/app9020225>.
104. Floros, M.C. and S.S. Narine, *Saturated linear diesters from stearic acid as renewable phase change materials*. *Materials Letters*, 2014. **137**: p. 252-255.<https://doi.org/10.1016/j.matlet.2014.09.041>.
105. Raghunanan, L., M.C. Floros, and S.S. Narine, *Thermal stability of renewable diesters as phase change materials*. *Thermochimica Acta*, 2016. **644**: p. 61-68.<https://doi.org/10.1016/j.tca.2016.10.009>.
106. Poopalam, K.D., L. Raghunanan, L. Bouzidi, S.K. Yeong, and S.S. Narine, *The anomalous behaviour of aliphatic fatty diamides: Chain length and hydrogen bonding interactions*. *Solar Energy Materials and Solar Cells*, 2019.<https://doi.org/10.1016/j.solmat.2019.110056>.
107. Raghunanan, L. and S.S. Narine, *Engineering Green Lubricants I: Optimizing Thermal and Flow Properties of Linear Diesters Derived from Vegetable Oils*. *ACS Sustainable Chemistry & Engineering*, 2016. **4**(3): p. 686-692.<https://doi.org/10.1021/acssuschemeng.5b01644>.
108. Noël, J.A., S. Kahwaji, and M.A. White, *Molecular structure and melting: implications for phase change materials*. *Canadian Journal of Chemistry*, 2017. **96**(7): p. 722-729.<https://doi.org/10.1139/cjc-2017-0578>.
109. Heym, F., B.J.M. Etzold, C. Kern, and A. Jess, *An improved method to measure the rate of vaporisation and thermal decomposition of high boiling organic and*

- ionic liquids by thermogravimetric analysis*. Physical Chemistry Chemical Physics, 2010. **12**(38): p. 12089-12100.<http://doi.org/10.1039/c0cp00097c>.
110. Solomons, T.W.G., C.B. Fryhle, and S.A. Snyder, *Organic Chemistry, Binder Ready Version*. 2016: Wiley.
 111. Zhao, C.Y., W. Lu, and Y. Tian, *Heat transfer enhancement for thermal energy storage using metal foams embedded within phase change materials (PCMs)*. Solar Energy, 2010. **84**(8): p. 1402-1412.<https://doi.org/10.1016/j.solener.2010.04.022>.
 112. Sun, T. and A.S. Teja, *Correlation and prediction of the viscosity and thermal conductivity of dense fluids*. Journal of Chemical & Engineering Data, 2009. **54**(9): p. 2527-2531.<http://doi.org/10.1021/jc900096n>.
 113. Yavari, F., H.R. Fard, K. Pashayi, M.A. Rafiee, A. Zamiri, Z. Yu, R. Ozisik, T. Borca-Tasciuc, and N. Koratkar, *Enhanced thermal conductivity in a nanostructured phase change composite due to low concentration graphene additives*. The Journal of Physical Chemistry C, 2011. **115**(17): p. 8753-8758.<https://doi.org/10.1021/jp200838s>.
 114. Di Nicola, G., E. Ciarrocchi, M. Pierantozzi, and R. Stryjek, *A new equation for the thermal conductivity of organic compounds*. J Therm Anal Calorim, 2014. **116**(1): p. 135-140.
 115. Wu, S., T. Yan, Z. Kuai, and W. Pan, *Thermal conductivity enhancement on phase change materials for thermal energy storage: A review*. Energy Storage Materials, 2020. **25**: p. 251-295.<https://doi.org/10.1016/j.ensm.2019.10.010>.
 116. Srivastava, G.P., *The Physics of Phonons*. 1990: Taylor & Francis.
 117. Minnich, A., *Advances in the measurement and computation of thermal phonon transport properties*. Journal of Physics: Condensed Matter, 2015. **27**(5): p. 053202.<https://doi.org/10.1088/0953-8984/27/5/053202>.
 118. Mehra, N., L. Mu, T. Ji, X. Yang, J. Kong, J. Gu, and J. Zhu, *Thermal transport in polymeric materials and across composite interfaces*. Applied Materials Today, 2018. **12**: p. 92-130.<https://doi.org/10.1016/j.apmt.2018.04.004>.
 119. Feng, B., J. Tu, J.-W. Sun, L.-W. Fan, and Y. Zeng, *A molecular dynamics study of the effects of crystalline structure transition on the thermal conductivity of pentaerythritol as a solid-solid phase change material*. International Journal of Heat and Mass Transfer, 2019. **141**: p. 789-798.<https://doi.org/10.1016/j.ijheatmasstransfer.2019.07.017>.
 120. Gunasekara, S.N., J. Stalin, M. Marçal, R. Delubac, A. Karabanova, J.N. Wei Chiu, and V. Martin, *Erythritol, glycerol, their blends, and olive oil, as sustainable phase change materials*. Energy Procedia, 2017. **135**: p. 249-262.<https://doi.org/10.1016/j.egypro.2017.09.517>.
 121. del Barrio, E.P., A. Godin, M. Duquesne, J. Daranlot, J. Jolly, W. Alshaer, T. Kouadio, and A. Sommer, *Characterization of different sugar alcohols as phase change materials for thermal energy storage applications*. Solar Energy Materials and Solar Cells, 2017. **159**: p. 560-569.<https://doi.org/10.1016/j.solmat.2016.10.009>.

122. Paul, A., L. Shi, and C.W. Bielawski, *A eutectic mixture of galactitol and mannitol as a phase change material for latent heat storage*. *Energy Conversion and Management*, 2015. **103**: p. 139-146.<https://doi.org/10.1016/j.enconman.2015.06.013>.
123. Lee, N.-E., J.-J. Zhou, L.A. Agapito, and M. Bernardi, *Charge transport in organic molecular semiconductors from first principles: The bandlike hole mobility in a naphthalene crystal*. *Phys Rev B*, 2018. **97**(11): p. 115203.<https://doi.org/10.1103/PhysRevB.97.115203>.
124. Inagaki, T. and T. Ishida, *Computational analysis of sugar alcohols as phase-change material: Insight into the molecular mechanism of thermal energy storage*. *The Journal of Physical Chemistry C*, 2016. **120**(15): p. 7903-7915.<https://doi.org/10.1021/acs.jpcc.5b11999>.
125. Kosny, J., N. Shukla, and A. Fallahi, *Cost analysis of simple phase change materials-enhanced building envelopes in Southern U.S. climates*. 2013: p. 1-55.<https://doi.org/10.2172/1219890>.
126. Cellat, K., B. Beyhan, Y. Konuklu, C. DüNDAR, O. Karahan, C. GüNGÖR, and H. Paksoy, *2 years of monitoring results from passive solar energy storage in test cabins with phase change materials*. *Solar Energy*, 2019.<https://doi.org/10.1016/j.solener.2019.01.045>.
127. Marani, A. and M.L. Nehdi, *Integrating phase change materials in construction materials: Critical review*. *Construction and Building Materials*, 2019. **217**: p. 36-49.<https://doi.org/10.1016/j.conbuildmat.2019.05.064>.
128. Kalnæs, S.E. and B.P. Jelle, *Phase change materials and products for building applications: A state-of-the-art review and future research opportunities*. *Energy and Buildings*, 2015. **94**: p. 150-176.<https://doi.org/10.1016/j.enbuild.2015.02.023>.
129. Sari, A., G. Hekimoğlu, and V.V. Tyagi, *Low cost and eco-friendly wood fiber-based composite phase change material: Development, characterization and lab-scale thermoregulation performance for thermal energy storage*. *Energy*, 2020. **195**: p. 116983.<https://doi.org/10.1016/j.energy.2020.116983>.
130. International, C. *Phase change Materials*. 2019 [cited 2019 12 July 2019]; Available from: <https://www.crodatherm.com/en-gb>.
131. PureTemp. *PureTemp Coated Fabrics: Temperature Control Technology*. 2019 [cited 2019 12 July 2019]; Available from: <https://www.puretemp.com/stories/about-puretemp-llc>.
132. Umair, M.M., Y. Zhang, K. Iqbal, S. Zhang, and B. Tang, *Novel strategies and supporting materials applied to shape-stabilize organic phase change materials for thermal energy storage—A review*. *Applied Energy*, 2019. **235**: p. 846-873.<https://doi.org/10.1016/j.apenergy.2018.11.017>.
133. Nkhonjera, L., T. Bello-Ochende, G. John, and C.K. King'ondeu, *A review of thermal energy storage designs, heat storage materials and cooking performance of solar cookers with heat storage*. *Renewable and Sustainable Energy Reviews*, 2017. **75**: p. 157-167.<https://doi.org/10.1016/j.rser.2016.10.059>.

134. Islam, M.M., A.K. Pandey, M. Hasanuzzaman, and N.A. Rahim, *Recent progresses and achievements in photovoltaic-phase change material technology: A review with special treatment on photovoltaic thermal-phase change material systems*. Energy Conversion and Management, 2016. **126**: p. 177-204.<https://doi.org/10.1016/j.enconman.2016.07.075>.
135. Oró, E., A. de Gracia, A. Castell, M.M. Farid, and L.F. Cabeza, *Review on phase change materials (PCMs) for cold thermal energy storage applications*. Applied Energy, 2012. **99**: p. 513-533.<https://doi.org/10.1016/j.apenergy.2012.03.058>.
136. Maxa, J., A. Novikov, and M. Nowotnick, *Thermal Peak Management Using Organic Phase Change Materials for Latent Heat Storage in Electronic Applications*. Materials, 2017. **11**(1): p. 31.<https://doi.org/10.3390/ma11010031>.
137. Sigurd Frohlich, Hans Jochen Koellner, and I. Salyer, *Food warming device containing a rechargeable phase change materials in United States Patent*. 2000, Phase Change Laboratories, Inc., San Diego, Calif.: US.
138. Sutterlin, W.R. *A phase change materials comparison: vegetable-based vs paraffin-based PCMs*. 2015 [cited 2019 12 July 2019]; Available from: <https://www.chemicalonline.com/doc/a-phase-change-materials-comparison-vegetable-based-vs-paraffin-based-pcms-0001>.
139. Navindra Soodoo, K.D.P., Laziz Bouzidi, Suresh S Narine, *Exploiting Aromaticity in Fatty Terephthalate Diesters to Enhance Melting Point and Prevent Polymorphism*. Solar Energy Materials and Solar Cells, 2021.
140. Butler, K.T., A. Walsh, A.K. Cheetham, and G. Kieslich, *Organised chaos: entropy in hybrid inorganic-organic systems and other materials*. Chemical Science, 2016. **7**(10): p. 6316-6324.<https://doi.org/10.1039/C6SC02199A>.
141. Yaghi, O.M., M. O'Keeffe, N.W. Ockwig, H.K. Chae, M. Eddaoudi, and J. Kim, *Reticular synthesis and the design of new materials*. Nature, 2003. **423**(6941): p. 705-714.<https://doi.org/10.1038/nature01650>.
142. McGillicuddy, R.D., S. Thapa, M.B. Wenny, M.I. Gonzalez, and J.A. Mason, *Metal-Organic Phase-Change Materials for Thermal Energy Storage*. Journal of the American Chemical Society, 2020. **142**(45): p. 19170-19180.<https://doi.org/10.1021/jacs.0c08777>.
143. Tao, Y.B. and Y.-L. He, *A review of phase change material and performance enhancement method for latent heat storage system*. Renewable and Sustainable Energy Reviews, 2018. **93**: p. 245-259.<https://doi.org/10.1016/j.rser.2018.05.028>.
144. Nazir, H., M. Batool, F.J. Bolivar Osorio, M. Isaza-Ruiz, X. Xu, K. Vignarooban, P. Phelan, Inamuddin, and A.M. Kannan, *Recent developments in phase change materials for energy storage applications: A review*. International Journal of Heat and Mass Transfer, 2019. **129**: p. 491-523.<https://doi.org/10.1016/j.ijheatmasstransfer.2018.09.126>.
145. Khan, Z., Z. Khan, and A. Ghafoor, *A review of performance enhancement of PCM based latent heat storage system within the context of materials, thermal stability and compatibility*. Energy Conversion and Management, 2016. **115**: p. 132-158.<https://doi.org/10.1016/j.enconman.2016.02.045>.

146. Skurkytė-Papievienė, V., A. Abraitienė, A. Sankauskaitė, V. Rubežienė, and K. Dubinskaitė, *Enhancement of thermal properties of bio-based microcapsules intended for textile applications*. Open Chemistry, 2020. **18**(1): p. 669-680.<https://doi.org/10.1515/chem-2020-0064>.
147. Al-Ahmed, A., A. Sarı, M.A.J. Mazumder, G. Hekimoğlu, F.A. Al-Sulaiman, and Inamuddin, *Thermal energy storage and thermal conductivity properties of Octadecanol-MWCNT composite PCMs as promising organic heat storage materials*. Sci. Rep., 2020. **10**(1): p. 9168.<https://doi.org/10.1038/s41598-020-64149-3>.
148. Al-Ahmed, A., A. Sarı, M.A.J. Mazumder, B. Salhi, G. Hekimoğlu, F.A. Al-Sulaiman, and Inamuddin, *Thermal energy storage and thermal conductivity properties of fatty acid/fatty acid-grafted-CNTs and fatty acid/CNTs as novel composite phase change materials*. Sci. Rep., 2020. **10**(1): p. 15388.<https://doi.org/10.1038/s41598-020-71891-1>.
149. Sarı, A., T.A. Saleh, G. Hekimoğlu, M. Tuzen, and V.V. Tyagi, *Evaluation of carbonized waste tire for development of novel shape stabilized composite phase change material for thermal energy storage*. Waste Manag, 2020. **103**: p. 352-360.<https://doi.org/10.1016/j.wasman.2019.12.051>.
150. Hekimoğlu, G., A. Sarı, T. Kar, S. Keleş, K. Kaygusuz, V.V. Tyagi, R.K. Sharma, A. Al-Ahmed, F.A. Al-Sulaiman, and T.A. Saleh, *Walnut shell derived bio-carbon/methyl palmitate as novel composite phase change material with enhanced thermal energy storage properties*. J Energy Storage, 2021. **35**: p. 102288.<https://doi.org/10.1016/j.est.2021.102288>.